Aalborg Universitet

AALBORG UNIVERSITY
DENMARK

Downlink Frequency-Domain Adaptation and Scheduling - A Case Study Based on the UTRA Long Term Evolution

Pokhariyal, Akhilesh

Publication date:
2007

Document Version
Publisher's PDF, also known as Version of record

Link to publication from Aalborg University

Downlink
Frequency-Domain Adaptation and Scheduling
- A Case Study Based on the UTRA Long Term Evolution

PhD Thesis

by

Akhilesh Pokhariyal

Supervisors:
Preben E. Mogensen, PhD,
Professor, Aalborg University, Denmark.
Troels E. Kolding, PhD,
System Competence Team Manager, Nokia Siemens Networks, Aalborg, Denmark.
Troels B. Sørensen, PhD,
Associate Professor, Aalborg University, Denmark.

Opponents:
Luis Lopes, PhD,
Director of Standards Strategy, Motorola, UK.
Klaus Hugl, PhD,
Research Team Leader, Nokia Research Center, Finland.
Luc Deneire, PhD,
Associate Professor, Aalborg University, Denmark.

To my wife Sangeeta, my parents, my family in-law, and my sister.

Abstract

Orthogonal Frequency Division Multiplexing (OFDM) and Orthogonal Frequency Division Multiple Access (OFDMA) have been selected by several standardization bodies for the implementation of next generation broadband wireless packet data systems. WiMAX and UTRAN Long Term Evolution (LTE) are examples of wide coverage and high mobility radio communication standards that employ these technologies. One of the reasons behind the popularity of OFDMA is that it facilitates frequency-domain adaptation and scheduling (FDAS). In this study, FDAS implies cross-layer optimization, as Physical layer measurements are used in resource allocation decisions at the MAC layer. Further, it involves multi-user packet scheduling, and link adaptation based on bandwidth and/or power adaptation as well as adaptive modulation and coding (AMC). These techniques can boost spectral efficiency by exploiting the frequency-selective fading experienced over the mobile multipath channel.

Two general FDAS scenarios have been investigated in this study: Frequency-Domain Link Adaptation (FDLA) and Frequency-Domain Packet Scheduling (FDPS). FDLA refers to the scenario where only a single user is selected for transmission in each scheduling interval, and both bandwidth and power can be adapted in frequency. The scheduler can exploit available multi-user diversity in time only. FDPS refers to user multiplexing in the frequency-domain, and here the scheduler can exploit multi-user diversity in frequency as well as in time. Both FDLA and FDPS are compared to a reference scheme based on full-bandwidth transmission, together with AMC, where the scheduler can exploit multi-user diversity in time only. In order to reduce the channel-quality feedback required to support FDAS a novel threshold-based reporting scheme has been proposed.

In contrast to known optimum adaptation algorithms, which allocate resources on sub-carrier level, we propose sub-optimal FDAS algorithms that are suitable for practical implementation and designed to interact with relevant system-level entities such as HARQ. A detailed system-level analysis of the practical FDAS algorithms has been performed, based on the 3GPP LTE Downlink cellular system framework. In the first part of the study we investigate the potential of available adaptation mechanisms such as bandwidth adaptation only, joint bandwidth, power and AMC adaptation, etc., using a simplified single-cell model. Extensive Monte Carlo simulations based on diverse operating conditions such as different multipath channel profiles, antenna configurations, bandwidths, etc., have been performed during the preliminary analysis. The FDAS algorithms with the largest potential were short-listed and further evaluated by using a state-of-the-art multi-cell system simulator in the final part of the study. As a result, realistic estimates of the FDAS gain potential at the system-level over time-domain only adaptation and scheduling have been obtained, which include the impact of limited and noisy channel-quality feedback.

The most important FDAS design parameter is the granularity of adaptation in frequency-domain, where generally an increase in the scheduling resolution leads to an improvement in spectral efficiency. The study has shown that it is sufficient to keep the scheduling resolution in the order of coherence bandwidth, i.e., around 350 kHz for the typically experienced channel profiles. FDLA is mainly a coverage enhancing mechanism, and equal-power distribution can

achieve most of the potential. Depending on the presence of receive antenna diversity, FDLA can provide a coverage gain of 10% - 40% over reference at 3 km/h, in the 3GPP Macro-cell scenario. Under similar assumptions, FDPS based on equal-power transmission can provide a cell throughput gain of 40% - 80%, and a coverage gain of 45% - 70%. The recommended strategy for HARQ management is to reserve adequate resources for retransmissions, while giving maximum flexibility to first transmissions. The results have been obtained for a 10 MHz system, using the best-effort traffic model and periodic channel-quality reporting (threshold-based) at the rate of 6 kbps. The FDAS gain potential is optimal below 10 km/h, while it cannot provide any gain beyond 30 km/h.

Dansk Resumé [1]

Orthogonal Frequency Division Multiplexing (OFDM) og Orthogonal Frequency Division Multiple Access (OFDMA) er valgt af flere standardiseringsorganer til realiseringen af næste generations trådløse bredbånds pakkedatasystemer. WiMAX og UTRAN Long Term Evolution (LTE) er eksempler på mobilkommunikationsstandarder, der benytter disse teknologier. OFDMA er populært, bl.a. fordi det muliggør frekvensdomæne adaptering og skedulering af pakkedata-trafikken. Konceptet, benævnt i dette studie som FDAS, indebærer krydslagsoptimering, idet fysiske målinger benyttes i MAC-laget til resurseallokering. Det indebærer også multi-bruger pakkeskedulering, linkadaptering baseret på tilpasning af båndbredde og/eller transmitteret effekt, såvel som adaptiv modulation og kodning (AMC). Disse teknikker kan forøge spektraleffektiviteten ved at udnytte den frekvensselektive fading der opstår ved flervejsudbredelse i radiokanalen.

Der er undersøgt to generelle FDAS scenarier i studiet: Frekvensdomæne linkadaptering (FDLA) og Frekvensdomæne pakkeskedulering (FDPS). FDLA hentyder til scenariet, hvor kun en enkelt bruger transmitterer i hvert skeduleringsinterval, med tilpasning af båndbredde og transmitteret effekt over frekvensdomænet. FDLA kan kun udnytte multi-bruger diversitet i tidsdomænet. FDPS derimod muliggør multiplexing af brugere i frekvensdomænet og kan dermed udnytte multi-bruger diversitet i frekvens- såvel som tids-domænet. Både FDLA og FDPS sammenlignes i afhandlingen med et referencescenarie baseret på transmission i den fulde båndbredde med AMC, i hvilket det kun er muligt at udnytte multi-bruger diversitet i tidsdomænet. For at begrænse mængden af channel-quality feedback til at supportere FDAS foreslås en ny tærskelbaseret rapporteringsmetode.

I modsætning til kendte optimale adapteringsmetoder, der tildeler resurser på sub-carrier niveau, foreslår vi sub-optimale FDPS algoritmer, der er anvendelige for praktisk implementering, og designet til at virke sammen med relevante system-enheder såsom HARQ. Der er foretaget en detaljeret system-niveau analyse af de praktiske algoritmer baseret på 3GPPs LTE downlink setup. I den første del af studiet undersøger vi potentialet i de tilgængelige adapteringsmekanismer såsom tilpasning af båndbredde eller for eksempel samtidig tilpasning af båndbredde, effekt og AMC, og i alle tilfælde med brug af en simplificeret enkeltcelle model. Der er foretaget omfattende Monte Carlo simuleringer baseret på forskellige systembetingelser, herunder forskellige flervejsudbredelsesprofiler, antennekonfigurationer, båndbredder, etc. De mest lovende algoritmer var yderligere analyseret i den sidste del af studiet vha. en state-of-the-art mutlicelle systemsimulator. Det har dermed været muligt at give realistiske estimater af potentialet af FDPS på systemniveau i sammenligning med scenariet hvor adaptering og skedulering kun foregår i tidsdomæne, bl.a. ved at inkludere indvirkningen af begrænset og støjfyldt channel-quality feedback.

Den mest betydningsfulde FDAS designparameter er granulariteten i frekvensdomænet, for hvilken spektraleffektiviteten generelt forbedres ved at mindske skeduleringsenheden. Resultaterne har vist, at det er tilstrækkeligt at benytte en mindste skeduleringsenhed, der modsvarer kohærensbåndbredden, dvs. omkring 350 kHz for de typisk forekommende kanalprofiler. FDLA

---

[1] Translation by Troels B. Sørensen, RATE Section, CTIF, Aalborg University, Denmark.

er hovedsageligt en mekanisme til forbedring af radiodækning, hvor forbedringen kan opnås uden avanceret vægtning i frekvens af den transmitterede effekt. Afhængig af tilstedeværelsen af antennediversitet i modtageren kan FDLA give en forbedring i dækning på 10% - 40% i forhold til referencen ved 3 km/h i 3GPP Macro-celle scenariet. Under tilsvarende antagelser kan FDPS forbedre cellekapaciteten med 40% - 80%, og dækningen med 45% - 70%. For en effektiv samvirkning med HARQ anbefales det at reservere tilstrækkeligt med resurser til retransmissioner, og maksimal fleksibilitet til de første transmissioner. De angivne resultater er for et 10 MHz system med periodisk (tærskelbaseret) channel-quality feedback ved en rate på 6 kbps, og best-effort trafik. Potentialet for FDAS er optimalt ved mobilitet under 10 km/h, og ubetydeligt ved hastigheder over 30 km/h.

Preface and Acknowledgments

This dissertation is the result of a three years research project carried out at the Radio Access Technology (RATE) section, Center for TeleInFraStruktur (CTIF), Institute of Electronic Systems, Aalborg University, Denmark, under the supervision and guidance of Professor Preben E. Mogensen (Aalborg University, Denmark), Dr. Troels E. Kolding (Nokia Siemens Networks, Aalborg, Denmark), and Associate Professor T. B. Sørensen (Aalborg University, Denmark). The dissertation has been completed in parallel with the mandatory course work, teaching, and project work obligations in order to obtain the PhD degree. This research project has been co-financed by the Danish Research Fund (FTP), Aalborg University (Tek NAT) and Nokia Networks R&D, Aalborg.

First of all I am grateful to my M.Sc. Thesis supervisor Dr. Troels E. Kolding for introducing me to the main topics of this research, namely OFDM, and Radio Resource Management. His enthusiasm and encouragement motivated me to undertake this challenging task. Further, I want to thank my Ph.D. supervisors for their guidance, advice and co-operation. Their input has been vital, especially our technical discussions were instrumental in improving my understanding of the subject, and enabled me to overcome the technical challenges. It has been a pleasure to work with a group of supervisors who are not only highly qualified technically, but are also very understanding when it comes to personal issues. I am grateful to Troels B. Sørensen for translating the abstract into Danish.

Further, I would like to thank the members of the assessment committee who through their detailed reading and constructive feedback have assisted me in the correction and clarification of the text throughout this dissertation.

The constant friendly support, assistance with administrative tasks, and the proofreading provided by our section secretaries Lisbeth Schiønning Larsen and Jytte Larsen is highly appreciated.

The presented work would not have been possible without being part of an inspiring network of colleagues, enabling interesting discussions and collaboration. In this respect I would like to particularly point out the good collaboration with Wei Na, Guillaume Monghal, Klaus. I. Pedersen, Frank Frederiksen, Istvan Z. Kovacs and Claudio Rosa, which has also led to common publications. Further, I want to thank Basuki E. Priyanto and Christian Rom for their valuable input. I would also like to express my gratitude to all the employees of Nokia Networks Aalborg, and the exchange students from Spain for their friendly support.

I am very grateful to the small but extremely helpful bunch of friends, Mangesh Ingale, Mohmmad Anas, Danish A. Khan and Oumer M. Teyeb, for making my stay in Aalborg enjoyable. Further, I am thankful to Shibu Chacko and Sunitha Chacko for being wonderful friends, and for helping us on numerous occasions. Finally, I want to sincerely thank my wife Sangeeta, my parents, my family in-law, and my sister, for their steadfast support, patience and affection.

Akhilesh Pokhariyal,

August 2007.

Notation

Abbreviations and mathematical conventions used in the thesis are listed below for quick reference. The abbreviations are additionally defined at their first occurrence.

Abbreviations

1G	First Generation
16QAM	16 Quadrature Amplitude Modulation
2G	Second Generation
3G	Third Generation
3GPP	3rd Generation Partnership Project
4G	Fourth Generation
64QAM	64 Quadrature Amplitude Modulation
AC	Admission Control
AMC	Adaptive Modulation and Coding
AMPS	Advanced Mobile Phone Services
AT	Allocation Table
AWGN	Additive White Gaussian Noise
BER	Bit Error Rate
BLER	BLock Error Rate
BPSK	Binary Phase Shift Keying
CC	Chase Combining
CDF	Cumulative Density Function
CP	Cyclic Prefix
CQI	Channel Quality Information
CSI	Channel State Information
DL	Downlink
DL-SCH	Downlink Shared Channel
eNode-B	E-UTRAN Node B
EESM	Exponential Effective SINR Metric
E-UTRA	Evolved Universal Terrestrial Radio Access
E-UTRAN	Evolved Universal Terrestrial Radio Access Network

FCF	Frequency Correlation Function
FDAS	Frequency-Domain Adaptation and Scheduling
FDD	Frequency Division Duplex
FDLA	Frequency-Domain Link Adaptation
FDM	Frequency Domain Multiplexing
FDPS	Frequency-Domain Packet Scheduling
FEC	Forward Error Correction
FFT	Fast Fourier Transform
FL	Fractional Load
GSM	Global System for Mobile Communication
HARQ	Hybrid Automatic Repeat reQuest
HSDPA	High-Speed Downlink Packet Access
HSPA	High-Speed Packet Access
HSUPA	High-Speed Uplink Packet Access
IFFT	Inverse Fast Fourier Transform
ICI	Inter-Carrier Interference
IR	Incremental Redundancy
ISI	Inter-Symbol Interference
KPIs	Key Performance Indicators
LA	Link Adaptation
LTE	Long Term Evolution
MAC	Medium Access Control
MCS	Modulation and Coding Scheme
MIMO	Multiple Input Multiple Output
MRC	Maximal Ratio Combining
OFDM	Orthogonal Frequency Division Multiplexing
OFDMA	Orthogonal Frequency Division Multiple Access
OLLA	Outer Loop Link Adaptation
PAPR	Peak-To-Average Power Ratio
PF	Proportional Fair
PHY	PHYsical Layer
PS	Packet Scheduler
QAM	Quadrature Amplitude Modulation
QoS	Quality of Service
QPSK	Quadrature Phase Shift Keying
RLC	Radio Link Control
RB	Resource Block
RRM	Radio Resource Management

SFTD	Space-Frequency Transmit Diversity
SINR	Signal-to-Interference-plus-Noise Ratio
SISO	Single Input Single Output
SNR	Signal-to-Noise Ratio
TDD	Time Division Duplex
TTI	Transmission Time Interval
TU	Typical Urban
UDO	User Diversity Order
UE	User Equipment
UL	Uplink
UMTS	Universal Mobile Telecommunications System
VoIP	Voice Over Internet Protocol
WiMAX	Worldwide Interoperability for Microwave Access
WCDMA	Wideband Code Division Multiple Access

Mathematical Conventions

The following mathematical conventions are used throughout the thesis:

$\ddot{\mathbf{a}}, \ddot{\mathbf{A}}$	Bold upper or lower case with double dots indicates a matrix.
$\dot{\mathbf{a}}, \dot{\mathbf{A}}$	Bold upper or lower case with a dot indicates a vector.
$\mathbb{A}$	Blackboard bold upper case denotes a set.
a, A	Non-bold indicates a scalar.
$\left(\ddot{\mathbf{A}}\right)_{[:,1:4]}$	Indexing notation, *e.g.* the first to fourth columns of $\mathbf{A}$.
$(\dot{\mathbf{a}})_{[2]}$	Indexing notation, *e.g.* the second element of $\mathbf{a}$.
$\mathrm{Re}\left\{\,\cdot\,\right\}$	Real component of complex number.
$\lceil\cdot\rceil$	Rounding up to the nearest integer.
$\left\|\cdot\right\|$	Absolute.
$\mathrm{pr}\left(x\right)$	Probability density function of x.
$\mathrm{Pr}\left(x\right)$	Cumulative probability density function of x.
$\overline{x}$	Short notation for the mean of x.
$\mathrm{Var}\left\{x\right\}$	Variance of random variable x, $$\mathrm{Var}\left\{x\right\} = \mathrm{E}\left\{\left(x - \mathrm{E}\left\{x\right\}\right)^2\right\}.$$
$\mathrm{Std}\left\{x\right\}$	Standard deviation of random variable x, $$\mathrm{Std}\left\{x\right\} = \sqrt{\mathrm{Var}\left\{x\right\}}.$$

Contents

Chapter 1

Thesis Introduction

1.1 Trends in Adaptive Resource Allocation for Mobile Communication Systems

Link Adaptation (LA) and smart *packet scheduling* are the key spectral efficiency enhancement techniques associated with radio resource allocation in mobile communication systems [1]. LA refers to techniques employed at the Medium Access Control (MAC) layer with the purpose to improve throughput over the radio-link, e.g., Adaptive Modulation and Coding (AMC) and power control [2]. The Packet Scheduler (PS) is employed to regulate the sharing of radio resources between users over a shared data channel, and it is usually applied at the MAC layer.

Mobile communication systems are usually classified into generations to reflect the evolution in technology, operating bandwidth as well as in the service capability [3]. Figure 1.1 illustrates the cellular system generations, their capabilities, as well as a few examples of relevant wireless standards. The First Generation (1G) radio systems such as Advanced Mobile Phone Services (AMPS) employed analog communication techniques to transmit mainly voice over radio. These systems were deployed in the 1970s and 1980s [4] and are characterized as *narrowband* on the basis of transmission bandwidth. They supported only circuit switched (CS) transmission, implying that the packet scheduling functionality was not required. Further, they employed very basic LA functionality such as fixed modulation scheme, open loop power control, etc. Multiple access was based on Frequency Division Multiple Access (FDMA), where users are differentiated on the basis of the transmission frequency. Due to narrowband transmission and basic LA the data rate was limited to around 2 kbps [3].

The Second Generation (2G) mobile communication systems such as the Global System for Mobile Communication (GSM), IS-54, IS-95, ushered the digital communications era. GSM is the most popular wireless standard globally. It employs a mixture of FDMA and Time Division Multiple Access (TDMA) to facilitate multiple access. In TDMA non-overlapping time-slots are allocated to the users. In terms of LA, GSM employs advanced channel coding techniques that can be combined with source coding to improve the cell range [6], [7]. However, the packet scheduling functionality is not required as only CS transmission is supported. GSM is usually classified as a narrowband system with a transmission bandwidth in the order of 200 kHz [8], [9]. Apart from supporting voice communications GSM can also provide limited data rates, in the order of several tens of kilobits per second [10]. The 2G systems were built and deployed in the 1980s and 1990s.
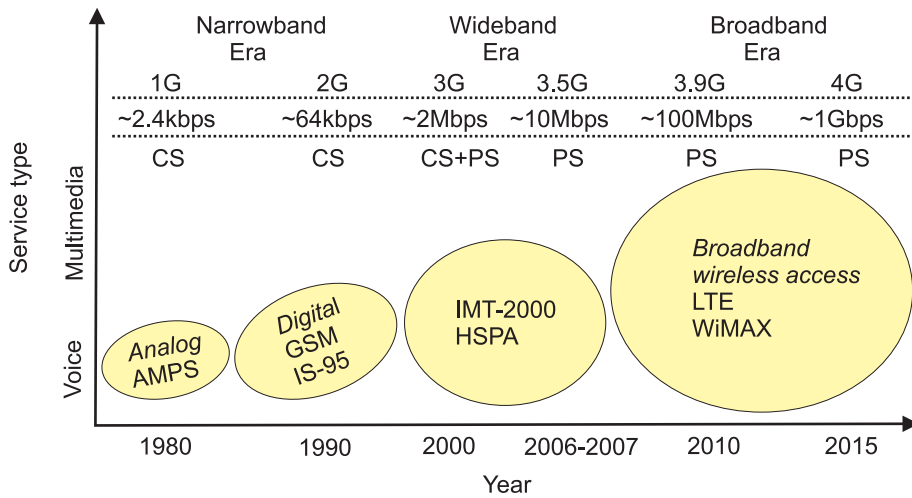
Figure 1.1: Evolution of cellular systems illustrating the shift in terms of service capability, from voice-only traffic in the past to multimedia services in the future. Note that all the wireless standards that constitute a particular wireless generation are not listed here. Further, PS denotes packet switching in the figure. It has been prepared by using material in [3], [5] and internal slides prepared by P. E. Mogensen.

Wideband Code Division Multiple Access (WCDMA) based radio networks whose specifications were developed by the 3rd Generation Partnership Project (3GPP) belong to the Third Generation (3G) of cellular systems [11]. It employs Code Division Multiple Access (CDMA), where users are differentiated on the basis of orthogonal spreading codes. WCDMA systems were launched in 2002 [1] and are classified as *wideband* systems with a transmission bandwidth of around 5 MHz. The first Release of WCDMA (Release-99) can provide data rates up to 2 Mb/s, 384 kb/s and 144 kb/s in Pico, Micro and Macro environments respectively [3]. WCDMA employs advanced LA techniques such as channel coding, variable spreading factor and closed-loop power control [1]. The aim of these features is to enable provision of multiple data rates with different reliability requirements. The PS entity was also introduced in WCDMA as it supports packet switching. The task of the PS functionality is to divide code and power resources between CS and packet switched services [1]. The PS entity is not located in close proximity of the radio channel, and as a result its decisions are updated at a slow rate, e.g., in the order of 100 ms to 1 s [12].

WCDMA evolution is denoted as High-Speed Packet Access (HSPA), and it is usually classified as 3.5 G. It consists of High-Speed Downlink Packet Access (HSDPA) and High-Speed Uplink Packet Access (HSUPA). Based on CDMA technology the first commercial HSDPA networks were available at the end of 2005, and the commercial HSUPA networks are expected to be available in 2007. The HSDPA peak data rate available in the terminals can potentially be beyond 10 Mbps, while the HSUPA peak data rate is expected to be in the order of 3-4 Mbps [2]. The LA functionality has been evolved to support advanced features such as AMC and physical layer Hybrid Automatic Repeat reQuest (HARQ). The PS entity has a significant role in HSPA, and it is located close to the radio channel, in the base station. Thus, it can operate at a fast rate, e.g., in HSDPA the scheduling decisions can be updated every 2 ms. Further, as the PS and LA entities are co-located in the base station, they can interact to improve utilization of radio resources [2].

In terms of switching technology radio systems are moving away from CS and towards the packet switching paradigm. Further, in terms of service capability modern wireless systems are primarily designed to support multimedia applications instead of just plain voice. Next generation of wireless systems are expected to support a wide range of high data rate multimedia applications,

with varying delay and reliability requirements. In order to meet the future demand for wireless broadband access 3GPP has launched the Study Item (SI) on the evolution of 3G and HSPA, termed as *Evolved Universal Terrestrial Radio Access (E-UTRA) and Evolved Universal Terrestrial Radio Access Network (E-UTRAN)* [13]. The purpose of the SI is to investigate technical solutions that can fulfill the performance targets of the Long Term Evolution (LTE) of Universal Mobile Telecommunications System (UMTS).

The commercial deployment of LTE (denotes E-UTRA & E-UTRAN henceforth) is expected to be around 2010. Long term goals for LTE include support for high peak data rates, 100 Mbps in the Downlink (DL) and 50 Mbps in the Uplink (UL), low latency (10 ms round-trip delay), improved system capacity and coverage, reduced operating costs, multi-antenna support, efficient support for packet data transmission, flexible bandwidth operations (up to 20 MHz) and seamless integration with existing systems [5]. LTE is usually referred to as 3.9 G and it will only support packet data transport over radio, which will require further refinements in LA and PS functionalities in comparison to HSPA. The most significant enhancement is expected to be the possibility to adapt transmission parameters in both time and frequency domains [14]. The thesis will primarily focus on the design of advanced LA and packet scheduling algorithms that can facilitate adaptation in time and frequency domains, within the framework of a modern cellular system such as LTE.

Fixed Worldwide Interoperability for Microwave Access (WiMAX) based on the IEEE 802.16-2004 Air Interface Standard is emerging as the key technology in the area of fixed broadband wireless metropolitan area networks [15]. It can support peak DL data rates up to 63 Mbps and peak UL data rates up to 28 Mbps in a 10 MHz channel. Mobile WiMAX, denoted as IEEE 802.16e, is an amendment to the original standard, and it can support mobility. WiMAX also supports scalable channel bandwidth from 1.25 MHz to 20 MHz. Further, smart antenna technologies such as beamforming and spatial multiplexing are also supported [15]. As LTE and WiMAX have several features in common, most of the findings of this study can be applied to WiMAX.

The Fourth Generation (4G) cellular systems are expected to support reliable transmissions with high peak data rates ranging from 100 Mbps for high-mobility applications to 1 Gbps for low-mobility applications. The spectrum efficiency is expected to be as high as 10 b/s/Hz in 20-100 MHz bandwidth [4], [16]. 4G is expected to be available around 2012-2015. Although we will not consider such a system explicitly in the analysis it is likely that some of the thesis findings can be applied to 4G systems.

1.2   Introduction to UTRAN LTE

With a view to maintain WCDMA competitiveness in the long-term future as well as to meet increasing user demands 3GPP has initiated the SI titled "Evolved UTRA and UTRAN" [13]. The aim of this SI is to propose technical solutions which can provide additional substantial leaps in terms of service provisioning and cost reduction over HSPA [17]. 3GPP has concluded on a set of targets and requirements for the LTE, which are enumerated in [18]. Important parts of such a long-term evolution include reduced latency, higher user data rates, improved system capacity and coverage, and reduced cost for the operator. In order to achieve this, an evolution of the radio interface as well as the radio network architecture is being considered.

One of the important requirements of LTE is spectrum flexibility, enabling deployment in many different spectrum allocations. Support for wide transmission bandwidth, up to 20 MHz,
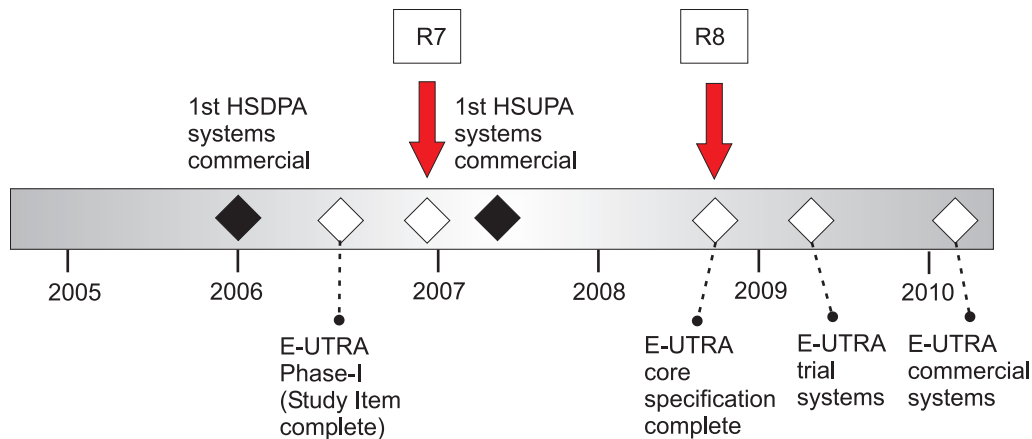
Figure 1.2: The E-UTRA standards timeline [5].

is envisaged in order to support the high data rates. At the same time support for much lower transmission bandwidths, less than 5 MHz, is also under investigation. The important targets for evolution of the UMTS radio-interface and radio-access network architecture are as follows [18]:

- Peak data rates exceeding 100 Mbps in the Downlink (DL) direction and 50 Mbps in the Uplink (UL) (in 20 MHz bandwidth).

- Improvement in average user throughput by factors of 2-3 and 3-4 in UL and DL respectively, over Release 6 HSDPA.

- Improvement in "cell edge bit rate" by a factor of 2-3 over Release 6 HSDPA, whilst maintaining the current inter-site distance.

- Significantly improved spectral efficiency, e.g., a factor of 3-4 times Release 6 HSDPA in a loaded network. Similarly the target for the UL is 2 to 3 times Release 6 Enhanced Uplink.

- Significantly reduced control-plane latency as well as user plane latency (10 ms round-trip delay [5]).

- Scalable bandwidth operation, i.e., 1.25, 2.5, 5, 10, 15 and 20 MHz.

- Reduced cost for operator and end user.

- Enhanced support for end-to-end QoS.

LTE will only support packet switching. Therefore, the overall goal is to develop an optimized packet based radio access system with high data rate and low latency. Examples of intended services include High Definition TeleVision (HDTV) broadcast, movies on demand, interactive gaming, and Voice Over Internet Protocol (VoIP) [5].

The E-UTRA standards timeline is shown in Figure 1.2. The first phase of the physical layer specification was completed in May 2006 with the conclusion that E-UTRA physical layer performance requirements are achievable. Complete specifications are then expected to be ready by the end of 2008. By 2009, trial E-UTRA systems are expected with commercial deployment by 2010 [5].

1.3 OFDM Transmission Technology for Wireless Broadband Communications

The wireless systems up to 3G are based on *single-carrier transmission* techniques. It is well known that the peak data rate of such a scheme is limited by the Inter-Symbol Interference (ISI) impairments that are experienced over a practical propagation channel [19]. As a result the provisioning of high date rates with reasonable reliability requires complex and expensive equalization at the receiver [20]. In order to overcome this limitation the research community has been focusing on *multi-carrier transmission* techniques. Here, the principle idea is to split the incoming high rate serial data stream into relatively low rate parallel streams, which modulate a group of orthogonal sub-carriers.

Among the contending multi-carrier transmission schemes Orthogonal Frequency Division Multiplexing (OFDM) has emerged as the strongest candidate for the provisioning of next generation wireless broadband communications in various standardization bodies, e.g., LTE, WiMAX and WLAN. It has been known since the sixties that OFDM can provide efficient high data rate communications over time-dispersive media, e.g., see [21], [22] and [23]. However, large scale production of OFDM transceivers at a feasible cost has only become possible in recent times. Apart from robustness against multipath the advantages of OFDM include inherent scalability in terms of bandwidth support, efficient modem implementation through the use of Fast Fourier Transform (FFT) and Inverse Fast Fourier Transform (IFFT), ease of combining with Multiple Input Multiple Output (MIMO) techniques, and flexibility in terms of *adaptive resource allocation* [23].

Figure 1.3 illustrates the time-frequency representation of an OFDM signal. The total system bandwidth is divided into a large number of spectrally overlapping, but mutually orthogonal non-frequency selective narrow-band sub-channels. ISI can be completely avoided by introducing an additional guard interval into each OFDM symbol [23], [25]. The purpose of the guard interval is to absorb all the ISI components prior to the start of the useful symbol. The time domain waveforms of the OFDM sub-carriers are orthogonal, yet the signal spectra corresponding to the different sub-carriers overlap in frequency, providing efficient utilization of the available
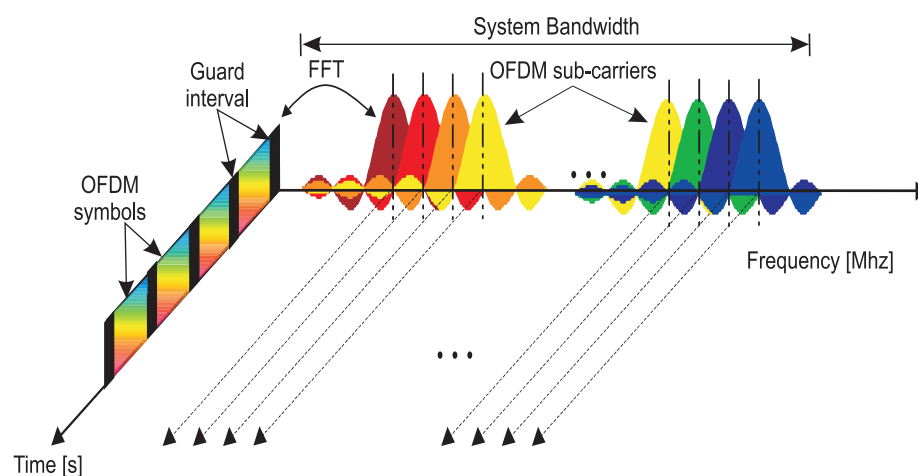
Figure 1.3: Time-frequency representation of an OFDM signal. Each OFDM symbol begins with a guard interval which is kept longer than the maximum excess delay experienced in the radio channel. At the receiver side the guard interval is discarded [24].
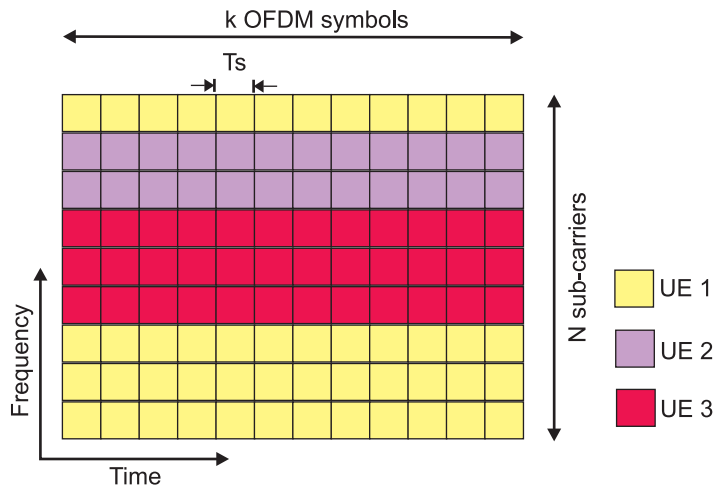
Figure 1.4: Illustration of the OFDMA multiple access scheme investigated in the thesis. It is based on block transmission (time-slotted), and the different UEs can be assigned flexibly to the sub-carriers. A single OFDM block consists of N sub-carriers transmitted over k OFDM symbols. T_s denotes the OFDM symbol duration.

bandwidth [4].

The main disadvantage of OFDM is the high Peak-To-Average Power Ratio (PAPR), due to multi-carrier transmission. As the amplitude of the time-domain signal is dependent on hundreds of sub-carriers, large signal peaks will occasionally reach the amplifier saturation region, resulting in non-linear distortion [4]. This will lead to both in-band and out-of-band emissions. PAPR can be reduced by e.g., use of data spreading techniques [25]. Further, OFDM is very sensitive to time and frequency synchronization errors [4]. Similarly, channel fading and narrowband co-channel interference can deteriorate the performance of OFDM. As a result channel coding (forward error correction) and interleaving are usually employed in conjunction with OFDM.

1.3.1   OFDMA Radio Access Scheme

In a multi-user scenario the system performance is highly dependent on the multiple access technique. As a result considerable research has been devoted to the investigation of a suitable access technique for the OFDM radio interface. The combination between the classical multiple access schemes TDMA, FDMA, CDMA and OFDM has been investigated in literature, e.g., in [26] and references therein. The performance of the schemes is compared in terms of flexibility with regard to data rate and radio channel adaptation, implementation complexity, signalling overhead and link-level performance. Studies show that the combination of OFDM and FDMA, denoted as Orthogonal Frequency Division Multiple Access (OFDMA), provides the best overall performance. It has also been selected for the DL of LTE [14].

Figure 1.4 illustrates the OFDMA scheme that is considered in the thesis. OFDM is a block modulation scheme [27], where a block of k information symbols are transmitted over N sub-carriers in parallel. Each of the N sub-carriers in Figure 1.4 is considered as a *time-frequency resource*. The figure illustrates possible user multiplexing scenario within a single OFDM block, where 3 UEs have been used as an example. Note that we do not consider the combination of TDMA and FDMA within a single OFDM block for complexity reasons. The OFDMA scheme

shown in Figure 1.4 has also been selected for the implementation of LTE [14].

It is clear that OFDMA supports adaptive resource allocation in the multi-user scenario. In principle, a fully flexible allocation of the sub-carriers to N users can be supported within a single OFDM block. However, sub-carrier level granularity in resource allocation is difficult to achieve in practice due to practical system constraints such as complexity. The objective of the thesis is to investigate the practical design of adaptive resource allocation algorithms for the OFDMA based air interface. Further, we will evaluate the gain potential of time-frequency domain adaptation over the simpler time-domain only adaptation (e.g., similar to HSDPA).

1.4 Recapitulation of Time-Domain Adaptation Techniques

In a real propagation environment the received radio signal strength experiences rapid fading, due to the presence of numerous scatterers along the transmission path. Further, the signal strength also changes with location. A typical example of the distribution of variation in signal envelope is Rayleigh fading, where the signal strength can easily vary by 5-10 dB [28]. Moreover, burst errors occur due to the correlated nature of channel fading. Such errors severely reduce the throughput at the higher-layer protocols such as TCP [29].

In order to provide reliable data communications over the fading radio channel the non-adaptive transmission scheme needs to be designed for the worst case channel conditions. For example, a more robust, but lower order modulation scheme will be employed in order to maintain an acceptable link-level performance when the channel quality is poor. This results in under utilization of the available channel capacity [30].

Adapting the transmission scheme to the signal fading on a fast basis allows for a more efficient use of the channel, as favorable channel conditions can be better exploited. As an example adjusting the modulation format according to the prevailing channel conditions has significant potential to improve the link-level throughput. Adaptive transmission was first proposed in the late 1960's [31]. Since then the topic has been widely researched, and a variety of adaptive schemes have been proposed that can exploit both narrowband and wideband fading behavior. Until recently time-domain adaptation was primarily in focus, as the 2G, 3G and 3.5G radio systems supported this adaptation mode. The basic idea behind adaptive transmission or LA is to maximize the link throughput under the given operating constraint, such as the Bit Error Rate (BER), total transmit power, data rate, etc.

The block diagram of the adaptive transmission scheme is illustrated in Figure 1.5, focusing on a single radio link. In a Frequency Division Duplex (FDD) system adaptive transmission requires feedback of the channel quality information [32]. The measurement of Channel State Information (CSI) is performed at the receiver, and it is fed back on the reverse control channel, e.g., in HSDPA periodic Channel Quality Information (CQI) reporting is supported with a time resolution of up to 2 ms [2]. The term CQI is used in 3GPP, and it denotes formatted CSI, e.g., in HSDPA it indicates the currently supported data rate estimated by the User Equipment (UE). We will use this term to denote CSI. Packet scheduling as well as adaptive modulation at the transmitter are based on the received CQI reports, e.g., in HSDPA the LA entity selects suitable number of DL orthogonal codes and a single Modulation and Coding Scheme (MCS) for each transmission [2]. Similarly, the PS dynamically allocates the shared data channel to a subset of UEs, on a fast basis.

In literature there are several flavors of time-domain adaptation algorithms in terms of which
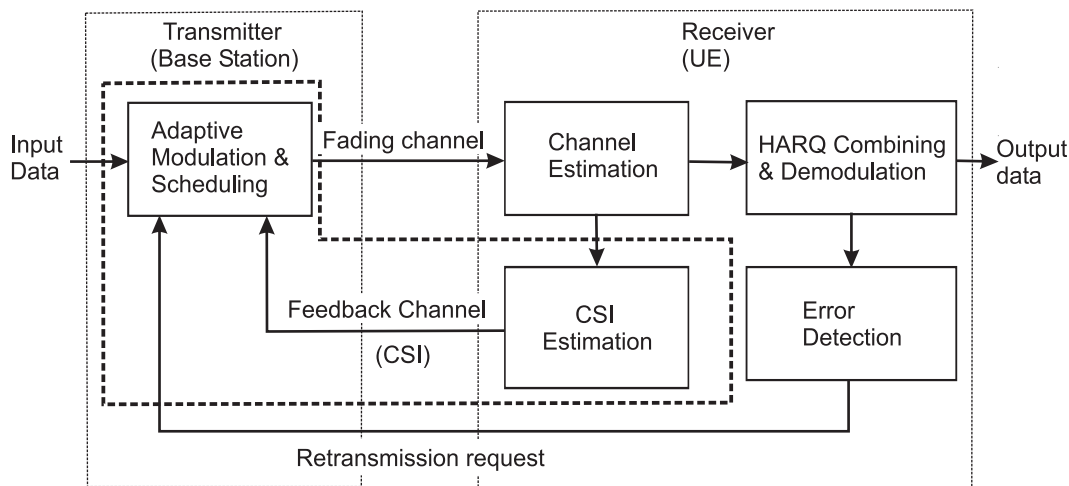
Figure 1.5: The block diagram illustrating the functional blocks of a general purpose adaptive transmission scheme, including HARQ combining and error detection. A single radio link has been shown for the sake of clarity.

parameters can be adjusted, e.g., transmit power level [31], symbol transmission rate [33], constellation size [34], coding rate/scheme [35], or any combination of these parameters [36]. It is reported that the adaptive schemes can provide high spectral efficiency by transmitting at high data rates under favorable channel conditions, while reducing the data rate as the fading becomes severe, e.g., see [30], [37], [38]. Apart from modern cellular systems adaptive transmission in time-domain has also been implemented in newer WLAN standards such as IEEE 802.11g [39].

1.5 Advanced Multi-Domain Adaptation and Packet Scheduling

The next generation wireless systems will be optimized for packet data transfer, e.g., LTE. In such a scenario the PS entity plays a key role in overall system performance. It is the network entity responsible for the allocation of system resources to users over the shared data channel [12]. The goal of the scheduler is to maximize spectral efficiency, while guaranteeing Quality of Service (QoS) [2]. The QoS requirements can vary from real-time conversational traffic, e.g., VoIP, characterized by stringent delay constraints, to best-effort traffic, e.g., email delivery and web browsing. The scheduler interacts with the LA functionality during the processing of the scheduling algorithm. The role of adaptive LA is to determine the optimal transport format that satisfies the reliability constraint, under fading channel conditions [12].

In a scenario where multiple users are sharing the same wireless media the PS can improve the spectral efficiency by utilizing the statistical behavior of the radio channel as well as that of traffic arrival [16]. The scheduler requires a priori knowledge of the prevailing channel conditions, in order to facilitate channel-aware scheduling. The aim is to exploit the available time, frequency, space and multi-user diversities in the system to improve spectral efficiency. For example, the scheduler can utilize *time diversity* by deferring the transmission on the radio links that are in a deep fade until the link quality recovers. *Multi-user diversity* exploits the independent channel fading statistics experienced by different users within the same coverage area. Similarly, *frequency diversity* refers to the uncorrelated fading statistics experienced on frequencies that are separated widely enough, and *space diversity* refers to the uncorrelated signals generated by a transmit or

receive antenna array when the spacing of the antennas has been selected carefully [28].

Packet scheduling for wireless systems has been investigated extensively in literature and several algorithms have been proposed. It was first applied to CDMA systems, e.g., in [40], [41] and [42] the authors have proposed channel-aware *opportunistic scheduling* schemes for the CDMA/High-Data-Rate (HDR) system. The term "opportunistic" implies that the scheduler picks those users for transmission that are experiencing fading peaks. In [29] the author has performed a detailed performance evaluation of the well known scheduling algorithms within the HSDPA framework. Schedulers are broadly classified in terms of the degree of fairness in distribution of throughput among the served users. Further, they are also classified on the basis of the rate at which the scheduling decision is updated. In the latter case scheduling policies are grouped into either *fast scheduling* or *slow scheduling* methods, depending on whether the scheduler can track instantaneous channel conditions. Table 1.1 lists the classification of scheduling algorithms with examples from literature. In general, the fast schedulers are located close to the radio channel and require frequent channel quality reports. In this study, the investigation will focus on fast packet scheduling techniques with different degrees of fairness.

In CDMA systems such as HSDPA the PS can benefit from the available time, multi-user and spatial diversities. Studies based on HSDPA have shown that channel aware opportunistic scheduling such as Proportional Fair (PF) in time-domain can provide a capacity gain of around 35% over the simple RR scheduler, which does not take channel conditions into consideration [2]. Thus, multi-domain scheduling is known to provide a significant gain potential in modern wireless packet data systems.

The OFDMA based wideband system makes another dimension available for the application of scheduling, namely the frequency domain. Figure 1.6 illustrates a snapshot of a typical wideband radio channel fading behavior, resolved in both time and frequency domains. It can be seen that the OFDM sub-carriers experience diverse fading conditions in both time and frequency domains. This, a suitably designed scheduler will have additional degrees of freedom, e.g., it can choose to allocate only good sub-carriers with a high Signal-to-Interference-plus-Noise Ratio (SINR) to each user. Furthermore, the number of sub-carriers for a specific user can be adjusted according to the required data rate, i.e., fine granularity for resource allocation is available with OFDMA [16]. Similarly, in terms of LA the link throughput can be enhanced by avoiding transmission on the sub-carriers that are experiencing deep fades.

Additionally, frequency-domain scheduling can improve the service provisioning of delay critical services such as VoIP, by limiting the delay in packet transmission that would normally be incurred if the system could only rely on time diversity. A similar advantage is foreseen for the case of static users, as the scheduler cannot rely on the limited time diversity to ensure adequate

Table 1.1: Classification of the packet scheduling algorithms applied to wireless systems, based on [29]. Note that this list only includes well known schedulers from literature.

Scheduling rate	Throughput fairness		
	Low	*Medium*	*High*
Slow (update rate in s)	C/I based	Round Robin (RR)	Fair throughput
Fast (update rate in ms)	Max. C/I	Proportional Fair (PF)	Fast fair throughput
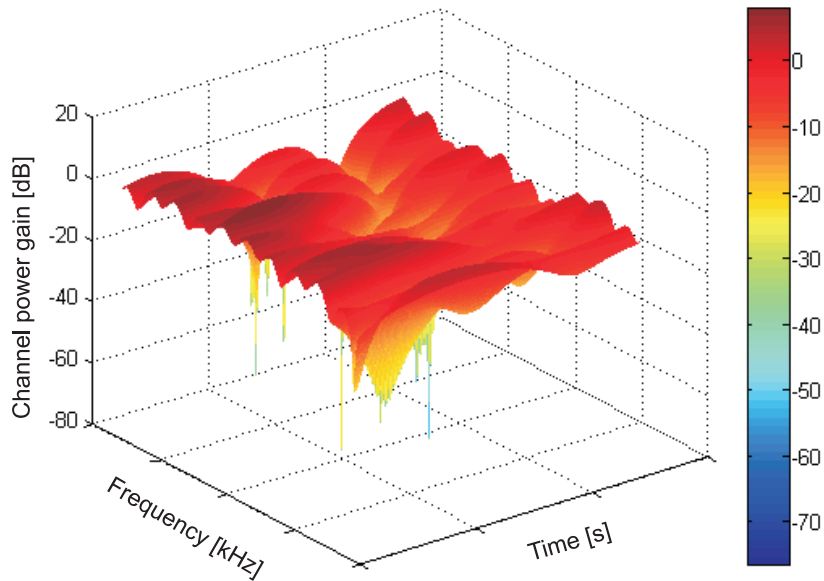
Figure 1.6: Time and frequency selective attenuation observed in a wideband radio channel. The ITU Ped. B channel profile [43] has been employed here.

system performance. In this study we will perform a detailed investigation of the performance of adaptation and scheduling in the frequency-domain, denoted as Frequency-Domain Adaptation and Scheduling (FDAS). Note that time and spatial diversities which are inherently present in the OFDMA system are also included in the FDAS concept.

MIMO techniques can significantly boost spectral efficiency without requiring additional power or bandwidth. However, processing complexity is increased at both the transmitter and the receiver [44]. A MIMO system takes advantage of the spatial diversity obtained by spatially separated antennas in a dense multipath scattering environment. MIMO systems can be implemented in a number of different ways, to obtain either a diversity gain or to obtain a capacity gain (spatial multiplexing) [4]. Recent developments in MIMO techniques promise a significant boost to the performance of OFDM systems [27]. Further, due to the relatively inexpensive frequency-domain equalization required for an OFDM signal a low complexity receiver implementation together with MIMO is feasible. Besides their robust performance over wireless media OFDM and MIMO are particularly suitable for adaptive resource allocation as they can provide orthogonal sub-channels in the frequency as well as in the spatial domains [16]. Preliminary studies on the potential of adaptive multi-user OFDM-MIMO in a practical cellular system scenario have shown significant potential, e.g., cell throughput gain in the order of 20%-30% has been reported in [45]. It is widely believed that the combination of MIMO and OFDM will be required to meet the data rate and spectral efficiency targets of 4G [4]. In this study we will only investigate the potential of spatial diversity together with FDAS, and spatial multiplexing will not be considered.

It appears that multi-domain adaptation and scheduling has the potential to improve the spectral efficiency. However, it requires extra complexity at the transmitter, as well as extra signaling overhead in both DL and UL. A major concern is the UL signaling overhead, which can be pro-

hibitively large in a wideband OFDM FDD[1] system. FDAS requires feedback of fairly detailed CQI reports with a fine granularity, in order to enable fast adaptation across multiple domains. Further, additional DL control overhead is required to convey the resource allocation information to the scheduled users. The amount of DL control overhead is dependent on the number of users multiplexed in frequency as well as on the allowed LA flexibility, i.e., number of transmit parameters that can be adjusted [2]. In general, the complexity of FDAS algorithms is high as throughput optimization is performed across multiple domains. This usually requires an exhaustive search over all possible combinations of transmit parameters.

1.6   Thesis Scope and Objectives

The aim of this research project is to investigate the potential of FDAS within a modern cellular system framework employing full frequency reuse. It is assumed that the multiple access is based on the OFDMA scheme with FDD being the duplexing mode. In contrast to previous mostly link-level studies, the aim here is to investigate the system-level performance of the FDAS schemes. The Key Performance Indicators (KPIs) of the system-level analysis are average cell throughput, average user throughput (dependent on location) and coverage. In order to make the study realistic we have employed the LTE framework and design guidelines in the analysis [14].

Research is mainly directed at the design and analysis of multi-domain adaptation and scheduling algorithms, taking into account interaction with features such as HARQ and antenna diversity that are present in a modern wireless system. The design of other Radio Resource Management (RRM) related functionalities, e.g., load control, handover control [2], required for efficient utilization of radio resources is not covered in the thesis. In terms of link-level performance we assume that ideal OFDM link-level performance is available, e.g., ISI imperfections are avoided by using a suitably designed guard interval. We also assume *ideal channel estimation*. The system-level performance evaluation is based on the *uni-cast* packet data transmission on the DL shared data channel of a multi-user radio access system.

We have investigated two general FDAS scenarios, single-user time-domain only channel-aware scheduling, denoted as Frequency-Domain Link Adaptation (FDLA), and multi-user channel-aware scheduling in time and frequency domains. The latter case is referred to as Frequency-Domain Packet Scheduling (FDPS). The single-user per transmission interval scenario (denoted as FDLA) has been used mainly to investigate the potential of frequency-domain LA techniques [46], while the multi-user case allows user multiplexing in the frequency-domain. The FDAS concept encompasses packet scheduling, LA based on bandwidth and/or power adaptation, AMC, HARQ, and transmit and/or receive antenna diversity, as shown in Figure 1.7. Further, fast adaptation and scheduling is assumed, e.g., time resolution of FDAS processing is in the order of 0.5 ms-1.0 ms. Note that smart antenna techniques such as beamforming as well as advanced MIMO techniques based on spatial multiplexing are outside the scope of this study.

The traffic model has a significant impact on scheduler performance, e.g., see [29]. We have used the simple *best-effort* traffic model in the analysis, which is also recommended by LTE [14]. Further, two variants of this traffic model have been employed. The *infinite buffer* best-effort traffic model is characterized by equal session time for all users, irrespective of their location in the cell [47], while the *finite buffer* model ensures that each user downloads an equal amount of data before

---

[1]In a Time Division Duplex (TDD) system the signaling overhead for channel quality feedback is not an issue due to the use of a common frequency in both UL and DL.
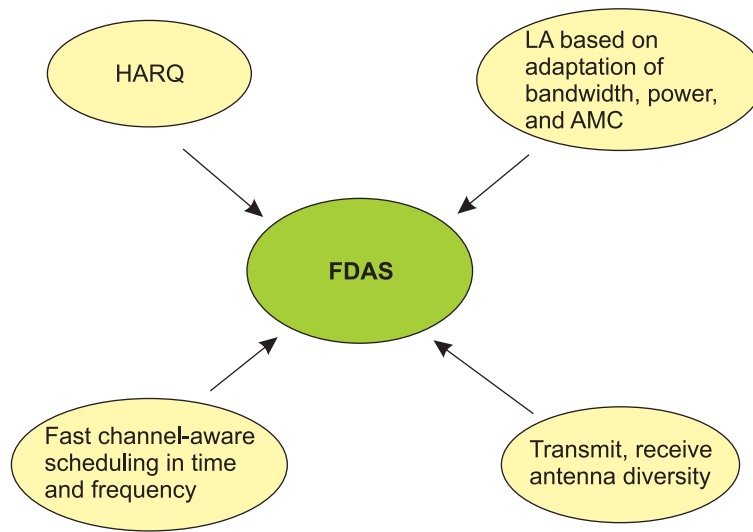
Figure 1.7: Key spectral efficiency enhancement mechanisms that are a part of the FDAS concept. These techniques are applied to the DL shared packet data channel of an OFDMA based wireless broadband system, e.g., 3GPP LTE.

exiting the system [48]. The best effort type of service was selected for the preliminary analysis of FDAS potential in order to avoid the additional restrictions imposed by the higher layer protocols. The KPIs are based on received throughput at the MAC layer, and packet delay characteristics are not considered in the evaluation.

The main objectives of the thesis are summarized below:

- Design of LA algorithms for an OFDMA system that can exploit the frequency-selective fading experienced in a wideband radio channel, including interaction with HARQ. This will be followed by detailed system-level performance evaluation of the proposed LA algorithms, based on a variety of operating scenarios. The evaluation will consider two typical cellular deployment scenarios, as well as different time-dispersive channel profiles, receiver types and mobility. Further, two variants of the best-effort traffic model will be employed. The overall goal of this investigation is to determine whether frequency-domain LA can provide sufficient gain over the simpler time-domain LA, at the system level. We will also make recommendations on suitable algorithms for practical implementation.

- Next, the design of multiuser scheduling algorithms that facilitate channel-aware packet scheduling will be investigated. A framework will be proposed for the scheduler, which will include the interaction with LA and HARQ. The trade-off between capacity and coverage will be evaluated for different scheduling policies. The system-level evaluation of the proposed PS schemes will be carried out under a variety of operating conditions, as listed in the previous bullet point. The overall aim of this study is to determine the gain potential of advanced frequency-domain scheduling over the simpler time-domain only scheduling technique.

- Finally, the design of low bandwidth CQI reporting schemes enabling FDAS operation will be investigated. This is one of the key areas of research, and it will determine whether it is feasible to implement FDAS in practice. A detailed system-level evaluation of the trade-off between UL signaling overhead and the achievable FDAS gain in DL will be performed.

Recommendations will be made on suitable CQI reporting schemes for practical implementation.

1.7   Scientific Methods Employed

A system-level study of a modern cellular system usually involves computer simulations based on a complex system model, as also recommended by LTE [14]. Analytical evaluation at the system-level is usually mathematically intractable as the system performance is dependent on a large number of parameters whose behavior cannot always be predicted beforehand. Consequently closed form analytical expressions characterizing system performance are seldom available. The majority of the results presented in this thesis have been obtained through extensive computer simulations using the system models that have been developed during the course of this project. A limited amount of analytical work has also been performed, mainly to determine the bounds of FDAS gain potential under ideal conditions. The evaluation of FDAS has been divided into two parts, based on the complexity of the system model.

The first part of the FDAS evaluation utilizes a simplified single-cell based system model. Here, only the most relevant parts of the system are implemented in detail. Among the simplifications introduced are model based implementation of features such as AMC, HARQ and link-to-system performance mapping [14]. Further, other-cell interference is assumed to be Additive White Gaussian Noise (AWGN). The PS and LA functionalities are implemented in detail, together with CQI measurement inaccuracies and reporting/processing delays. A detailed investigation of FDAS algorithm design, as well as the potential of the available adaptation mechanisms has been performed using the simplified model.

The modeling simplifications were motivated by two factors. Firstly, at the beginning of the study there was little information available about the system-level assumptions such as control channel overhead, scheduling resolution/flexibility, link-to-system performance mapping, etc. As a result it was not feasible to develop a complex multi-cell based system model that was generic enough for long-term use. Secondly, in order to facilitate algorithm development and testing a model that was relatively easy to program, and had a reasonable execution time was required. A thorough evaluation of the FDAS potential based on a variety of operating scenarios such as different system bandwidths, multipath channel models, speeds, cellular deployment scenarios, etc., using a multi-cell system model was not feasible within the time-frame of the project. Thus, the simplified single-cell model was used at the beginning to investigate whether FDAS could provide sufficient gain potential over time-domain only scheduling and adaptation. Further, the evaluation was used to short-list candidate FDAS algorithms for further analysis.

In the final part of the thesis the FDAS potential is evaluated using a state-of-the-art multi-cell *system simulator*. This model was developed in co-operation with other colleagues in Nokia, and the research group. The cellular deployment as well as the modeling assumptions are based on the latest 3GPP recommendations, given in [14] and [49]. This model includes detailed implementation of LA based on real AMC, explicit scheduling of HARQ processes including retransmissions, link-to-system mapping technique suitable for OFDM and dynamic other-cell interference. The aim is to obtain accurate estimates of the FDAS gain potential at the system-level, as well as to recommend suitable algorithms for practical implementation. Additionally, we will investigate FDAS performance under the Fractional Load (FL) scenario, i.e., when the system is not operating at full load. It should be noted that the multi-cell system model utilizes a static UE mobility model, i.e.,

a fully dynamic multi-cell network simulator has not been implemented in this study.

1.8   Novelty and Contributions

The main contribution of this study is the system-level performance evaluation of FDAS, within the context of an OFDMA based wireless broadband cellular system. The study provides realistic estimates of the FDAS gain potential over time-domain only scheduling and adaptation. The analysis is based on recommendations taken from the ongoing standardization activities within LTE [14]. Unlike most previous studies we have investigated the interaction of resource allocation schemes with throughput enhancement features such as HARQ and spatial diversity.

There are theoretical studies in open literature which provide useful insight into the design of adaptation algorithms for OFDMA, e.g., [50], [51], [52]. They provide optimal as well as sub-optimal solutions for sub-carrier based resource allocation. The performance evaluation is usually based on ideal assumptions such as perfect channel coding performance, adaptive power allocation with infinite granularity and perfect knowledge of channel quality at the transmitter. These studies can at best provide the upper bound throughput performance of adaptive resource allocation under idealized assumptions.

The majority of the published studies are confined to link-level performance analysis of the adaptive schemes. The typical approach has been to report performance improvement in terms of Signal-to-Noise Ratio (SNR), at a selected BER level. However, it is not clear whether the link-level performance improvement that has been shown over a limited range of SNR values can translate into a tangible gain at the system-level.

The design of the reference scheme in most of the previous studies has not been optimized, e.g., non-adaptive transmission is mostly assumed. Thus, the gain from adaptation can be quite significant. In comparison, the reference scheme used here can exploit both fast adaptation and opportunistic scheduling in the time-domain. Thus, a fair comparison of techniques has been made in this study. Further, we have employed sub-band based resource allocation in this study in order to limit the UL signaling overhead as well as the complexity of the scheduling algorithm. Thus, the proposed FDAS algorithms are suitable for practical implementation.

The first topic of research in this study is the design and analysis of LA algorithms for an OFDMA based system. Here we have investigated in detail the potential of available adaptation mechanisms, e.g., adaptive bandwidth allocation, joint bandwidth and power allocation. Performance has been investigated under different user speeds, deployment scenarios, system bandwidths, channel profiles, and antenna schemes. Further, we have included CQI measurement inaccuracies as well as interaction with HARQ in the analysis. Based on a thorough system-level analysis using computer simulations we have made recommendations on suitable LA algorithms for practical implementation. The following article has been published based on the findings of this study:

- A. Pokhariyal, T. E. Kolding, F. Frederiksen, P. Olives, T. B. Sørensen and P. E. Mogensen, "Investigation of Frequency-Domain Link Adaptation for a 5-MHz OFDMA/HSDPA System," *Proceedings of the IEEE Vehicular Technology Conference (VTC)*, vol. 3, pp. 1463-1467, Stockholm, Sweden, May, 2005.

Next, we investigate the potential of PS algorithms that can exploit multi-user diversity in both time and frequency domains. Here, we have proposed a scheduling framework to manage time and frequency channel-aware scheduling under the constraints imposed by HARQ. Further, frequency-domain extension of legacy time-domain PS algorithms has been performed. Different combinations of time and frequency domain scheduling algorithms have been considered, which provide a trade-off between throughput and fairness. The inter-working of PS, LA and HARQ entities has been investigated in detail.

The performance of the schedulers is reported at the cell-level as well as at the user-level. The impact of CQI measurement errors, Frequency Domain Multiplexing (FDM) order, User Diversity Order (UDO), spatial diversity, mobility and fairness constraints has been analyzed based on a state-of-the-art simulation platform. The following articles related to FDPS have been published:

- A. Pokhariyal, T. E. Kolding and P. E. Mogensen, "Performance of Downlink Frequency Domain Packet Scheduling for the UTRAN Long Term Evolution," *Proceedings of the IEEE Personal Indoor and Mobile Radio Communications Conference (PIMRC)*, pp. 1-5, Helsinki, Finland, September, 2006.

- T. Kashima, M. Rinne, T. Roman, S. Visuri, S. Jarot, J. Kahtava, A. Pokhariyal, T. E. Kolding and O. Tirkkonen , "Design of channel structures for the Evolved UTRA downlink," *Proceedings of the Japan Society for Simulation Technology Mobile Communications Working Group Workshop JSST-MM 2006*, Evolved UTRA Special Session, pp. 11-17, Tokyo, Japan, October, 2006.

- A. Pokhariyal, K. I. Pedersen, G. Monghal, I. Z. Kovacs, C. Rosa, T. E. Kolding and P. E. Mogensen, "HARQ Aware Frequency Domain Packet Scheduler with Different Degrees of Fairness for the UTRAN Long Term Evolution", *Proceedings of the IEEE Vehicular Technology Conference (VTC)*, pp. 2761-2765, Dublin, Ireland, April, 2007.

- A. Pokhariyal, G. Monghal, K. I. Pedersen, P. E. Mogensen, I. Z. Kovacs, C. Rosa and T. E. Kolding, "Frequency Domain Packet Scheduling Under Fractional Load for the UTRAN LTE Downlink," *Proceedings of the IEEE Vehicular Technology Conference (VTC)*, pp. 699-703, Dublin, Ireland, April, 2007.

- W. Na, A. Pokhariyal, T. B. Sørensen, T. E. Kolding, P. E. Mogensen, "Performance of MIMO with Frequency Domain Packet Scheduling in UTRAN LTE downlink," *Proceedings of the IEEE Vehicular Technology Conference (VTC)*, pp. 1177-1181, Dublin, Ireland, April, 2007.

- P. E. Mogensen, W. Na, I. Z. Kovacs, F. Frederiksen, A. Pokhariyal, K. I. Pedersen, T. E. Kolding, K. Hugl and M. Kuusela, "LTE Capacity compared to the Shannon Bound," *Proceedings of the IEEE Vehicular Technology Conference (VTC)*, pp. 1234-1238, Dublin, Ireland, April, 2007.

The results of the PS study were also presented in the following 3GPP contributions:

- 3GPP, R1-060188, "Frequency-domain user-multiplexing for the E-UTRAN downlink - Nokia," TSG RAN WG1 LTE Ad Hoc Meeting, Helsinki, Finland, January, 2006.

- 3GPP, R1-071960, "LTE Performance Benchmarking - Nokia & Nokia-Siemens-Networks," TSG RAN WG1 LTE Ad Hoc Meeting, April, 2007.

Lastly, we have investigated the design of low bandwidth CQI reporting schemes enabling FDAS operation. This is an important research topic as the performance of FDAS is highly dependent on the accuracy of the CQI reports. In practice, the channel-quality feedback needs to be minimized as bandwidth is a scarce and expensive resource. Thus, additional constraints are imposed on the system in the form of CQI measurement inaccuracies, quantization and delay. Further, as it is not practical to feedback the channel quality pertaining to each time-frequency resource independently, low bandwidth CQI schemes have to be designed. In this regard we have proposed a *Threshold-based* CQI scheme which provides an attractive trade-off between UL signaling overhead and performance in the DL. Additionally, we have investigated FDAS potential with reduced CQI reporting rate, as well as evaluated the impact of time-domain averaging on the CQI estimation accuracy. Further, known CQI schemes with potential have also been included in the analysis. The following articles have been published based on the findings of the CQI study:

- T. E. Kolding, A. Pokhariyal, N. Wei and P. E. Mogensen, "Impact of Channel Quality Signaling on Frequency-Domain Link Adaptation Performance," *Proceedings of the Wireless Personal Multimedia Communications (WPMC) Symposium*, pp. 932-936, Aalborg, Denmark, September, 2005.

- T. E. Kolding, F. Frederiksen and A. Pokhariyal, "Low-Bandwidth Channel Quality Indication for OFDMA Frequency Domain Packet Scheduling," *Proceedings of the International Symposium on Wireless Communication Systems (ISWCS)*, Valencia, Spain, September, 2006.

- W. Na, A. Pokhariyal, T. B. Sørensen, T. E. Kolding and P. E. Mogensen, "Mitigating Signalling Requirements for MIMO with Frequency Domain Packet Scheduling," *Proceedings of the IEEE Vehicular Technology Conference (VTC)*, pp. 2771-2775, Dublin, Ireland, April, 2007.

- K. I. Pedersen, G. Monghal, I. Z. Kovacs, T. E. Kolding, A. Pokhariyal, F. Frederiksen and P. E. Mogensen, "Frequency Domain Scheduling for OFDMA with Limited and Noisy Channel Feedback," *Accepted for publication in the IEEE Vehicular Technology Conference (VTC)*, Baltimore, USA, October, 2007.

- I. Z. Kovacs, K. I. Pedersen, T. E. Kolding, A. Pokhariyal and M. Kuusela, "Effects of Non-Ideal Channel Feedback on Dual-Stream MIMO-OFDMA System Performance," *Accepted for publication in the IEEE Vehicular Technology Conference (VTC)*, Baltimore, USA, October, 2007.

In addition to the above mentioned topics a detailed OFDM link-level simulator was also developed during the course of the project. The tool is based on LTE recommendations [14] and was developed in co-operation with other PhD students in the research group. The single-cell based system model utilizes link-level traces obtained from the link simulator. The following article has been published based on the link-level study:

- N. Wei, A. Pokhariyal, C. Rom, B. E. Priyanto, F. Frederiksen, C. Rosa, T. B. Sørensen, T. E. Kolding and P. E. Mogensen, "Baseline E-UTRA Downlink Spectral Efficiency Evaluation," *Proceedings of the IEEE Vehicular Technology Conference (VTC)*, pp. 1-5, Montreal, Canada, September, 2005.

The following article on system-simulator speed optimization has been published, based on collaborative work with colleagues in the research group:

- G. Monghal, I. Z. Kovacs, A. Pokhariyal, K. I. Pedersen, C. Rosa and P. E. Mogensen, "Fast Fading Implementation Optimization in an OFDMA System Simulator," *Proceedings of the IEEE Vehicular Technology Conference (VTC)*, pp. 1214-1218, Dublin, Ireland, April, 2007.

The following provisional patent applications have been filed based on the findings of this study:

- F. Frederiksen, T. E. Kolding, P. E. Mogensen and A. Pokhariyal, "Mapping Strategy for OFDM-Based Systems Using H-ARQ", United States Provisional Patent Application, January, 2005.

- K. I. Pedersen and A. Pokhariyal, "Apparatus, Method and Computer Program Product Providing HARQ-Aware Packet Schedule", United States Provisional Patent Application, August, 2006.

- K. I. Pedersen, P. E. Mogensen, G. Monghal and A. Pokhariyal, "Frequency-Domain Packet Scheduling under Fractional Load", United States Provisional Patent Application, United States Provisional Patent Application, April, 2007.

1.9   Thesis Outline

The structure of the thesis reflects the progression of the research project. It is divided into nine chapters in the main part, and four appendix chapters. A brief description of the different chapters is provided below:

- Chapter 1: *Thesis Introduction* - It provides background information as well as the state-of-the-art on the main topics of the research project. Further, the goals of the project as well as the scientific methods employed are also outlined in this chapter.

- Chapter 2: *UTRAN LTE System Model* - This chapter introduces the general system model applicable to this study. It describes the relevant network nodes as well as the protocol layers. Further, it provides a general description of the LA, PS, HARQ and cross-layer resource allocation concepts. It also provides the description of the single-cell based system model that is used in the initial evaluation of FDAS.

- Chapter 3: *Frequency Domain Adaptation and Scheduling: Concept and Algorithm Design* - This chapter provides a detailed description of the FDAS concept as well as the associated terms. Further, it covers FDAS algorithm design aspects including the reference scheme. The design of low bandwidth CQI schemes enabling FDAS is also described here.

- Chapter 4: *Evaluation of Frequency-Domain Link Adaptation Based on the Single-Cell Model* - This chapter covers the performance evaluation of Frequency-Domain Link Adaptation, which refers to bandwidth, power and data rate optimization in the frequency domain, for the single-user per transmission interval scenario. The LA algorithms are evaluated based on a variety of operating conditions and include the impact of mobility, time-domain scheduling policy, and CQI measurement inaccuracies.

- Chapter 5: *Analysis of Frequency-Domain Packet Scheduling* - This chapter describes the performance evaluation of packet scheduling algorithms that can exploit multi-user diversity in both time and frequency domains. The detailed performance evaluation includes the impact of scheduling resolution in frequency, CQI measurement inaccuracies, mobility, and traffic model on the gain potential of multi-domain packet scheduling.

- Chapter 6: *Evaluation of the Low Bandwidth CQI Schemes Enabling FDAS* - This chapter covers the optimization of low bandwidth CQI schemes individually for the single-user (FDLA) and multi-user (FDPS) scenarios. Further, the gain potential of proposed LA and PS schemes based on limited and noisy channel quality feedback is evaluated.

- Chapter 7: *Practical FDAS Algorithm Design* - This chapter introduces the advanced multi-cell based system simulator. Further, the modifications to the proposed LA and PS algorithms in order to include practical aspects such as real AMC, HARQ retransmissions are described here.

- Chapter 8: *System Simulator Based Evaluation of the FDAS Potential* - This chapter covers the detailed evaluation of selected FDAS schemes based on the multi-cell system simulator. Further, the comparison of performance between the two system models is also presented here.

- Chapter 9: *Overall Conclusions and Recommendations* - The final chapter provides a summary of the overall study. Further, recommendations on suitable algorithms covering the three main areas of the study are provided. The estimates of FDAS gain potential for a set of reference simulation scenarios are also presented.

The following appendix chapters have been provided to support the work outlined in the main part of the thesis:

- Appendix A: *OFDM Link-Level Model: Description and Performance Analysis* - This chapter covers the description and validation of the detailed OFDM link-level model developed during the course of this project. The tool was used to evaluate the OFDM link-level performance. Further, detailed link-level traces were generated by using this tool and employed in the simplified single-cell system model.

- Appendix B: *Verification of the EESM Link-To-System Performance Mapping Model* - This chapter describes the verification of the employed link-to-system performance mapping technique.

- Appendix C: *Low Bandwidth CQI Schemes Enabling FDAS: Supplementary Results* - This chapter provides supplementary results for Chapter 6, covering the evaluation of low bandwidth CQI schemes enabling FDAS.

- Appendix D: *Statistical Significance Assessment* - In this chapter we provide an analysis of the statistical significance of key performance indicators, for a number of important simulation scenarios taken from the study.

Chapter 2

UTRAN LTE System Model

2.1 Introduction

In this chapter we will introduce the general system framework as well as the role of PS, LA and HARQ functionalities. Further the single-cell based system model is also described here. The chapter is organized as follows: Section 2.2 introduces the general system model, highlighting the location of the important RRM related functionalities as well as the relevant control channels. Section 2.3 describes the E-UTRAN user plane protocol architecture, while Section 2.4 introduces the cross-layer resource allocation concept. Section 2.5 presents a general description of the LA functionality, as well as discusses the modeling of AMC. Section 2.6 provides a description of HARQ and its modeling, while Section 2.7 presents the packet scheduling concept. The remaining sections of the chapter are devoted to the modeling aspects of the system-level model.

2.2 System Model for the Investigation of Downlink Packet Scheduling

The generalized system model for the investigation of DL packet scheduling in a cellular packet data system such as LTE is illustrated in Figure 2.1. For the sake of clarity only a single site within the multi-site deployment is shown in detail. There are three sectors at each site, based on 3GPP assumptions, and it is assumed that a hexagonal coverage pattern is generated by the overlapping beams of the sectorized antennas. The base station denoted as E-UTRAN Node B (eNode-B) establishes radio links with a number of UEs within its coverage area. We focus on the performance of the shared data channel, denoted as Downlink Shared Channel (DL-SCH), between the eNode-B and the UEs. The dynamic resource allocation at each sector/cell is managed by the following functional entities: PS, LA, and HARQ. They are located at the eNode-B in order to support fast channel-aware adaptation and scheduling [53].

Before transmission on the DL-SCH can begin several control channels are required to be set up in both DL and UL directions, as shown in Figure 2.1. The UL control channel is used to transmit HARQ Ack/Nack information as well as CQI reports to the eNode-B. The definition of CQI is provided in Section 2.4.1. In order to support FDAS frequency-selective CQI reports are required at the eNode-B, i.e., CQI is estimated and reported on a time-frequency resource

19
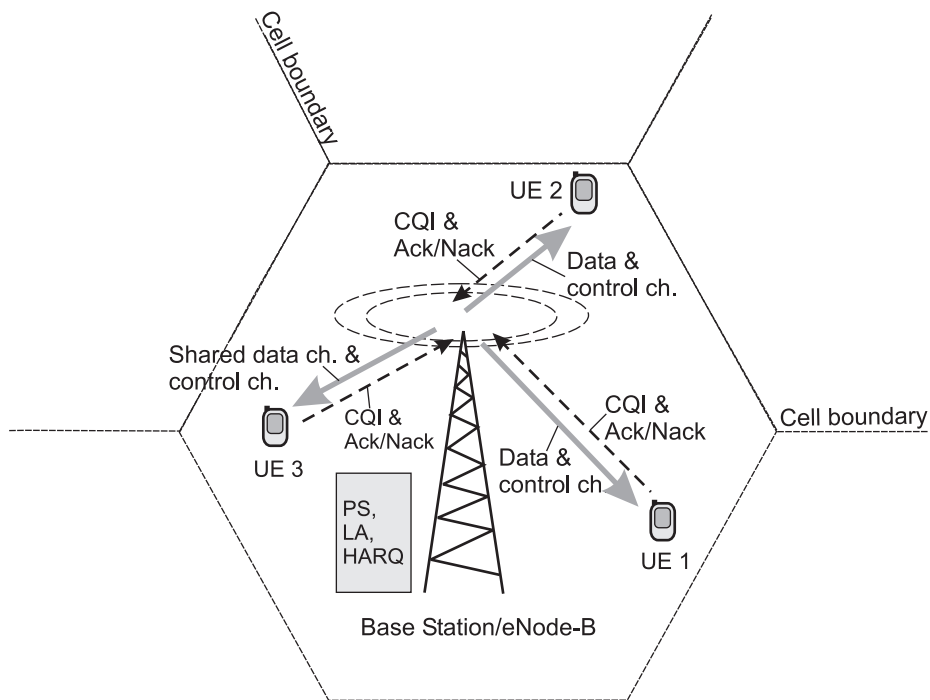
Figure 2.1: Generalized system model for the investigation of packet scheduling in the downlink of a cellular system such as LTE. The DL shared data channel and the DL & UL control channels between one eNode-B and a number of UEs are shown. For the sake of clarity only a single site within the multi-site deployment is illustrated.

basis. The frequency-selective CQI reports are used in the processing of LA and PS decisions. The DL control channel is required to transmit the *allocation table* (AT), which notifies the UEs of incoming transmissions as well as contains information required for correct decoding of the packets, e.g., MCS format, HARQ process identification, [14].

2.3   E-UTRAN User Plane Protocol Architecture

Figure 2.2 illustrates the interaction between the protocol layers of the eNode-B and the UE, focusing on the PHYsical Layer (PHY) and MAC layers within the E-UTRAN user plane protocol stack. The following PHY layer functions have been included in the link-level analysis conducted in this study [53]:

- Forward Error Correction (FEC) encoding/decoding, which provides robustness against a fading channel by introducing redundancy. Channel coding of the data channel is based on the UTRA Release 6 Turbo coding, possibly extended to lower rates and extended to longer code blocks.

- Error detection is based on the Cyclic Redundancy Check (CRC) encoding/decoding technique.

- Support for HARQ with soft combining. These concepts are explained later in Section 2.6.

- Modulation and demodulation of the physical channels.
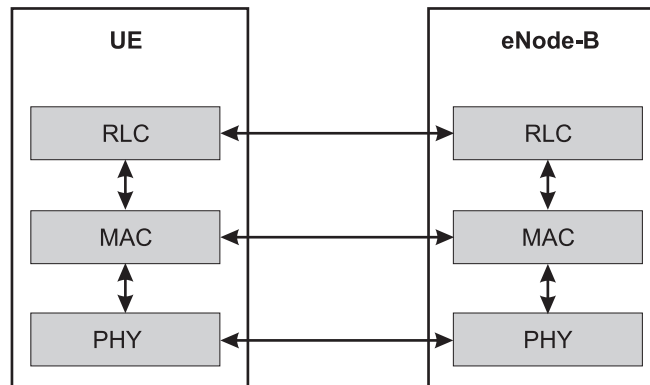
Figure 2.2: The interaction between the protocol layers of the eNode-B and the UE, focusing on PHY and MAC layers within the E-UTRAN user plane protocol stack.

- CQI estimation and reporting to higher layers.

The DL frame structure for the E-UTRA FDD mode is shown in Figure 2.3. Each 10 ms radio frame is divided into 20 equally sized sub-frames. The sub-frame duration is 0.5 ms, and it characterizes the minimum Transmission Time Interval (TTI) duration [14]. This setting was later changed in 3GPP, but we have used the original TTI duration in the initial evaluation of FDAS.

The Radio Link Control (RLC) sub layer of the Layer 2 (L2) performs segmentation and reassembly of higher layer Protocol Data Units (PDU) as well as retransmissions in order to improve the reliability of the radio link. The RLC layer retransmissions are not included in the current analysis. The MAC sub layer within L2 is responsible for packet scheduling, LA and HARQ, which are the key topics of this study.

2.4   Cross MAC-PHY Layer Resource Allocation

Efficient management of radio resources is crucial in wireless networks as radio spectrum is scarce and often expensive. Adaptive cross-layer resource allocation that exploits interdependencies and interactions across the PHY, MAC, and higher protocol layers has recently attracted extensive research interest, e.g., see [54], [55], [56]. The basic idea of cross-layer resource allocation is to
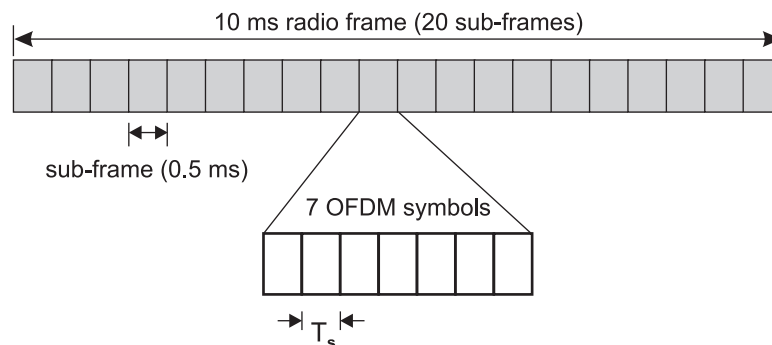
Figure 2.3: The DL frame structure of the E-UTRA FDD mode consisting of 7 OFDM symbols per sub-frame [14]. T_s denotes the OFDM symbol duration.
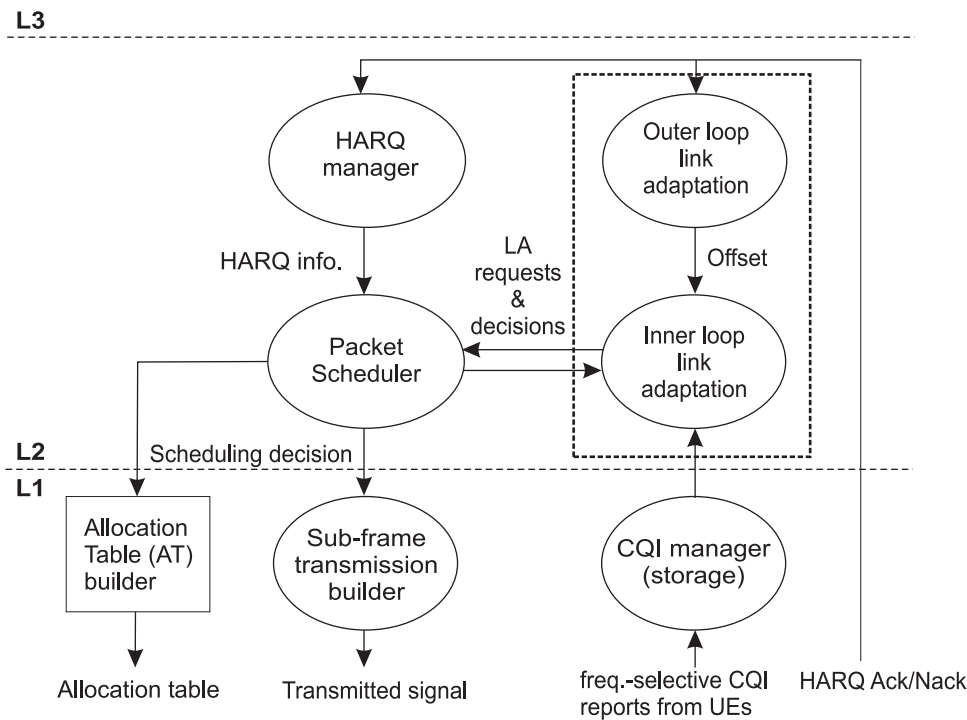
Figure 2.4: Interaction between functional entities involved in packet scheduling and their location in the protocol stack [59].

adapt bandwidth, power allocation as well as other transmission parameters jointly across the protocol stack, in order to improve the resource utilization efficiency significantly. Here, we consider cross-layer adaptation based on the PHY and MAC layers only. The joint MAC-PHY layer optimization of resource allocation can take into account the user's QoS requirements, queuing states observed in the MAC layer based on traffic arrival, as well as the channel quality observed in the PHY layer based on CQI reports available at the eNode-B.

One example of cross MAC-PHY layer resource allocation is opportunistic scheduling, described in [57] and [58]. Opportunistic scheduling, e.g., PF in time, endeavors to maximize the system capacity by scheduling users when their instantaneous channel quality is near the peak. In this study we will investigate the potential of cross MAC-PHY layer opportunistic scheduling when the scheduler can exploit channel dynamics in both time and frequency domains.

2.4.1 Interaction Between PHY and MAC Based RRM Entities Involved in Packet Scheduling

Figure 2.4 illustrates the interaction between the different functional entities involved in packet scheduling, i.e., PS, LA, HARQ manager and CQI manager [12]. The controlling entity is the MAC sublayer based PS entity, where the scheduling policy is applied. The PS can consult the LA entity to obtain an estimate of the supported data rate for certain users in the cell, for a given allocation of time-frequency resources. Furthermore, LA tries to ensure that the estimate of the supported data rate corresponds to a certain BLER target for the first transmission.

LA normally consists of both Inner Loop Link Adaptation (ILLA), which refers to the actual LA algorithm, and Outer Loop Link Adaptation (OLLA). OLLA is required in a scenario where

the target BLock Error Rate (BLER) cannot be guaranteed by ILLA alone. Such a situation can arise in the presence of CQI measurement uncertainties. Previous studies have shown that a suitably designed OLLA algorithm can reduce the impact of biased CQI errors on the LA performance [60]. As depicted in Figure 2.4 the OLLA algorithm provides an adaptive Offset to the ILLA. The details of the OLLA algorithm will be provided in Section 2.5.2. We denote ILLA as simply LA hereafter.

Scheduling and LA entities employ CQI feedback from users, while HARQ employs Ack/Nack's from past transmissions. In the single-cell model based evaluation the frequency-selective CQI is defined as the geometric average of the SINR over the OFDM symbols contained within the specified time-frequency resource. The SINR is measured at the input of the decoder. Thus, CQI is given by:

$$\text{CQI}_i = \Big(\prod_{j=1}^{N} SINR_j \Big)^{\frac{1}{N}} \quad , \tag{2.1}$$

where CQI_i denotes the CQI corresponding to the ith time-frequency resource, $SINR_j$ denotes the SINR of the jth OFDM symbol within the ith time-frequency resource, and N denotes the number of OFDM symbols contained within the time-frequency resource. The motivation behind employing geometric averaging is explained in Section 3.7.

The CQI manager stores the CQI values received from the users and forwards them to the LA module upon request. The HARQ manager provides buffer status information of new transmissions and pending HARQ retransmissions as well as information related to the transmission format of those. The packet is discarded after reaching the maximum allowed number of unsuccessful transmission attempts. The HARQ manager uses Ack/Nack's received on the UL control channel to determine whether a packet was correctly received or not. The DL control information is formatted in the PHY layer and inserted into the AT, based on the input of the scheduler.

2.5   Link Adaptation

The key to successfully deploying broadband wireless systems is to secure a low BLER over the frequency-selective fading channels that can be expected [61]. The single-user fading channel capacity can be maximized if the transmitter adapts its transmit power, data rate, and coding scheme according to the channel variations [30]. LTE supports fast adaptive LA in order to exploit the
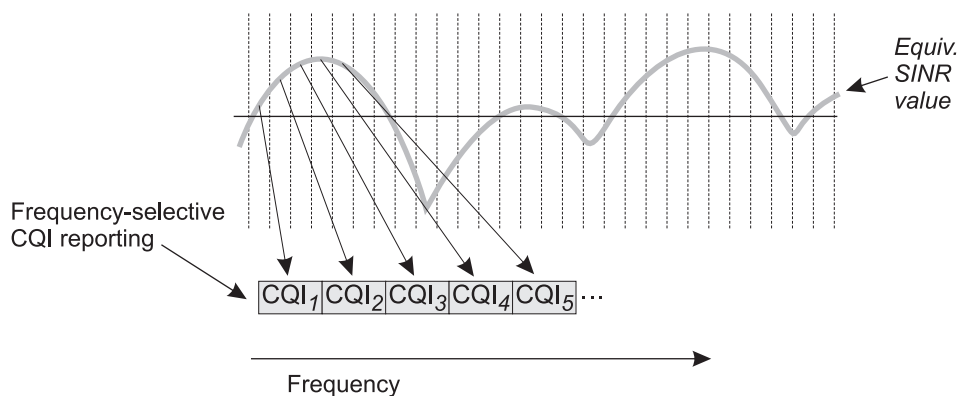
Figure 2.5: Illustration of the frequency-selective CQI reporting scenario.
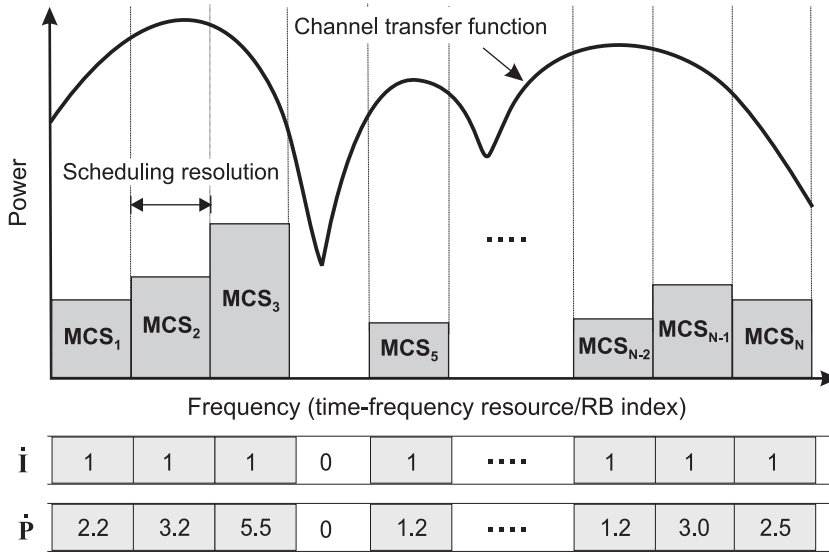
Figure 2.6: A snapshot of the wideband channel transfer function and illustration of the terminology used with frequency-domain LA. An example of the Resource Block (RB) resource allocation ($\dot{\mathbf{I}}$), as well as the power allocation vector ($\dot{\mathbf{P}}$) is also shown.

radio channel dynamics in time, frequency and spatial domains. Adaptive LA can improve the spectral efficiency and reliability in wireless systems. The operating principle of the adaptive LA algorithm is to define a suitable CQI metric, which provides some knowledge of the channel, and to ensure that the most efficient transmission format is always used regardless of the underlying channel conditions [16].

The link-level throughput optimization in time and frequency domains is mathematically formulated hereafter. Let N denote the total number of time-frequency resources available within the system bandwidth, which depends on the scheduling resolution in the frequency-domain. The scheduling resolution will be denoted as the *resource block* (RB) hereafter, following LTE naming convention [14]. The RB consists of a group of adjacent OFDM sub-carriers. In order to enable frequency-domain LA the network directs the UE to report a CQI value for each RB, as shown in Figure 2.5.

The various components and associated terminology for adaptive LA in a frequency-selective fading scenario are depicted in Figure 2.6. The task of the LA algorithm is to select the combination of transmission parameters that optimizes effective throughput, i.e., the mode that yields the largest throughput while remaining within the BLER target bound. The general form of LA based throughput optimization, operating under the total power constraint is given by:

$$\{\dot{\mathbf{I}}^*, \dot{\mathbf{P}}^*, \dot{\mathbf{MCS}}^*\} \;=\; \operatorname*{argmax}_{\dot{\mathbf{I}}, \dot{\mathbf{P}}, \dot{\mathbf{MCS}}} \left\{ TP_{eff}\left(\dot{\mathbf{CQI}}, \dot{\mathbf{I}}, \dot{\mathbf{P}}, \dot{\mathbf{MCS}}\right) \right\} \;, \qquad (2.2)$$

subject to:

$$
\begin{aligned}
\mathbf{C\dot{Q}I} &= (\mathrm{CQI}_1, \mathrm{CQI}_2, \cdots, \mathrm{CQI}_N) \quad, \\
\mathbf{\dot{I}} &= (\mathrm{I}_1, \mathrm{I}_2, \cdots, \mathrm{I}_N); \quad \mathrm{I}_i \in \{0, 1\} \quad, \\
\mathbf{M\dot{C}S} &= (\mathrm{MCS}_1, \mathrm{MCS}_2, \cdots, \mathrm{MCS}_N); \quad \mathrm{MCS}_i \in \mathbb{MCS} \quad, \\
\mathbf{\dot{P}} &= (\mathrm{P}_1, \mathrm{P}_2, \cdots, \mathrm{P}_N); \quad 0 \leq \mathrm{P}_i \leq \mathrm{P}_{\text{total}} \quad, \mathrm{P}_i \in \mathbb{R} \quad, \\
\sum_{i=1}^{N} \mathrm{P}_i &= \mathrm{P}_{\text{total}} \quad,
\end{aligned}
$$

where TP_{eff} denotes the total effective throughput, i.e., throughput taking the first transmission BLER target into account. The exact expression of TP_{eff} is based on the LA algorithm, and this topic is covered in detail in Chapter 3. $\mathrm{P}_{\text{total}}$ denotes the total power available for the data channel, $\mathbf{C\dot{Q}I}$ denotes the received vector (1xN) of CQI values from the UE. $\mathbf{\dot{I}}$ denotes the RB allocation vector, while $\mathbf{M\dot{C}S}$ denotes the vector of the selected MCS formats. $\mathbb{MCS}$ denotes the set of the available MCS formats. The power allocation vector is denoted by $\mathbf{\dot{P}}$, specified on a RB basis, while $\mathbb{R}$ denotes the set of real numbers. The combination $\{\mathbf{\dot{I}}^*, \mathbf{\dot{P}}^*, \mathbf{M\dot{C}S}^*\}$ represents the optimal LA parameters under the given channel conditions, and LA algorithm.

The LA processing is followed by several PHY layer processing steps, as shown in Figure 2.7, which are described hereafter in brief. First, CRC encoding is performed on the L2 PDU. This is done to enable error detection at the receiver. It is followed by channel coding and HARQ rate matching. The rate matcher has the task of matching the size of the encoded block at the output of the turbo decoder to the capacity on the PHY layer [62]. In doing so it adjusts the base code rate of the decoder to the one requested by LA. Finally the rate matched bits are modulated according
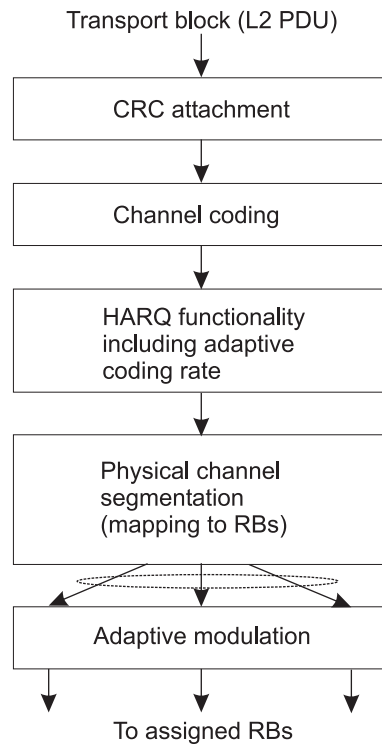
Figure 2.7: Block diagram of the PHY layer processing executed on each L2 PDU after the execution of LA algorithm [14].
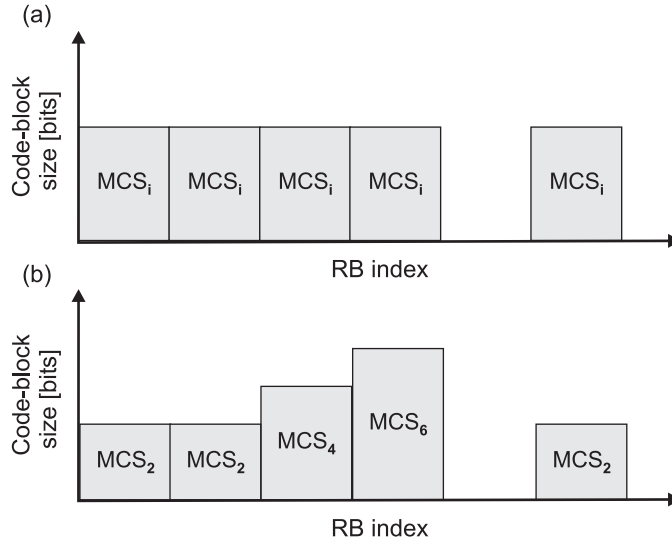
Figure 2.8: (a) Single-block transmission, where the same MCS format is used for all the allocated RBs, (b) Multi-block transmission, where the data rate can be optimized on each selected RB independently, resulting in multiple coding blocks per UE.

to the selected QAM scheme and multiplexed on to the selected RBs, as depicted in Figure 2.7. The link-level processing steps are described in detail in Appendix A.

2.5.1   Modeling of AMC

It is well known that AMC can significantly improve the spectral efficiency of a wireless system [63]. As a result this feature has been included in several wireless standards, e.g., HSDPA [2], WiMAX [15], LTE [14]. In LTE the supported DL data-modulation schemes are Quadrature Phase Shift Keying (QPSK), 16 Quadrature Amplitude Modulation (16QAM) and 64 Quadrature Amplitude Modulation (64QAM).

In the simplified system model we have employed a model based abstraction of AMC performance. The single code-block and multi-block transmission scenarios have been investigated, which are illustrated in Figure 2.8. In single-block transmission the same MCS format is used to encode all the selected RBs, while in multi-block transmission the MCS format can be optimized separately for each selected RB. Single-block transmission is modeled as follows:

$$\overline{SINR}_{block,1} \;=\; \left(\prod_{i=1}^{nRBs} \left(\overline{SINR}_{la,i} \cdot \mathrm{I}_i \right) \right)^{\frac{1}{nActRBs}} , \qquad (2.3)$$

$$\overline{SINR}_{la,i} \;=\; \frac{\overline{SINR}_i \cdot \mathrm{P}_i}{\mathrm{P}_{ref}} , \qquad (2.4)$$

$$nActRBs \;=\; \sum_{i=1}^{nRBs} \mathrm{I}_i ,$$

where $\overline{SINR}_i$ denotes the geometric average SINR over the symbols within the ith RB , $\overline{SINR}_{la,i}$ denotes the modified SINR of the ith RB taking into account the reference power used in CQI estimation (P_{ref}), and the RB specific power allocation (P_i). $\overline{SINR}_{block,i}$ denotes the geometric

average SINR of the ith coding block used in LA, I_i denotes a member of the resource allocation vector $\dot{\mathbf{I}}$, $nActRBs$ denotes the number of active RBs, and $nRBs$ indicates the total number of RBs within the system bandwidth. In case of multi-block transmission (2.4) gives the block SINR for each encoding block, as in this case $\overline{SINR}_{block,i} = \overline{SINR}_{la,i}$.

Based on (2.3) and (2.4) the following expressions are used to determine the supported throughput for the different block encoding options:

$$
\begin{aligned}
TP_{SB} &= \frac{BW \cdot nActRBs}{nRBs} \\
&\quad \cdot \log 2 \left(1 + \min \left(\frac{\overline{SINR}_{block,1}}{10^{4/10}}, 10^{18/10} \right) \right), \quad\quad (2.5) \\
TP_{MB} &= \sum_{i=1}^{nActRBs} \frac{BW}{nRBs} \\
&\quad \cdot \log 2 \left(1 + \min \left(\frac{\overline{SINR}_{block,i}}{10^{4/10}}, 10^{18/10} \right) \right), \quad\quad (2.6)
\end{aligned}
$$

where TP_{SB} represents the supported throughput for single-block transmission, TP_{MB} denotes the supported throughput in multi-block transmission, and BW denotes the system bandwidth. (2.5) and (2.6) are based on the modified *Shannon theorem* including an Implementation margin. The Implementation margin takes into account system imperfections resulting from bandwidth utilization, real modulation, limited code block length, etc. The maximum SINR is limited to 18 dB for the 3GPP Macro cell scenario, based on previous system-level studies, e.g., see [64]. It is assumed that the channel fading rate is slow enough so that the frequency response does not change within a coding block. The Implementation margin is set at a fixed value of 4 dB, which has been taken from previous HSDPA studies.

The curves depicting spectral efficiency versus SINR obtained with the Shannon Theorem and
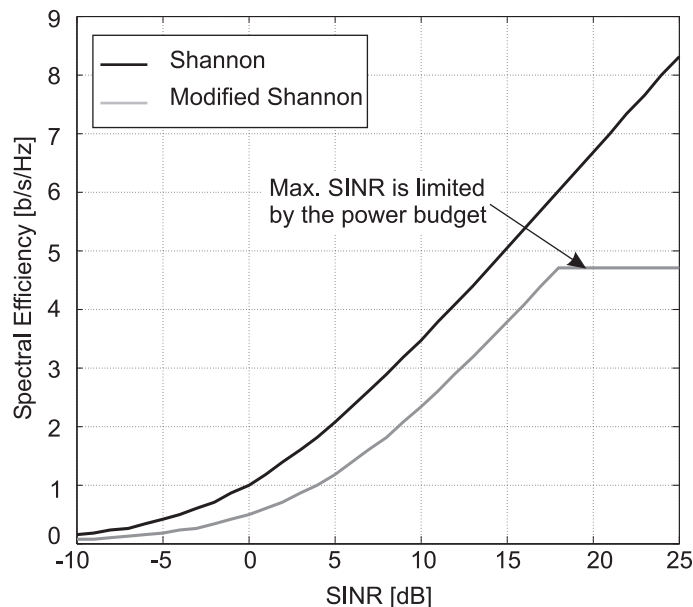

Figure 2.9: The spectral efficiency versus instantaneous SINR curves obtained with the Shannon Theorem and the modified Shannon Theorem (max. SINR is limited to 18 dB for the 3GPP Macro cell case).

the modified Shannon Theorems are illustrated in Figure 2.9. The modified Shannon theorem is a simplified version of the model proposed in a recent study [65], where it is recommended to use a BW efficiency factor in addition to the Implementation margin/SNR efficiency factor. The BW efficiency factor is to be determined from system-level parameters such as pilot and common channel overhead. As the control overhead was not known at the time of this study, we have ignored the BW efficiency factor in the current analysis. Further, the authors in [65] have recommended to optimize the SNR efficiency factor according to the antenna configuration and receiver type. However, we have used a fixed Implementation margin for all antenna-receiver configurations in order to simplify the analysis. Note that multi-block transmission is less efficient with respect to the CRC overhead as each coding block has to be CRC encoded separately. This aspect is not included in (2.5) and (2.6). Furthermore, the coding overhead is not included in the throughput calculation.

2.5.2   Outer Loop Link Adaptation

The performance of LA is highly dependent on the accuracy of the CQI reports [48]. It is well known from previous HSDPA studies that an OLLA algorithm is needed in scenarios where the CQI feedback from the UEs is subject to errors and reporting delays, e.g., see [60], [66]. OLLA is a closed-loop mechanism that can be used to reduce the impact of biased CQI errors on LA performance.

The CQI measurement is subject to errors as it is based on a limited number of pilot symbols that are inserted into each sub-frame, e.g., in LTE FDD mode the pilot symbol overhead is around 5% for the single-stream case [14]. Further, the time available to perform CQI estimation and reporting is also quite limited, e.g., 0.5 ms in LTE. Thus, there is limited scope of applying averaging techniques to reduce the measurement error. These factors contribute towards CQI measurement inaccuracies in a practical scenario, e.g., even though the UE performs CQI measurement over a 5 MHz band in HSDPA the commonly used CQI error model assumes a *lognormal distribution* of error with a standard deviation (std.) of 1 dB [48]. The CQI measurement is performed over a 2 ms period in HSDPA [2].

In an OFDMA system supporting FDAS the challenge of providing an accurate CQI report is even greater, since it is estimated over a narrow bandwidth, e.g., in the extreme case over a single sub-carrier. Based on a similar error model as used in HSDPA it will be shown in Figure 3.18 that for a fixed pilot overhead the CQI error increases rapidly as the scheduling resolution is increased. When the scheduling resolution is equal to 375 kHz, i.e., 24 RBs within 10 MHz, the std. of CQI error is around 2.5 dB [67]. Thus, it is important to consider CQI measurement inaccuracies in the system-level analysis of the FDAS gain potential.

In the scenario where CQI errors cannot be totally avoided, the OLLA algorithm is usually employed to stabilize the overall LA performance. Without the OLLA the BLER for the actual transmissions will tend to be higher than the originally anticipated BLER target. This is especially true when the packet scheduling algorithm is also making decisions based on the CQI reports.

The OLLA algorithm considered here is motivated from previous HSDPA studies [1]. It monitors success of past transmissions to each user, based on received Ack/Nack's, which are used to calculate an offset parameter as input to the LA algorithm, as previously shown in Figure 2.4. The LA algorithm adjusts CQIs according to the OLLA offset before using them in the processing of the algorithm. Only one OLLA offset is available per user for simplicity reasons. We describe here

the OLLA algorithm, which only targets at controlling the BLER target for the first transmission to users. This OLLA algorithm adjusts the offset factor, A_{CQI}, according to two simple rules [68]:

- If an Ack is received for a first transmission, then decrease A_{CQI} by $A_{StepDown}$ decibels:

$$A_{CQI} = A_{CQI} - A_{StepDown} \quad . \tag{2.7}$$

- If a Nack is received for a first transmission, then increase A_{CQI} by A_{StepUp} decibels:

$$A_{CQI} = A_{CQI} + A_{StepUp} \quad . \tag{2.8}$$

Note that only Ack/Nack from the first transmissions are used for adjusting the offset A_{CQI} parameter. Ack/Nack for HARQ retransmissions are not used by the considered OLLA algorithm. The recursive algorithm requires initialization of the A_{CQI} parameter. Furthermore, it has to be ensured that the dynamic range of the offset factor remains within a predefined interval, to avoid reaching saturation as a result of unexpected errors. The relation of A_{StepUp} and $A_{StepDown}$ is suggested to be [60]:

$$A_{StepDown} = A_{StepUp} \cdot \frac{BLER}{1 - BLER} \quad . \tag{2.9}$$

Hence, for a certain desired BLER target and a known A_{StepUp}, the $A_{StepDown}$ parameter can be determined using (2.9). When using the OLLA algorithm, the CQI reports received from the UE and expressed in decibels are offset by using the current A_{CQI} value:

$$CQI_{i,eff} = CQI_i - A_{CQI} \quad . \tag{2.10}$$

It should be noted that the same offset A_{CQI} is applied to all the CQI reports of a user across the frequency domain.

2.5.2.1   Simplified Model of OLLA

As the HARQ retransmissions have not been implemented in the single-cell model a simplified model for OLLA is used, where the A_{StepUp} and $A_{StepDown}$ parameters are kept equal. They are given by:

$$A_{StepUp} = A_{StepDown} = 0.05 \, \text{dB} \quad . \tag{2.11}$$

The step size of the OLLA algorithm has been taken from previous HSDPA studies. Further, direct BLER estimation is used to determine whether (2.7) or (2.8) is employed to update the A_{CQI} parameter.

2.6   HARQ

LTE supports the HARQ functionality to ensure packet delivery between peer entities at Layer 1 [53]. HARQ provides robustness against LA errors caused by the uncertainties in CQI measurement and reporting. As an example, in HSDPA the effective probability of packet error for the first transmission is typically in the order of 10-40%, due to LA errors [69]. Further, if the service can tolerate additional delay, HARQ can improve the spectral efficiency by allowing LA to be more aggressive [12]. The HARQ within the MAC sublayer has the following characteristics [53]:

- N-process Stop-And-Wait (SAW) protocol based HARQ is used between the eNode-B and the UE. The transmitter persists with the transmission of each packet for a given number of transmission attempts, before discarding the packet. The HARQ processes are transmitted over N parallel time channels in order to ensure continuous transmission to a single UE. The choice of the N parameter depends on the length of the TTI, feedback delays and QoS delay constraints. Increasing N leads to extra buffering requirement at the receiver and transmitter, longer delay per HARQ process, and increased signaling load in the DL. In practice N is kept in the order of 4-6 [2].

- The HARQ is based on Ack/Nack's. The data packets are acknowledged after each transmission. A Nack implies that a retransmission is requested either for additional redundancy (Incremental Redundancy (IR)) or a combining gain (Chase Combining (CC)), to enable error free packet delivery to the higher protocol layers.

- Asynchronous retransmissions with adaptive transmission parameters are supported in the DL, to maximize the scheduling flexibility available at the PS. *Asynchronous HARQ* implies that (re)transmissions for a certain HARQ process may occur at any time. Explicit signaling of the HARQ process number is therefore required on the AT. *Adaptive HARQ* operation in the frequency-domain implies that the re-transmission can be scheduled on different RBs in comparison to the first transmission. However, additional restrictions can still be applied on retransmissions, e.g., use of the same MCS. These restrictions are imposed to ease the implementation of combining schemes at the receiver, as well as to avoid the associated control signaling overhead.

If the HARQ retransmissions fail or exceed the maximum number of retransmissions allowed, the RLC layer handles further ARQ retransmissions. Such RLC based retransmissions are not considered in this study. The HARQ gain comes at the cost of increased memory requirement at the UE, required to buffer the soft values at the output of the Turbo decoder. Further, HARQ combining also increases the packet delay.

2.6.1   HARQ Modeling

The explicit scheduling of HARQ processes is not implemented in the simplified system model. The combining gain is modeled using a simple HARQ process model, taken from [70]. Only CC type of combining is considered, where the block SINR after HARQ combining is given by:

$$\left(\overline{SINR}_{block,i}\right)_{C,n} = \epsilon^{n-1} \cdot \sum_{k=1}^{n} \left(\overline{SINR}_{block,i}\right)_k \quad , \tag{2.12}$$

where $\left(\overline{SINR}_{block,i}\right)_{C,n}$ represents the combined block SINR after n transmissions, ϵ denotes the CC efficiency and $\left(\overline{SINR}_{block,i}\right)_k$ denotes the block SINR of the ith block after the kth transmission, given by (2.3) or (2.4). We have used $\epsilon = 0.95$ in these studies, which is the recommended value in [70]. Note that (2.11) is only valid when n is relatively small, e.g., around 3-4, which is also the case in a practical system. In this study the HARQ process allows a maximum of three retransmissions per block before discarding a code block, i.e., $n = 4$.

A simple statistical recursive HARQ model is used to calculate the effective throughput after

retransmissions:

$$
\begin{aligned}
TP_{eff,harq} \;=\; & TP \cdot (1 - BLER_1) + \frac{TP}{2} \cdot BLER_1 \cdot (1 - BLER_2) \\
& + \frac{TP}{3} \cdot BLER_1 \cdot BLER_2 \cdot (1 - BLER_3) \\
& + \frac{TP}{4} \cdot BLER_1 \cdot BLER_2 \cdot BLER_3 \cdot (1 - BLER_4) \,, \qquad (2.13)
\end{aligned}
$$

where $TP_{eff,harq}$ denotes the effective throughput after HARQ combining gain, TP denotes either single-block throughput (TP_{SB}) or TP_{MB} given by (2.5) and (2.6) respectively, $BLER_1$ denotes the BLER for the first transmission, $BLER_2$ denotes the BLER for the first retransmission, and so on. Note that (2.13) is applied only if the code-block is correctly received after the fourth transmission, i.e., $BLER_4 = 0$, else $TP_{eff,harq}$ is set to 0. The SINR-to-BLER mapping curve in Figure 2.14 is used to determine $BLER_i$ for a given SINR after taking the HARQ combining gain into account. These aspects are explained further in Section 2.8. The general form of the expression in (2.13) is given by:

$$
TP_{eff} = \sum_{i=1}^{n} \left(\frac{TP}{n} \prod_{i=1}^{n-1} BLER_i \cdot \left(1 - BLER_n \right) \right) \quad . \qquad (2.14)
$$

The HARQ model presented here assumes *non-adaptive* HARQ operation. This is also clear from (2.13) since we assume that the transmit parameters are not changed between transmissions of the same code-block. Further, no signaling delays or errors in the transmission of HARQ Ack/Nack's are assumed.

2.7 Packet Scheduling

In order to utilize the DL-SCH resources efficiently a scheduling function is used in the MAC sub layer. The radio channel fading which used to be regarded as a fundamental limitation on the performance of wireless systems, is now considered as an advantage since it can be exploited by a channel-aware scheduler. Here, an overview of the scheduler is given in terms of its operation, signalling of scheduler decisions, and UE measurements facilitating scheduler operation.

Figure 2.10 illustrates the management of users' queues within the HARQ manager as well as its interaction with the scheduler. The PS entity assigns radio resources dynamically between UEs, taking into account channel conditions, traffic volume and the QoS requirements of each UE [53]. Different scheduling algorithms can be applied at the MAC layer that provide a trade-off between throughput and fairness, as exemplified in Table 1.1. We assume that the radio resource allocation determined by the PS can be changed on a TTI basis, i.e., fast scheduling can be employed. In this study, resource assignment consists of performing a mapping between the UEs and the available RBs in the frequency domain. The UEs identify whether resources are assigned to them by receiving a scheduling related control channel, i.e., AT, which indicates the selected transport format as well as the RB allocation pattern.

The scheduler can instantaneously choose the best multiplexing strategy from the available methods, i.e., localized or distributed transmissions. In this study we will only consider the *frequency localized* transmission scenario [14], characterized by flexible user multiplexing in the
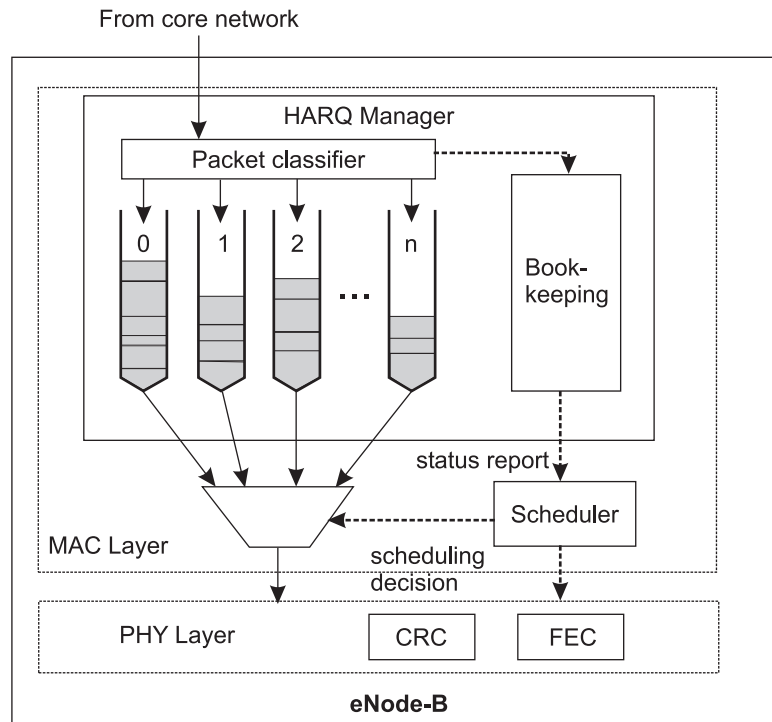
Figure 2.10: Management of users' queues within the HARQ manager and the interaction with the DL scheduler. Packets arrive at the top of their respective queues. The HARQ manager submits a status report to the scheduler when requested, containing information about the priorities and the size of the queues. The figure has been adapted from [71].

frequency domain with a view to fully exploit the available multi-user diversity gain, as illustrated earlier in Figure 1.4. Scheduling is tightly integrated with LA and HARQ entities. The UE performs channel quality measurement and the CQI reports are used in the processing of the scheduling algorithm. The time and frequency granularity of the UE radio environment measurement reports has a significant impact on the performance of channel-aware scheduling [72]. The scheduling decision can be based on QoS parameters, payloads buffered in the eNodeB, pending HARQ retransmissions, CQI reports from the UEs, UE capabilities, UE sleep cycles and measurement gaps/periods and system parameters such as bandwidth and interference level/patterns [14]. We will consider only a subset of these parameters in the current analysis, e.g., UE capabilities, QoS parameters, are not included.

An effective trade-off between spectral efficiency, fairness, and QoS is desired in wireless resource allocation [48]. Packet scheduling is an optimization problem, and has been formulated mathematically in previous studies, e.g., see [73]. We now provide a brief review of such a theoretical formulation based on the use of utility functions [54].

Kelly [73] proposed the use of utility function to quantify the degree to which a network satisfies requirements of users' applications, based on similar studies in economics. The utility function maps the network resources a user utilizes into a real number [54]. Since a reliable data rate is the most important factor to determine the satisfaction of users, the utility function is a non-decreasing function of the data rate r. The cross-layer optimization aims at maximizing the

aggregate utility of the network, which can be expressed as [74]:

$$\text{maximize} \quad \sum_{i=1}^{k} U_i(r_i) \quad , \tag{2.15}$$

subject to

$$\sum_{i=1}^{k} r_i < C \,, \quad r_i \geq 0 \quad , $$

where k denotes the number of active users in the cell, r_i denotes the average throughput of user i, C denotes the channel capacity, and $U_i(\cdot)$ denotes the utility function of user i. The average user throughput is computed in a recursive manner as follows [74]:

$$r_i[n+1] = \begin{cases} \left(1 - \frac{1}{\tau}\right) r_i[n] + \frac{d_i[n]}{\tau} & \text{if user } i \text{ is served in slot } n \quad , \\ \left(1 - \frac{1}{\tau}\right) r_i[n] & \text{otherwise} \quad , \end{cases} \tag{2.16}$$

where $d_i[n]$ is the instantaneous bit rate of the user i if served during the nth period, and τ is the time constant of the smoothing filter.

Assuming that the utility function of each user is strictly concave and differentiable, the optimal set of rates denoted by $\{r_i^*\}$ have the property that $U_i'(r_i^*)$ is the same for all users [74]. The optimal solution varies with time since the channel capacity and the number of active users both vary with time. Further, the system can only move towards the optimum at each decision point by going in the direction of steepest ascent, given by [74]:

$$i^* = \underset{i}{\arg\max} \left\{ d_i[n] U_i'(r_i[n]) \right\} \quad . \tag{2.17}$$

The argument of $\arg\max\{.\}$ in (2.17) is usually referred to as the *scheduling priority metric* $\left(P(i)\right)$. As an example, if the utility function is a linear function of the data rate, i.e.,

$$U(r) \quad = \quad \alpha \cdot r \quad , \tag{2.18}$$

the scheduler should pick the user i^* which satisfies:

$$i^* = \underset{i}{\arg\max} \left\{ d_i[n] \right\} \quad . \tag{2.19}$$

It means that the scheduler should pick the user with the highest data rate, i.e., Max. Throughput scheduler. However, such a scheduler will always serve those users who are in good conditions and will rarely serve those who are in bad conditions, leading to an unfair allocation of resources. This problem can be addressed by using the PF utility function, given by:

$$U(r) = \log(r) \quad . \tag{2.20}$$

The resulting scheduler picks the user such that:

$$i^* = \underset{i}{\arg\max} \left\{ \frac{d_i[n]}{r_i[n]} \right\} \quad . \tag{2.21}$$

The scheduler calculates the priority metric $P(i)$ for all users, and picks the one which satisfies (2.17) for scheduling in the next TTI. Some of the popular utility functions which will also be employed in this study are listed in Table 2.1.

Table 2.1: List of some of the utility functions that are employed in this study.

Utility function	$U(r)$
Max Throughput (MT)	$\alpha \cdot r$
Proportional Fair (PF)	$\log(r)$
Blind Equal Throughput (BET)	$\frac{\log(r)}{d}$

2.8   Link-To-System Performance Mapping Function

In order to estimate the performance at the system-level with reasonable accuracy, an evaluation based on extensive simulations under a variety of scenarios is crucial. A single simulator approach would be preferable, but the complexity of such a simulator including everything from link-level processing to multi-cell network is too high for the required simulation resolutions [1]. Therefore, separate link-level and system-level simulators are needed. The link and system levels are connected through a *link-to-system performance mapping* function, which is used to predict the instantaneous BLER at system-level without performing detailed link-level processing steps. This function is estimated using link-level simulations, and it takes into account factors such as MCS format, receiver type, and channel state [75]. The desired characteristics of the link-to-system mapping function are that it should be general enough to cover different multiple access strategies and transceiver types, including different antenna techniques. Further, it should be possible to derive the parameters of the model from a limited number of link-level evaluations.

We have selected the Exponential Effective SINR Metric (EESM) link-to-system performance mapping function, based on previous OFDM studies [76], [75] and LTE recommendations [14]. The EESM model maps the instantaneous channel state experienced by the OFDM sub-carriers within the code-block into a single scalar value, an effective SINR, which is then used to find an estimate of the BLER for this specific channel state. In the general form, the EESM model is given by [76]:

$$\gamma_{eff} = -\beta \cdot \ln \left(\frac{1}{N} \sum_{i=1}^{N} e^{\frac{-\gamma_i}{\beta}} \right) \quad , \tag{2.22}$$

where γ_{eff} denotes the scaler EESM value, γ_i denotes the SINR (at the input of decoder) of the ith sub-carrier, β is a parameter which is obtained from link-level simulations and is adjusted for each MCS separately, and N denotes the number of active OFDM sub-carriers. As seen in (2.22) the effective SINR is similar to the geometric average SINR over the symbols within the code-block. A similar recommendation was made in other OFDM based studies [46], [77], where it was shown that the decoder performance depends not only on the average SINR, but also on the inter-symbol SINR variability.

The effective SINR from (2.22) is used to find an estimate of the BLER for the relevant MCS using basic AWGN link-level-performance curves [76]. The reference AWGN curves used in this study are shown in Figure 2.11, and are based on the 3GPP Rel. 6 compliant Turbo coding scheme operating with the basic rate of 1/3 [78]. The detailed link-level processing chain used to generate these performance curves is illustrated in Figure A.1. Further, in Appendix B we show that the EESM model is able to provide a reliable estimate of decoder performance. Note that a simplified link-to-system performance mapping function will be employed in the single-cell based model.
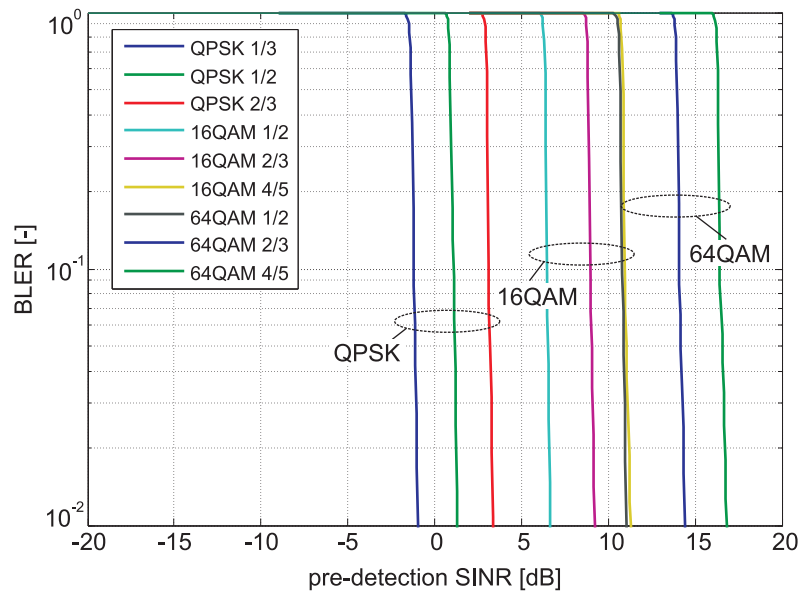
Figure 2.11:   Reference BLER versus SNR curves (measured at the input of decoder) for the AWGN channel. These performance curves are based on the 3GPP Rel. 6 compliant Turbo coding scheme operating with the basic rate of 1/3 [78].

This technique is described in Subsection 2.12.2.

2.9   OFDM Physical Layer Parameters

The OFDM PHY layer parameters used in the evaluation of the E-UTRA DL are listed in Table 2.2, and are taken from [14]. We consider three of the possible six system BW scenarios supported by LTE. Further, the short CP length has been assumed for each BW case. For information purposes, LTE also supports a long CP option where the CP length has been increased to $16.67\,\mu$s.   Note that the TTI duration has recently been increased to $1.0\,$ms, and the new setting will be used in the

Table 2.2: The OFDM PHY layer parameters used for the analysis of E-UTRA DL performance [14].

Parameter	*Setting*		
Transmission BW [MHz]	5	10	20
Sub-frame duration [ms]	0.5		
Sub-carrier spacing [kHz]	15		
Sampling frequency [MHz]	7.68	15.36	30.72
FFT size [-]	512	1024	2048
Number of occupied sub-carriers [-]	300	600	1200
Number of OFDM symbols per sub-frame [-]	7		
Cyclic Prefix (CP) length [μs]	4.75		

multi-cell simulator based evaluation.

2.10   Traffic Modeling

The *infinite buffer* and the *finite buffer* traffic models have been employed in this study, to abstract the behavior of best-effort services. These models differ in terms of the session time of the users. In the infinite buffer model all users experience equal session time irrespective of their location within the cell. This implies that the users close to the eNode-B download a much larger amount of data in comparison to those located near the cell edge (due to superior SINR conditions near the cell center). The cell and user throughput statistics are collected over several simulation runs, each of a fixed duration, i.e., Monte-Carlo simulation approach is utilized. In each run a fixed number of user locations within the coverage area are sampled.

The finite buffer model allows each user to download the same amount of data. Once the download is finished the session is terminated, and a new user is immediately admitted to the system. Hence, the session time is proportional to the experienced data rates. Thus, users close to the cell edge are expected to stay longer in the system in comparison to the users located near the cell center. The data rates delivered to the cell edge users will dominate the resultant cell throughput. Only a single simulation run is performed in this case, which is of a relatively long duration, in order to collect sufficient user statistics. This is also required to sample most of the locations within the coverage area of a cell. For both traffic models it is assumed that data is always available in the eNode-B buffers, waiting to be served by the PS. Note that bursty traffic arrival process within an ongoing packet session is not modeled in this study.

2.11   Reference Antenna Schemes

We have considered three popular single-stream based antenna schemes from the LTE standardization activities for analysis purposes. They differ in terms of the available order of transmit and/or receive diversity. The selected antenna schemes are as follows [14]:

1x1 - It is the simple Single Input Single Output (SISO) antenna scheme, which does not include any transmit or receive diversity.

1x2 MRC - This scheme includes two branch receive diversity, and signal combining is performed using the well known Maximal Ratio Combining (MRC) technique [28].

2x2 SFTD - The Space-Frequency Transmit Diversity (SFTD) antenna scheme considered in this study is based on the Alamouti Space Time Coding scheme, applied to neighboring OFDM sub-carriers instead of adjacent time symbols [62]. Open Loop transmit diversity is used here in addition to the receive diversity, while combining is based on the MRC technique. The transmit signals are assumed to be uncorrelated, due to the wide inter-antenna spacing at the eNode-B.
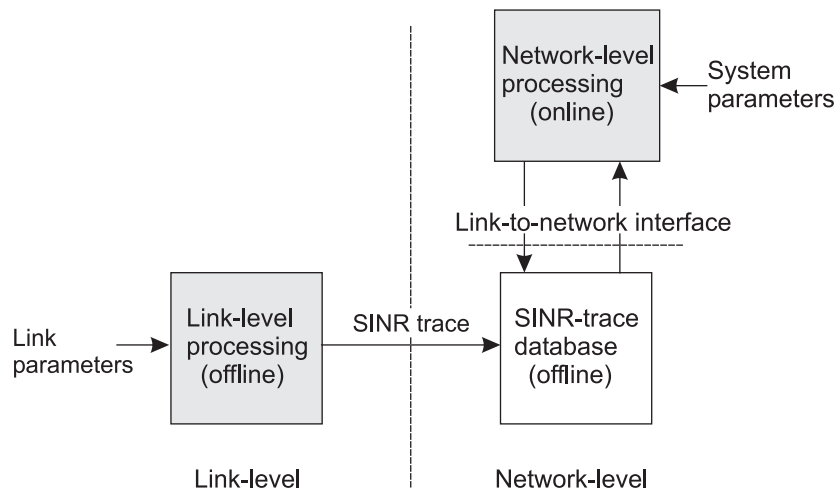
Figure 2.12: Decoupled link and network level simulation methodology for run-time efficient network performance evaluation, adapted from [79, p. 16].

2.12   Simulation Methodology Employed in the Single-Cell Model

A quasi-static *decoupled* link and network level simulation methodology [79] has been employed in the initial evaluation of FDAS. In this technique the link-level processing is modeled in the form of pre-generated RB-level SINR traces, while the network-level processing is implemented in real-time within a single cell. The simulation methodology is illustrated in Figure 2.12. It is a practical trade-off between simulation inaccuracy due to the modeling simplifications, and the processing load caused by the complexity of real-time joint modeling of link and system levels.

At the system-level the implementation of some features such as HARQ, AMC, OLLA and link-to-system performance mapping has been simplified. However, the most relevant functional entities at the network level, e.g., PS and LA, have been implemented in detail. Further, other-cell interference is assumed to be AWGN. This model is preferred in the initial phase of the study where we will be focusing on algorithm design issues. Further, preliminary analysis of the gain potential of FDAS schemes will also be performed using this model.

The decoupled simulation approach requires a link-to-network interface concept, as shown in Figure 2.12, where the network simulator reads the link-level performance in the form of a SINR trace from a database. The advantage of this technique over fully dynamic network simulators is that time consuming link-level simulation results can be pre-computed and reused, for example, to test the performance of different network level packet scheduling strategies. Moreover, the impact on system performance due to changes in PHY layer parameters, e.g., antenna deployment, system bandwidth, speed, can be evaluated with relative ease by the introduction of corresponding link-level SINR distributions. The link and network level modeling steps are outlined hereafter.

2.12.1   Link-Level Modeling

A detailed OFDM link-level simulator has been used to generate the raw SINR trace on an OFDM sub-carrier basis. The link model is based on the LTE and HSDPA recommendations [80], and includes implementation of the spatial multi-path channel model, support for transmit and re-
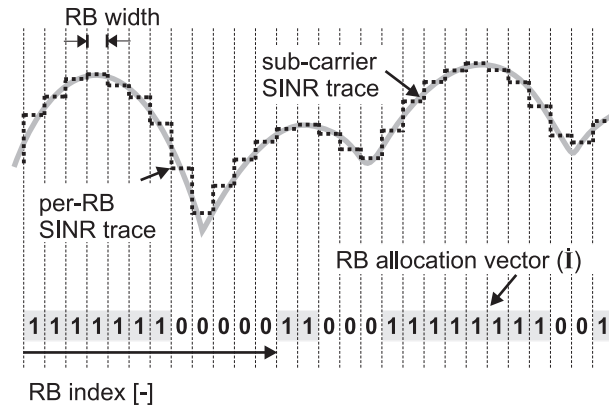
Figure 2.13: Snapshot of the sub-carrier SINR measured at the input of decoder, as well as the per RB SINR trace in the frequency-domain. An example RB allocation pattern of the frequency-domain LA algorithm is also shown.

ceive antenna diversity techniques, E-UTRA PHY layer processing modules such as Turbo coding/decoding, HARQ rate matching and combining, interleaving and constellation rearrangement for higher order QAM. A detailed description of the link-level model as well as the validation of its performance is outlined in Appendix A.

The sub-carrier level SINR trace (measured at the input of decoder) obtained from the link-level model is formatted into a RB-level SINR trace, as illustrated in Figure 2.13. The SINR at the RB-level is calculated by taking the geometric average of the SINR over the sub-carriers contained within the RB. This technique was selected on the basis of an initial performance analysis of the impact of different averaging techniques on the throughput performance. The details of the study are provided in Section 3.7.

2.12.2 Network-Level Modeling

The quasi-static network overlay shown in Figure 2.12 provides traffic modeling, multi-user scheduling, and LA including HARQ (CC). A single-cell is implemented in detail, and it is assumed that users are uniformly distributed in the reference cell with respect to area. The system is based on a simple Admission Control (AC) strategy which keeps the number of users in the cell constant. In terms of propagation modeling, the combined effect of path loss, shadowing and other-cell interference is modeled as AWGN adjusted to an equivalent *Geometry* factor (G-factor) distribution, while fast-fading is modeled using the RB-level SINR trace.

The G-factor distribution is dependent on the cellular deployment scenario, e.g., 3GPP Macro-cell [14]. The G-factor is defined as the ratio of totally received wideband eNode-B/intra-cell power to other-cell interference plus noise, measured at the receive antenna. It is averaged over short-term fading, but not over shadowing [2], and is given by:

$$G = \frac{P_{own}}{P_{other} + P_{noise}} \quad , \tag{2.23}$$

where P_{own} denotes the wideband intra-cell power, P_{other} denotes the wideband other-cell interference, and P_{noise} denotes the thermal noise. Note that the G-factor is normally defined for a fully loaded system, where all cells are transmitting with a flat power spectral density (PSD) over entire bandwidth. However, these assumptions are not valid for some advanced FDAS schemes,
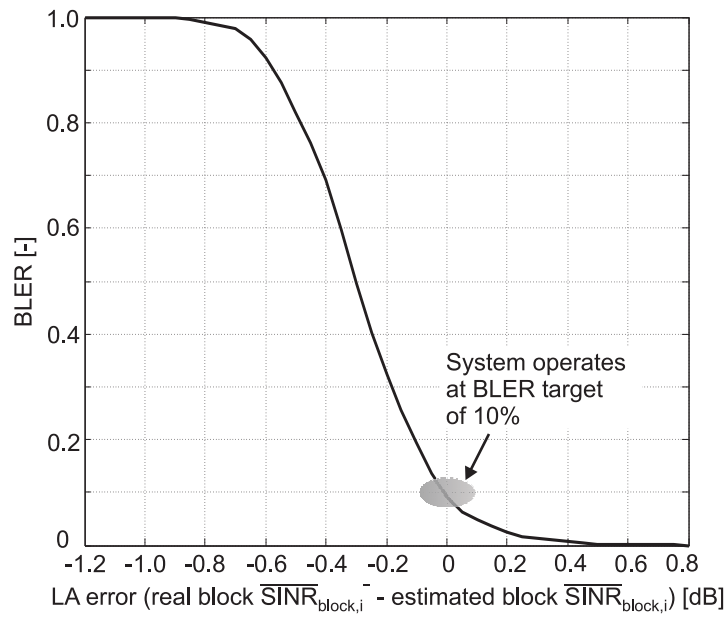
Figure 2.14: The LA error versus BLER curve that is used as the link-to-system performance mapping function in the simplified system model.

e.g., when the allocation of power in frequency is according to the Water-filling distribution [81]. However, in order to simplify analysis we utilize a common G-factor distribution, irrespective of the FDAS scheme. This assumption is discarded in the system simulator based evaluation outlined in Chapter 8.

The G-factor distribution is dependent on factors such as inter-site distance, path loss, shadowing loss, antenna pattern, transmit power, penetration loss, etc. The reference distributions used in this study are illustrated in Figure 2.15, and have been obtained from system-level simulations. The average G-factor remains constant for a user during a session, thus assuming that the packet call is short compared to the coherence time of shadow fading. The DL control and pilot channel overhead are not considered in the preliminary study. Further, error free reception of the DL control channel has been assumed throughout.

The SINR trace file obtained from the link-level tool is also used to build the frequency-selective CQI reports, according to (2.1). Further, the CQI report also includes measurement errors and quantization. LA is conducted on the potentially delayed CQI reports, taking into account UE and eNode-B processing delays [2]. The frequency-domain LA algorithm determines which RBs will be used in the next transmission based on the optimization of throughput. At the receiver, the CQI imperfections will result in a *LA error*, which is defined as the difference between the real and the estimated value of the SINR measured over the code-block. The LA error is mapped into an equivalent BLER, by using the simplified link-to-system performance mapping function that is shown in Figure 2.14. This curve has been obtained from previous HSDPA studies, and it models the behavior of a rate 1/3 Turbo decoder.

The system is operated at the first transmission BLER target of 10%. The LA scheme is allowed to be aggressive since it can rely on HARQ retransmissions to get the packet through. Further, the OLLA algorithm is employed to stabilize the first transmission BLER in the presence of CQI errors, where the OLLA offset is updated by using direct BLER estimation, only for the first transmission.

Table 2.3: Summary of the key differences in simulation assumptions between the reference cellular deployment scenarios. Macro-cell parameters are obtained from [14], while the Micro-cell parameters are obtained from [82].

Parameter	Deployment scenario	
	Macro case 1	Micro out-to-in
Inter-site distance [m]	500	130
Total eNode-B TX power [dBm]	46	38
Total antenna gain [dBi]	14	6
Min. coupling loss [dB]	70	53
Shadow fading std. [dB]	8	10
Path loss model	$128.1 + 37.6 \log_{10}(d)$	$7 + 56 \log_{10}(d)$
Penetration loss [dB]	20	-
Min. distance between UE and cell [m]	>=35	>=10
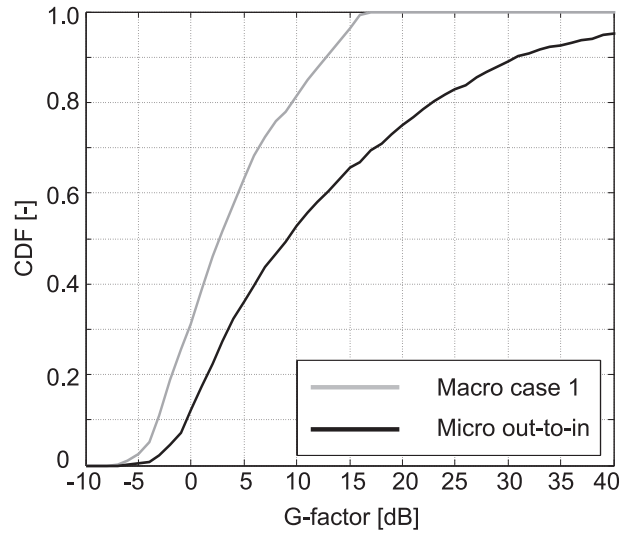
Figure 2.15: CDF of the G-factor for the reference system deployment scenarios obtained from system level simulations [59], [49].

2.13 Reference Cellular Deployment Scenarios

The G-factor distribution is used to model the experienced wideband SINR conditions within the coverage area of the cell. Two popular 3GPP cellular deployment scenarios have been employed in the analysis. These are the Macro-cell case 1 and the Micro-cell outdoor-to-indoor (out-to-in) scenarios [14]. They mainly differ in terms of the resulting coverage area. The detailed list of system-level parameters for the two deployment cases is provided in Chapter 7, while the key differences are listed in Table 2.3. The carrier frequency is equal to 2 GHz in both cases [14]. A 3-sector network topology with 70 degree eNode-B antennas is assumed for the Macro-cell cases, while the Micro-cell case assumes an omni directional eNode-B antenna.
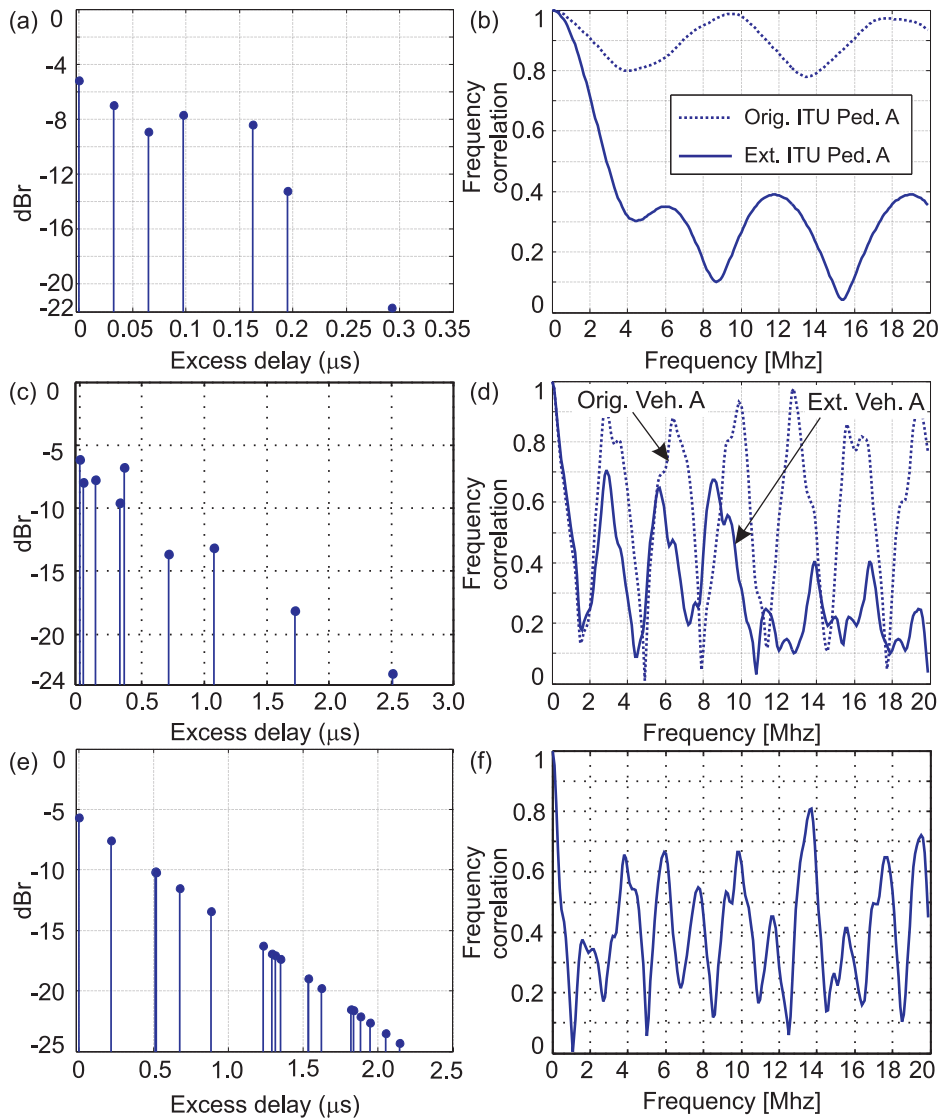
Figure 2.16: (a) Ext. ITU Ped. A PDP. (b) Orig. & Ext. ITU Ped. A FCF. (c) Ext. ITU Veh. A PDP. (d) Orig. (in dotted line) & Ext. ITU Veh. A FCF. (e) COST259 TU PDP. (f) COST259 TU FCF. All the PDPs are shown on a 32.55 ns sampling grid corresponding to a sampling rate of 30.72 MHz.

The G-factor Cumulative Density Function (CDF) curves for the investigated deployment scenarios are illustrated in Figure 2.15. These curves have been obtained from system-level simulations [59], [49]. The G-factor is approximately 8 dB higher for the Micro-cell scenario as compared to the Macro-cell environment at the median value. This behavior is observed due to the higher isolation between the Micro cells. The Micro out-to-in scenario will be denoted as Micro case 1 hereafter.

2.14 Reference Multipath Channel Models

We investigate the potential of the FDAS schemes by considering three well known multipath radio channel profiles, which differ in terms of the *coherence bandwidth*. The channel impulse response is based on a *sample spaced* tapped-delay line implementation, corresponding to the LTE

Table 2.4: Rms delay spread and the coherence BW $\left(B_c \approx 1/(2\pi \cdot \sigma_\tau) \right)$, corresponding to the correlation level of 0.7 [43].

Channel model	Rms delay spread (σ_τ) [μs]	Coherence BW (B_c) [kHz]
Ext. ITU Ped. A	0.06	2.65e3
Ext. ITU Veh. A	0.36	442.1
COST259 TU	0.5	318.3

sampling frequency. Each channel profile is characterized by the following parameters: number of taps in the impulse response, time delay relative to the first tap, average power relative to the strongest tap, and the power spectrum of each tap.

The three channel profiles considered in this study are as follows: Extended (Ext.) ITU Ped. A, Ext. ITU Veh. A [43] and the COST259 Typical Urban (TU) [83]. The first two models are extensions of the original ITU channel models that were proposed for use within 5 MHz [84], [85]. The Ext. ITU Ped. A profile (denoted as Ped. A) consists of 7 taps and represents relatively flat-fading conditions within the considered bandwidth (20 MHz). The Ext. ITU Veh. A profile (denoted as Veh. A) has 9 taps while the TU profile consists of 20 taps. The latter two channel profiles represent highly frequency-selective conditions. The detailed list of tapped-delay line parameters for the considered channel models are provided in Table A.1.

It is important that the channel models have realistic frequency correlation properties as the evaluation of wideband system concepts that exploit frequency dependent characteristics such as FDAS is highly dependent on it [43]. In this regard we investigate the Frequency Correlation Function (FCF) curves of the considered channel profiles in Figure 2.16. The FCF is defined as the Fourier Transform of the PDP [43]. Figure 2.16 also illustrates the stem plots of the considered PDPs, as well as the FCF curves of the original ITU channel models.

Propagation modeling based studies as well as measurement data collected for the wideband channel indicate that the channel correlation should normally decay steadily with increasing frequency separation [43]. This implies that a high order of frequency selection diversity is available in a wideband channel. However, observing the FCF curves of the original ITU channel models in Figure 2.16 (b) and (d) we can see an apparent periodicity in their frequency correlation properties, with high correlation levels even for large frequency separations. This behavior can significantly deteriorate the FDAS gain potential due to reduction in the order of frequency selection diversity, e.g., in Figure 2.16 (b) the diversity order is reduced by a factor of three. In comparison, the FCF curves of the extended ITU channel models have reasonable frequency correlation properties within the maximum considered system bandwidth of 20 MHz.

Table 2.4 lists the rms delay spread and the coherence BW of the considered channel models, based on a well known measure of coherence BW [43]. As can be seen from the FCF behavior as well as the tabulated values, the Ext. ITU Ped. A has the largest coherence BW among the considered models, while the TU and Veh. A profiles have similar coherence BW. Further, as the TU model is characterized by an exponentially decaying PDP, the minima of its FCF is located close to the peak value. However, due to the irregular shape of the PDP of the Ext. ITU Veh. A profile its minima is located further away from the the peak value.

2.15 Key Performance Indicators

Being a system-level study the Key Performance Indicators (KPIs) are as follows; average cell throughput, spectral efficiency, average user throughput and coverage. The average cell throughput $\overline{TP}_{cell}$ is defined as:

$$\overline{TP}_{cell} = \frac{\text{total bits correctly delivered}}{\text{simulation time}} \quad , \tag{2.24}$$

where the numerator is an aggregate of the correctly delivered bits at the MAC layer over all active sessions in the system. The spectral efficiency measured at the MAC layer is given by:

$$\eta_{spectral} = \frac{\overline{TP}_{cell}}{BW} \quad . \tag{2.25}$$

The average user throughput for the ith user is defined as:

$$\overline{TP}_i = \frac{\text{bits correctly delivered to user } i}{\text{session time}} \quad . \tag{2.26}$$

Note that the session time of the user depends on the traffic model. Coverage, denoted by $\overline{TP}_{cov}$, is determined from the CDF of the average user throughput taken over all the completed sessions. It is defined as the data rate with 95% coverage, i.e., only 5% of users experience a lower average data rate than the coverage rate. This KPI is a measure of the fairness in throughput distribution provided by the packet scheduler. A detailed analysis of the statistical significance of KPIs obtained for a set of reference simulation scenarios is provided in Appendix D.

Chapter 3

Frequency Domain Adaptation and Scheduling: Concept and Algorithm Design

3.1 Introduction

This chapter describes the FDAS concept in detail including the algorithm design aspects. The key terms and definitions associated with this study are also introduced here. The chapter is organized as follows: We begin by introducing the FDAS concept in Section 3.2. Section 3.3 introduces the important terms, while Section 3.4 discusses the design of the Ref scheme. Section 3.5 introduces the design of frequency-domain LA schemes, while Section 3.8 covers the design of PS algorithms that can utilize multi-user diversity in time and frequency. Finally, Section 3.9 discusses the design of low bandwidth CQI schemes that can support FDAS.

3.2 The FDAS Concept

Time-domain adaptation and scheduling is sufficient to exploit the radio channel dynamics in a flat-fading scenario. However, it cannot provide the full spectral efficiency potential in a frequency-selective environment, whereas FDAS can improve performance in such a scenario [63]. In general, depending on the ratio of channel coherence BW to system BW, either time-domain or frequency-domain adaptation is required to maximize the spectral efficiency, as shown in Table 3.1.

In this study FDAS consists of cross-layer optimization, as PHY layer measurements (CQI reports) are used in resource allocation decisions at the MAC layer. Further, it involves multi-user packet scheduling, and link adaptation based on bandwidth and/or power adaptation as well as AMC. Similarly, HARQ is integral to the FDAS concept as it can improve the spectral efficiency over a fading channel. FDAS can be classified into sub-carrier based adaptation and *sub-band based adaptation*, depending on the scheduling resolution in the frequency domain.

Table 3.1: The potential of spectral efficiency enhancement through the use of time/frequency-domain scheduling and adaptation techniques, depending on the ratio of channel coherence BW to system BW.

$\frac{\text{coherence BW}}{\text{system BW}}$	*Time-domain adaptation*	*Frequency-domain adaptation*
≥ 1 (Narrow band channel)	Full potential	No additional gain
$\ll 1$ (Wideband channel)	Reduced potential	Full potential

3.2.1   State-Of-The-Art of Sub-Carrier Based Adaptation for OFDMA

LA in time and frequency based on OFDM sub-carrier level granularity has been studied in detail in literature, e.g., see [30], and the references therein. When an OFDM signal is transmitted over a time-dispersive channel the different sub-carriers will experience diverse fading conditions, as seen in Figure 1.6. In such a scenario an adaptive frequency-domain LA scheme will normally select only those sub-carriers for transmission that are experiencing constructive fading [32]. An example of a Threshold based LA scheme is illustrated in Figure 3.1, which does not allocate those portions of system BW that are experiencing a lower SINR than the Threshold value.

According to theory, distribution of power according to the *Water-filling* principle maximizes the capacity of an OFDM system [16]. It states that under a given power constraint the overall information rate of an arbitrary channel is maximized by transmitting more power where the channel attenuation and noise are weaker. In other words, a higher transmission rate should be used when the channel is experiencing favorable conditions and vice versa [30].

Several studies have proposed both optimal and sub-optimal resource allocation schemes for OFDM, based on sub-carrier level granularity, see e.g., [23], [37], [50], [86], and the references therein. For the single-user case resource allocation is normally divided into two steps, selection of sub-carriers and the appropriate MCS (*sub-carrier and bit loading*) followed by adaptive power allocation (*power loading*). Single-user adaptive resource allocation has been discussed in [87], [88] while the multi-user scenario is investigated in [89], [50]. The proposed schemes typically assign data rate to different sub-carriers on the basis of experienced SNR. Often sub-carriers with
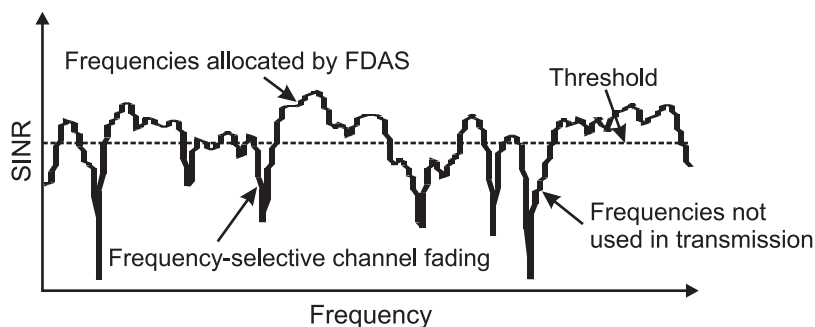

Figure 3.1: Illustration of the resource allocation executed by a frequency-domain LA algorithm. The Threshold based LA scheme does not allocate those portions of system BW where the channel quality is below the Threshold value.

very low SNR are not used at all. Similarly, the data rate adaptation per OFDM symbol is usually done by varying the size of signal constellation, e.g., from Binary Phase Shift Keying (BPSK) to 256 Quadrature Amplitude Modulation (QAM) or even larger signal sets, [52].

Most of the previous studies are dealing with link-level performance of the adaptive schemes. Further, they do not include features such as HARQ and channel coding in the analysis, which are important in the context of modern wireless systems. Similarly, the impact of dynamic other-cell interference is not included. Another significant limitation of these studies is that they mostly assume ideal channel feedback on a sub-carrier basis, which cannot be achieved in practice. As an example, using LTE assumptions there are 600 useful sub-carriers within the system BW of 10 MHz [14]. If a 5-bit CQI report (similar to HSDPA) is fed back for each sub-carrier every 0.5 ms, the required UL overhead will be 6 Mbps. Such a large overhead will significantly reduce the useful data rate in UL. Moreover, the computational complexity of optimal sub-carrier based loading algorithms is quite large, since resource allocation is a non-linear combinatorial optimization problem in which there is no general approach to achieve optimality [90], [56].

The DL resource allocation in a cellular system needs to be updated frequently, due to factors such as channel quality variation induced by mobility, traffic fluctuations and variations in the inter-cell interference from neighboring cells in a reuse 1 network. If sub-carrier based resource allocation is employed the DL control overhead (AT) will also become prohibitively large, as the UE needs to be informed about the MCS format and power allocation on a sub-carrier basis. Due to these practical concerns we will focus on the performance of sub-optimal *sub-band based adaptation* techniques. This strategy has also been adopted in LTE [14] and WiMAX [15].

3.2.2   Sub-Band Based Adaptation

In order to reduce the signaling overhead and the complexity of DL resource allocation, the system bandwidth is divided into a number of equal-width chunks/sub-bands, as illustrated in Figure 3.2. Each sub-band, denoted as RB, consists of a fixed number of adjacent OFDM sub-carriers. The granularity of adaptation and scheduling in the frequency-domain is determined by the RB width, which implies that FDAS can allocate at most a single MCS and a single user to each RB.

The rationale behind sub-band adaptation is based on the observation that the channel transfer factors and consequently the SNRs of neighboring sub-carriers are highly correlated. Thus, only marginal performance degradation is expected by introducing blocks of sub-carriers which are smaller than the channel coherence BW. Mathematically speaking, if the ratio of RB width
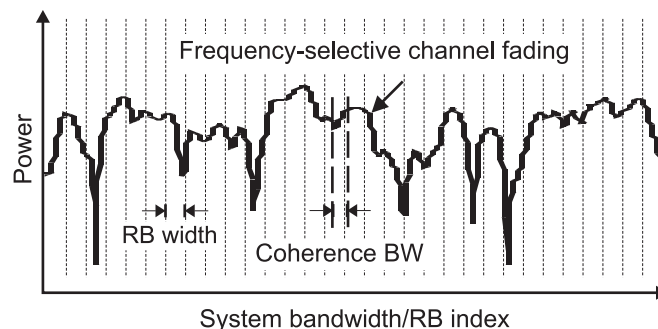

Figure 3.2: Relationship between system bandwidth and the RB width. In this example the RB width is in the order of the coherence BW of the channel.
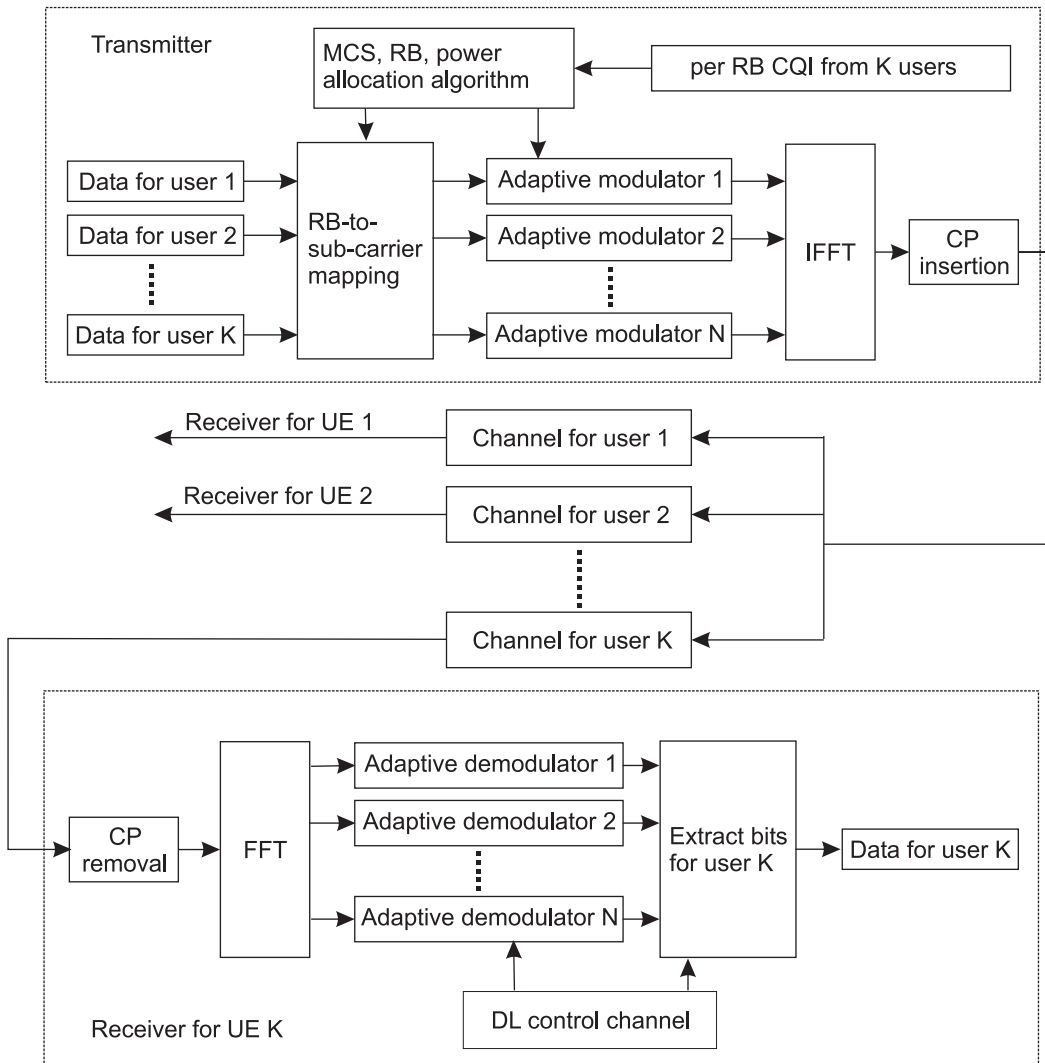
Figure 3.3: System model for the multiuser adaptive OFDMA transmission scheme, where the minimum scheduling resolution is one RB. The figure has been adapted from [91].

to coherence bandwidth is $\ll 1$, each RB will experience nearly flat-fading characteristics, otherwise frequency-selective fading is seen within the RB [19]. In the latter case some of the FDAS potential will be lost as the SNR peaks will be reduced. To summarize, the RB size in time and frequency should ideally be determined using the minimum coherence time (dependent on maximum supported speed) and the minimum coherence bandwidth respectively. The trade-off between RB width and the achievable FDAS performance will be investigated in this study.

A schematic diagram of the multi-user adaptive OFDMA transmission scheme is illustrated in Figure 3.3, where K denotes the total number of active users, and N denotes the total number of sub-carriers. At the transmitter, the serial data streams from the K users are fed into the RB-to-sub-carrier mapping block. The assignment of UEs to RBs is determined by the FDAS algorithm, based on factors such as the CQI reports. The adaptation process also determines the MCS format as well as the power allocation for each RB. This information is used to configure the adaptive modulators shown in Figure 3.3, and the input data is modulated accordingly. The complex symbols at the output of the adaptive modulators are transformed into time-domain samples by the IFFT block. Next, a cyclic prefix is prepended to each OFDM symbol to ensure orthogonality in a multipath

environment. The transmit signal then passes through separate frequency selective fading channels to the scheduled UEs.

At the receiver, the cyclic prefix is removed to eliminate ISI, and the time samples of the Kth user are transformed by the FFT block into modulated symbols. The MCS format and power allocation information carried by the DL control channel (AT) is used to configure the adaptive demodulators, while the RB allocation related information is used to extract the demodulated bits from the sub-carriers assigned to the Kth user.

3.2.2.1 State-Of-The-Art of Sub-Band Based Adaptation

Sub-band based adaptation for a single-user OFDMA scenario has previously been investigated in [92]. It has been reported that the throughput performance of such a scheme is quite similar to the sub-carrier bit loading algorithms, and is achieved at a fraction of the computational complexity as well as signaling overhead. This study is based on the HIPERLAN/2 system and employs a discrete set of MCS values.

In [93], a sub-band based adaptation algorithm has been proposed for the multi-user OFDMA scenario. The algorithm minimizes the total required transmit power while satisfying multiple users data rate and BER requirement. This link-level study reports a gain of 4 dB in average bit SNR over the non-adaptive scheme. The computational complexity of the proposed algorithm is still quite large due to the joint optimization of sub-carrier/bit allocation and power allocation under the total power constraint. The simulation assumptions are based on the Wireless LAN IEEE 802.11a system. The analysis is based on relatively low number of sub-carriers, e.g., around 50.

In [91] and [90] decentralized multiuser resource allocation algorithms have been proposed where each UE attempts to occupy the sub-band with the highest average channel gain. These studies propose techniques to resolve conflicts arising from multiple users staking claim to the same sub-band. Further, each user is allocated an equal number of sub-bands, and adaptive modulation is applied on a sub-band basis. Simulation results show a gain in link-level SNR of around 3 dB-4 dB over the non-adaptive scheme. Further, these studies do not include the gain from channel coding and HARQ combining.

In [94] the potential of multi-user frequency-domain adaptation and scheduling based on the sub-band approach has been investigated under realistic system assumptions. This system-level study concludes that significant gains are possible in terms of both cell throughput (around 70%) and data-rate fairness over time-domain only scheduling. However, some of the assumptions are not in line with LTE, e.g., the system BW is set at 100 MHz. Moreover, single-user optimization is not included in the analysis. Further, the impact of factors such as speed, HARQ management strategy, limited CQI, antenna configuration, deployment scenario, etc., have not been investigated in [94]. Thus, it appears that sub-band based adaptation for OFDMA radio access can provide an attractive trade-off between complexity and performance. We now proceed to undertake a detailed analysis of this technique, based on a modern cellular system framework.

Table 3.2: Classification of the investigated scenarios based on the FDM order.

FDM order	Scheme
1	FDLA, Ref
> 1	FDPS

3.3 Investigated FDAS Scenarios

Two general FDAS scenarios are included in the analysis, which differ in terms of the allowed FDM order, i.e., number of users that can be multiplexed in frequency, on a TTI basis. These are Frequency-Domain Link Adaptation (FDLA), and Frequency-Domain Packet Scheduling (FDPS). In order to determine the potential of the FDAS schemes over time-domain only adaptation and scheduling a suitable design for the Reference (Ref) scheme has been proposed. The classification of the investigated scenarios is given in Table 3.2.

3.3.1 Frequency-Domain Link Adaptation - Definition

In this scenario, the eNode-B is allowed to transmit to only a single-user in each TTI. The user selection criterion is dependent on the time-domain PS algorithm, e.g., opportunistic scheduling in time. The transmission parameters over the radio link, e.g., RB indices, transmit power for each RB, MCS, are determined by the FDLA algorithm [46].

3.3.2 Frequency-Domain Packet Scheduling - Definition

FDPS or frequency localized transmission refers to the scenario where the scheduler can exploit multi-user diversity in time and frequency, i.e., user multiplexing in frequency is allowed. The packet scheduler interacts with LA and HARQ entities to determine the mapping of UEs to RBs.

3.4 Reference Scheme - Definition

The performance of the FDLA and the FDPS schemes is compared against the Ref scheme, which is characterized by frequency-blind transmission to a single UE on a TTI basis. In this case the CQI overhead can be reduced to a single wideband report per UE, similar to HSDPA. Thus, the CQI overhead is limited to e.g., 5 bits/CQI report [2], resulting in the CQI rate of 10 kbps. In terms of scheduling the Ref scheme can benefit from opportunistic scheduling in time-domain. The aim is to optimize the design of the Ref scheme, in order to make a fair comparison with the FDAS schemes.

```
sortCQI(1:nPRBs) = sort CQI values in descending order;
sortedIndices(1:nPRBs) = Indices of the sorted CQI values;
maxTP = 0;
PRBallocVector = zeros(1:nPRBs);
powerAllocVector = zeros(1:nPRBs);
nActPRBs = 0;
for s=1:nPRBs
    tempPowerVector=[ ];
    tempPowerVector = P_total/s;
    calculate TP_eff,FDLA-EP using sortCQI(1:s), tempPowerVector and (2.5)
    or (2.6);
    if ( TP_eff,FDLA-EP > maxTP )
        maxTP = TP_eff,FDLA-EP ;
        nActPRBs = s;
    end
end
for r=1:nPRBs
    if ( r is found in sortedIndices(1:nActPRBs) )
        PRBallocVector(r) = 1;
        powerAllocVector(r) = P_total/nActPRBs;
    end
end
```

Figure 3.4: Pseudo-code of the FDLA-EP algorithm, based on Matlab notation. The output of the algorithm is the set of optimal transmit parameters $\{\dot{\mathbf{I}}^*, \dot{\mathbf{P}}^*\}$, as given by (3.1).

3.5 FDLA Algorithm Design

Sub-band based FDLA for an OFDMA system has been investigated previously in [95], [92] and [96]. The key components of adaptive LA design are the determination of adaptation thresholds, adaptation rate and the choice of a suitable CQI metric [96]. Adaptation thresholds are required to switch between the available transmission *modes*, e.g., MCS formats.

The FDLA algorithm aims at optimization of the transmit throughput under the constraints of total power and the target first transmission BLER. As mentioned earlier in Section 2.5, the FDLA algorithm selects the appropriate set of transmit parameters, given by $\{\dot{\mathbf{I}}^*, \dot{\mathbf{P}}^*, \dot{\mathbf{MCS}}^*\}$, for each UE. The decision is based on available CQI reports, as well as HARQ status. As we will be using the modified Shannon Theorem based model for AMC the $\dot{\mathbf{MCS}}$ term is ignored in the analysis hereafter.

Two FDLA algorithms are proposed that differ in terms of the power allocation strategy. These are the simple equal-power distribution based scheme and the advanced Water-filling power distribution [81] based FDLA algorithm.

3.5.1 Equal-Power Distribution Based FDLA

The equal-power based link throughput optimization (FDLA-EP) is given by:

$$\{\dot{\mathbf{I}}^*, \dot{\mathbf{P}}^*\} = \operatorname*{argmax}_{\dot{\mathbf{I}}, \dot{\mathbf{P}}} \left\{ TP_{eff, FDLA-EP}\left(\mathbf{C}\dot{\mathbf{Q}}\mathbf{I}, \dot{\mathbf{I}}, \dot{\mathbf{P}}\right) \right\} \quad , \tag{3.1}$$
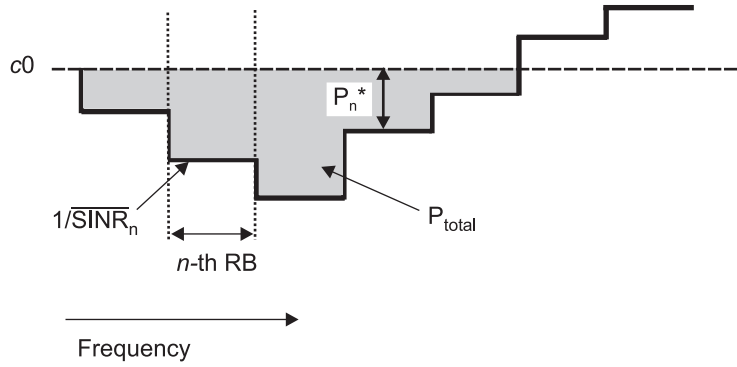
Figure 3.5: Illustration of the power distribution in the frequency-domain based on the FDLA-WF scheme. The figure is based on the slides prepared by T. E. Kolding.

based on the following power allocation strategy:

$$
P_n^* = \begin{cases} \frac{1}{nActRBs} \cdot P_{\text{total}} & \text{if} \quad I_n^* = 1 \quad, \\ 0 & \text{otherwise} \quad. \end{cases} \tag{3.2}
$$

The terminology has been introduced earlier in Section 2.5. The SINR of RB n used in LA is denoted by $\overline{SINR}_{la,n}$, and given by (2.4), where $\overline{SINR}_n$ is replaced by CQI_n. Further, if OLLA is enabled CQI_n is adjusted according to the OLLA offset, as described in Subsection 2.5.2. In case of single-block transmission, $TP_{eff,FDLA-EP} = TP_{SB}$, and (2.5) is used to calculate the supported throughput. Similarly, (2.6) gives the total throughput when multi-block transmission is employed. The pseudo-code for the FDLA-EP algorithm is given in Figure 3.4. This scheme has been used in most of the LTE contributions, since it is relatively simple to implement and it can limit the interference variations in the cellular network.

3.5.2   Water-Filling Power Distribution Based FDLA

According to the Water-filling scheme the power on the nth RB is given by [38]:

$$
P_n^* = \begin{cases} c_0 - \frac{1}{\overline{SINR}_n} & \text{if} \quad \left(c_0 - \frac{1}{\overline{SINR}_n}\right) > 0 \quad, \\ 0 & \text{otherwise} \quad, \end{cases} \tag{3.3}
$$

where c_0 is the water-level that must be chosen according to the total power constraint:

$$
P_{\text{total}} \quad = \quad \sum_{i=1}^{nRBs} P_n^* \quad. \tag{3.4}
$$

The RB allocation vector ($\dot{\mathbf{I}}^*$) is determined from the knowledge of $\dot{\mathbf{P}}^*$, as follows:

$$
I_n^* = \begin{cases} 1 & \text{if} \quad P_n^* \neq 0 \quad, \\ 0 & \text{otherwise} \quad. \end{cases} \tag{3.5}
$$

Figure 3.5 depicts the working of the FDLA-WF algorithm. It potentially requires additional DL control overhead, in order to communicate the unique reference power on each RB to the UE. The

```
sortInvSINR(1:nPRBs) = sorted 1/ SINRₙ values in descending order;
sortedIndices(1:nPRBs) = Indices of the sorted 1/ SINRₙ values;
maxTP = 0;
PRBallocVector = zeros(1:nPRBs);
powerAllocVector = zeros(1:nPRBs);
tempPowerAllocVec2 = [ ];
nActPRBs = 0;
for s=1:nPRBs
      nTemp=1;
      pwRem = Ptotal;
      nTempAllocPRBs = 1;
      tempPowerAllocVec1 = zeros(1:s);
      while (pwRem > 0) & (nTemp < s)
            pwAdd = min(pwRem, (sortInvSINR(nTemp+1) -
            sortInvSINR(nTemp))*nTemp);
            pwRem = pwRem - pwAdd;
            tempPowerAllocVec1(1:nTemp) = tempPowerAllocVec1(1:nTemp)
            + pwAdd/nTemp;
            nTemp = nTemp +1;
            if (pwRem > 0)
                    nTempAllocPRBs = nTemp;
            end
      end
      tempPowerAllocVec1(1:nTempAllocPRBs) =
      tempPowerAllocVec1(1:nTempAllocPRBs) + pwRem/s;
      calculate TPeff,FDLA-WF using 1/sortInvSINR(1:nTempAllocPRBs),
      tempPowerAllocVec1(1:nTempAllocPRBs)  and either (2.5) or (2.6);
      if ( TPeff,FDLA-WF > maxTP )
            maxTP = TPeff,FDLA-WF ;
            nActPRBs = nTempAllocPRBs;
            tempPowerAllocVec2(1:nActPRBs) =
            tempPowerAllocVec1(1:nActPRBs);
      end
end
for r=1:nPRBs
      if ( r is found in sortedIndices(1:nActPRBs) )
            x = Index of r in sortedIndices(1:nActPRBs);
            PRBallocVector(r) = 1;
            powerAllocVector(r) = tempPowerAllocVec2(x);
      end
end
```

Figure 3.6: Pseudo-code of the FDLA-WF algorithm, based on Matlab notation.

power allocation is quantized to a finite resolution, denoted by $resWF$. The quantization process is carried out as follows:

$$\bar{P}_n = \text{round}\left(\frac{P_n^*}{resWF}\right) \cdot resWF \quad ,$$

$$\hat{P}_n = \left(\frac{\bar{P}_n}{\sum_{i=1}^{nActRBs} \bar{P}_n}\right) \cdot P_{\text{total}} \quad , \tag{3.6}$$

where $\bar{P}_n$ and $\hat{P}_n$ denote the power after quantization and normalization respectively.   It is clear that the FDLA-WF algorithm will only be used in practice if it can provide a significant performance gain over the FDLA-EP scheme. The pseudo-code of the FDLA-WF algorithm is shown in

Figure 3.6.

3.5.3 Gain Potential of FDLA-WF Over FDLA-EP, based on a Simple Two-Channel Model

We now evaluate the gain potential of the FDLA-WF algorithm over the FDLA-EP scheme, using a simple two-channel model and for the single user case. Channel 1 or RB 1 is characterized by $SINR_1$, provided that $\frac{P_{total}}{2}$ is used as the reference power. Similarly, Channel 2 is characterized by $SINR_2$, based on the reference power being equal to $\frac{P_{total}}{2}$. Without loss of generality we will assume that $SINR_1 > SINR_2$.

The optimum power allocation based on the FDLA-WF algorithm can be found by using (3.3), as follows:

$$
\begin{aligned}
P_1 &= \max\left(0, \min\left(1, 0.5 \cdot P_{total} \cdot \left(\frac{1}{2 \cdot SINR_2} - \frac{1}{2 \cdot SINR_1} + 1\right)\right)\right) \quad, \qquad (3.7)\\
P_2 &= P_{total} - P_1 \quad. \qquad\qquad\qquad\qquad\qquad\qquad\qquad\qquad\qquad\qquad (3.8)
\end{aligned}
$$

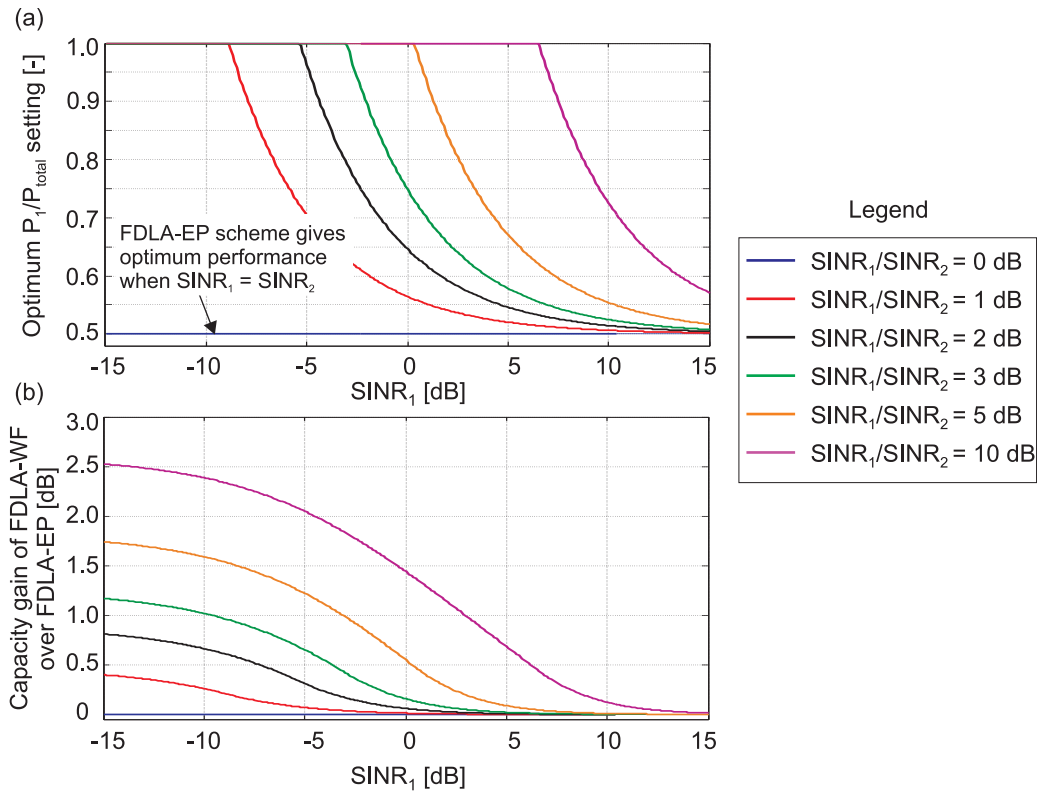The normalized capacity achieved by the different FDLA algorithms is given by:

Figure 3.7: (a) The variation of the FDLA-WF power setting on the best channel relative to the total power, for a simple two-channel model. (b) The capacity gain of the WF power allocation relative to the EP power allocation scheme.
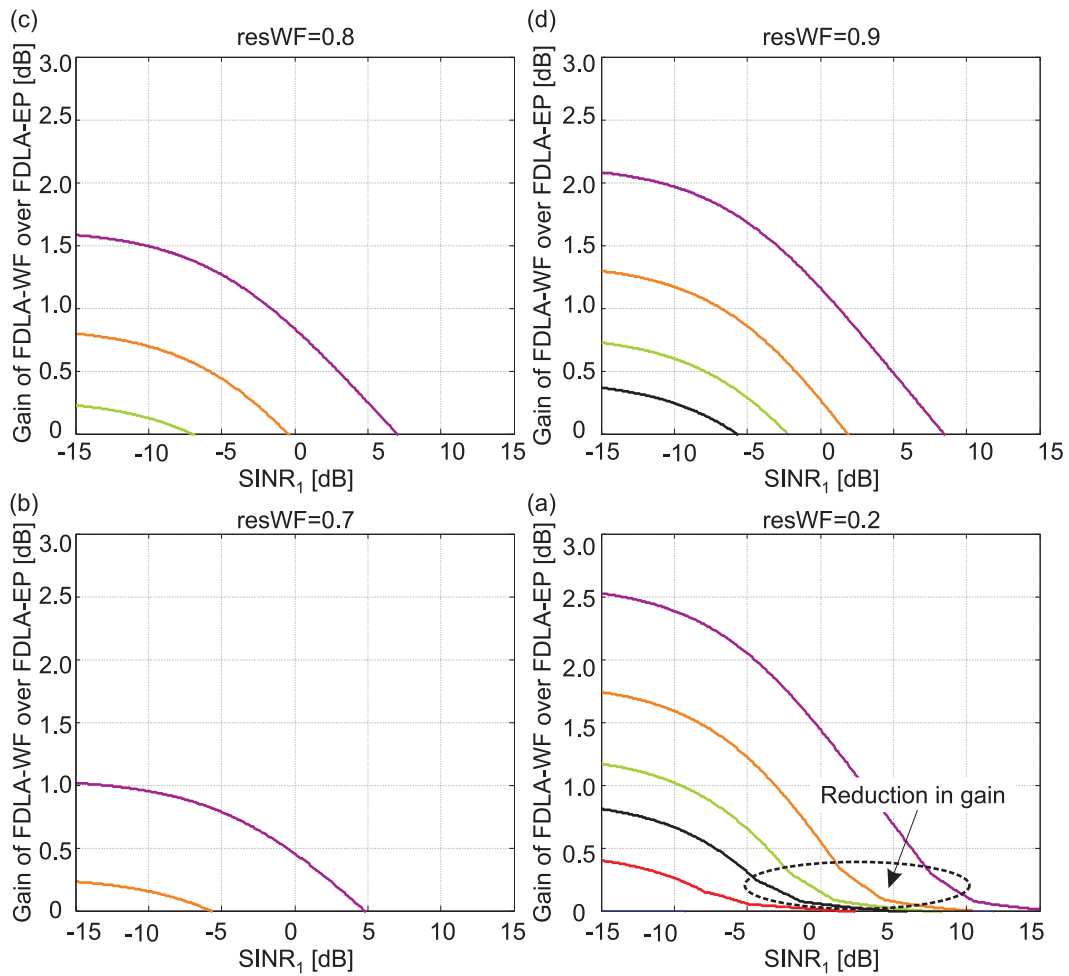
Figure 3.8: Impact of $resWF$ on the FDLA-WF performance. The legend in this figure is the same as that used in Figure 3.7.

$$C_{FDLA-EP} = \log 2(1 + \mathrm{SINR}_1) + \log 2(1 + \mathrm{SINR}_2) \quad , \tag{3.9}$$

$$C_{FDLA-WF} = \log 2\left(1 + \frac{P_1 \cdot 2 \cdot \mathrm{SINR}_1}{P_{\text{total}}}\right) + \log 2\left(1 + \frac{P_2 \cdot 2 \cdot \mathrm{SINR}_2}{P_{\text{total}}}\right). \tag{3.10}$$

Figure 3.7 (a) shows the optimum FDLA-WF power for the best channel relative to the total power $\left(\frac{P_1}{P_{\text{total}}}\right)$, while Figure 3.7 (b) illustrates the capacity gain of the WF power allocation over the EP allocation scheme. These results indicate that the optimum power setting on the best channel depends on the absolute power level of Channel 2. It is more useful to allocate larger proportion of the power on Channel 1 when SINR_1 is low, due to the near-linear mapping between SINR and throughput, as given by the Shannon theorem. Further, when $\mathrm{SINR}_1 = \mathrm{SINR}_2$, the EP algorithm provides optimum performance. The theoretical maximum capacity gain of WF power allocation over the EP allocation for the simple channel model considered here is $3\,\mathrm{dB}$, which is obtained from (3.9) and (3.10).

Figure 3.8 illustrates the impact of the $resWF$ parameter on performance, based on the simple two-channel model. The results show that it is difficult to predict the behavior without a detailed numerical evaluation, due to the iterative nature of the WF algorithm. In general, there are several values of $resWF$ that can provide the optimum performance.

In addition to the equal power and water-filling schemes, the inverse water-filling power distribution scheme has also been investigated in [46]. The study has shown that the equal-power scheme provides the best trade-off between performance and complexity, especially under frequency-selective fading conditions.

3.6   Link Adaptation for the Reference Scheme

The Ref scheme is based on transmission to a single user in each TTI. The selection of the user is based on the scheduling policy. LA for the Ref scheme is based on frequency-blind transmission. Thus, the transmit throughput is given by:

$$TP_{Ref} \quad = \quad BW \cdot \log 2\left(1 + \min\left(\frac{\overline{SINR}_{block,1}}{10^{4/10}}, 10^{18/10}\right)\right) \quad , \tag{3.11}$$

where $\overline{SINR}_{block,1}$ is the single-block geometric average SINR evaluated over the entire system BW.

3.7   Selection of the Averaging Technique for LA

Earlier we have mentioned that the geometric averaging technique has been employed to calculate the CQI in (2.1), as well as to calculate the effective SINR over a RB $(\overline{SINR}_i)$ in (2.3). We now present results to support the selection of this averaging technique. The performance of the FDLA-EP algorithm is evaluated for both single and multi-block transmission cases. Further, in terms of averaging techniques linear and geometric averaging are investigated.

The 10 MHz bandwidth is divided into 24 RBs, which used to be the default assumption in LTE. The current assumption is that there are 50 RBs within 10 MHz. However, only 25 CQI reports are forwarded by the UE, in order to reduce the CQI overhead. Further, the TTI duration has now been increased to 1.0 ms [14]. Note that we have not used these new settings in the initial
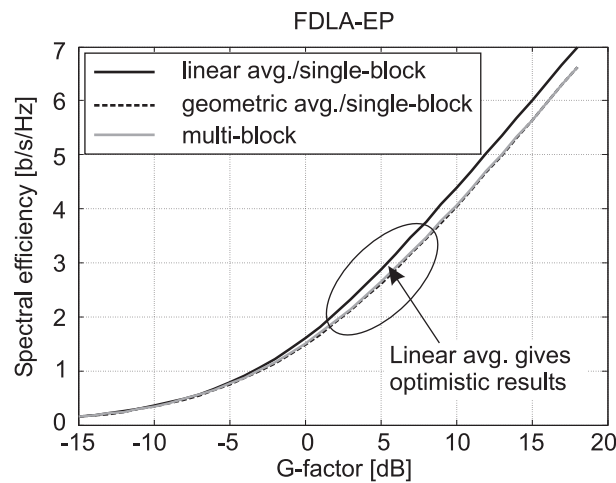

Figure 3.9: Average user throughput as a function of the G-factor, based on the 1x2 antenna scheme, RR scheduler and Macro case 1 scenario.

evaluation of FDAS. We do not expect the new parameter settings to have a major impact on the conclusions. This is also supported by the latest reported LTE system-level results, e.g., see [97].

A simplified simulation methodology has been used in this analysis. An imaginary channel model is employed, which is highly frequency-selective, e.g., each RB is experiencing ideal Rayleigh fading statistics. Further, the fading is assumed to be independent between the RBs. The simple infinite buffer traffic model is employed in this analysis. Time-domain scheduling is based on the simple RR priority metric. The simulation methodology consists of the following steps:

1. The per RB SINR statistics are calculated for a UE, and adjusted by the G-factor (G), assuming ideal OFDM reception. Further, it is assumed that the channel is constant over the entire code block.

2. The average throughput of the UE at a given G-factor is obtained using Monte Carlo realizations of the channel. It is assumed that the per RB CQI is instantaneously available at the eNode-B without any measurement errors and with infinite resolution. Further, perfect reception of the DL and UL control channels is assumed. In terms of LA it is assumed that the system can perform ideal mapping of SINR to throughput according to the Shannon Theorem. The throughput is calculated on the basis of the selected block-encoding scheme, i.e., SB or MB.

3. The average cell throughput is computed by conditioning the average user throughput obtained in the previous step with the G-factor distribution for the Macro case 1 scenario.

Figure 3.9 illustrates the spectral efficiency as a function of the G-factor, for the FDLA-EP algorithm. From theory, the MB transmission scheme is optimal in terms of throughput. However, in Figure 3.9 it is seen that the linear averaging technique together with SB transmission gives a higher spectral efficiency than the MB case, when the G-factor is above 0 dB. The curve for geometric averaging together with SB transmission is just below the MB curve. Similar trends were observed with the FDLA-WF algorithm. It was concluded that the linear averaging technique gives an optimistic estimate of the throughput performance when it is used in conjunction with the Shannon Theorem. Therefore, the geometric averaging technique will be employed in the single-cell model based evaluation.

3.7.1 Cell Throughput Gain of FDLA over Reference based on Ideal System Settings

Next, we evaluate the cell throughput gain of FDLA over Ref based on ideal system settings. The analysis will be used to benchmark performance results that will be obtained from the more detailed system model. The simplified simulation methodology introduced in Section 3.7 will be employed here.

Figure 3.10 illustrates the cell throughput gain of FDLA over Ref for both SB and MB transmission schemes. Further, results for the 1x1 and the 1x2 MRC antenna configurations have been shown. Interestingly, FDLA-WF can only provide a marginal gain over FDLA-EP, that also when MB transmission is employed. These trends are supported by the findings based on theory that have been published in [32]. Further, MB transmission cannot provide a significant gain over SB transmission, e.g., below 5 %. The cell throughput gain of FDLA over Ref is in the order of 15% - 20% for the 1x1 case, and around 3% - 5% for the 1x2 case, depending on the block encoding

scheme. In the 1x2 MRC case the 3 dB array gain from coherent combining together with the diversity gain is able to stabilize the channel dynamics, thus reducing the gain potential of FDLA.

The low throughput gain of FDLA-WF over FDLA-EP can be explained on the basis of the Macro-cell G-factor distribution shown in Figure 2.15 and the performance curves of Figure 3.7. The majority of the UEs experience a G-factor in the range of -2 dB to 10 dB. Further, as a result of FDLA the SINR of the selected RBs is usually above the G-factor. In the region around $G = 0$ dB the FDLA-WF gain over FDLA-EP is around 5%, as seen in Figure 3.7, unless the algorithm schedules RBs with significantly different SINR conditions, e.g., a difference of 5 dB - 10 dB in the SINR of selected RBs. This event will happen rarely due to the presence of several RBs with similar channel quality. Further, the power constraint will also restrict the possibility of allocating RBs with significantly different channel quality.

Figure 3.11 illustrates detailed performance results with FDLA. Figure 3.11 (a) shows the throughput gain of FDLA over Ref, as a function of the G-factor. It is observed that FDLA *is mainly a coverage enhancing mechanism*, since the performance improvement over frequency-blind transmission is mainly seen at low G-factor values. The results can be explained on the basis of the Shannon Theorem, which tells us that at low SINR values it is beneficial to trade bandwidth for improvement in SINR, due to the near-linear mapping of SINR to throughput in this region. However, when the SINR is high it is better to transmit on the maximum possible bandwidth (due to the non-linear mapping of SINR to throughput in this region).

Figure 3.11 (b) depicts the number of RBs scheduled by FDLA as a function of the G-factor, for the 1x2 antenna configuration and MB transmission. As the RB quality can easily vary by around 10 dB for a given G-factor, the FDLA algorithm optimizes the throughput by allocating fewer RBs at low G-factor values. Further, due to the additional degrees of freedom available to the FDLA-WF algorithm (in the power domain) its RB allocation is greater than the FDLA-EP scheme when the G-factor is low. This translates into a marginal throughput gain over the FDLA-EP scheme, as seen in Figure 3.10. However, the trends are reversed when SB transmission is utilized, as WF power distribution is no longer the optimal solution.
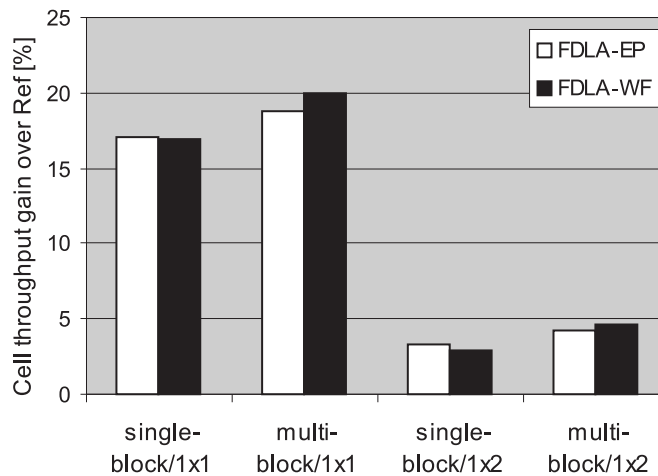

Figure 3.10: Cell throughput gain of FDLA over Ref based on ideal system settings, RR scheduler and Macro case 1 deployment scenario.
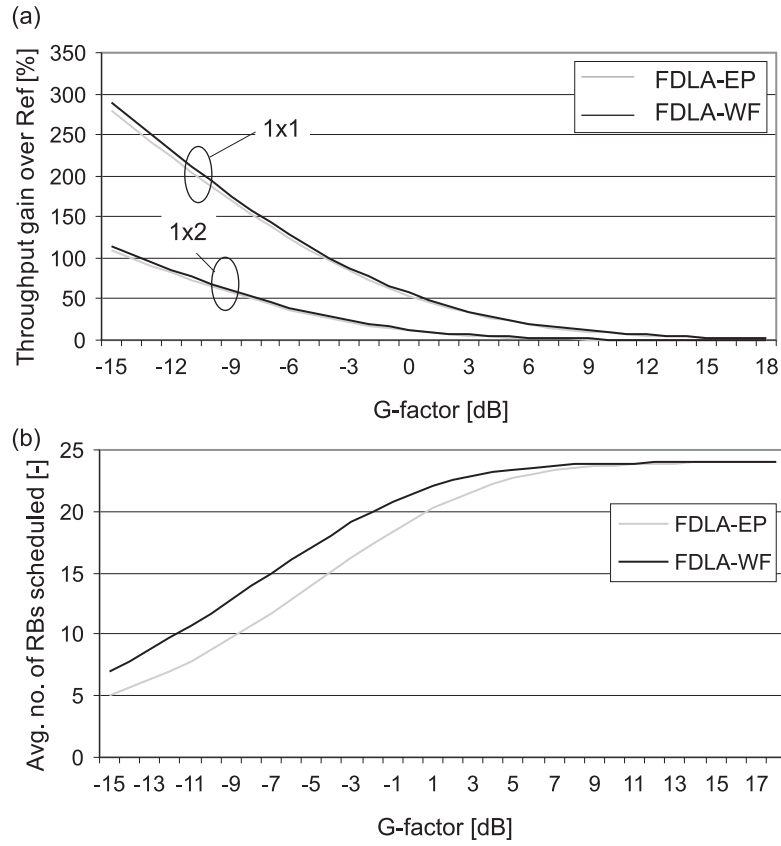
Figure 3.11: (a) Throughput gain over Ref as a function of the G-factor. The results are obtained for multi-block transmission. (b) Average number of RBs allocated as a function of the G-factor and the FDLA algorithm. The results are shown for MB transmission and the 1x2 antenna configuration.

3.8   Design of the Frequency-Domain Packet Scheduler

The optimal solution to the multiuser resource allocation problem for an OFDMA system is well known, e.g., see [54]. It requires joint optimization over all the available domains, i.e., exhaustive search over all possible combinations of transmit parameters and users. Further, WF power distribution is needed across the user domain. Optimal multi-user resource allocation at the sub-carrier level granularity is not a feasible solution, for complexity reasons [56]. Further, the optimal solution does not include the inter-user fairness aspect, which is important in a practical scenario. Similarly, the theoretical approach does not include the impact of HARQ constraints. The solution for practical scheduler design proposed in the thesis is to decouple the overall scheduler into a time-domain (TD) part followed by the frequency-domain (FD) part, as illustrated in Figure 3.12.

Scheduling consists of the following simple two step algorithm: in Step # 1, the TD scheduler selects a sub-set of N users from the available users in the cell, which are frequency multiplexed by the FD scheduler in Step # 2 [59]. This framework is attractive from a complexity point of view, since the FD scheduler only has to consider frequency multiplexing of maximum N users per TTI. The value of N is set according to potential DL signaling constraints as well as the number of
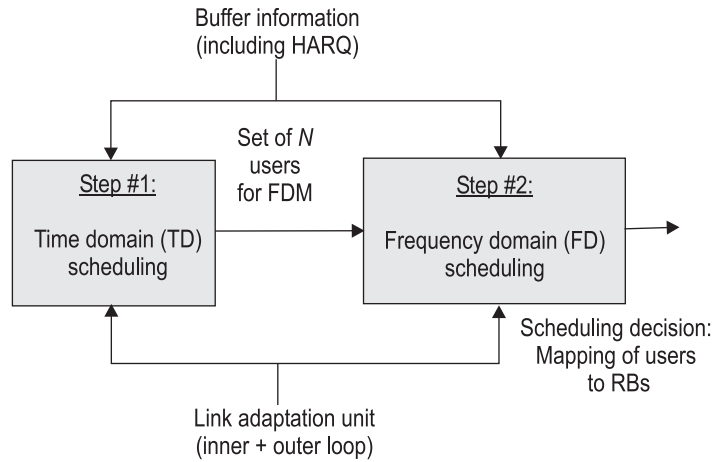
Figure 3.12: Packet scheduler framework illustrating the split between the time-domain scheduling and the frequency-domain scheduling parts [59].

RBs in the scheduling bandwidth. Assuming that the number of users in the cell, D, is larger than N, i.e., $(D > N)$, the TD scheduler provides the primary mechanism for controlling inter-user fairness, while the FD scheduler mostly tries to optimize spectral efficiency per TTI, given the input from the TD scheduler. Note that the overall scheduler performance will be sub-optimum due to the limited user diversity order at the FD scheduler. Although the scheduling framework consists of two successive steps, there is in many cases a dependency between the TD and the FD schedulers. This is especially the case for those TD schedulers which depend on average delivered throughput to users in the past (i.e., dependent on the FD scheduler decisions). Given this scheduling framework, the QoS aware scheduling algorithms studied for WCDMA/HSDPA [2] are also applicable for the TD scheduler in Step # 1, with minor modifications.

3.8.1   TD Scheduling Policies

The TD scheduler in Figure 3.12 selects the N users with the highest scheduling priority for subsequent FD scheduling, where N is a parameter for the TD scheduler. Let us denote the instantaneously supported throughput of user m as $\hat{r}_m[n]$. It is obtained from the LA unit assuming simple full bandwidth transmission, with the eNode-B transmit power divided equally among all the RBs. For each TD scheduler variant we define a priority metric for each user m, denoted by P_m. The scheduler selects those N users that at the scheduling time have the highest value of the priority metric. With a view to investigate the trade-off between cell throughput and coverage, the following TD scheduling priority metrics have been considered in the study:

- Time-Domain Round Robin (TD-RR) - This scheduler allocates an equal amount of time to each UE. In other words, the scheduler distributes the time resource among users in a fair manner.

- Time-Domain Proportional Fair (TD-PF) -

$$P_m \quad = \quad \frac{\hat{r}_m[n]}{T_m[n]} \quad , \qquad\qquad (3.12)$$

where $T_m[n]$ denotes the average delivered user throughput in the past, calculated by the recursive method outlined in [41], also given by (2.16), and n denotes the current scheduling

(a) F-FDM

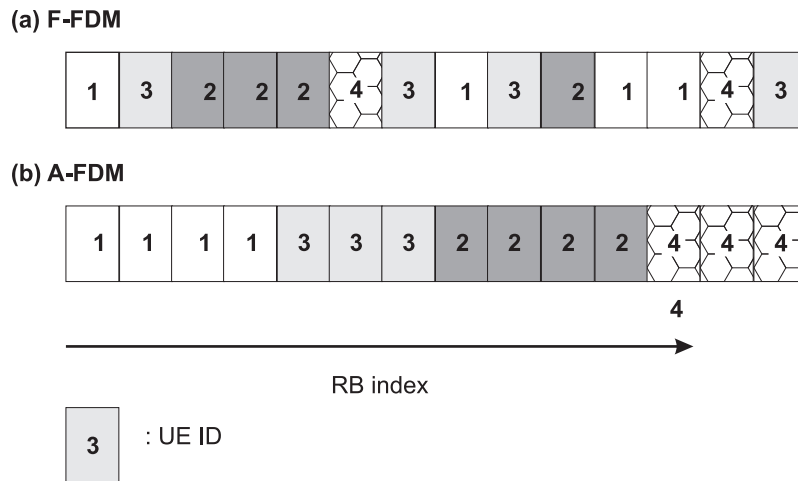**(b) A-FDM**

RB index

: UE ID

Figure 3.13: The investigated FD scheduler user-multiplexing scenarios, exemplified using 4 UEs.

interval. The average delivered throughput is based on transmitted (but not acknowledged) throughput.

- Time-Domain Maximum Throughput (TD-MT) -

$$P_m = \hat{r}_m[n] \quad .$$ (3.13)

This scheduler prioritizes users that are closer to the eNode-B. However, it provides poor inter-user fairness.

- Time-Domain Blind Equal Throughput (TD-BET) -

$$P_m = \frac{1}{T_m[n]} \quad .$$ (3.14)

This scheduling policy aims at maintaining an equal delivered throughput among all the users, irrespective of their location in the cell. Unlike the previous schedulers, it does not require a priori knowledge of the radio channel.

The set of users considered by the TD scheduler includes both users with new data as well as those with pending retransmissions. Further, users with pending retransmissions are not prioritized by the TD scheduler.

3.8.2 FD Scheduler Design

FDPS requires additional control overhead (AT) in the DL to inform the UEs about the transport format, e.g., RB allocation, MCS. The AT overhead is mainly dependent on the allowed user multiplexing flexibility at the FD scheduler. Further, the signaling information bits are typically much less spectrally efficient than data-channel bits, due to limited encoding and lack of Hybrid ARQ. Thus, besides the fully flexible FDM solution, denoted as F-FDM, we propose another solution which limits the AT overhead by applying restrictions on the FD scheduler. In this scheme the FD scheduler is restricted to allocate only adjoining RBs to a single UE. The technique is denoted as the *adjacent allocation* (A-FDM) scheme [98]. The two FD scheduler multiplexing scenarios are illustrated in Figure 3.13, and their main characteristics are listed in Table 3.3.

Table 3.3: The main characteristics of the F-FDM and the A-FDM scheduling techniques.

F-FDM	A-FDM
Full user selection diversity in the frequency-domain	Limited user selection diversity in the frequency-domain
Full averaging diversity in the frequency-domain	Limited averaging diversity in the frequency-domain
Complex AT implementation	Simple AT implementation
Known optimization techniques	Complicated optimization procedure due to the additional constraint

Next, we evaluate the AT overhead of the considered FDPS schemes. It is assumed that the number of supported RBs is known to the UE through broadcast of the system information. It is possible to encode the AT information either in a joint manner in which case the entire AT can be decoded by each UE, or separately for each UE based on code multiplexing. In case of joint encoding, the information about the total number of UEs in the current allocation is known, and it can be used to reduce the AT overhead. For the A-FDM case with joint encoding the UE only needs to know the starting index of its RB allocation, while for F-FDM the complete RB allocation pattern has to be sent. The resulting control overhead for both FDPS schemes using joint and separate encoding of the AT is illustrated in Figure 3.14. Taking the 24 RBs case as a reference, numerical evaluation shows that F-FDM requires an increase in DL overhead of up to 190% for joint encoding, and 140% for the separate encoding case (i.e., UDO=5). Due to the significant savings in DL overhead we will also include the A-FDM scheme in the analysis. In LTE the separate encoding scheme has been selected for AT transmission [14].

The goal of the FD scheduler is to determine the mapping of the N users to the available RBs. Since we will not be considering the explicit scheduling of HARQ processes initially, the design of the FD scheduler is simplified. The strategy used to manage HARQ retransmissions will be described in Chapter 7. In order to gain from the multi-user frequency diversity it is desirable to map users to those RBs where they experience relatively good channel quality. Let us denote the instantaneous throughput of user m on RB b by $\hat{r}_{m,b}[n]$. This throughput estimate is obtained from link adaptation based on the CQI report for the particular RB and assuming equal power per RB. Given this starting point we investigate the performance of the following FD scheduler options:

- Frequency-Domain Equal Resource (FD-ER) - The scheduler picks user m' for scheduling on RB b which maximizes

$$m' \;=\; \arg\max_{m} \left\{ \hat{r}_{m,b}[n] \right\} \quad , \tag{3.15}$$

subject to the constraint that a maximum of $\lceil (nRBs/N) \rceil$ RBs are allocated to each user, i.e., equal distribution of RBs among the FD multiplexed users.

- Frequency-Domain Proportional Fair (FD-PF) - It is an extension of the time domain PF
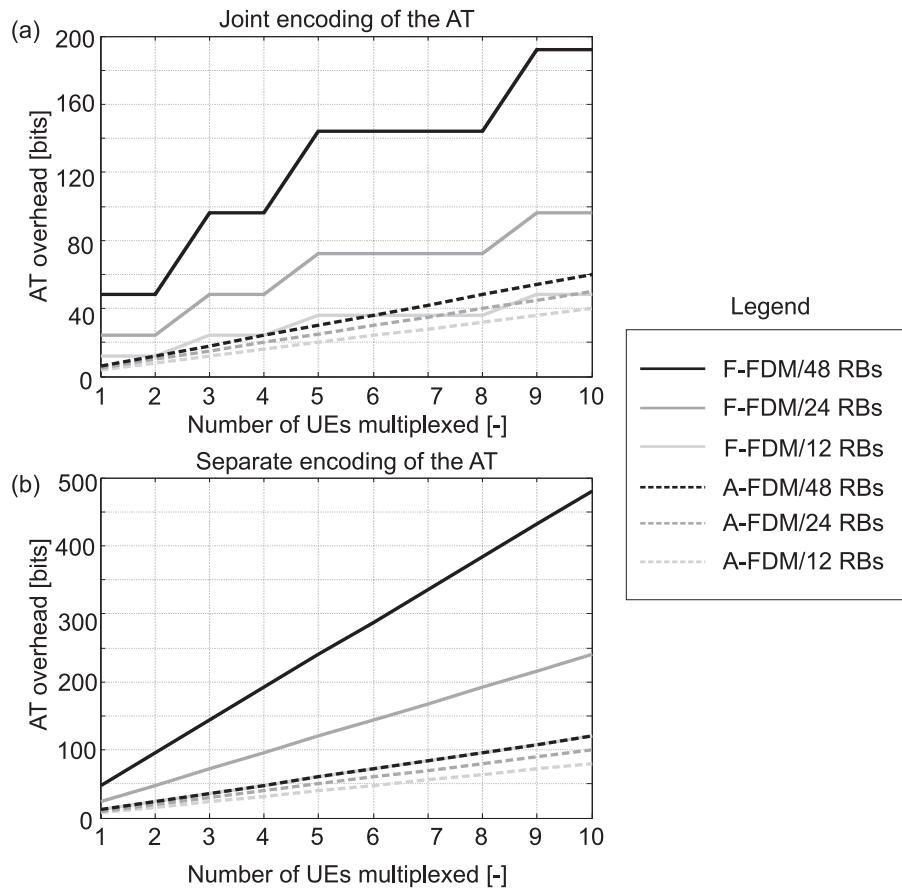
Figure 3.14: (a) The DL control overhead resulting from the joint encoding of the AT, as a function of the number of multiplexed UEs. (b) The DL control overhead based on separate encoding of the AT information to each UE.

scheduling, where the priority metric is given by:

$$m' = \arg\max_m \left\{ \frac{\hat{r}_{m,b}[n]}{T_m[n]} \right\} . \tag{3.16}$$

- Frequency-Domain Throughput-to-Average (FD-TA) - In order to investigate the fairness potential of FD scheduling we consider the following priority metric:

$$m' = \arg\max_m \left\{ \frac{\hat{r}_{m,b}[n]}{\hat{r}_m[n]} \right\} , \tag{3.17}$$

where $\hat{r}_m[n]$ denotes the instantaneous supported throughput based on full BW transmission. The aim of this priority metric is to improve the working of the FD-PF scheduler, by avoiding the dependency on the average throughput term ($T_m[n]$). The average throughput, which is calculated using a recursive method [41], can experience variations that can affect the fairness performance of the traditional PF scheduler.

3.8.3 Theoretical Gain Potential of FDPS Over Ref

We now evaluate the theoretical gain of F-FDM over Ref, based on ideal Rayleigh fading statistics on each RB. In this evaluation the F-FDM scheduler is allowed to allocate each RB to the user with
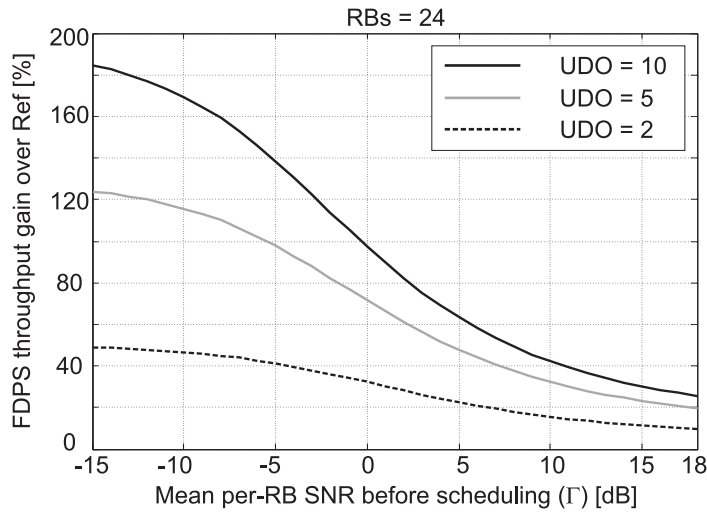
Figure 3.15: Throughput gain of F-FDM over Ref, based on theory.

the best channel quality. Thus, the working principle of F-FDM is similar to Selection Diversity from antenna theory [28]. The mean per-RB SNR after F-FDM scheduling (γ_s) based on Selection Combining is given by:

$$\gamma_s \;\; = \;\; \Gamma \cdot \sum_{k=1}^{UDO} \frac{1}{k} \quad , \tag{3.18}$$

$$\text{TP}_{\text{F-FDM}} \;\; = \;\; \sum_{k=1}^{nRBs} BW_{\text{RB}} \cdot \log 2\Big(1 + \gamma_s\Big) \quad , \tag{3.19}$$

where Γ denotes the per-RB average SNR before scheduling, UDO denotes the number of users in the cell, $\text{TP}_{\text{F-FDM}}$ denotes the throughput after FDPS, and BW_{RB} denotes the RB bandwdith. It is assumed that all the users experience the same average SNR conditions. Further, the signals are assumed to be uncorrelated on the RBs.

Figure 3.15 illustrates the variation in throughput gain of F-FDM over Ref as a function of the average per-RB SNR. The throughput is based on the Shannon Theorem, and the F-FDM scheduler always uses the entire bandwidth for transmission. Three curves have been shown in Figure 3.15, representing different settings of the UDO parameter. The key difference between FDPS and FDLA is that FDPS does not depend on bandwidth reduction for the improvement in SNR. Thus, in contrast to Figure 3.11 (a), FDPS can provide a significant improvement over Ref even at high SNR values, depending on the UDO. However, at low SNR values a sight deterioration in the gain is seen in comparison to Figure 3.11 (a), as FDLA has not been used on top of FDPS in the current analysis. Further, in general the FDPS gain is improved with UDO, as a result of the increase in the multi-user diversity order.

3.8.4 Potential of Different LA Techniques Together With FDPS

Once the FD scheduler has determined the mapping of UEs to RBs, it is the task of LA to determine the final transport format. Depending on the allowed flexibility, several adaptation mechanisms are available. We will perform a preliminary analysis of these mechanisms, which are as follows:
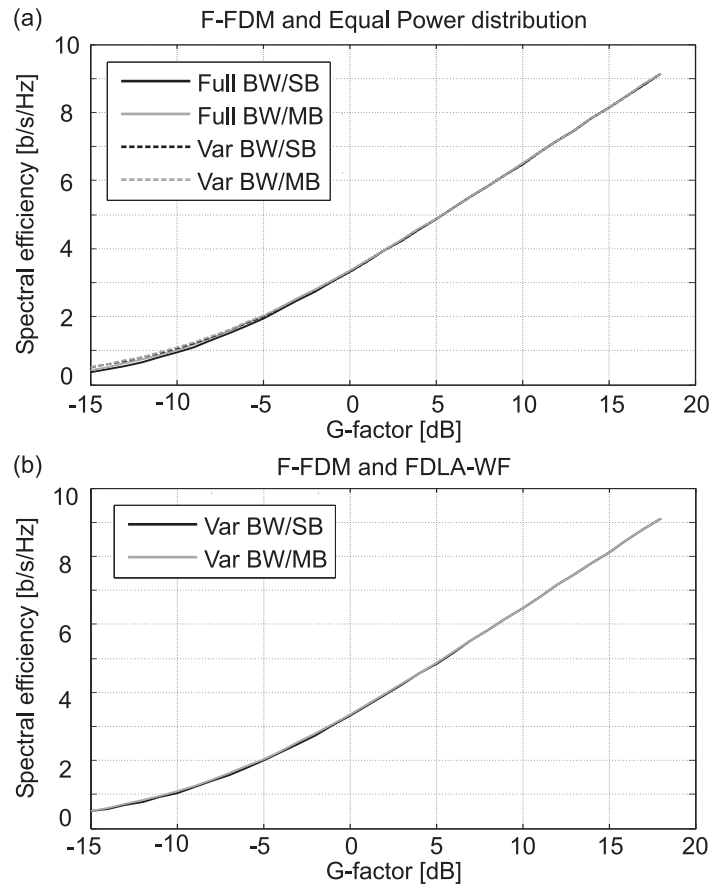
Figure 3.16: (a) Spectral efficiency performance of different EP distribution options together with FDPS, based on the 1x2 receiver. (b) Spectral efficiency performance of different FDLA-WF options versus G-factor. The results are based on the 1x2 receiver.

- Full BW, single-block transmission, and equal power distribution (Full BW/SB/EP)- In this case LA transmits on all the RBs selected for the given UE by the FD scheduler. Since the FD scheduler divides the entire BW among active UEs this scheme is characterized by full BW transmission. The division of power among UEs is based on the proportion of allocated RBs to each UE, e.g., if the number of RBs allocated to the mth UE is L, then the power available to this UE is given by:

$$Pow_m = \left(\frac{P_{total}}{nRBs}\right) \cdot L \quad.\tag{3.20}$$

Further, the power given by (3.20) is divided equally among the allocated RBs. In terms of block encoding SB transmission is employed.

- Full BW, multi-block transmission, and equal power distribution (Full BW/MB/EP) - It is similar to the previous case, except that MB transmission is allowed.

- Optimized/variable BW transmission, based on the FDLA-EP scheme and single-block transmission (Var BW/SB/EP) - In this case the FDLA-EP algorithm determines if it is optimum to transmit on all the RBs allocated to a certain UE by the FD scheduler. Further. only a single TB is allowed, and the distribution of power among the UEs is given by (3.20).

- Optimized BW transmission, based on the FDLA-EP scheme and multi-block transmission (Var BW/MB/EP) - It is similar to the previous case, except that MB transmission is enabled.
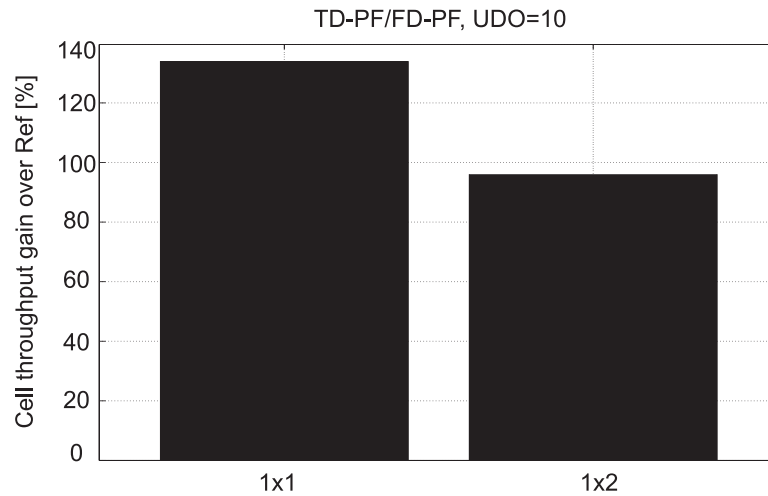
Figure 3.17: Cell throughput gain of F-FDM Full BW/SB/EP over Ref for the Macro case 1 scenario.

- Optimized BW transmission, based on the FDLA-WF algorithm and single-block transmission (Var BW/SB/WF).

- Optimized BW transmission, based on the FDLA-WF scheme and multi-block transmission (Var BW/MB/WF).

The preliminary investigation of these schemes is based on the simplified system-model described earlier in Section 3.7. The evaluation is based on the F-FDM technique and assumes that there are always $N = 3$ UE's available at the FD scheduler at any given G-factor. The TD and FD scheduling metrics are based on the PF principle, given by (3.12) and (3.16) respectively. Figure 3.16 illustrates the spectral efficiency versus G-factor for the different LA options. As seen in Figure 3.16 (a), there is marginal difference between the performance of Full BW and Var BW cases, as well as between SB and MB transmission, when FDLA-EP is applied. Further, similar trends are observed for the FDLA-WF scheme, shown in Figure 3.16 (b). The reason for the observed behavior is that the F-FDM scheme inherently operates at a high SINR value, and the possibility to improve its performance further through advanced LA techniques is very limited. The FD scheduler selects the best RBs for a given user, and these are likely to be similar in quality. The SINR of the selected RBs can be 3 dB - 5 dB higher than the G-factor, even for a moderate UDO. Considering the G-factor range for the Macro case 1 scenario, the potential of FDLA on top of F-FDM is limited. Based on this analysis the Full BW/SB/EP option is selected for further investigation of FDPS, which is also the preferred transmission mode in LTE [14]. Similar recommendations have been made by other related studies, e.g., see [99].

The cell throughput gain of FDPS over Ref is shown in Figure 3.17, assuming UDO is equal to 10. Here, the Ref scheme is also based on the TD-PF scheduler, in order to make a fair comparison. The modeling of the Ref scheme assumes perfect PF scheduling, where each UE is active $1/K$ of the time when the channel conditions are best (UDO=K). The average throughput at a given G-factor based on the PF scheduler is calculated by using the best $1/K$ throughput samples. Preliminary analysis based on the simplified system model indicates significant potential of FDPS, e.g., it can provide a capacity gain of around 100% over Ref. Note that this is an optimistic estimate of the FDPS gain potential, due to the ideal assumptions.
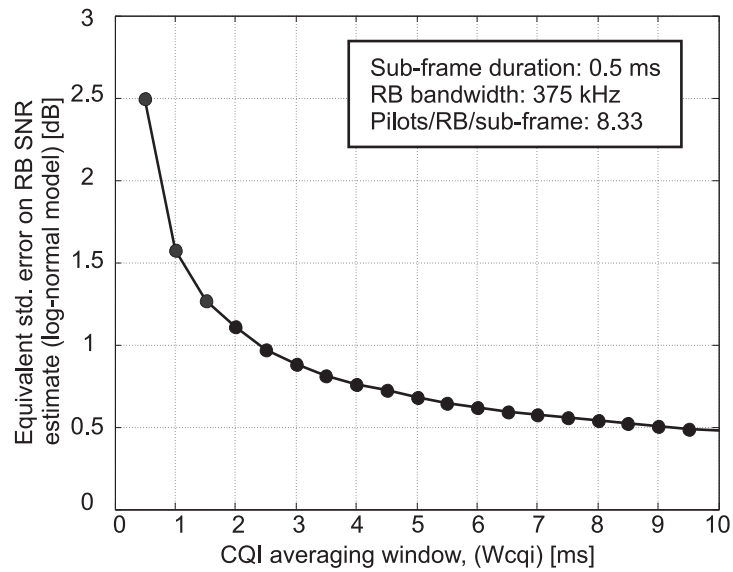
Figure 3.18: Impact of time-domain averaging on RB SNR estimation error.

3.9   Design of Low Bandwidth CQI Schemes Enabling FDAS

The gain potential of the FDAS schemes depends significantly on the quality of CQI reports. Further, ideal CQI signalling on a RB basis is not practically achievable due to the limited number of pilot symbols, as well as the overhead concerns. It is clear that the CQI feedback needs to be minimized since it consumes resources that would otherwise be used for transmission of useful data in UL. The accuracy of the CQI report depends mainly on three factors: (1) Available number of pilot symbols within the RB, pilot pattern, and measuring time, (2) Signaling resolution of the CQI report, denoted by $resSinr$, and (3) Delay from the instant CQI is measured at the UE until it is used by the eNode-B in scheduling decisions [72].

We consider *periodic CQI reporting* in the study, which has also been selected in LTE [14]. This technique was earlier employed in WCDMA/HSDPA, where the CQI measurement is conducted over a 5-MHz bandwidth and a 2 ms period. For LTE with the shorter sub-frame size we can expect significantly larger error levels when considering only a single RB, since the bandwidth is also significantly lower, e.g., 375 kHz.

To quantify the impact of available pilot symbols on the accuracy of CQI estimation, a set of idealized simulations have been conducted. The simulations were based on the AWGN channel, and ideal channel estimation. For this setup, the pilot symbol pattern selected for LTE and described in [14] was used. Based on this setup, an average of 8.33 pilot symbols per sub-frame and per RB are available for CQI estimation. Further, the estimation of CQI is based on an unbiased estimate of the standard deviation (std.) of the noise samples received at the time-frequency locations of the pilot symbols. The numerical results are shown in Figure 3.18. By introducing time domain averaging the effective number of pilot symbols is increased, thus improving the per RB estimation accuracy of the noise power, as shown in Figure 3.18. Simulations show that averaging over the full system bandwidth of 10 MHz and over the sub-frame duration yields a log-normal std. of approximately 0.4 dB. However, in the absence of any time-averaging the error in CQI estimation over a single RB can be quite large, e.g., up to 2.5 dB.

To lower the CQI bandwidth, a generic approach is to lower the rate at which the UE reports its channel quality. The basic CQI reporting loop is shown in Figure 3.19. The UE reports the frequency selective channel quality every Δ_{cqi} sub-frames, and the reported value is based on a time averaging over the past W_{cqi} sub-frames. The averaging window need not be limited in practice to a per-sub-frame resolution. Once the UE has transmitted the CQI report, it takes some processing time before the eNode-B is able to utilize it in LA and scheduling. This processing delay is denoted by D_{cqi}. It is evident that Δ_{cqi} can be increased directly to save CQI signalling bandwidth at the expense of LA and PS delays.

By increasing the averaging window, W_{cqi}, we average the CQI measurement noise and im-prove the CQI measurement accuracy. It is clear from Figure 3.18 that a large potential is available from increasing the averaging window duration. On a negative note, averaging causes more effec-tive LA and PS delay since we base current CQI estimate on older samples. Further, averaging reduces the channel dynamics, which create the multi-user diversity gain in the first place. From a signalling perspective, it is best to consider the mobility requirements and then employ as much averaging as possible on the UE side. An alternative approach is to let the UE send frequent reports and then conduct the CQI averaging in the eNode-B. The latter clearly yields a more flexible and dynamic solution from a network and multi-user perspective, but has an inherent penalty in terms of signalling overhead [72]. Hence, for this study we consider only the cases where $W_{cqi} \leq \Delta_{cqi}$. For WCDMA/HSDPA, the maximum CQI reporting rate is 5 bits per 2 ms per 5 MHz which scales to an equivalent of 10 kbit/s for LTE based on a TTI duration of 0.5 ms. This is taken to be a rea-sonable amount of CQI overhead, and it is sufficient to support the Ref scheme.

Based on Figure 3.19, the experienced LA delay after averaging and processing of the CQI reports is modeled as follows [72]:

$$D_{LA} = \lceil (\max\{W_{cqi}, \Delta_{cqi}\}/2 + D_{cqi}) \rceil \quad \text{(sub-frames)} \quad . \tag{3.21}$$

At the UE, the SINR measurement is formatted and compressed into a finite number of bits (called the CQI word) before being reported to the eNode-B. The dynamic range of allowed LTE modu-lation and coding schemes from QPSK with excessive coding to 64QAM with marginal coding is approximately 25 dB [62], which means that $N_{abs} = 5$ bits are needed to signal the CQI report with 1 dB resolution [49]. Further, the received CQI word is also subject to errors due to imperfect decoding of the received signal [97]. However, this aspect is not included in the analysis.

The most straightforward way to implement CQI is to send an absolute SINR for every single RB. This technique is denoted as the *Absolute-CQI* (AB-CQI) scheme. The AB-CQI approach has the drawback that it will require a lot of signaling bandwidth but very accurate channel quality
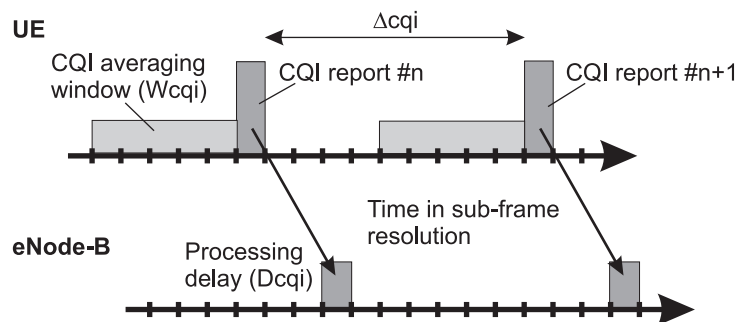

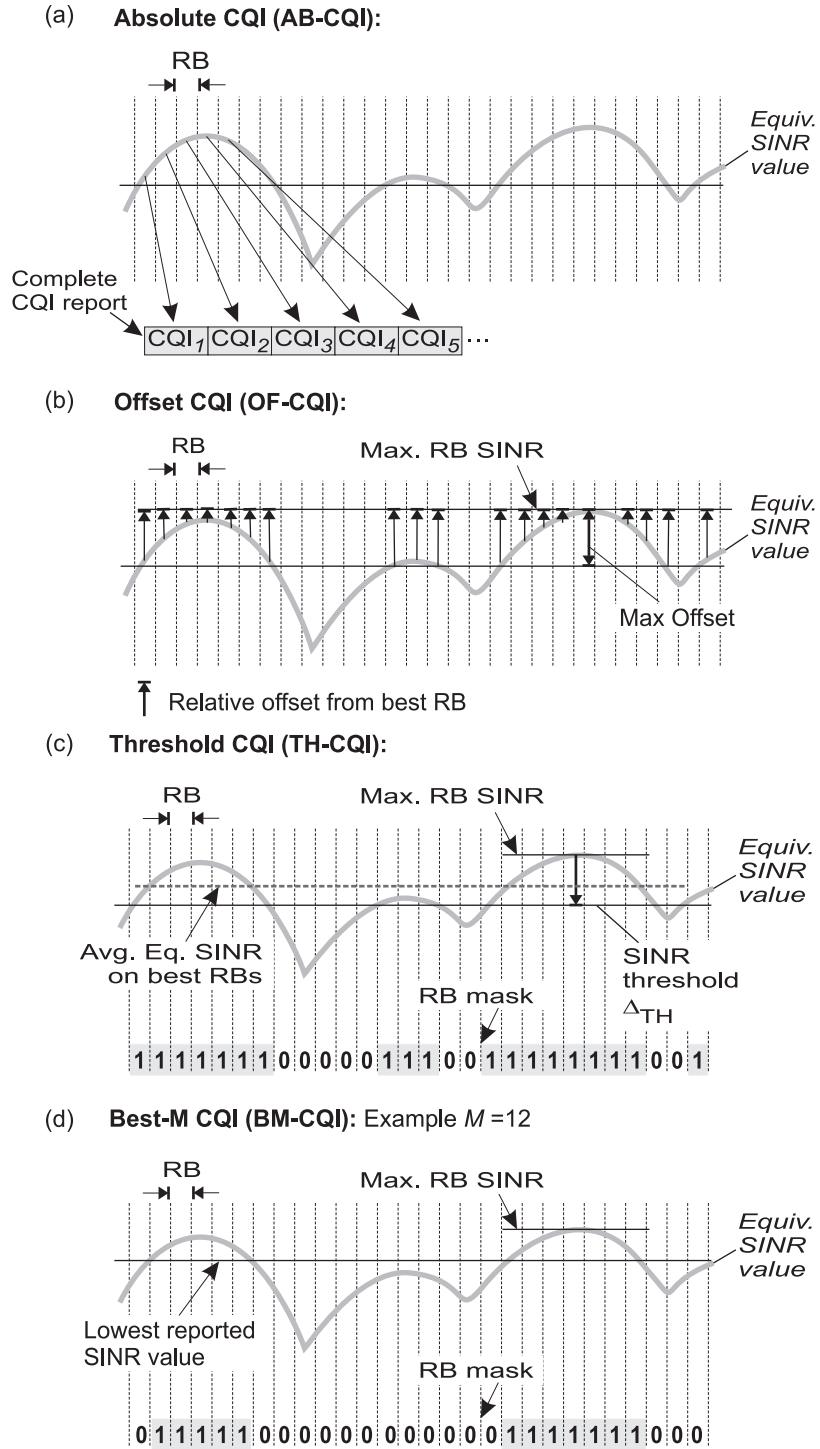**Figure 3.19:** The CQI measurement and reporting process.

Figure 3.20: Illustration of the CQI schemes considered in this study.

information is available for scheduling. We investigate CQI overhead reduction using the signaling of offset information in comparison to the signaling of absolute value of SINR. The following CQI schemes enabling both FDLA and FDPS are considered:

- Absolute-CQI (AB-CQI) - The absolute value of SINR measured at each RB is transmitted to the eNode-B using N_{abs} bits. This is the ideal CQI signaling scheme from the perspective of FDAS performance. It is illustrated in Figure 3.20 (a).

- Ref (Ref-CQI) - The Ref scheme is based on frequency-blind transmission. Thus, a single CQI report is sufficient to signal the wideband channel quality, using N_{abs} bits.

- Offset-CQI (OF-CQI) - We propose to reduce the bandwidth of the AB-CQI scheme by utilizing offset signaling. The absolute SINR value of the best RB is signaled using N_{abs} bits. Next, the relative SINR offset of each RB from the best RB is calculated and signaled using offset signaling. Further, N_{off} bits are utilized for offset signaling. If the offset of a certain RB is greater than the maximum defined offset, an out-of-range indication is signaled for this RB [67], [100].

  When transmitting a CQI report there is the option of having both dynamic length and fixed length messages. If only a small amount of RBs are active on an average then it makes sense to signal the offset information only for the active RBs. However, previous studies have shown that there is limited potential of dynamic length CQI reporting, e.g., [67]. Therefore we will consider only fixed length CQI reports. The OF-CQI scheme is depicted in Figure 3.20 (b).

- Threshold CQI (TH-CQI) - In this proposal the average SINR for all RBs within a specified fixed threshold from the best RB is signaled using N_{abs} bits, and the good RBs are signalled using a bit mask [67], [72]. This scheme can provide a significant reduction in the CQI overhead. However, it can only by applied together with equal power LA, e.g., FDLA-EP. The motivation is that if LA is only allowed to select one MCS per UE, then the average SINR over the best RBs should be sufficient to realize the gain from fast adaptation. The scheme is depicted in Figure 3.20 (c).

- Best-M CQI (BM-CQI) - In this CQI scheme the absolute SINR of the best M RBs are reported to the eNode-B [101], using N_{abs} bits each. The rationale is that the resource allocation will usually employ only those RBs that have relatively good channel quality. It is therefore better to utilize the available CQI BW to signal the absolute value of the best M RBs. The scheme is depicted in Figure 3.20 (d), using $M = 12$ as an example.

  The best M RBs are indicated using a bit mask. In order to reduce the overhead for signaling the bit-mask combinatorial techniques can be utilized. This is based on the assumption that both eNode-B and the UE have ordered the possible combinations in the same sequence.

- Best-M Offset CQI (BM-OF-CQI) - We propose to reduce the overhead of the BM-CQI scheme by utilizing offset signaling, similar to OF-CQI. The best RB is signaled using N_{abs} bits, and the relative offset of each RB from the best RB is signaled using N_{off} bits. The selected combination of M RBs is signaled using a bit mask, similar to the BM-CQI scheme.

For the Offset signaling techniques, a SINR level signaling resolution is also defined between each offset step, and denoted by Δ_{off}. Assuming N_{off} bits are used for the signaling of offset information, the total allowed offset from the best RB is equal to $(2^{N_{off}} - 1) \cdot \Delta_{off}$ (in dB). One combination is reserved for indicating the out-of-range value. Based on these definitions the

Table 3.4: CQI overhead in bits per report for the considered schemes. The numerical evaluation is based on $nRBs = 24$, $N_{abs} = 5$, $N_{off} = 3$, and $M = 10$.

CQI scheme	Expression to calculate overhead	Signaling overhead [bits/report]
AB-CQI	$nRBs \cdot N_{abs}$	120
OF-CQI	$N_{off} \cdot nRBs + N_{abs}$	77
TH-CQI	$N_{abs} + nRBs$	29
BM-CQI	$N_{abs} \cdot M + \lceil \log_2 \binom{nRBs}{M} \rceil$	71
BM-OF-CQI	$N_{off} \cdot M + N_{abs} + \lceil \log_2 \binom{nRBs}{M} \rceil$	56
Ref-CQI	N_{abs}	5

associated overhead per CQI report for each CQI scheme is given by the expressions listed in Table 3.4.

The numerical evaluation of the CQI overhead of the different schemes is depicted in Figure 3.21, based on 24 RBs. Calculations show that the maximum reduction in CQI overhead can be achieved with the TH-CQI scheme, e.g., the overhead is reduced by up to 76%, over the AB-CQI scheme. Similarly, for a moderate value of M, e.g., 10, the saving in CQI overhead from using BM-CQI and BM-OF-CQI ($N_{off} = 3$) is 41% and 53% respectively. Further, if the BM-OF-CQI scheme is employed instead of the BM-CQI scheme the maximum reduction in overhead is up to 36%, in the considered range of M. In terms of the potential of OF-CQI scheme the overhead can be reduced by 36%, based on $N_{off} = 3$. Further, the BM-OF-CQI scheme has a lower overhead
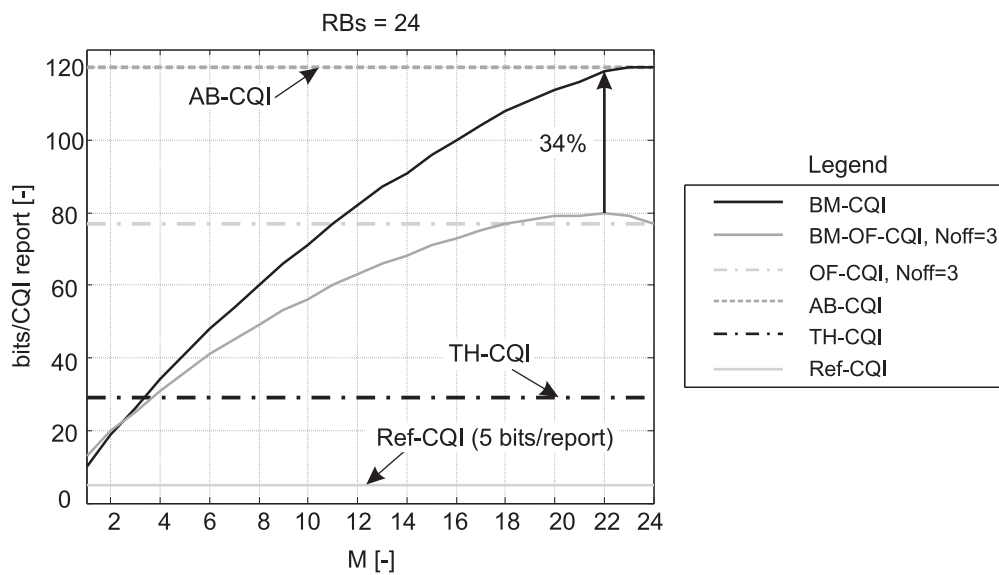

Figure 3.21: Numerical evaluation of the CQI overhead for the different schemes investigated in the thesis, based on 24 RBs.

in comparison to the OF-CQI scheme if M is below 18. In comparison to the Ref scheme the best low BW CQI scheme for FDAS (i.e., TH-CQI) still requires an additional 480% in overhead. The potential of further savings in overhead by utilizing delayed CQI reporting will be investigated in Chapter 6.

Chapter 4

Evaluation of Frequency-Domain Link Adaptation Based on the Single-Cell Model

4.1 Introduction

This chapter is devoted to the performance analysis of the considered LA algorithms, i.e., FDLA-EP, FDLA-WF, and Ref. We investigate the potential of the various adaptation mechanisms available to the system. The evaluation is carried out under a variety of operating conditions in order to make a generalized analysis of LA for an OFDMA system.

The chapter is organized as follows: The main modeling assumptions are introduced in Section 4.2. The verification of the single-cell based system model is presented in Section 4.3. This is followed by the detailed performance evaluation of the gain potential of FDLA, starting from Section 4.4 and onwards. The conclusions are presented in Section 4.13.

4.2 Modeling Assumptions

The simulation methodology used here has been introduced in Chapter 2. We employ the quasi-static decoupled link and network level simulation methodology. A single-cell is modeled in detail, while the interference from the surrounding cells is modeled as AWGN. The average experienced SINR dependent on the user location is based on known G-factor distributions. The system is based on a simple admission control strategy which keeps the number of users per cell constant.

The PS and LA functionalities have been modeled according to the description in Section 3.5 and Section 3.8 respectively, while OLLA is modeled according to Subsection 2.5.2. The frequency-selective CQI reports are modeled with measurement inaccuracies due to the limited number of pilot symbols within each RB. The CQI reporting delay used here is 2 ms, which corresponds to the existing WCDMA/HSDPA delay scaled for a shorter TTI length of LTE [102]. Similarly, as D_{cqi} is not specified in LTE, we use the existing WCDMA/HSDPA setting and scale it according to the shorter TTI length. Further, the effect of CQI quantization is also included in the analysis.

Table 4.1: Default simulation parameters.

Parameter	Setting
Physical layer parameters	See Table 2.2
System bandwidth, (BW)	10 MHz
RB bandwidth	375 kHz
Number of users (UDO)	20
Cell-level user distribution	Uniform
Power delay profile	TU
CQI reporting scheme	AB-CQI, periodic reporting
CQI error std.	1 dB
CQI reporting resolution ($resSinr$)	1 dB
CQI reporting interval (Δ_{cqi})	2 ms
N_{abs}	5 bits
Processing delay (D_{cqi})	1.5 ms
LA block encoding scheme	single-block
WF resolution in the power domain ($resWF$)	0.01
TD scheduling	PF
AMC model	See Subsection 2.5.1
HARQ model	Chase combining
LA target	10% BLEP (1st Transmission)
UE speed	3 km/h
UE receiver	1x2 MRC
Channel estimation	Ideal
Carrier frequency	2 GHz
Deployment scenario	3GPP Macro case 1
PF filter length	300
Initial T_m value	$BW \cdot \log_2(1 + \hat{G}/2.5)$‡

‡$\hat{G}$ *is estimated using the first available CQI reports of the user.*

As the study was performed before the pilot pattern was agreed upon in LTE, we have used the setting of 1 dB as std. of the CQI error for all the schemes, based on the WCDMA/HSDPA setting [48].

In terms of the modeling of the DL control channel (AT) we assume that it is received without any errors throughout the coverage area of the cell. Similarly, it is assumed that the UL control channel carrying the HARQ Ack/Nack information is always received correctly. Further, the decoding errors experienced on the UL control channel transmitting CQI reports are ignored.

The simple infinite buffer traffic model is used in the initial performance evaluation of FDLA, and the speed is fixed at 3 km/h. The results for the finite buffer model, where each user downloads a fixed 2 Mbit packet before leaving the system, are also presented. The default simulation assumptions are summarized in Table 4.1.
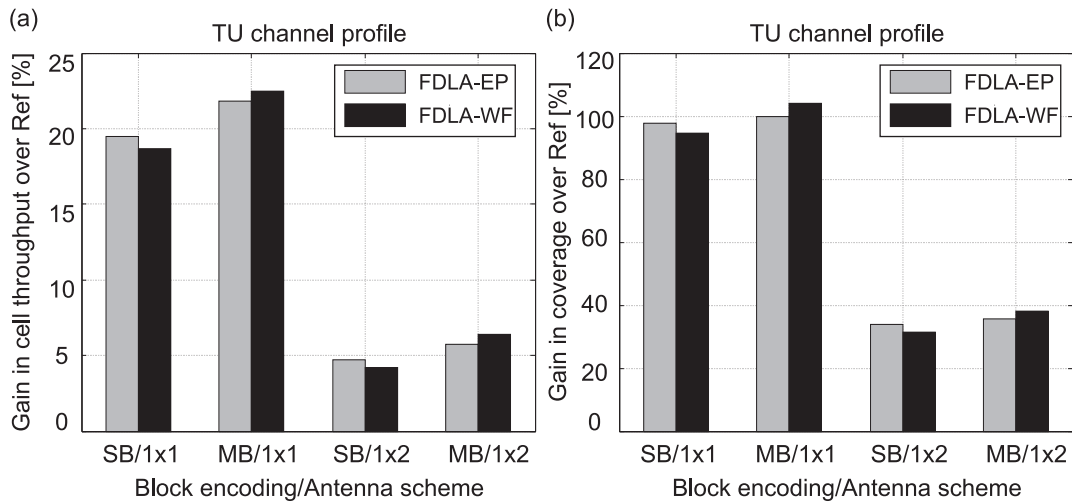
Figure 4.1: FDLA gain potential over Ref, based on ideal CQI conditions and the RR scheduler. The results are based on the infinite buffer traffic model.

4.3   Validation of the System-Model

The functioning of the system-model is validated against the numerical evaluation carried out in Subsection 3.7.1. The FDLA cell throughput gain over Ref is evaluated for the Macro case 1 scenario under ideal CQI conditions, i.e., no measurement errors or reporting delay is assumed. Further, infinite resolution of CQI reporting is assumed, and the RR scheduler is employed. The 10 MHz bandwidth is divided into 24 RBs, and the highly frequency-selective TU channel profile is selected. The results are illustrated in Figure 4.1.

The FDLA cell throughput gain obtained with the more detailed system model is similar to that observed in Figure 3.10 for all the investigated cases, e.g., within 2% - 3%. The improvement in coverage with FDLA is shown in Figure 4.1 (b). Similar to the trends observed in Figure 3.11, it is seen that FDLA can provide a substantial improvement in coverage, e.g, in the order of 100% for the 1x1 case. Further, these results confirm that FDLA-EP is the preferred LA technique with SB transmission, owing to its superior performance and implementation simplicity. In terms of the preferred block encoding option, it is clear that the MB transmission provides marginal gain over SB encoding (around 2%). Thus, we will exclude the MB encoding option in future FDLA analysis.

4.4   Impact of Scheduling Resolution on the FDLA Potential

As the dynamic range of SINR is dependent on the scheduling resolution in frequency-domain, the gain potential of FDLA will vary as a function of the RB width. We investigate this dependence in Figure 4.2. The three channel profiles introduced in Section 2.14 have been employed in the analysis. Further, results are obtained for the 1x1 and the 1x2 MRC antenna configurations. Ideal CQI conditions are assumed here together with the RR scheduler.

Based on the results for all the channel profiles we conclude that most of the FDLA gain potential, e.g., within 5% of the maximum potential, can be achieved by having a RB width in the order of the coherence BW. This corresponds to around 3 RBs within 10 MHz for the Ped. A
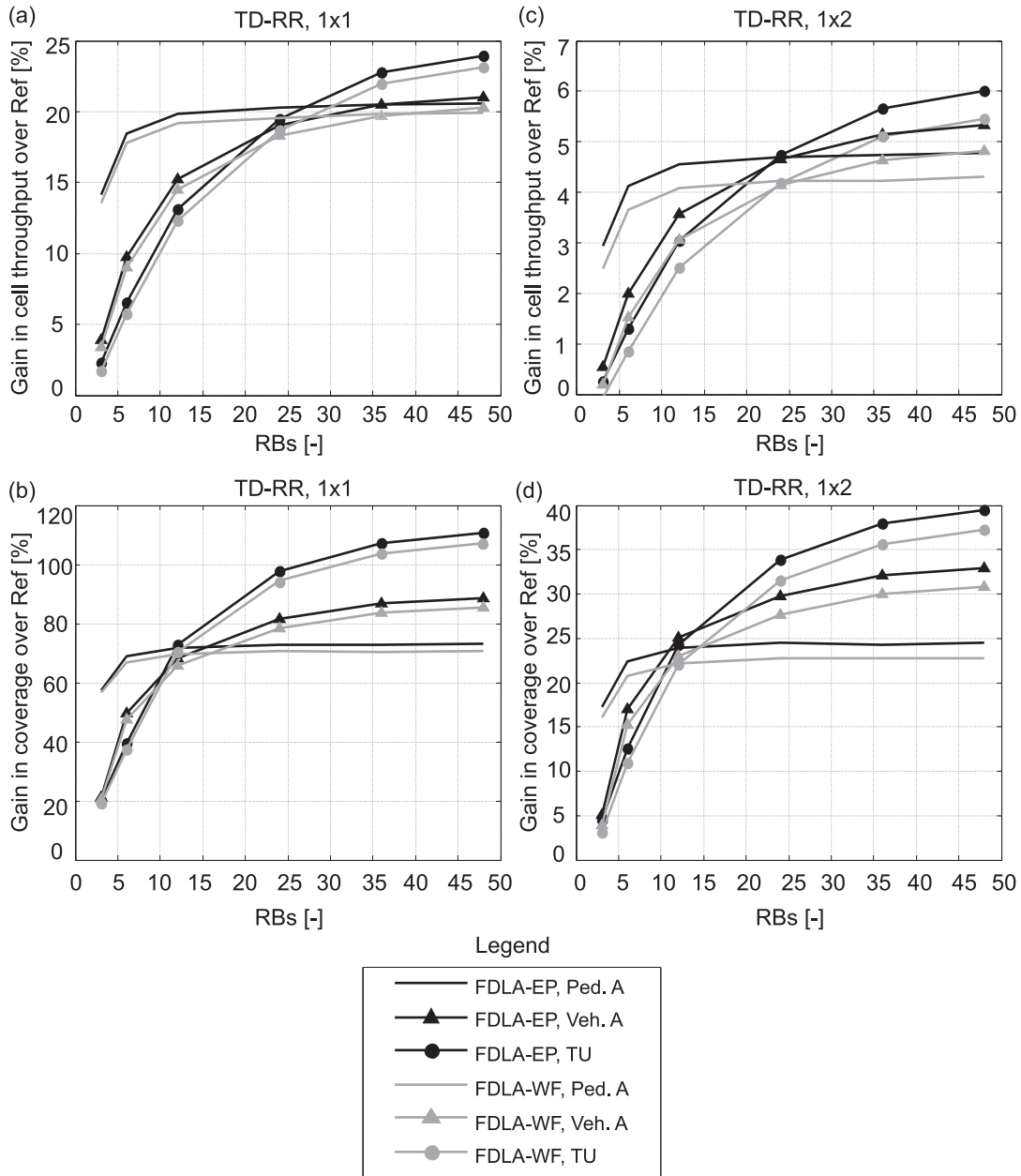
Figure 4.2: Cell throughput and coverage gain of FDLA over Ref, as a function of the number of RBs, antenna configuration and coherence BW. Ideal CQI conditions, single-block transmission, infinite buffer traffic model, and the RR scheduler have been employed.
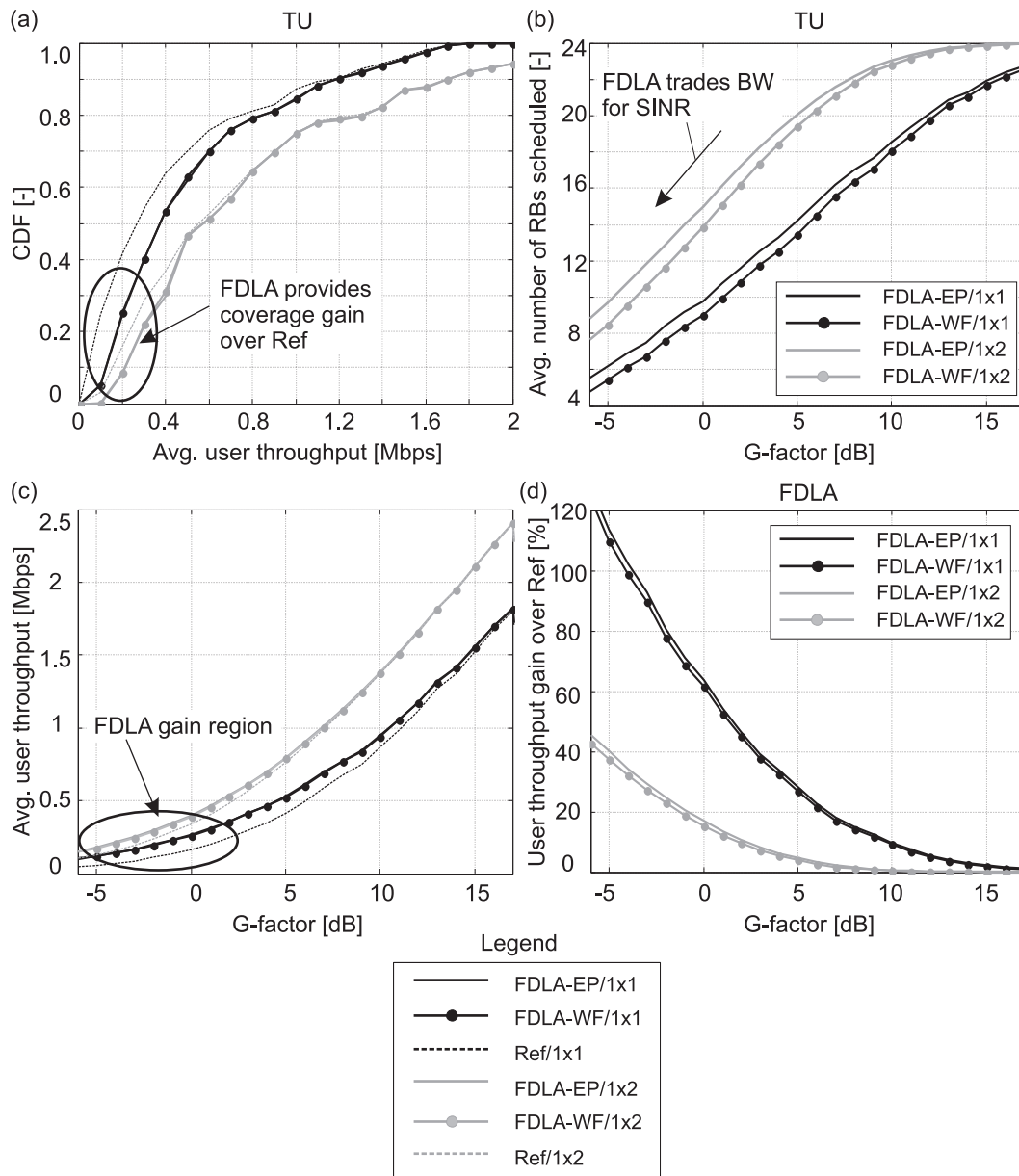
Figure 4.3: Detailed FDLA performance curves, based on ideal CQI settings, SB transmission, infinite buffer traffic model and the RR scheduler.

profile, and around 24 RBs for the Veh. A and the TU channel profiles. Further, the maximum FDLA gain potential is improved with an increase in frequency-selectivity of the channel, as FDLA is able to exploit the improvement in frequency selection diversity order. Thus, the maximum gain is seen in the TU profile. The maximum cell throughput gain is around 24% and 6% for the 1x1 and the 1x2 antenna configurations respectively. Similarly, the maximum FDLA coverage gain is around 110% and 40%, depending on the antenna configuration. As an example of the sensitivity to scheduling resolution, the FDLA gain potential is halved when the ratio of coherence BW to RB width is reduced to around 0.4 (TU).

4.5   Detailed Analysis of the FDLA Performance

The results in Figure 4.3 illustrate the FDLA performance in detail. These results are based on ideal CQI settings, SB transmission and the RR scheduler. Figure 4.3 (a) shows the CDF of the average user throughput for the considered LA schemes. It is seen that FDLA mainly improves the performance at the tail of the distribution, i.e., in terms of coverage. Receive diversity can improve the median user throughput by 110% for Ref, and around 50% for FDLA, based on the 1x1 scheme.

Figure 4.3 (b) illustrates the average number of scheduled RBs as a function of the G-factor. In the low G-value range FDLA trades BW for improvement in SINR, as there is a near-linear mapping between SINR and throughput. However, the situation is reversed when G-factor is high. In this case it is beneficial to transmit on the entire BW. In case of the 1x1 antenna deployment it is interesting to note that due to the presence of large channel dynamics FDLA does not utilize the entire BW for transmission, even at the high G-factor values.

Figure 4.3 (c) illustrates the average user throughput as a function of the G-factor. Due to the large channel dynamics experienced with the 1x1 antenna configuration and the use of the geometric average SINR metric in LA, the FDLA schemes can provide a gain over Ref up to around 15 dB. The predominant gain is at the low G-factor values.

Figure 4.3 (d) illustrates the gain in average user throughput over Ref as a function of the G-factor. The improvement in coverage achieved by FDLA can be up to 120% for the 1x1 case and 40% for the 1x2 antenna case. The performance is reduced in comparison to the results shown in Figure 3.11 (a), due to the use of SB transmission and a more realistic channel profile with a reduced dynamic range.

4.6   Evaluation of OLLA Performance

In order to evaluate FDLA performance under more realistic conditions we introduce a finite CQI resolution and reporting delay, based on the settings given in Table 4.1. Further, PF scheduling in time domain according to (3.12) is introduced. Figure 4.4 (a) illustrates the FDLA cell throughput gain over Ref with and without OLLA. Similarly, Figure 4.4 (b) shows the impact of OLLA on the coverage performance. These curves are obtained for the TU channel profile and the 1x2 antenna case.

The trends are similar for both FDLA schemes. The performance deteriorates with increase in std. of CQI error. The curve without OLLA has a steep slope, indicating that FDLA is very sensitive to CQI errors. As the std. of the log-normal CQI error increases, FDLA tends to schedule on PRBs which are experiencing a positive value of error, i.e., a positive bias is introduced. The impact of CQI error can be reduced through the use of the OLLA algorithm. As an example, when the std. of CQI error is 1 dB, OLLA is able to improve the cell throughput gain by around 20%. Similarly, the coverage gain is enhanced by around 15%.

Looking at the OLLA curves it is seen that the CQI error should be kept under 1.5 dB in order to achieve gain from FDLA. Further, the open loop ILLA cannot guarantee FDLA gain alone, and the OLLA algorithm is required to stabilize performance. If the std. of CQI error is kept at 1 dB, the FDLA cell throughput gain is around 12%, while the coverage gain is around 35% for the 1x2
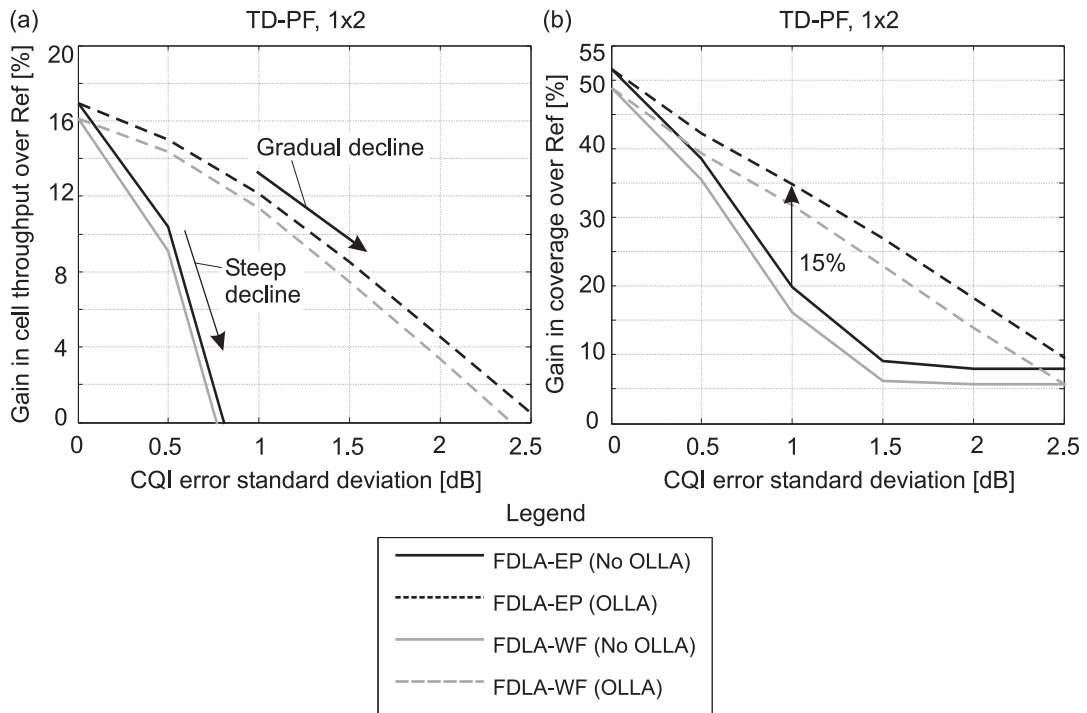
Figure 4.4: Performance of OLLA together with FDLA. PF scheduling in time domain is employed, together with the infinite buffer traffic model. The number of users in the cell is fixed at 20.

case.

4.7   Impact of the Scheduling Policy on Fairness

Figure 4.5 illustrates the impact of the time-domain scheduling policy on the CDF of user throughput. In terms of fairness, it is clear that the optimal scheduler is the one that provides equal throughput distribution among the users, i.e., the slope of the CDF curve should be close to 90 degrees. Among the considered scheduling policies, the PF and the RR schedulers provide similar performance. This is due to the gain of FDLA on top of packet scheduling. Further, the two aforementioned schedulers can significantly improve fairness in comparison to the MT scheduler.

The PF scheduler provides a good trade-off between fairness and cell throughput. Comparing it to the RR scheduler, it is observed that the coverage performance of the PF scheduler is slightly improved. The MT scheduler is biased in favor of the cell-center users. These observations are similar to those reported in previous WCDMA/HSDPA based studies [2].

4.8   Impact of Speed on the FDLA Performance

The mobility support of FDLA is investigated in Figure 4.6. The results are obtained with non-ideal CQI settings, according to Table 4.1. It is intuitive that the ability of LA to track channel variations on the basis of CQI is reduced with speed. Similar observations have been reported in previous studies e.g., see [48]. Due to the LA/PS processing delay there can be a significant
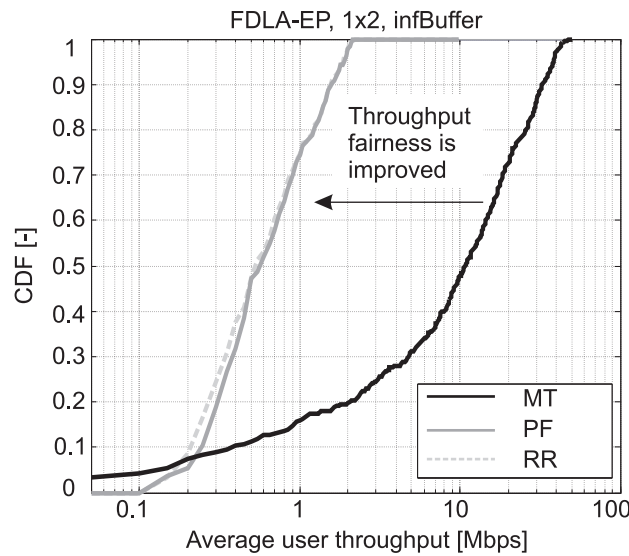
Figure 4.5: Impact of the time-domain scheduler on FDLA performance. Non-ideal CQI, FDLA-EP, infinite buffer traffic model and the 1x2 antenna scheme is assumed.

difference in the channel quality from the time of CQI measurement to the time that the packet is finally received, when the UE speed is high.

The results in Figure 4.6 show that the FDLA cell throughput gain is halved when the UE speed is increased to 30 km/h. Within the considered range of speeds, the FDLA cell throughput gain is reduced by around 8% from the maximum value. Similarly, the coverage gain is reduced by around 16%. The trends are similar for both FDLA algorithms.

Coverage performance is more sensitive to speed due to the near-linear mapping of SINR to throughput for the cell-edge users. In this case, the available degrees of freedom for FDLA are reduced, and throughput optimization is based on transmission on only a few RBs. Results show that FDLA-EP can provide a coverage gain of around around 30% at 30 km/h, while still maintaining a higher cell throughput than the Ref scheme.
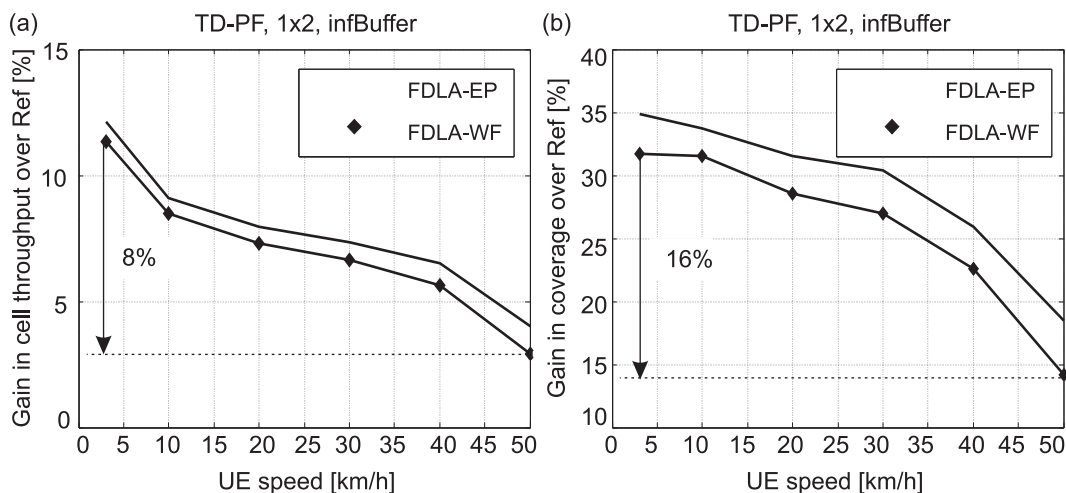

Figure 4.6: Impact of UE speed on the FDLA performance. The results are based on the infinite buffer traffic model, 1x2 antenna configuration, non-ideal CQI, and the PF scheduler.
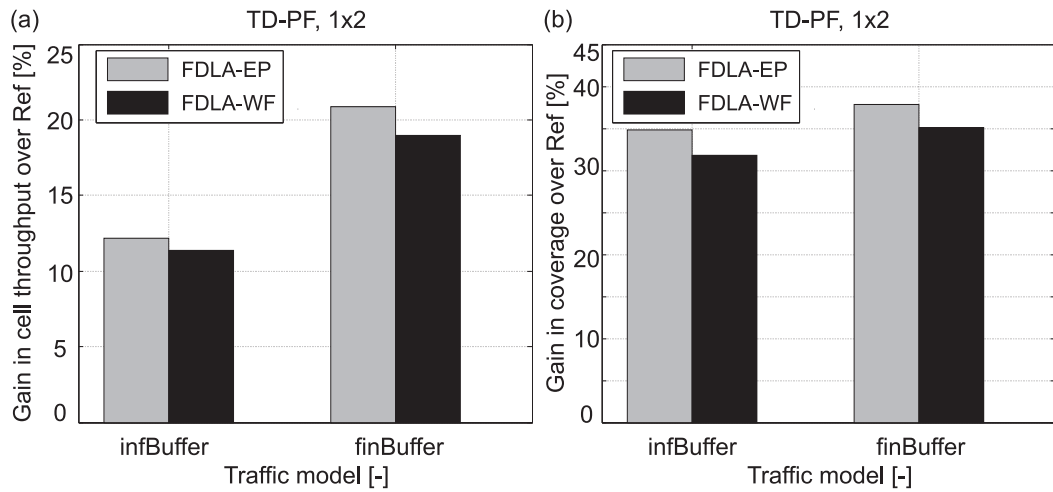
Figure 4.7: FDLA performance under different traffic models. The results are based on non-ideal CQI.

4.9 FDLA Performance under Different Traffic Models

The impact of the traffic model on FDLA performance is illustrated in Figure 4.7. By utilizing the finite buffer (finBuffer) traffic model it is seen that the FDLA cell throughput gain is improved by around 8%, over the infinite buffer (infBuffer) model. Similar trends are observed for both FDLA schemes. The results are based on the PF scheduler and non-ideal CQI. The infinite buffer model is characterized by equal session time to all users. This implies that the cell-edge users download a much lower amount of data in comparison to the cell-center users, during the fixed session time. As a result this traffic model is biased in favor of the cell-center users, in terms of data.

The finite buffer traffic model ensures that all users download an equal amount of data, irrespective of their location in the cell. It implies that cell-edge users remain active longer than the cell-center users, due to the less favorable channel conditions. Thus, depending on the scheduling policy and the LA algorithm the experienced G-factor distribution can vary in time.
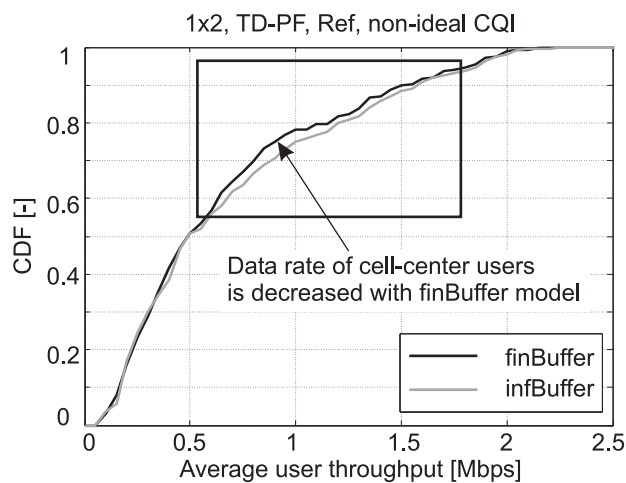

Figure 4.8: CDF of the user throughput obtained with the Ref scheme under the two types of best effort traffic models considered in the study.

Under the finite-buffer traffic model the coverage limited users need to be scheduled more often by the PF scheduler in order to compensate for the poor SINR conditions. This leads to a reduction in the scheduling time of the cell-center users, which results in a performance deterioration. As a result the overall cell throughput is also reduced. Among the LA schemes considered, the reduction in cell throughput is most severe in case of the Ref scheme due to the limited degrees of freedom. Thus, the FDLA cell throughput gain over Ref increases when the finite buffer model is applied. Figure 4.8 illustrates the CDF of the user throughput for the Ref scheme, under the two types of traffic models. It is seen that the cell-center users experience slightly higher data rates under the infinite buffer traffic model.

In terms of coverage performance there is no significant difference between the two traffic models. As mentioned earlier the coverage limited users will be scheduled more often under the finite buffer model. The results show that the increase in scheduling time can compensate almost fully for the increase in data, and the coverage performance is not reduced significantly. This is also verified by the CDF curves in Figure 4.8.

4.10   Analysis of the Multi-User Diversity Gain

The ability of the PF scheduler to harness the available multi-user diversity in the time-domain is investigated in Figure 4.9. Simulations are based on the finite buffer traffic model and show that the cell throughput of the Ref scheme is enhanced by 14% when the UDO is increased from 1 to 20.

Observing the cell throughput curve of the FDLA-EP scheme we see that the maximum increase in throughput is equal to 7%, and it is achieved around UDO of 10. Thereafter there is a slight decrease in the cell cell throughput. This is due to the adverse impact of CQI errors on FDLA performance, as the probability of utilizing CQI reports with a positive value of error increases with UDO. The difference in the multi-user diversity gain potential of the two schemes is due to the difference in their operating points. In general, due to the nature of the mapping between SINR and throughput the scheme operating at lower SINR values (Ref) has higher potential for
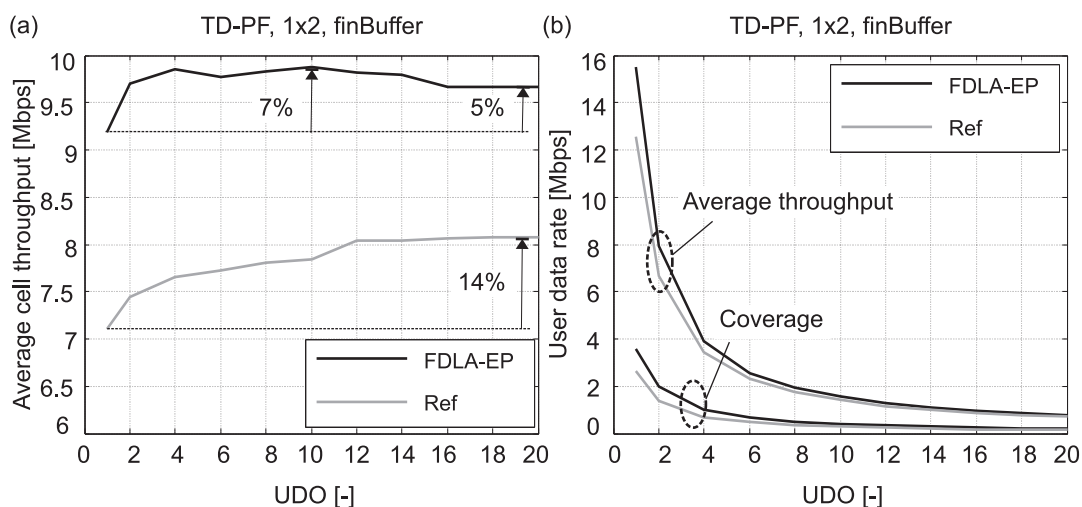

Figure 4.9: Multi-user diversity gain analysis based on the PF scheduler. Non-ideal CQI, finite buffer traffic model, and the 1x2 antenna scheme is assumed.

performance enhancement through advanced features.

Figure 4.9 (b) illustrates the coverage and mean data rate as a function of the UDO. As expected the user experienced data rate decreases with the increase in UDO, due to the shared access on the data channel.

4.11   FDLA Performance as a Function of System Bandwidth

As LTE is expected to operate in different system bandwidths, we have selected three different bandwidth scenarios and evaluated the FDLA gain over Ref. The results are illustrated in Figure 4.10, where the ratio of the number of RBs to system BW is kept constant. Further, the ratio of offered traffic to the system bandwidth is also kept constant.

The results show that the FDLA cell throughput and coverage gain is improved with the increase in the system bandwidth, which can be attributed to two factors. Firstly, it is due to the deterioration in the performance of the Ref scheme at larger bandwidths. With the increase in bandwidth there is also an increase in the channel dynamics due to frequency-selective fading. The geometric average, which is used as the metric for effective SINR calculation in LA, is reduced with an increase in the channel variations, leading to the reduction in throughput.

Secondly, due to the increase in UDO there will be an improvement in the multi-user diversity gain available from PF scheduling in time. FDLA can exploit the improved SINR conditions more effectively than the Ref scheme, due to the higher degrees of freedom. The combination of these factors lead to an improvement in the FDLA cell throughput gain by around 5%, as the system bandwidth is doubled. Similarly, the FDLA coverage gain is also improved by around 15% with the doubling of the system bandwidth.
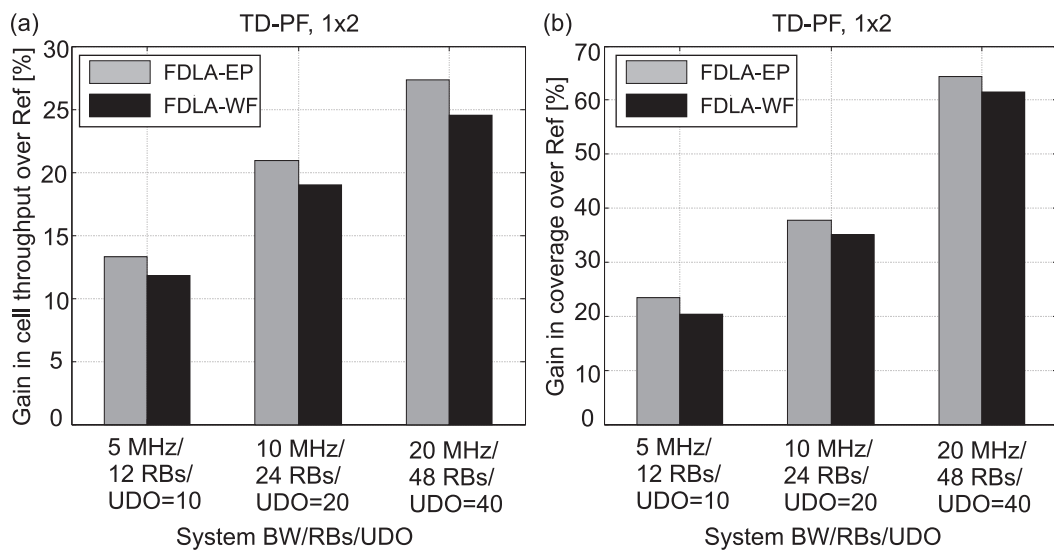

Figure 4.10: FDLA performance as a function of the system BW, based on the finite buffer traffic model and non-ideal CQI.
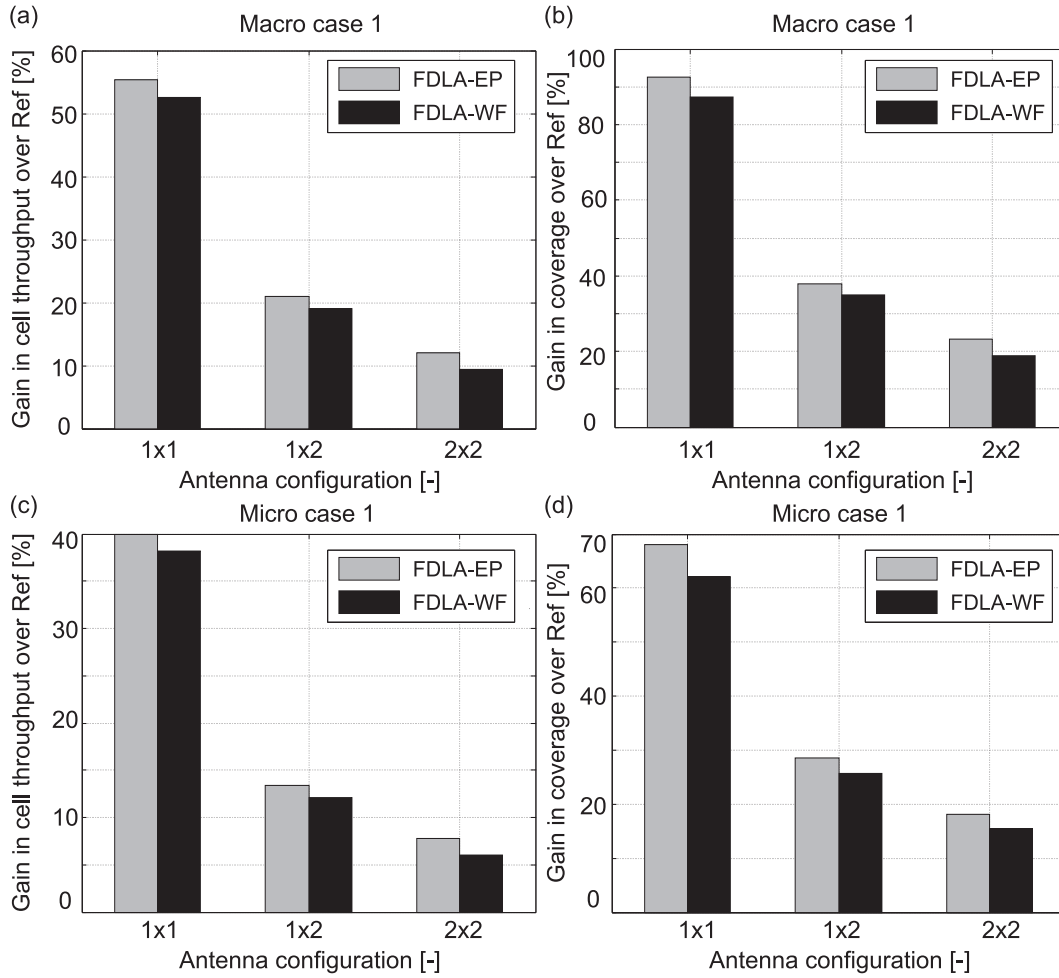
Figure 4.11: Impact of the antenna scheme and the deployment scenario on the FDLA performance. The results are based on the time-domain PF scheduler, non-ideal CQI and the finite buffer traffic model.

4.12 Impact of Antenna Scheme and Deployment Scenario on FDLA Performance

The impact of the antenna scheme and the cellular deployment scenario on FDLA cell throughput and coverage gain is evaluated in Figure 4.11. The results are based on the PF scheduler, non-ideal CQI and the finite buffer traffic model. It is obvious that the maximum FDLA gain potential is available with the 1x1 antenna scheme. Even with non-ideal CQI, the cell throughput gain is around 55%, while the coverage gain is close to 90%, in the Macro case 1 deployment scenario.

In case of the 2x2 SFTD scheme, the FDLA cell throughput gain is reduced to around 11%, while the coverage gain is reduced to around 20%, in the Macro case 1 scenario. The reduction in the gain potential of FDLA in comparison to the 1x2 case is due to the stabilization of the channel resulting from the addition of open loop transmit diversity, which has a two fold effect on performance. Firstly, the dynamic range of the channel is reduced, which reduces the SINR peaks as well as the throughput enhancement available from FDLA. Secondly, the performance of the Ref scheme is improved due to reduction in the channel dynamics. In general, the addition of transmit and/or receive diversity will reduce the FDLA gain potential.

The probability of experiencing a high G-factor value is increased substantially in the Micro case 1 scenario, as seen in Figure 2.15. In the high G-factor range the ability of FDLA to improve throughput over Ref is reduced, leading to a reduction in the corresponding cell throughput and coverage gain. As an example, the cell throughput gain with the 1x2 antenna scheme is reduced to 13%, while the coverage gain is reduced to around 29%, based on the FDLA-EP scheme.

4.13   Conclusions

In this chapter we have described the performance evaluation of FDLA based on the simplified single-cell model. The three algorithms considered for link throughput optimization are FDLA-EP, FDLA-WF and Ref. First, the functioning of the system model was validated by comparing performance results with those obtained in the preliminary evaluation of Subsection 3.7.1. A close match was found between the two sets of results.

To begin with the system-level evaluation of FDLA was based on ideal CQI reporting, the infinite buffer traffic model, and the TD-RR scheduler. The dependence of FDLA gain on the scheduling resolution in frequency was determined by conducting simulations under three multi-path channel profiles. It was found that most of the FDLA gain potential can be achieved if the RB width is in the order of the coherence bandwidth of the channel. Thus, 24 RBs within 10 MHz are sufficient to achieve within 5% of the maximum FDLA gain, in a highly frequency-selective channel such as the TU.

In terms of block encoding options, it was seen that SB transmission provides a good trade-off between complexity and performance. Further, the FDLA-WF scheme can provide a marginal improvement in the cell throughput gain over FDLA-EP (1% - 2%), only if MB transmission is employed. The detailed performance curves such as the CDF of the average user throughput as well as the variation in user throughput as a function of the G-factor revealed that FDLA is mainly a coverage enhancement mechanism. This results from the Shannon Theorem, which recommends to trade BW for SINR improvement at the low SINR values.

Next, non-ideal CQI measurement and reporting delays were introduced in the system model. Further, the TD-PF scheduler was also introduced in order to evaluate the FDLA potential under realistic conditions. It was found that the open loop LA is not able to stabilize the link quality in the presence of CQI errors. It is due to the tendency of LA to allocate those RBs that have a positive value of error, thus introducing a positive bias in LA decisions. The impact of CQI errors is reduced by the closed loop OLLA mechanism.

The impact of UE speed on FDLA performance was evaluated for the 1x2 antenna scheme. The general trend was that the FDLA gain is reduced with increase in speed, due to the inability of LA to track fast variations in the channel quality on the basis of CQI reports. It was shown that FDLA can provide an improvement of 30% in coverage over Ref even at 30 km/h, while maintaining a similar cell throughput as the Ref scheme. Next, the impact of the traffic model on performance was evaluated. It was seen that the finite buffer traffic model improved the FDLA cell throughput gain by around 8%, over the infinite buffer model. This is mainly due to the deterioration in performance of the cell-center users under the data-fair traffic model.

Next, the ability of the TD-PF scheduler to improve cell throughput by exploiting the multi-user diversity gain was demonstrated. It was seen that the PF scheduling in time improves the cell throughput of the Ref scheme by 14%, as the UDO is increased from 1 to 20. The improvement in

the FDLA throughput was lower at around 5%, due to the higher operating point of the algorithm.

The evaluation of FDLA under different system bandwidths has shown that the gain potential is improved in wider bandwidths, up to 20 MHz. The ratio of total number of RBs to system bandwidth as well as of the offered traffic to system bandwidth was kept constant in these simulations. The improvement in the FDLA gain with bandwidth is attributed to the deterioration in performance of the Ref scheme, due to an increase in the channel dynamics. Further, there is a marginal improvement in FDLA performance due to the increase in the multi-user diversity gain.

The evaluation of FDLA gain under different antenna configurations has shown that the gain potential is reduced in the presence of transmit and/or receive diversity. This is caused by the reduction in the channel dynamic range, i.e., stabilization of the channel. The FDLA gain is also reduced if the isolation between cells is improved, e.g., in the Micro case 1 scenario. This is due to the increase in the operating point (SINR), which will generally limit the potential of throughput enhancement.

In terms of the preferred LA scheme, the analysis demonstrates that the FDLA-EP scheme with SB transmission provides the best trade-off between implementation complexity and performance. The same conclusion has been reached by several recent studies submitted to 3GPP [14].

The following mobility scenarios of interest are defined:

- *Static*: In this scenario the users are stationary, and the PF scheduler is not able to exploit multi-user diversity in time-domain. However, the frequency selection diversity is still available to FDLA. Further, the CQI overhead needed to support FDLA can be reduced significantly, e.g., the CQI report for the first RB is transmitted at TTI=1, the CQI for the second RB is transmitted at TTI=2, and so on. Thus, in principle the CQI overhead for FDLA can be reduced to that of the Ref scheme.

- *Low mobility*: This scenario corresponds to a UE speed of up to 3 km/h. In this case, the system is able to fully exploit the available diversities in time, frequency and multi-user domains. However, the signaling requirements are extensive in order to support fast multi-domain adaptation.

- *Medium mobility*: This scenario corresponds to a UE speed of up to 30 km/h. In this case, the potential of fast link adaptation is reduced as CQI does not provide a reliable estimate of the prevailing channel conditions.

- *High mobility*: This scenario corresponds to UE speeds in excess of 30 km/h. As the system is no longer able to track fast channel variations the "open loop" or "averaging" diversity techniques are beneficial to stabilize user performance. The distributed transmission scheme is an example of such a technique [14]. We have not investigated the FDLA performance in the high mobility scenario.

The FDLA-EP/SB cell throughput and coverage gain over Ref under non-ideal CQI conditions and based on the 1x2 antenna scheme are summarized in Table 4.2. The results are given for both traffic models and are based on the Macro case 1 deployment scenario. The maximum FDLA potential is available in the static scenario, as the Ref scheme suffers from the lack of multi-user diversity gain. The FDLA gain potential is reduced with the increase in UE speed, e.g., the cell throughput gain is reduced from 25% (static case) to 13% at 30 km/h, while the coverage gain is

Table 4.2: FDLA gain over Ref for the 1x2 MRC case and the 3GPP Macro case 1 scenario. The results are based on the AB-CQI reporting scheme, and the TD-PF scheduler.

Mobility scenario	Cell throughput gain [%]		Coverage gain [%]	
	Finite buffer	Infinite buffer	Finite buffer	Infinite buffer
Static	25	15	40	40
Low mobility (3 km/h)	20	12	35	35
Medium mobility (30 km/h)	13	7	25	25

reduced from 40% to 25%. The findings of this study have been published in a conference article [46].

Chapter 5

Analysis of Frequency-Domain Packet Scheduling

5.1 Introduction

This chapter covers the system-level evaluation of the two FDPS schemes, namely A-FDM and F-FDM, that were introduced in Subsection 3.8.2. The analysis is based on LTE assumptions. It has been carried out under a variety of operating conditions, e.g., different antenna schemes, channel profiles, system bandwidths, in order to make an accurate assessment of the FDPS potential, as well as determine the key factors that influence its performance.

The chapter is organized as follows: The main modeling assumptions are summarized in Section 5.2. The preliminary analysis of FDPS performance based on a simplified system model is presented in Section 5.3. It is followed by the detailed analysis of FDPS potential using the single-cell based evaluation technique outlined in Section 2.12. The main conclusions are presented in Section 5.12.

5.2 Modeling Assumptions

The evaluation of FDPS performance is based on the quasi-static link and network level simulation methodology, introduced in Section 2.12. It consists of a single-cell implementation, where the LA and PS functionalities are implemented in detail, while the other cell interference is based on a known G-factor distribution. The G-factor distribution represents average SINR conditions based on full-load transmission from all the cells in a multi-cell deployment [14]. The transmit parameters used to obtain the G-factor distribution have been specified by the 3GPP, e.g., Macro case 1 parameters are specified in [14]. Further, a uniform distribution of users in area is assumed.

The link-level SINR experienced by each user is precalculated for a known G-factor, based on the detailed OFDM link-level model. The CQI reports are generated using the delayed and formatted version of the link-level SINR trace, as explained in Subsection 2.12.2. The CQI error is characterized by a lognormal distribution, taken from WCDMA/HSDPA settings [48]. The default

Table 5.1: Default simulation parameters.

Parameter	Setting
System bandwidth, (BW)	10 MHz
RB bandwidth	375 kHz
Number of users (UDO)	10
Cell-level user distribution	Uniform
Power delay profile	TU
CQI reporting scheme	AB-CQI, periodic reporting
CQI error std.	1 dB
CQI reporting resolution ($resSinr$)	1 dB
CQI reporting interval (Δ_{cqi})	2 ms
N_{abs}	5 bits
Processing delay (D_{cqi})	1.5 ms
TD scheduling	PF
FD scheduling	PF
Selected LA scheme	single-block, EP, Full BW
AMC model	See Subsection 2.5.1
HARQ model	Chase combining
LA target	10% BLEP (1st Transmission)
UE speed	3 km/h
UE receiver	1x2 MRC
Channel estimation	Ideal
Carrier frequency	2 GHz
Deployment scenario	3GPP Macro case 1
PF filter length	150
Initial T_m value	$BW/UDO \cdot \log_2(1 + \hat{G}/2.5)$‡

‡$\hat{G}$ *is estimated using the first available CQI reports of the user.*

value of the std. of CQI error is 1 dB [2]. The remaining CQI related parameter settings are based on the description in Section 3.9.

A simple admission control strategy is applied which maintains a constant number of active users within the cell, denoted by UDO. The analysis includes both infinite and finite buffer traffic models, based on the description in Section 2.10. In case of the finite buffer model, each user downloads a fixed 2 Mbit packet before exiting the system. Upon the termination of a session a new user is immediately added to the system.

In terms of the modeling of the DL control channel (AT) we assume that it is received without any errors throughout the coverage area of the cell. Similarly, it is assumed that the UL control channel carrying the HARQ Ack/Nack information as well as the CQI reports is always received correctly. The default simulation assumptions are summarized in Table 5.1.
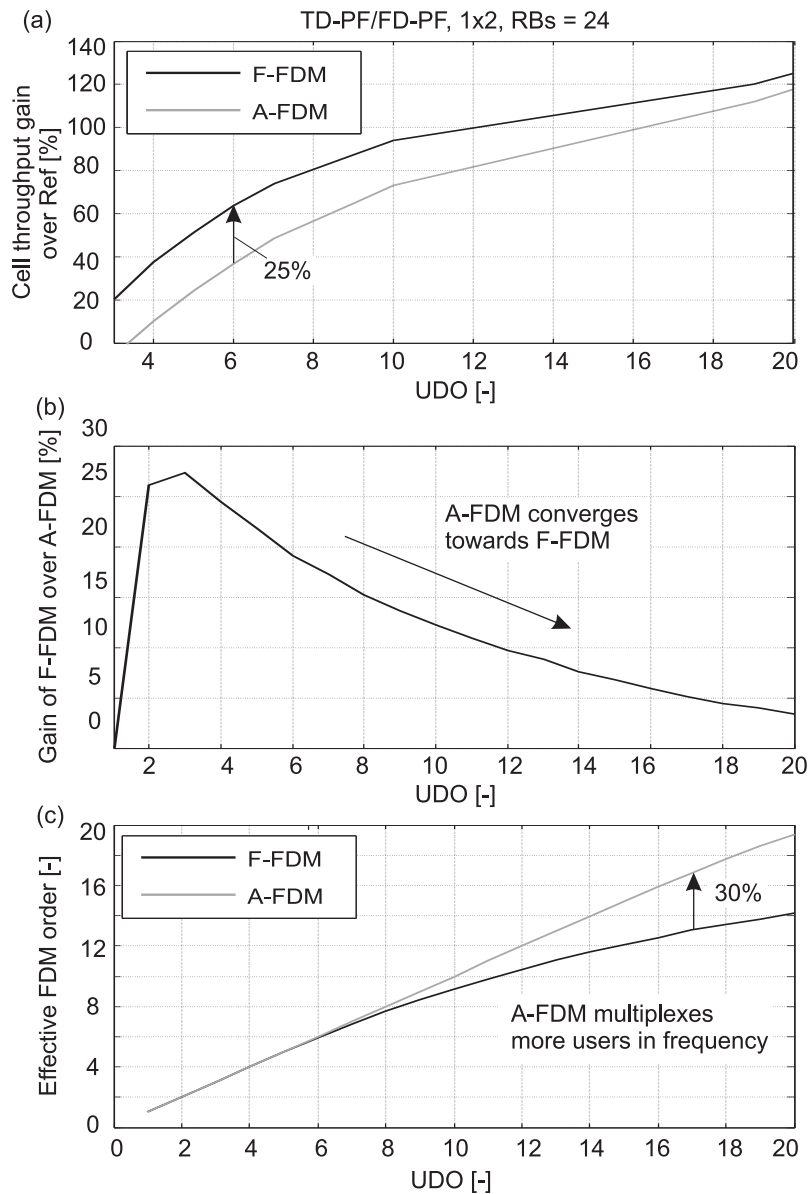
Figure 5.1: Preliminary evaluation of the FDM techniques, based on the 1x2 MRC receiver and 24 RBs.

5.3 Preliminary Analysis of the FDM Techniques

We begin by investigating the performance of the A-FDM and the F-FDM schemes using a simplified system model, which was introduced earlier in Section 3.7. The analysis is based on the 1x2 antenna scheme, and the 10 MHz bandwidth is divided into 24 RBs. The modeling of FDPS assumes that there are always UDO number of UEs present at any G-factor. Scheduling is based on the PF priority metrics given by (3.12) and (3.16). Perfect CQI measurement and reporting is assumed in these results.

Figure 5.1 (a) shows the cell throughput gain of both FDPS schemes over Ref as a function of the UDO. As FDPS is able to exploit the multi-user diversity in both time and frequency domains, its gain potential is improved with an increase in UDO. Further, as the A-FDM technique is limited by the multiplexing constraint that allows only adjacent RB allocations to any UE, its performance

is inferior to the fully flexible F-FDM scheme. The difference between the two schemes is significant at low-moderate UDO, and it decreases at large UDO. As an example, the cell throughput gain is reduced by as much as 25% with A-FDM (UDO=6) in these idealized simulations.

Figure 5.1 (b) illustrates the gain of F-FDM over A-FDM as a function of the UDO. It increases initially with UDO, and thereafter the performance of the two schemes begins to converge. The behavior can be explained intuitively, as with a very large number of users the probability that F-FDM will allocate more than one RB to any user is negligible. Thus, at large UDO values with both schemes allocating a unique user to each RB the impact of the A-FDM multiplexing constraint becomes insignificant.

Figure 5.1 (c) shows the effective FDM order, defined as the average number of UEs multiplexed in frequency, as a function of the FDM scheme and UDO. Interestingly, although in principle the A-FDM scheme requires fewer AT signaling bits than the F-FDM scheme for the same effective FDM order as seen in Figure 3.14, it multiplexes more users in frequency for a given UDO. This behavior is observed as the UDO is increased beyond 8. Thus, the potential of saving AT signaling bandwidth with the use of A-FDM scheme is reduced. As an example, A-FDM multiplexes around 30% more users in comparison to F-FDM at large UDO values.

5.4 FDPS Gain Potential as a Function of the Scheduling Resolution

We now evaluate the FDPS potential based on the single-cell system model. In order to investigate the dependence of FDPS gain on the scheduling bandwidth, we have performed system-level simulations with the TU and the Ped. A channel profiles. The results are shown in Figure 5.2, based on the TD-PF/FD-PF scheduler and ideal CQI reporting. In terms of LA, we have used the Full BW/SB transmission scheme, described earlier in Subsection 3.8.4.

By comparing the FDPS potential with the results shown in Figure 5.1 (a) it is seen that the maximum cell throughput gain potential of F-FDM is reduced to around 60%, when more realistic system modeling assumptions are introduced. The results for the TU channel profile show that most of the F-FDM potential is achieved by having the RB width close to coherence bandwidth of the channel, e.g., with 24 RBs the cell throughput gain is within 5% of the maximum gain potential, and within 10% of the maximum coverage gain. In this case the ratio of RB width to coherence BW is 0.85. However, the Ped. A curves indicate that around twice the number of RBs are required to achieve similar F-FDM gain potential. We conclude that the RB width should be between 1-2 times the coherence BW of the channel profile, in order to achieve most of the F-FDM gain potential.

The A-FDM curves for the TU profile show that for a fixed UDO the performance of this scheme deteriorates with increase in the number of RBs. The complexity of cell throughput optimization with A-FDM under a highly frequency-selective environment will increase with the addition of RBs. The A-FDM scheduler design proposed here is clearly not optimal, as seen in the performance deterioration at large number of RBs. A similar trend is observed in the coverage performance. Comparing it to the A-FDM performance in the relatively flat fading Ped. A channel profile, it is seen that although there is no deterioration in cell throughput, the coverage is reduced initially. We conclude that the proposed algorithm for A-FDM requires optimization.
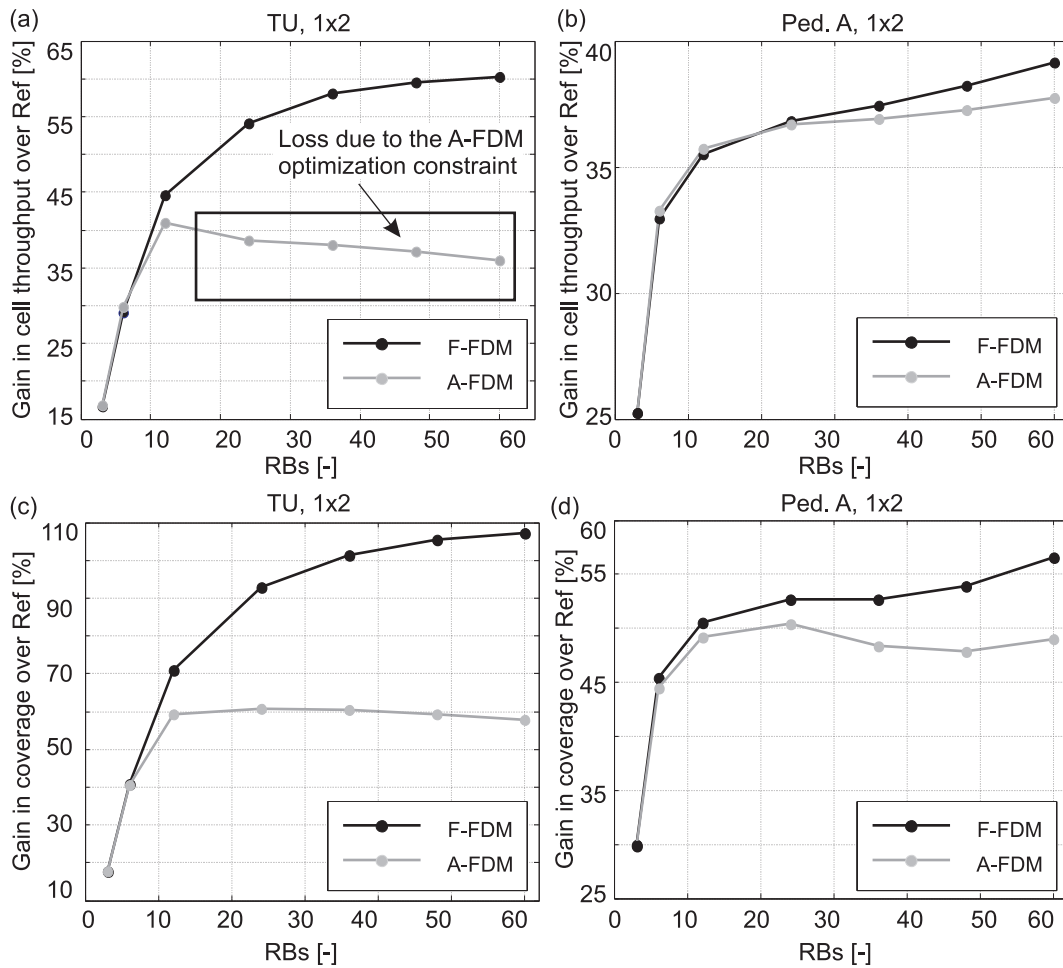
Figure 5.2: FDPS performance as a function of the number of RBs, based on the TD-PF/FD-PF scheduler, 1x2 antenna scheme, ideal CQI, and the infinite buffer traffic model.

5.5   Detailed Analysis of FDPS Performance

Figure 5.3 shows the behavior of the FDM schemes in terms of the most relevant performance indicators. In Figure 5.3 (a) it is seen that FDPS can provide an improvement in throughput over the complete range of G-factors experienced in the Macro case 1 deployment scenario. Figure 5.3 (b) illustrates the throughput gain over Ref as a function of the G-factor. As expected, the gain is a decreasing function of the G-factor.

Figure 5.3 (c) illustrates the CDF of the average user throughput for the considered schemes. It is seen that FDPS can provide a significant improvement in data rate over the entire CDF range. The curves in Figure 5.3 (d) show the CDF of the scheduled SINR for the 24 RBs case. It is observed that the A-FDM multiplexing constraint leads to a SINR penalty of around 0.8 dB in the median sense.
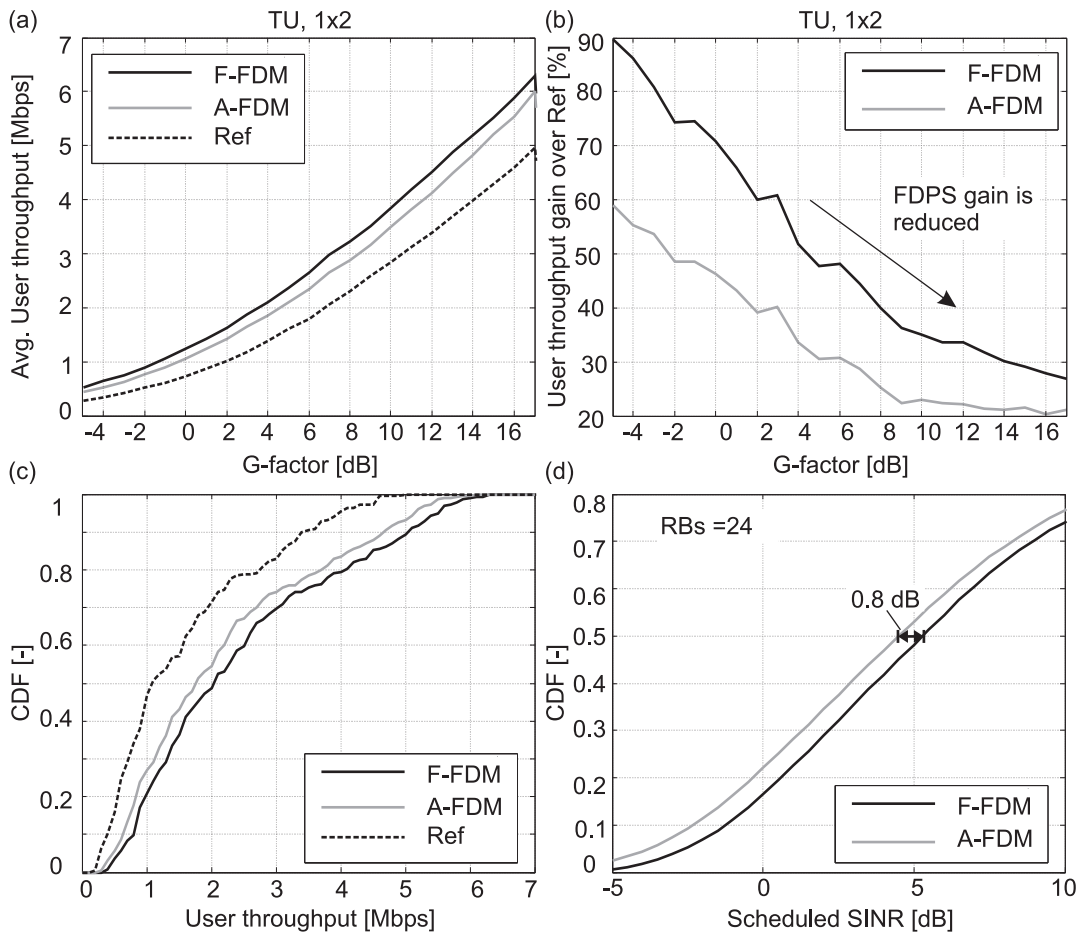
Figure 5.3: Detailed analysis of the FDM, based on TU channel profile, ideal CQI, 1x2 antenna scheme and the infinite buffer traffic model.

5.6   FDPS Performance as a Function of the User Diversity Order

Figure 5.4 (a) shows the FDPS cell throughput gain over Ref, as a function of the UDO. Ideal CQI is assumed in these simulations. Similar trends were seen in Figure 5.1 (a), though the absolute gain is reduced here due to more realistic assumptions. The F-FDM scheme improves the gain potential over A-FDM initially. However, the two curves converge at large UDO values. Figure 5.4 (b) illustrates the coverage gain of FDPS over Ref. The F-FDM coverage gain saturates around UDO of 10, due to the high operating point of the algorithm. However, the A-FDM coverage gain grows almost uniformly in the considered range of UDO values, due to the limited degrees of freedom.

For low to moderate UDO the A-FDM scheme experiences a 15% - 20% loss in gain potential in comparison to F-FDM. Additionally, the multiplexing constraint of the A-FDM scheme makes it difficult to implement schedulers that can provide strict fairness control.
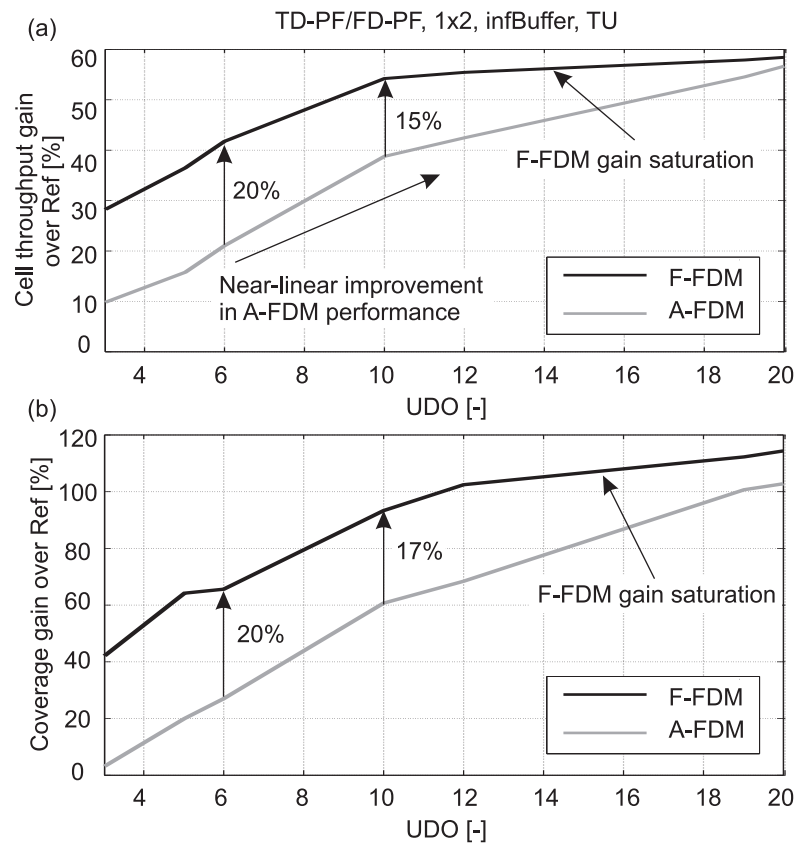
Figure 5.4: FDPS performance as a function of the UDO, based on the TU channel model, and the 1x2 receiver. Further, ideal CQI has been assumed.

5.7 Impact of CQI Measurement Inaccuracies on FDPS Performance

We now include realistic assumptions related to the CQI measurement accuracy as well as quantization and reporting delay. Figure 5.5 (a) and (b) illustrates that LA is not able to provide reliable performance in the presence of CQI errors. Similar trends are observed for both FDPS schemes. As the std. of the lognormal error increases, the probability of LA scheduling on RBs with a large positive error also increases. Consequently, a closed loop mechanism is needed to stabilize the performance.

The OLLA performance curves in Figure 5.5 show that it can significantly improve FDPS performance in the presence of CQI inaccuracies. As an example, when the std. of CQI error is equal to 1 dB, the F-FDM cell throughput gain over Ref is improved by 25% due to OLLA. Similarly, the A-FDM cell throughput gain is improved by around 10%. Similar trends are seen in terms of coverage. Thus, in a practical system implementation OLLA type of closed loop mechanism is required to provide robustness against CQI imperfections.

5.8 FDPS Performance as a Function of the UE Speed

The impact of mobility on FDPS performance is illustrated in Figure 5.6. The results are based on the infinite buffer model and assume non-ideal CQI. The ability of LA to track the channel
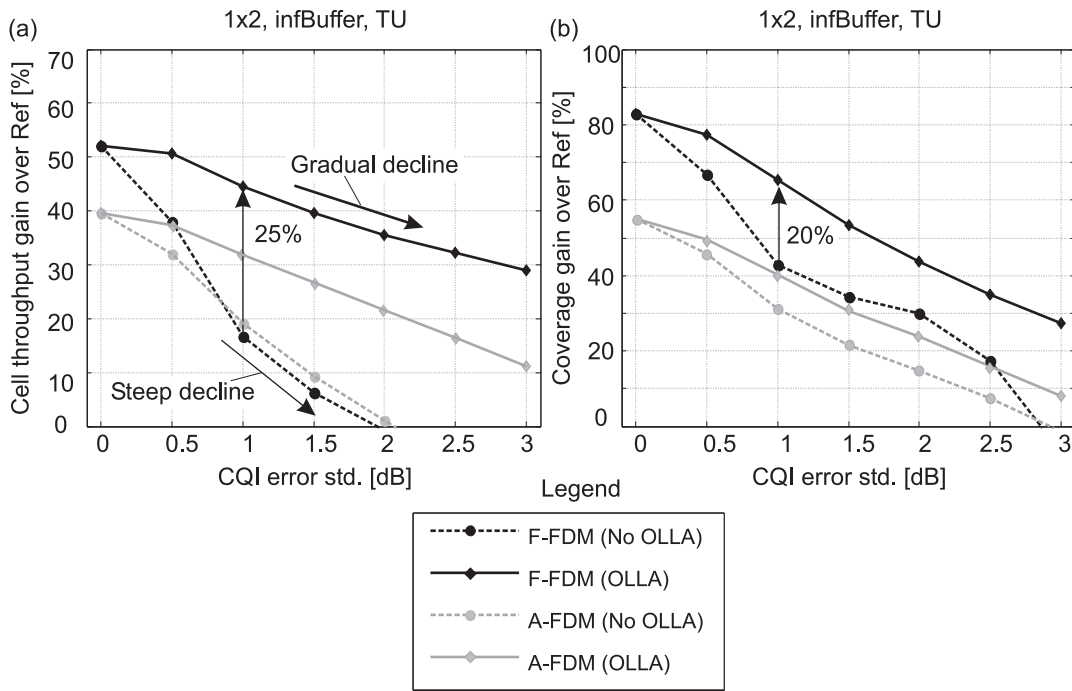
Figure 5.5: FDPS performance in the presence of CQI measurement inaccuracies and reporting delay. The ability of OLLA to stabilize FDPS performance is also shown. The results assume CQI quantization and reporting delay according to settings in Table 5.1.

quality variations on the basis of CQI reports is reduced with the increase in UE speed [48]. The finite LA/PS delay in a practical system implies that at high speeds the channel quality can change significantly between the time it is used in scheduling decisions and the instant when the packet finally arrives at the UE.

The results show that the FDPS cell throughput as well as coverage gain is halved at a speed of around 40 km/h. However, F-FDM can still provide a gain of around 25% - 30% in cell throughput and coverage at 40 km/h. The A-FDM scheme is equally sensitive to UE speed as can be seen
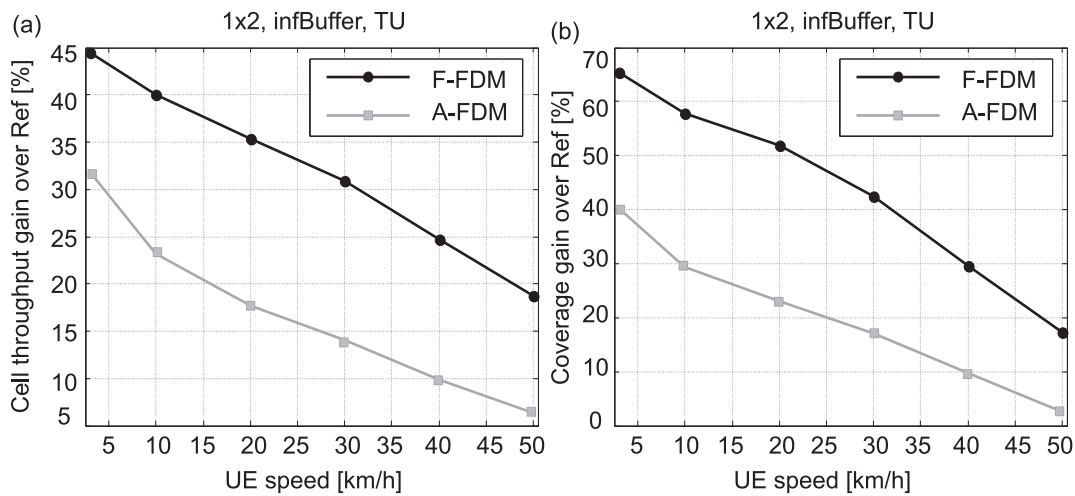

Figure 5.6: FDPS performance as a function of the UE speed, based on the 1x2 antenna configuration, non-ideal CQI, and the infinite buffer traffic model.
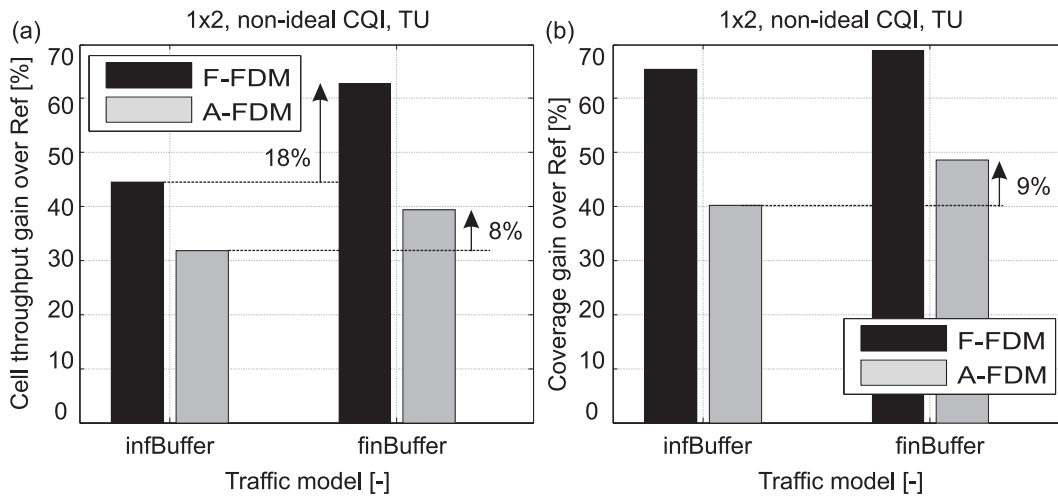
Figure 5.7: FDPS performance as a function of the traffic model. The results are based on non-ideal CQI and the 1x2 antenna scheme.

from the slope of the curves. However, as its gain potential is lower than F-FDM, the available cell throughput as well as coverage gain is reduced to around 10% at 40 km/h. The results suggest that FDPS can provide a significant improvement in performance for low-moderate UE speeds, i.e., below 30 km/h - 40 km/h. For higher UE speeds techniques that exploit frequency-diversity, such as distributed transmission of LTE [14], could provide an improvement in throughput performance. Further, the CQI overhead can be reduced in the high speed scenario.

5.9   Impact of Traffic Model on FDPS Performance

The comparison of the FDPS gain potential under the two types of best-effort traffic models considered in this study is illustrated in Figure 5.7. Similar to the FDLA observations in Figure 4.7, the FDPS gain potential is increased with the data-fair finite buffer traffic model. The cell throughput gain of F-FDM is improved by around 18%, while that of A-FDM is improved by around 8%.

Under the data-fair traffic model, the overall cell throughput is reduced as a result of reduction in the data rate experienced by cell-center users. The PF scheduler needs to allocate more time to the cell-edge users in order to compensate for the less favorable channel conditions. Among the considered schemes the Ref scheme experiences the most severe reduction, which leads to an improvement in the FDPS gain potential.

In terms of coverage, the F-FDM scheme does not experience a significant difference due to the finite buffer model, e.g., within 1% - 2%. However, the coverage gain with the A-FDM scheme is improved by around 9% under the finite buffer model.

5.10   FDPS Performance as a Function of System Bandwidth

Figure 5.8 illustrates FDPS performance as a function of the system bandwidth. We have used three bandwidth cases: 5 MHz, 10 MHz and 20 MHz in the analysis. The PHY layer parameters
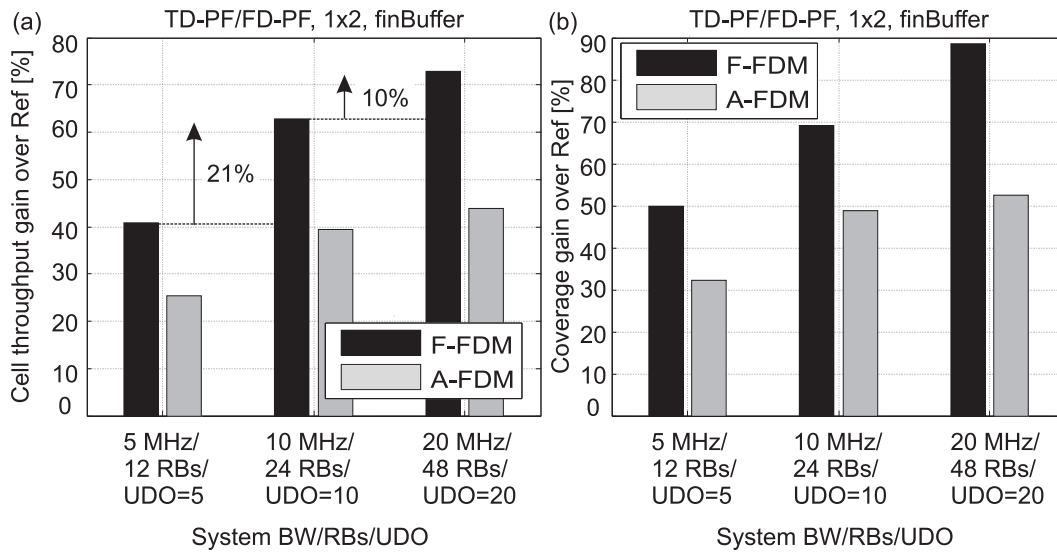
Figure 5.8: Impact of system bandwidth on FDPS performance, based on non-ideal CQI, TD-PF/FD-PF scheduler and the finite buffer traffic model.

for these cases are based on LTE assumptions [14]. The ratio of number of RBs to the system BW as well as of the offered traffic to the system BW is kept constant in these simulations.

The general trend is that the FDPS gain is increased with bandwidth. In terms of cell through-put, the gain from F-FDM is improved by about 21% when the BW is increased from 5 MHz to 10 MHz. A similar improvement in the coverage performance is also seen. A-FDM shows sim-ilar trends although the absolute performance numbers are lower than the corresponding F-FDM values.

The improvement in performance with bandwidth is due to the deterioration in the performance of the Ref scheme at larger bandwidths, arising from the increase in channel dynamics which leads to a reduction in the geometric average SINR. Secondly, the multi-user diversity gain available to the FDPS scheduler is also improved with an increase in UDO. This effect is seen in Figure 5.9, illustrating the CDF of the scheduled SINR as a function of system bandwidth. For example, there is an increase of 1.5 dB in the median value of SINR between the 5 MHz and the 20 MHz cases.

The results in Figure 5.8 (b) illustrate that the coverage gain is also improved significantly with the increase in bandwidth. Looking at the F-FDM performance, the coverage gain is improved by around 20% with doubling of the system BW. However, A-FDM performance is increased only marginally beyond 10 MHz, due to the complex optimization procedure.

5.11 Impact of Antenna Scheme and Deployment Scenario on FDPS Performance

Figure 5.10 illustrates the impact of the cellular deployment scenario and antenna scheme on FDPS performance. Similar to the trends in Figure 4.11, the maximum FDPS gain potential is observed in the 1x1 antenna case. Further, the gain potential is reduced significantly with the addition of transmit and/or receive diversity. In the Macro case 1 scenario, the F-FDM scheme can provide a cell throughput gain of 120% with the 1x1 receiver, while the gain is halved with A-FDM. Similar
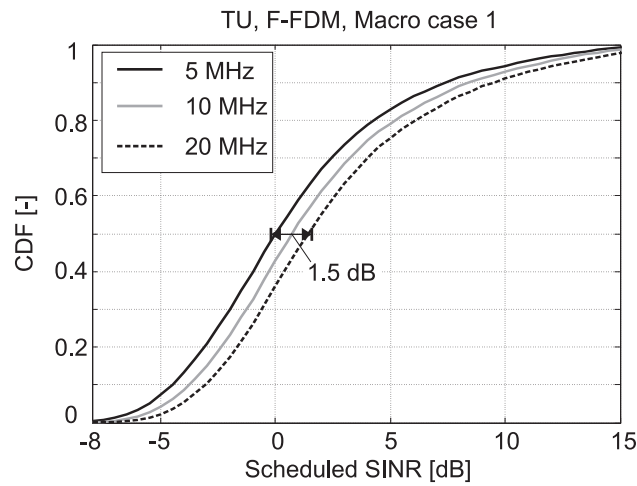
Figure 5.9: CDF of the scheduled SINR as a function of the system bandwidth for F-FDM scheduling, based on the 1x2 antenna scheme and the Macro case 1 deployment scenario.
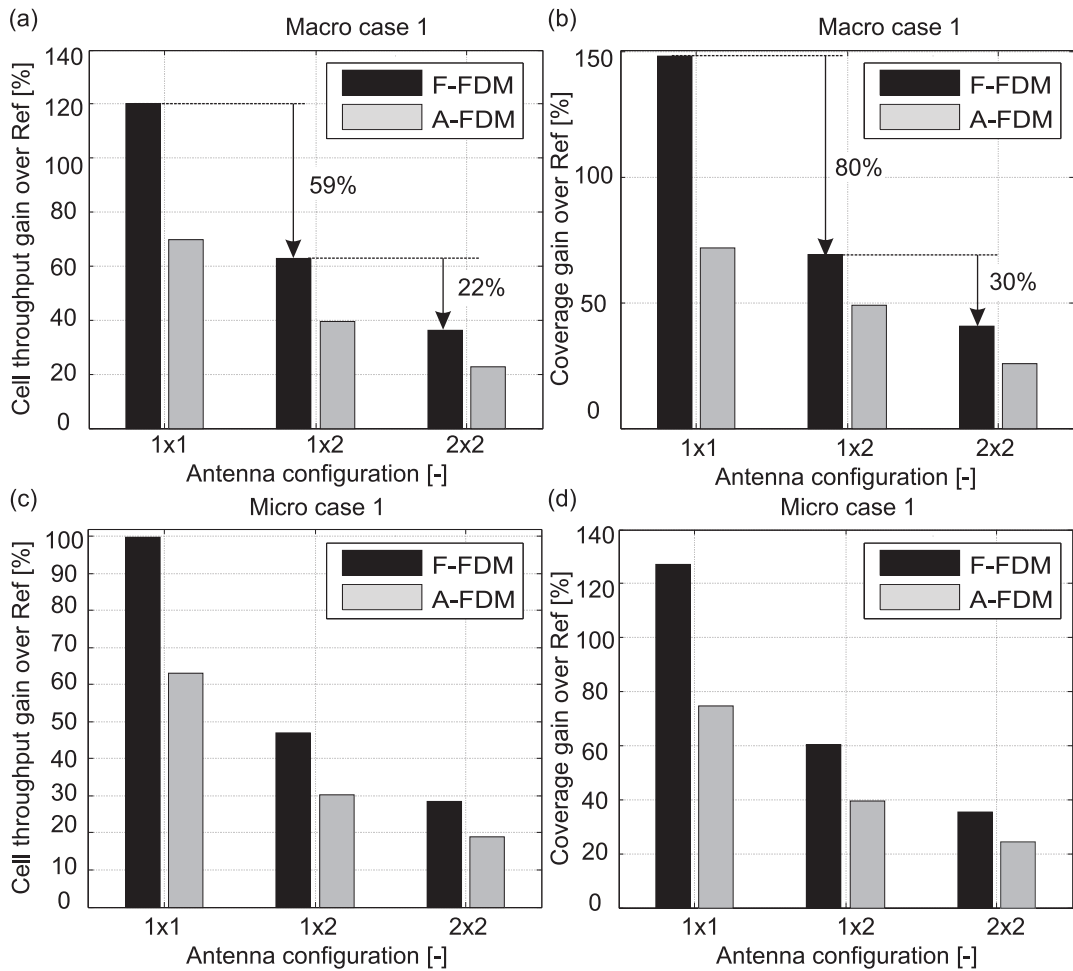

Figure 5.10: FDPS performance in the Macro case 1 and the Micro case 1 cellular deployment scenarios. The cell throughput and coverage gain for the three antenna configurations considered in the study are reported. The results are based on the finite buffer traffic model, non-ideal CQI, and the TD-PF/FD-PF scheduler.

trends are seen in terms of coverage. The cell throughput gain is reduced to 36% and 21% with F-FDM and A-FDM respectively, when the 2x2 scheme is employed. This represents a reduction in cell throughput gain of around 84% over the 1x1 scheme. The FDPS cell throughput gain is around 60% for the 1x2 antenna scheme.

The Micro case 1 deployment provides better isolation between cells, which increases the probability of experiencing good channel conditions, e.g., there is a 50% probability that the SINR will be larger than 10 dB. In this case the FDPS gain potential will be reduced due to significant improvement in the performance of the Ref scheme. Figure 5.10 (c) and (d) shows that the FDPS cell throughput and coverage gain with the 1x2 antenna scheme is around 45% and 60% respectively.

5.12   Conclusions

In this chapter we have evaluated the gain potential of the two considered FDM scenarios, namely, F-FDM and A-FDM, under a variety of operating conditions. It has been shown earlier in Figure 3.14, that A-FDM can reduce the DL signaling overhead significantly, e.g., by around 140%, in comparison to the fully flexible F-FDM scheme. This is achieved by introducing an additional multiplexing constraint in A-FDM, which ensures that only adjoining RBs can be allocated to any user. However, system level simulations have shown that the A-FDM scheme will multiplex more users on an average, in low-medium UDO. Thus, the potential to save signaling bandwidth with the A-FDM scheme is reduced.

Starting with ideal CQI assumptions and the infinite buffer traffic model we have shown that in order to achieve most of the F-FDM gain potential, the RB width should be within 1-2 times of the coherence bandwidth of the channel. Using the 1x2 antenna scheme as reference it was found that the F-FDM cell throughput and coverage gain over Ref is around 55% and 90% respectively, under a highly frequency-selective channel. A-FDM can provide a cell throughput gain of 40% and a coverage gain of 60% under similar conditions. In addition to the loss in gain potential the performance trends of the A-FDM scheme are difficult to predict as a result of the complex optimization procedure.

In terms of the FDPS gain dependence on location, it was seen that the most significant improvement is experienced by the coverage limited users. The ability of FDPS to harness the available multi-user diversity gain in time and frequency was investigated by sweeping over the UDO parameter. It was seen that the F-FDM gain potential saturated around UDO of 10, while the A-FDM gain is improved in a uniform manner over the considered UDO range. In general, the performance of A-FDM converges towards F-FDM as the UDO is increased.

When realistic assumptions on the CQI measurement accuracy and reporting delay are introduced it is seen that the FDPS gain potential is reduced significantly. Further, F-FDM was found to be more sensitive to CQI errors in comparison to A-FDM. For example, when the CQI error std. is equal to 1 dB the two FDM schemes have similar performance. Under CQI errors, the LA algorithm tends to favor those RBs which have a positive value of the CQI error, leading to an optimistic estimation of the supported throughput. The results have shown that the closed loop OLLA mechanism is able to provide robustness against CQI errors. It reduces the impact of the positive error bias, e.g., the improvement in the F-FDM cell throughput gain with OLLA is 25%, at the CQI error of 1 dB.

Next, the impact of UE speed on the FDPS performance is investigated. It is seen that the

ability of LA to track channel variations is reduced as the UE speed is increased. This is due to the CQI and LA/PS processing delays experienced in the practical system scenario. Simulations have shown that the FDPS gain potential is halved when the speed is increased to 40 km/h. For higher UE speeds it is recommended to employ open loop or averaging diversity techniques, such as the distributed transmissions [14], which exploit frequency diversity to stabilize link-level performance.

Among the traffic models, the finite buffer traffic model ensures that all users download an equal amount of data, irrespective of their location. It implies that the coverage limited users remain active longer than the cell-center users. Further, the use of PF scheduling results in increased allocation time for the coverage limited users, which leads to a deterioration in the data rate of the cell-center users. Thus, the overall cell throughput is reduced. Further, as the decrease in cell throughput is maximum for the Ref scheme, the FDPS gain is improved under the finite buffer traffic model, e.g., the F-FDM cell throughput gain is improved from 45% (infinite buffer) to 62% (finite buffer).

The FDPS gain potential is improved when the system bandwidth is increased from 5 MHz to 20 MHz. The ratio of RBs to the system bandwidth as well as the offered traffic to the system bandwidth is kept constant in these simulations. This results from deterioration in the performance of the Ref scheme at larger bandwidths due to the increased channel dynamics. Further, FDPS benefits from the increase in the multi-user diversity gain at larger bandwidths.

The FDPS gain potential is reduced by the addition of transmit and/or receive diversity. Further, if the average SINR conditions are improved due to better isolation between cells, the FDPS gain is also reduced. In order to provide significant gain FDPS requires that the underlying radio channel experiences large SINR dynamics. Further, due to the nature of the mapping between SINR and throughput, the operating point of the system should be low in order to improve the potential from FDPS.

In terms of the preferred FDM technique the detailed analysis under a variety of operating conditions suggests that the F-FDM scheme should be selected for implementation. It can maximize the gain potential, and its optimization is relatively simple. Further, scheduling policies that enable different degrees of fairness can be easily extended to the frequency domain. The performance of the F-FDM scheme can be predicted based on a sub-set of simulations. Another important advantage of this scheme over A-FDM is that it can support full averaging diversity, which is beneficial for high mobility users. Similar conclusions have been reached in the LTE standardization project

Table 5.2: F-FDM cell throughput and coverage gain over Ref for the 1x2 MRC case, Macro case 1 scenario, and based on the AB-CQI reporting scheme.

Mobility scenario	*Cell throughput gain [%]*		*Coverage gain [%]*	
	Finite buffer	*Infinite buffer*	*Finite buffer*	*Infinite buffer*
Static	75	60	90	90
Low mobility (3 km/h)	60	45	65	65
Medium mobility (30 km/h)	40	30	40	40

[14].

The F-FDM cell throughput and coverage gain over Ref for the 1x2 antenna scheme, Macro case 1 scenario, and based on non-ideal CQI settings are summarized in Table 5.2. Results are provided for the important mobility scenarios that were introduced in Section 4.13. The maximum gain potential is seen in the static case as FDPS is able to exploit the available frequency selection diversity, while the Ref scheme performance deteriorates due to the reduction in the multi-user diversity gain. Further, in the static scenario the CQI reporting overhead can be reduced significantly. The FDPS gain potential is reduced with UE speed, due to the inability of LA to track fast channel variations. It is concluded that F-FDM can provide a significant gain over frequency-blind transmission in an OFDMA system, even in the presence of receive antenna diversity. The findings of this study have been published in several conference articles, e.g., [102], [98].

Chapter 6

Evaluation of the Low Bandwidth CQI Schemes Enabling FDAS

6.1 Introduction

This chapter describes the evaluation of the low bandwidth CQI schemes that can facilitate FDAS. The trade-off between CQI overhead in the UL and the achievable FDAS performance in the DL is investigated based on system-level simulations. The following CQI schemes are considered in the analysis: Absolute-CQI (AB-CQI), Offset-CQI (OF-CQI), Threshold CQI (TH-CQI), Best-M CQI (BM-CQI) and its variant based on offset signaling, namely the Best-M Offset CQI (BM-OF-CQI). Additionally, the reference scheme based on the Ref-CQI scheme is also evaluated. These schemes have been introduced earlier in Section 3.9.

The investigation of FDLA potential with reduced CQI signaling is considered first, followed by the evaluation of FDPS. The chapter is organized as follows: Section 6.2 describes the modeling assumptions. Section 6.3 onwards up to Section 6.6 covers the evaluation of FDLA potential with different CQI schemes. Section 6.8 describes the performance with reduced CQI reporting rate. The conclusions of the CQI analysis for FDLA are presented in Section 6.10.

The evaluation of FDPS potential (F-FDM) with low bandwidth CQI schemes is described from Section 6.11 onwards and up to Section 6.18. The conclusions of the FDPS analysis are presented in Section 6.19. Supplementary results of the CQI analysis are presented in Appendix C.

6.2 Modeling Assumptions

The CQI measurement and reporting control loop was introduced in Figure 3.19. The accuracy of the per RB CQI estimation is dependent on the pilot symbols embedded within the RB. Based on LTE assumptions there are 8.33 reference symbols per sub-frame and per RB [14]. Assuming that the CQI error distribution is lognormal, which is similar to WCDMA/HSDPA [2], the numerical evaluation has shown that without any averaging in time the std. of per RB CQI error is around 2.5 dB (see Figure 3.18). This assumes a RB width of 375 kHz. At this value of CQI error, the cell throughput gain of FDLA is reduced by 15% and that of FDPS is reduced by 20%, as seen in

Table 6.1: Default simulation parameters.

Parameter	Setting
System bandwidth, (BW)	10 MHz
RB bandwidth	375 kHz
$nRBs$	24
Number of users (UDO)	20 (FDLA), 10 (FDPS)
Cell-level user distribution	Uniform
Power delay profile	TU
CQI error std.	1 dB (FDLA, FDPS), 0.4 dB (Ref)
CQI reporting resolution ($resSinr$)	1 dB
Offset resolution (Δ_{off})	1 dB
CQI reporting interval (Δ_{cqi})	2 ms (FDAS), 0.5 ms (Ref)
CQI averaging window (W_{cqi})	2 ms (FDAS), 0.5 ms (Ref)
N_{abs}	5 bits
N_{off}	[1:4] bits
Processing delay (D_{cqi})	1.5 ms
TTI duration	0.5 ms
TD scheduling	TD-PF, TD-RR
FD scheduling	F-FDM, FD-PF
LA parameters	single-block (FDLA), single-block, EP, Full BW (FDPS)
AMC model	See Subsection 2.5.1
HARQ model	Chase combining
LA target	10% BLEP (1st Transmission)
UE speed	3 km/h
UE receiver	1x1, 1x2 MRC
Channel estimation	Ideal
Carrier frequency	2 GHz
Deployment scenario	3GPP Macro case 1

Figure 4.4 and Figure 5.5 respectively. The CQI error can be reduced by performing time-domain averaging. This study assumes that the averaging window is fixed at 2 ms, at the receiver side.

The potential of reducing the CQI overhead through delayed reporting, i.e., by increasing Δ_{cqi} (in Figure 3.19), will also be investigated here. The disadvantage of this strategy is that the LA and PS delay will be increased, thereby reducing the ability of LA to track the channel variations. In other words, the mobility support will be affected adversely with a reduction in the CQI reporting rate. As mentioned earlier, it is assumed that the system supports periodic CQI reporting, which is also the recommendation in LTE [14].

The analysis will be based on the quasi-static decoupled link and network level simulation methodology, described in detail in Section 2.12. The LA and PS functionalities are implemented in detail within the center-cell, while a AWGN based model is used for the other-cell interference. The FDLA evaluation assumes single-block transmission, which was selected as the preferred block encoding scheme in Chapter 4. Further, both FDLA-EP and FDLA-WF algorithms are

employed in the CQI analysis. Note that it has been assumed that each RB contains enough data symbols for the UE to perform blind QAM detection when the FDLA-WF technique is employed, i.e., we do not assume that the reference power is signalled to the UE. In terms of the FDPS algorithm we will investigate the impact of reduced CQI overhead on the F-FDM scheme, which was chosen as the preferred scheme in Chapter 5.

The simple infinite buffer traffic model as well as the finite buffer model is used in the performance evaluation. In case of the infinite buffer model, several iterations are conducted wherein a set of users is created based on the G-factor distribution. The user and cell level statistics are collected at the end of each iteration. In case of the finite buffer model each user downloads a fixed 2 Mbit packet before leaving the system. The creation of users is dependent on the G-factor distribution. Further, when the session is terminated, a new user is immediately admitted. A simple admission control policy is employed which ensures that there is always a fixed number of UEs in the cell, given by UDO. The default simulation assumptions are summarized in Table 6.1.

6.3 FDLA Performance Based on the OF-CQI Scheme

The reference CQI scheme for FDAS is AB-CQI, where a detailed CQI report for each RB is forwarded to the eNode-B. Since the Ref scheme is able to utilize the entire system bandwidth in CQI estimation, the equivalent error is quite small, e.g., the std. of CQI error is 0.4 dB, according to Figure 3.18. Table 6.2 summarizes FDLA gain based on the AB-CQI scheme. The performance numbers are slightly different in comparison to Table 4.2 as the CQI error for the Ref scheme has been reduced. These results will be used to benchmark the performance of the reduced CQI schemes.

The OF-CQI scheme utilizes offset signaling in order to reduce the CQI overhead, as described in Section 3.9. Figure 6.1 (a), (b) illustrates the relative loss in cell throughput and coverage over the AB-CQI scheme. Results are presented for both FDLA-EP and FDLA-WF algorithms and are based on the Macro case 1 deployment scenario. Further, the 1x1 and the 1x2 antenna cases are considered, and the TD scheduler is based on PF scheduling, given by (3.12). Figure 6.1 (c), (d) show the available FDLA gain over Ref with the OF-CQI scheme. We consider four different settings of N_{off} in the analysis. Further, for each setting of N_{off} the optimum setting for maximum offset has been extracted from extensive simulations.

Table 6.2: Reference results giving FDLA gain over Ref based on the AB-CQI scheme. The results are based on the Macro case 1 scenario, TD-PF scheduler, and the UE speed is set at 3 km/h.

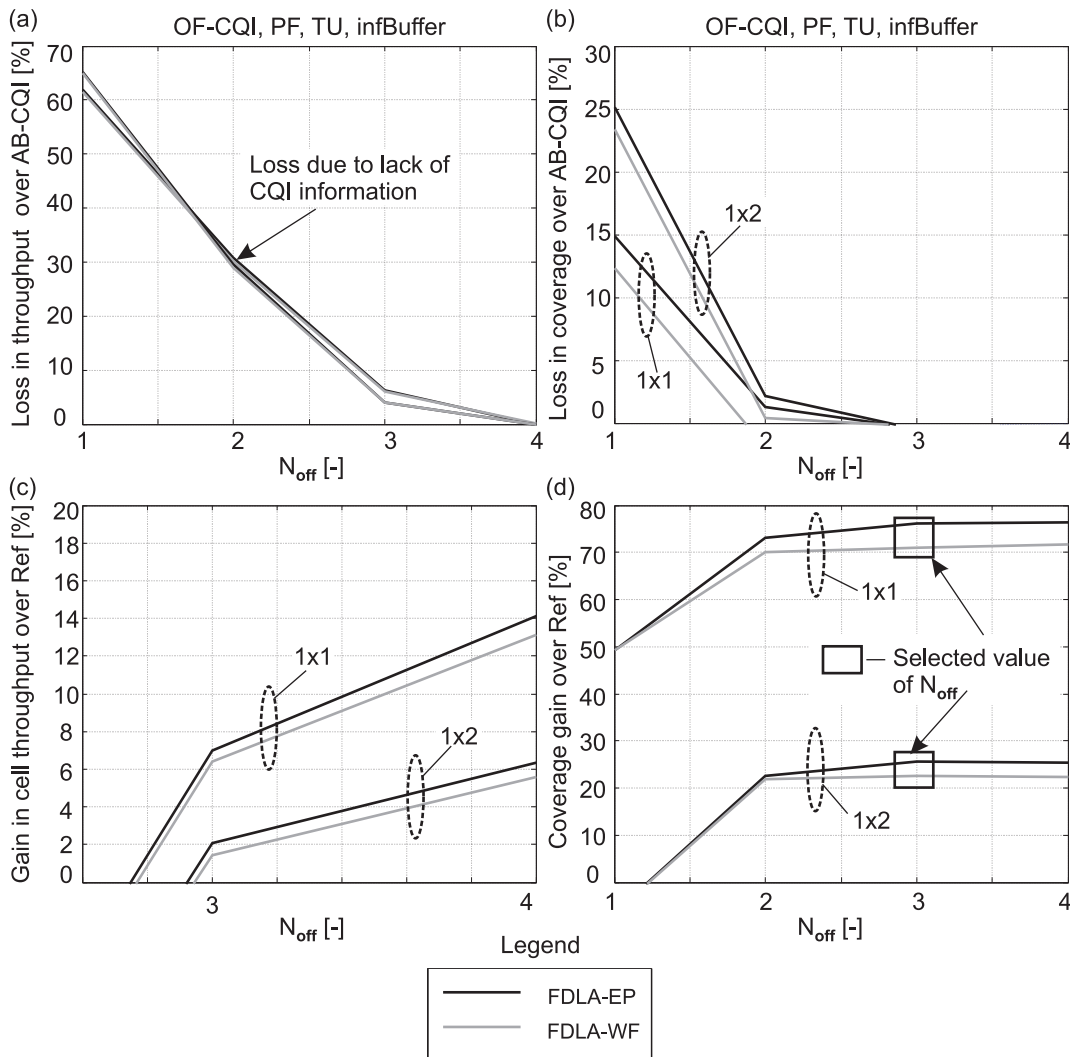| FDLA scheme (antenna conf.)	Cell throughput gain based on AB-CQI [%]		Coverage gain based on AB-CQI [%]	
	Finite buffer	Infinite buffer	Finite buffer	Infinite buffer
FDLA-EP (1x1)	49	14	77	76
FDLA-WF (1x1)	46	13	72	71
FDLA-EP (1x2)	14	6	30	26
FDLA-WF (1x2)	12	5.5	27	22

Figure 6.1: FDLA performance based on the OF-CQI scheme, TD-PF scheduler and the infinite buffer traffic model. Results are presented for both FDLA schemes as well as for both 1x1 and 1x2 antenna schemes.

It is seen that the FDLA performance is sensitive to the choice of N_{off}, e.g., a near-linear improvement in gain potential with N_{off} is seen. When it is set to a small value, i.e., 1 or 2, there is a significant loss in performance in comparison to the AB-CQI scheme. This can be explained as follows: The maximum value of offset is given by $(2^{N_{off}} - 1) \cdot \Delta_{off}$. An out-of-range indication is transmitted for the RBs whose offset relative to the best RB is greater than the maximum offset. As a result, when N_{off} is small, the transmitter does not have knowledge of the instantaneous channel conditions at a large number of RBs, which reduces the throughput potential.

The results in Figure 6.1 show that the FDLA performance converges in N_{off}. Further, the setting of $N_{off} = 3$ is sufficient to capture most of the available FDLA coverage potential, while still providing a better cell throughput than the Ref scheme. It corresponds to a maximum offset of 7 dB, based on $\Delta_{off} = 1$ dB. The trends are similar for both antenna schemes. Additional results for the OF-CQI scheme based on the TD-RR scheduler are presented in Figure C.1. The trends are quite similar to the TD-PF case, and $N_{off} = 3$ is sufficient to enable most of the FDLA coverage potential. At this value of N_{off} the saving in CQI overhead is around 36%, in terms of bits per

CQI report, relative to the AB-CQI scheme.

The dependence of the N_{off} parameter on the channel profile is investigated in Figure C.2 (a) and (b), where the Ped. A channel profile has been employed. It is seen that $N_{off} = 3$ is sufficient to achieve most of the FDLA gain potential. Based on this analysis it appears that $N_{off} = 3$ is a suitable setting for LTE.

6.4 FDLA-EP Performance Based on the TH-CQI Scheme

The proposed TH-CQI scheme requires that the average channel quality of the RBs within a specified threshold from the best RB is reported to the eNode-B. Further, the identity of the selected RBs is indicated by using a bit mask. The scheme has been illustrated in Figure 3.20 (c). The potential of savings in CQI overhead is quite significant, e.g., numerical evaluation for the 24 RBs case has shown that in terms of bits/report the overhead can be reduced by 76%, in comparison to the AB-CQI scheme.

The motivation behind this scheme is based on the LA algorithm, which utilizes SB transmission. As LA selects a single MCS format for transmission, it makes sense to utilize signaling bits to transmit the average channel quality over the best RBs. Further, as the quality of the individual RBs is not known, this scheme should only be applied with the EP power distribution.

There are several methods to implement the TH-CQI scheme, e.g., the threshold can be applied in the SINR domain, or in the throughput domain. In the latter case the SINR at each RB is mapped into throughput, and the threshold is applied in the throughput domain. In terms of threshold optimization it can either be optimized for each G-factor separately, or a single threshold can be applied at the cell-level. Although the former can potentially improve throughput performance, it has a higher implementation complexity, as the UE needs to estimate the G-factor over time. We evaluate the performance of these TH-CQI schemes next.

6.4.1 Evaluation of the TH-CQI Scheme Based on Cell-Level Threshold

Figure 6.2 illustrates the potential of the TH-CQI scheme based on a single threshold applied at the cell-level. Here, the threshold is applied in the SINR domain. The TD-PF and TD-RR schedulers as well as 1x1 and 1x2 antenna schemes have been used in the analysis. It is seen that the FDLA performance is sensitive to the threshold value. When the threshold is set at a low value there is lack of CQI information at the transmitter as only a few RBs lie within the specified threshold. This leads to a deterioration in cell throughput as observed in Figure 6.2 (a) and (c). For example, if the threshold is set at 5 dB, the loss in cell throughput over AB-CQI is around 22% for the 1x2 TD-RR case and 11% for the 1x2 TD-PF case. The TD-RR scheduler is more sensitive to the threshold value as it is unable to exploit smart scheduling techniques to compensate for the lack of CQI information.

As the threshold value is increased the cell throughput performance with the TH-CQI scheme begins to improve and reaches an optimum at the threshold value of around 10 dB, for all the considered cases. By increasing the threshold beyond the optimal value the cell throughput begins to decrease, as the average channel quality deteriorates. Note that even at the optimum threshold value there is a performance loss in comparison to the AB-CQI scheme. This results from the
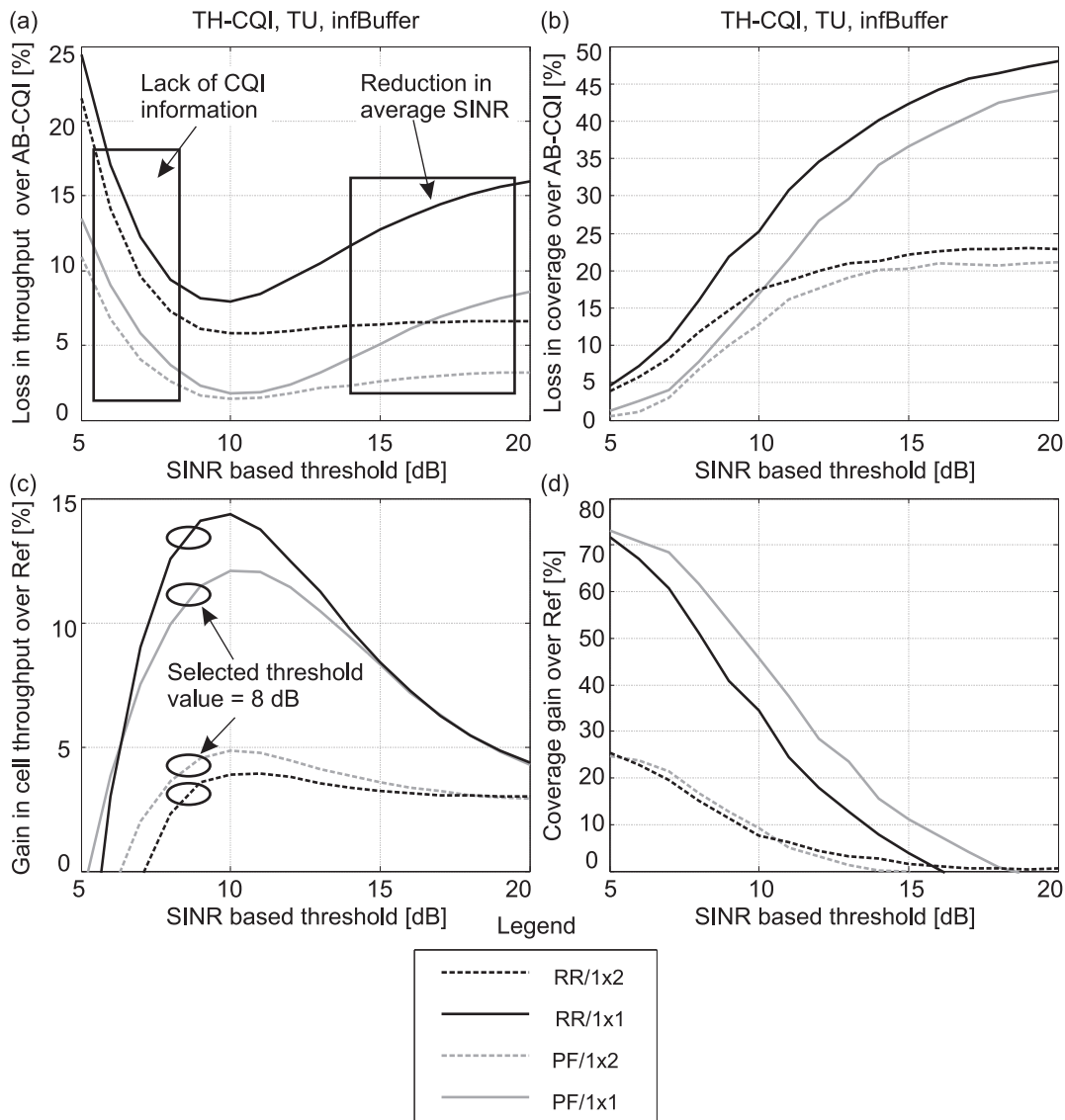
Figure 6.2: FDLA-EP performance based on the TH-CQI scheme, TU channel profile and Macro case 1 scenario. In terms of PS options both TD-PF and TD-RR schedulers are used in the investigation.

unavailability of detailed channel knowledge of the RBs at the transmitter side.

The variation in the coverage performance as a function of the threshold value is different from the behavior of cell throughput. In order to achieve the maximum FDLA coverage potential the threshold should be set at a low value, e.g., for the 1x2 TD-PF case the optimum value of threshold is around 5 dB. This is due to the fact that in case of the coverage limited users it is best to transmit on a few RBs with better channel quality, as was seen in the FDLA performance curves of Figure 4.3 (b). However, by doing so the cell throughput performance will deteriorate due to a reduction in the effective number of RBs, as seen in Figure 6.2 (a). The threshold value of 8 dB is selected for all the considered cases, as it provides a good trade-off between cell throughput and coverage. Supplementary results of the TH-CQI scheme based on the Ped. A channel profile are shown in Figure C.2 (c). It is seen that the optimization of the threshold value is specific to the channel profile.
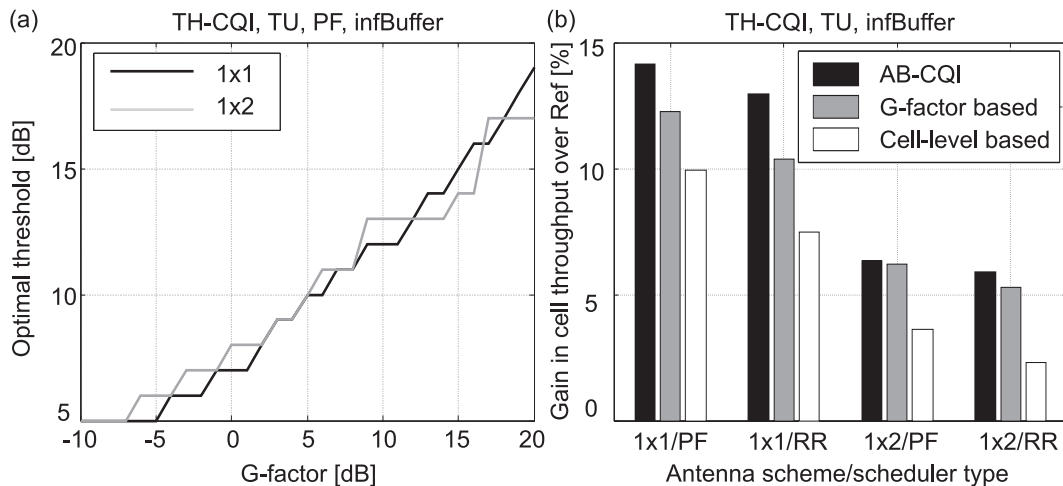
Figure 6.3: FDLA performance with the TH-CQI scheme, based on the G-factor level threshold.

6.4.2 Evaluation of the TH-CQI Scheme Based on G-Factor Level Threshold

The optimal threshold value in terms of cell throughput depends on the actual SINR values and the intra-RB dynamics. Figure 6.3 (a) illustrates the variation in the optimal threshold value as a function of the G-factor. This analysis assumes that the threshold is applied in the SINR domain. Here, the TD-PF scheduler is employed, and results are obtained for the 1x1 and the 1x2 antenna schemes. In general, a larger threshold value is required for a given G-factor in the presence of receive antenna diversity. This is expected as the system is operating at a higher mean SINR level. Further, the optimum threshold value increases with the G-factor due to similar reasons.

Figure 6.3 (b) illustrates the comparison between the cell-level and the G-factor level threshold optimization. Results for the TD-RR scheduler are also provided here. It is seen that there is only marginal improvement in the performance through the use of G-factor dependent optimization, e.g., in the order of 2% - 3%, over the cell-level based Threshold optimization. Further, the trends are similar for both scheduler types.

6.5 FDLA Performance With the BM-CQI Scheme

The CQI overhead is reduced by the BM-CQI scheme by transmitting the CQI reports only for the best M RBs, as depicted in Figure 3.20 (d). The scheme is based on the principle that FDLA normally utilizes only the RBs with favorable channel conditions in resource allocation. It can support both FDLA algorithms as detailed knowledge of the channel quality at the M RBs is available at the transmitter. In terms of optimization of the M parameter both cell-level and G-factor based optimization can be employed. Here, we will only consider cell-level optimization of the M parameter.

Figure 6.4 illustrates the performance of the BM-CQI scheme for both FDLA algorithms and the TU channel profile. The aim is to determine that value of M which can provide most of the FDLA coverage gain, while providing a cell throughput that is similar to the Ref scheme. It is seen that a fairly large value of M is required to ensure that the cell throughput loss over AB-CQI is within 5%, e.g., $M = 20$ for the 1x2 scheme, and $M = 18$ for the 1x1 scheme. When M is small,
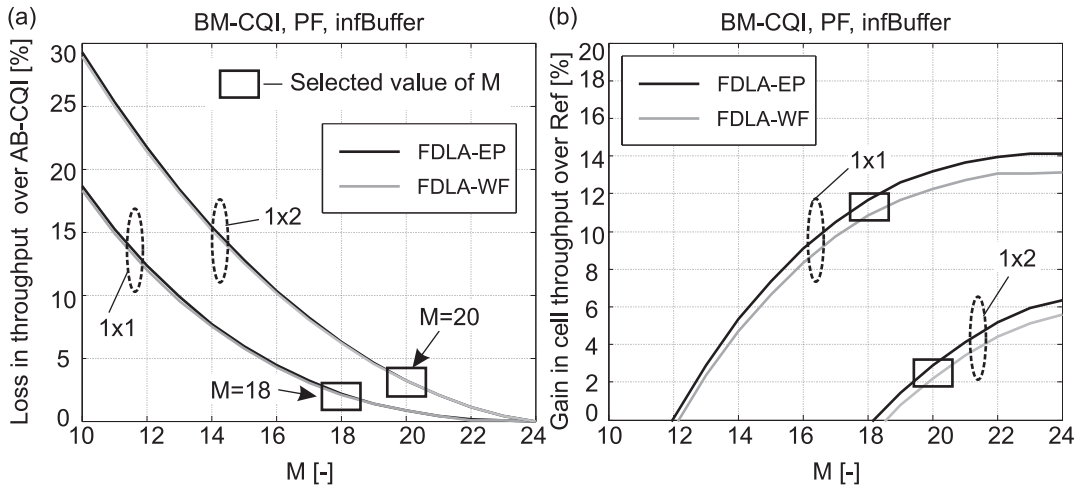
Figure 6.4: FDLA performance based on the BM-CQI scheme. Results are provided for the TD-PF scheduler, both antenna schemes and the infinite buffer traffic model.
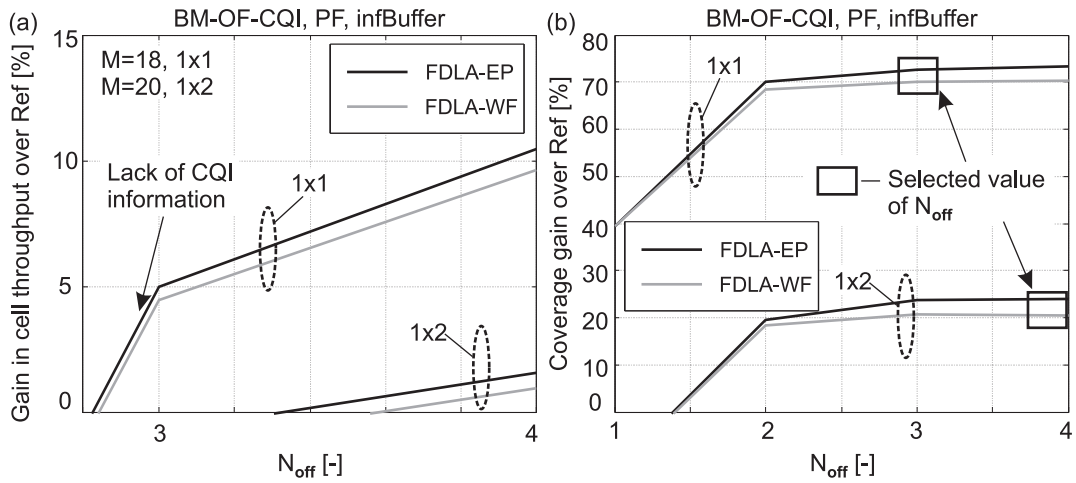

Figure 6.5: FDLA performance based on the BM-OF-CQI scheme, and the infinite buffer traffic model.

the cell throughput performance deteriorates due to reduction in the degrees of freedom, i.e., the effective number of RBs whose channel quality is known at LA is reduced. Further, due to the higher operating point of the 1x2 scheme it requires a larger value of M in comparison to the 1x1 scheme, for similar gain performance.

Although not shown here it was seen that the coverage performance is not as sensitive to M, and a moderate value of M (e.g., $M = 10$ for the 1x2 scheme) is sufficient to achieve most of the FDLA coverage potential. This is due to fact that FDLA trades bandwidth for improvement in the SINR, in case of coverage limited users. For the selected values of M the CQI overhead can be reduced by 10% for the 1x1 case and by 5% for the 1x2 case, in comparison to the AB-CQI scheme. Next the optimization of the BM-OF-CQI scheme is conducted based on the selected values of M.

6.6   FDLA Performance Based on the BM-OF-CQI Scheme

Figure 6.5 illustrates the optimization of the BM-OF-CQI scheme. The aim of this technique is to reduce the overhead of the BM-CQI scheme by utilizing offset signaling, as described in Section 3.9. When N_{off} is small, there is a loss in cell throughput due to the lack of CQI information at the transmitter side. Results show that below $N_{off} = 3$ there is a cell throughput loss in comparison to the Ref scheme, irrespective of the antenna scheme.

In Figure 6.5 (b) we see that coverage performance is not as sensitive as cell throughput to the N_{off} parameter, e.g., most of the FDLA coverage potential is achieved at $N_{off} = 2$, for both antenna configurations. However, in order to provide at least a similar cell throughput as the Ref scheme N_{off} needs to be set at 3 for the 1x1 scheme. Similarly, $N_{off} = 4$ is selected for the 1x2 antenna case. For these values of N_{off} the CQI overhead can be reduced by 36% for the 1x1 case and by 18% for the 1x2 case, in comparison to the AB-CQI scheme. In comparison to the BM-CQI scheme the CQI overhead is reduced by 29% and 13%, depending on the presence of receive antenna diversity.

The FDLA performance with the BM-OF-CQI scheme under the Ped. A channel profile is shown in Figure C.2 (d). It is seen that due to the nearly-flat fading channel a large value of M is required to achieve similar cell-level performance as the Ref scheme. In such cases the Best M schemes are not suitable for implementation as they cannot provide a significant reduction in signaling overhead over the AB-CQI scheme.

6.7   FDLA Gain as a Function of the CQI Overhead, for Optimized CQI Schemes

We now proceed to evaluate the trade-off between UL signaling overhead (bits/CQI report) and FDLA gain potential in the DL. Figure 6.6 illustrates FDLA performance results for all the considered CQI schemes. For comparison purposes reference FDLA results for the AB-CQI scheme are also reported here. Further, both antenna schemes have been considered.

The results show that in general the FDLA cell throughput performance is more sensitive to CQI overhead in comparison to the coverage performance. The best trade-off in terms of cell throughput is achieved with the TH-CQI scheme, as the loss in comparison to AB-CQI is around 2% - 3%, while the reduction in overhead is around 76%. However, the coverage loss with the TH-CQI scheme is higher, around 13% for the 1x1 case and around 8% for the 1x2 antenna scheme. In terms of overall performance the TH-CQI scheme still provides the most attractive trade-off between reduction in UL signaling overhead and the achievable gain in the DL.

Among the CQI schemes relying on offset signaling the analysis has shown that the BM-OF-CQI scheme is more sensitive to bits per CQI report, in comparison to the OF-CQI scheme. Further, between these two schemes the OF-CQI scheme provides better FDLA performance for a similar value of CQI overhead. The difference in performance is more significant for the 1x1 case, e.g., when the CQI overhead is set at 50 bits/report the coverage gain with OF-CQI is around 70%, while it is 55% with the BM-OF-CQI scheme. In terms of improvement over the BM-CQI scheme results show that the BM-OF-CQI scheme can reduce the overhead by 10% - 20% for a similar cell throughput performance.
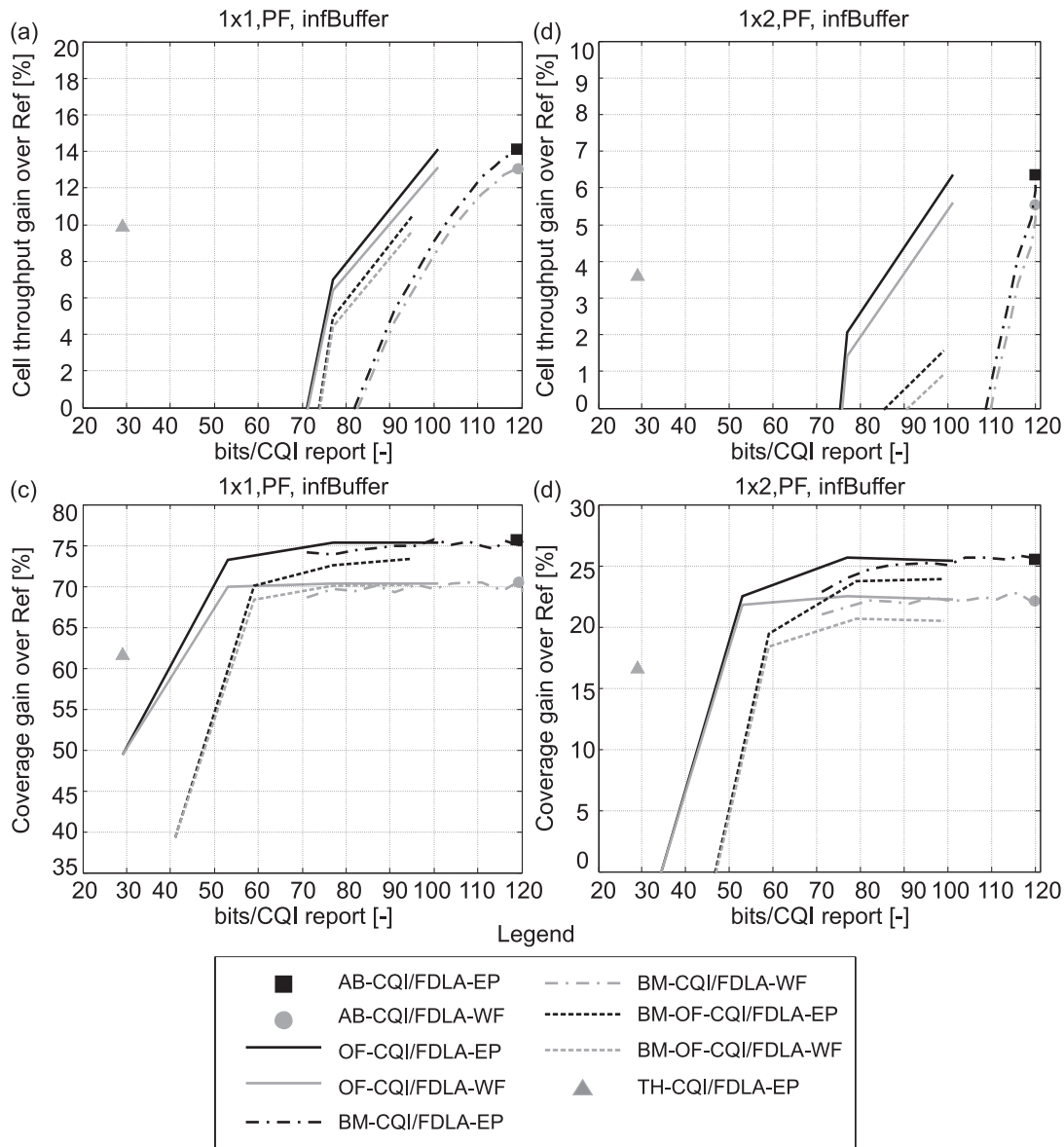
Figure 6.6: FDLA gain over Ref as a function of the CQI overhead, for the investigated CQI schemes. The results are based on the infinite buffer traffic model.

Based on these results it is concluded that the TH-CQI scheme is the preferred reduced bandwidth CQI scheme for FDLA. Further, if the system supports the more complex WF power distribution then the preferred CQI scheme is OF-CQI. Due to limited potential the Best M schemes will not be considered hereafter in the FDLA analysis. For similar reasons the FDLA-WF scheme will also be excluded from future analysis.

6.8   Impact of Reduced CQI Reporting Rate on FDLA Performance

We now investigate the impact of reduced CQI reporting rate on the FDLA potential, for the optimized CQI schemes. This is a basic mechanism available for reducing the CQI overhead. However, it will impact the mobility support of the system. Figure 6.7 illustrates the variation
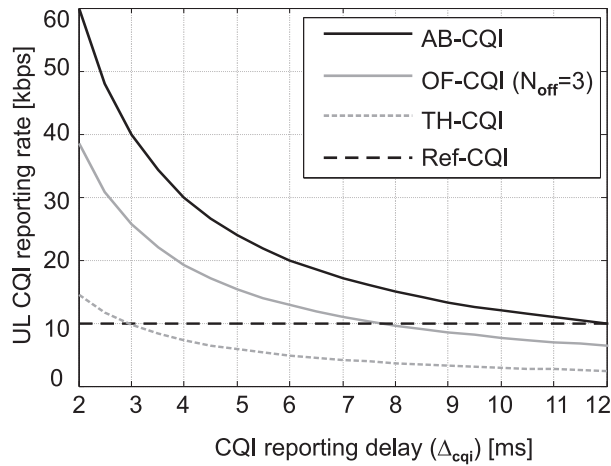
Figure 6.7: CQI rate as a function of the reporting delay for the optimized CQI schemes.

Table 6.3: CQI parameters for the investigation of delayed CQI reporting, together with FDLA. D_{cqi} is kept constant at 1.5 ms.

CQI scheme	Δ_{cqi} [ms]	W_{cqi} [ms]	CQI rate [kbps]	D_{LA} [sub-frames]
Ref-CQI	0.5	0.5	10	4
AB-CQI	2	2	60	5
OF-CQI	2	2	38.5	5
($N_{off} = 3$)	4	2	19.3	7
	6	2	12.8	9
	8	2	9.6	11
TH-CQI	2	2	14.5	5
	3	2	9.7	6
	4	2	7.3	7

of the CQI rate as a function of the reporting delay (Δ_{cqi}). The goal is to select those values of reporting delay for each scheme for which the resulting CQI overhead is similar to the Ref scheme. Based on the curves in Figure 6.7 the cases selected for further evaluation of the FDLA potential are listed in Table 6.3. Here, the effective LA delay, denoted by D_{LA}, is calculated using (3.21).

Figure 6.8 illustrates the impact of reduced CQI rate on the FDLA-EP potential, with the OF-CQI scheme. The results are based on the 1x2 scheme and the infinite buffer traffic model. The maximum FDLA cell throughput gain is around 2% for the optimized settings, while the coverage gain is up to 25%, similar to Figure 6.6. The results in Figure 6.8 show that the minimum CQI rate at which FDLA-EP can provide a gain over Ref is 19.3 kbps. However, the mobility support is severely affected at this CQI rate, and FDLA is not a feasible solution beyond 3-4 km/h.
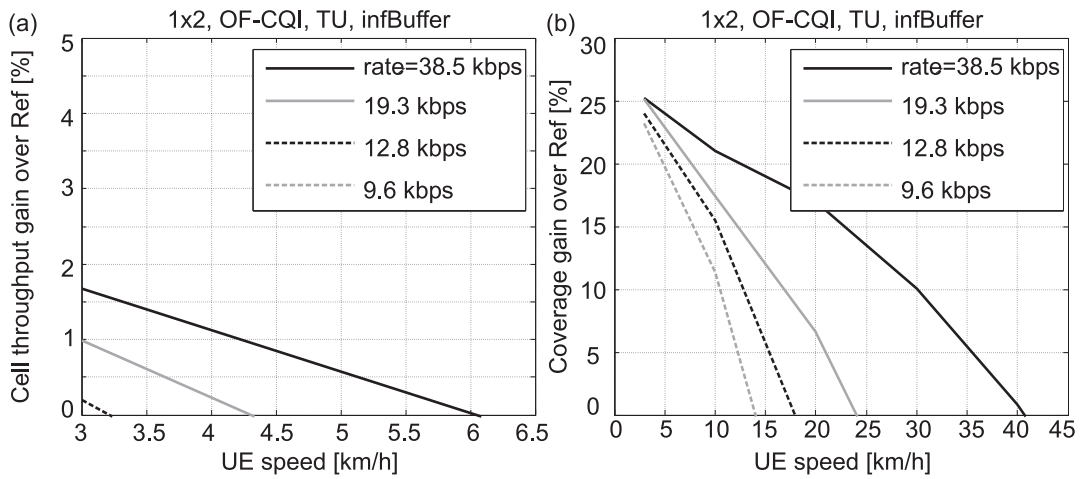
Figure 6.8: FDLA-EP performance as a function of the UE speed and CQI reporting delay, for the OF-CQI scheme. Results are based on the infinite buffer traffic model.
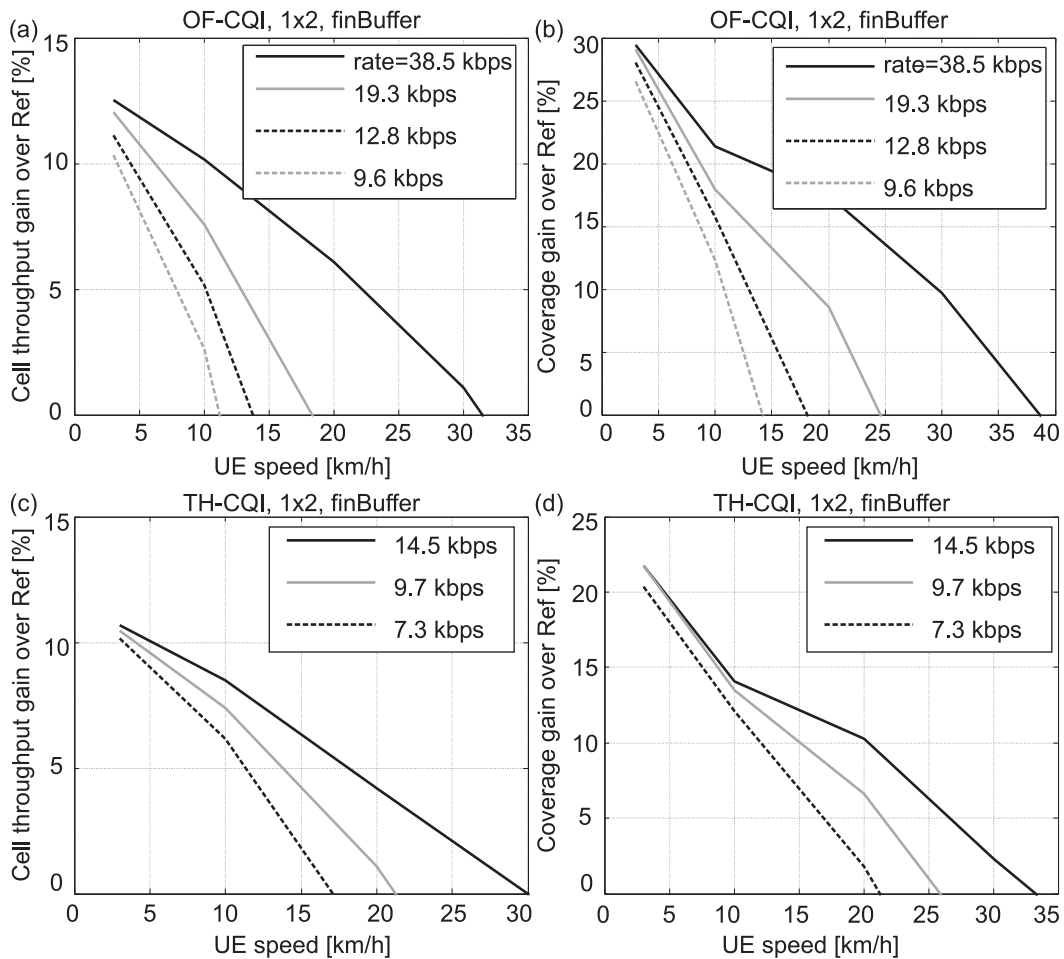

Figure 6.9: FDLA-EP performance as a function of the UE speed and CQI reporting rate, for the finite buffer traffic model. The results are provided for the OF-CQI and the TH-CQI schemes.
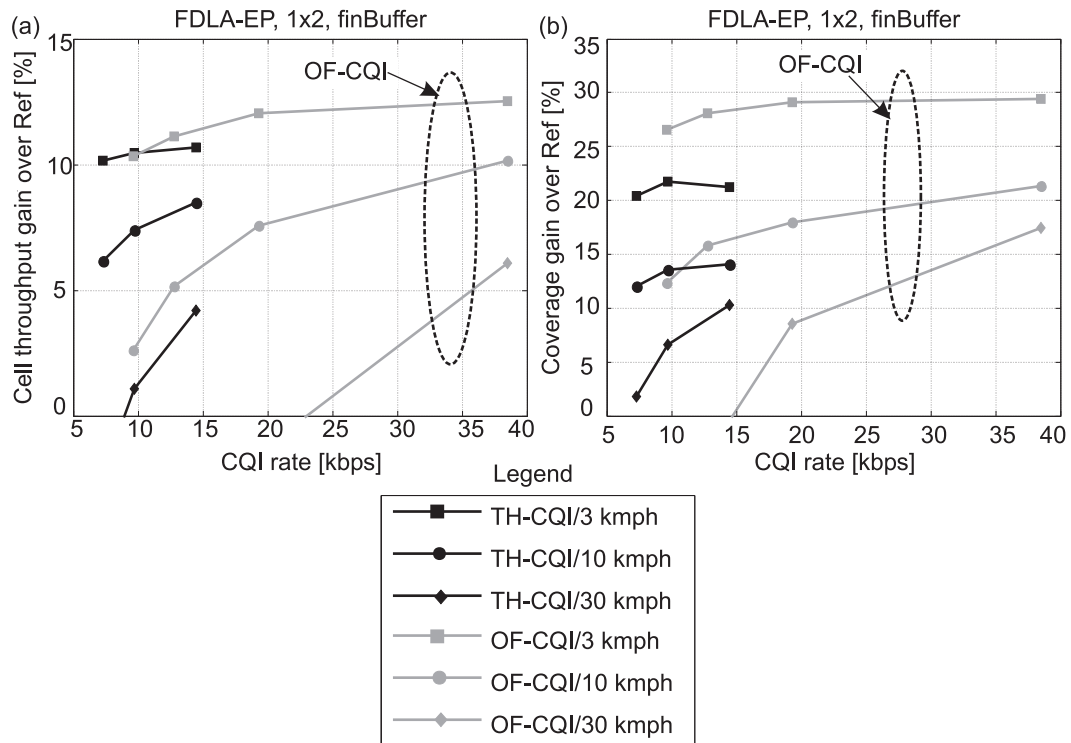
Figure 6.10: Trade-off between FDLA potential in the DL and CQI overhead in the UL, based on the finite buffer traffic model.

6.9 FDLA Potential With the Finite Buffer Traffic Model and Limited CQI

Next, the impact of finite buffer traffic model on FDLA potential is evaluated. Extensive simulations have shown that the optimized CQI parameter settings do not change when the finite buffer model is introduced. We have seen earlier in Section 4.9 that under the data-fair traffic model there is an improvement in the FDLA cell throughput gain potential by around 8%. Similarly, the coverage gain is also improved marginally. These trends are supported by the results in Figure 6.9 for the 1x2 case, although the increase in cell throughput gain is slightly higher.

The performance curves for the OF-CQI scheme show that under the data-fair traffic model most of the FDLA gain potential can be achieved even when the CQI rate is reduced to 9.6 kbps, which is similar to the Ref scheme. At this CQI rate the UE mobility of up to 10 km/h can be supported.

Figure 6.9 (c) and (d) illustrate the FDLA potential with the TH-CQI scheme as a function of speed, based on the finite buffer model and the 1x2 antenna configuration. Comparing the performance with the OF-CQI scheme we see that the TH-CQI scheme is more robust to speed. As an example FDLA can be supported up to 20 km/h, with the CQI rate of 9.7 kbps.

Similar results for the 1x1 antenna configuration can be seen in Figure C.4. In this case, the OF-CQI scheme can support FDLA up to 15 km/h, while the TH-CQI can support FDLA up to 30 km/h, with similar CQI rate.

Figure 6.10 illustrates the FDLA potential as a function of the CQI rate, for selected values of

UE speed. Results are shown for both OF-CQI and the TH-CQI schemes. In general, the FDLA potential is reduced as the CQI rate is decreased. Further, the slope of the OF-CQI curves is steeper in comparison to the curves of the TH-CQI scheme. Thus, the latter scheme is more robust to speed, and it provides a better FDLA gain potential as long as the speed is above 10 km/h. Similar trends are observed for the 1x1 antenna case, and these results have been illustrated in Figure C.5.

6.10 Conclusions of the FDLA Analysis Based on the Low-Bandwidth CQI Schemes

We have considered several low bandwidth CQI schemes in the evaluation of the trade-off between reduction in UL signaling overhead and the available FDLA gain in the DL. Each CQI scheme was optimized individually, depending on the channel profile, antenna configuration, and the packet scheduling policy. The AB-CQI scheme characterized by detailed reporting of the channel quality on each RB was used as reference in this analysis. Although this scheme can provide the maximum FDLA potential, the CQI overhead is around 60 kbps, which is six times larger than the overhead required by the Ref scheme (10 kbps).

Considering the OF-CQI scheme we found that the cell throughput performance is sensitive to the choice of N_{off}, which determines the maximum offset that can be used in the signaling. When N_{off} is low, there is a reduction in the effective number of RBs with known channel quality at the transmitter. However, as coverage is dependent on transmission using the best RBs it is more robust to the choice of N_{off}. Detailed analysis of the OF-CQI scheme with the TD-PF, TD-RR schedulers as well as the 1x1 and 1x2 antenna schemes has shown that $N_{off} = 3$ is sufficient to exploit most of the FDLA coverage potential, while still providing marginal improvement in cell throughput over the Ref scheme. The resulting reduction in CQI overhead is around 36%, relative to the AB-CQI scheme.

Next, the optimization of the TH-CQI scheme was carried out. It was seen that when the threshold value is low there is a loss in FDLA-EP cell throughput due to the lack of CQI information. As the threshold is increased the cell throughput is improved until it reaches optimum. Thereafter, the performance is reduced with an increase in the value of threshold. This is due to deterioration in the average SINR conditions, as the transmitter cannot distinguish between RBs.

Based on detailed analysis under the TU profile, we have seen that the threshold value of 8 dB provides a good trade-off between coverage and cell throughput. Further, the same setting of threshold can be used for both antenna schemes as well as the two considered schedulers. The more complex G-factor level threshold optimization can provide only marginal improvement in FDLA potential in comparison to the single cell-level based threshold. The TH-CQI scheme provides the best trade-off between overhead and FDLA gain potential, e.g., with the optimized TH-CQI scheme the achievable FDLA cell throughput potential is within 3%-4% of AB-CQI, and the reduction in CQI overhead is around 76%. It was also shown that the threshold optimization is dependent on the channel profile.

The analysis of the BM-CQI scheme has shown that a fairly large value of M, e.g., around 18-20, is required to achieve sufficient FDLA gain. Due to the limited potential of overhead reduction for such a large value of M, the Best M schemes are not recommended for the implementation of FDLA.

Table 6.4: Tabulated results of FDLA gain with optimized CQI schemes, as a function of CQI rate and antenna scheme. The speed is set at 3 km/h, and the finite buffer traffic model has been employed.

Parameter	CQI scheme							
	OF-CQI				TH-CQI			AB-CQI
CQI rate [kbps]	38.5	19.3	12.8	9.6	14.5	9.7	7.3	60
FDLA-EP cell throughput gain over Ref [%] (1x1)	47	46	45	44	45	44.5	44	49
FDLA-EP coverage gain over Ref [%] (1x1)	76	75	74	73	66	75	64	77
FDLA-EP cell throughput gain over Ref [%] (1x2)	13	12	11	10.5	11	10.5	10	14
FDLA-EP coverage gain over Ref [%] (1x2)	30	29	28	26.5	22	21	20	30

The potential savings in overhead with delayed CQI reporting was evaluated for the short listed CQI schemes, namely the OF-CQI and the TH-CQI schemes. The analysis included the investigation of mobility support at different CQI rates. Results show that a FDLA cell throughput gain of 10% and a coverage gain of around 26% is achievable with the OF-CQI scheme (1x2 antenna configuration) at 3 km/h, when the CQI rate is reduced to 9.6 kbps. At a similar CQI rate (9.7 kbps) the TH-CQI scheme can support a slightly reduced FDLA gain. However, the mobility support is increased up to 20 km/h. We conclude that FDLA can provide a significant improvement in coverage (i.e., 20%-25%), at a fairly reasonable CQI transmission rate of around 10 kbps. Further, FDLA should be the preferred LA scheme as long as the UE speed is below 20 km/h. For reference purposes the FDLA gain potential with the optimized CQI schemes at 3 km/h is summarized in Table 6.4. The findings of this study have been published in a conference article [67]. This concludes the analysis of FDLA with reduced CQI schemes.

6.11 Evaluation of FDPS Potential Based on the OF-CQI Scheme

Next, we evaluate the potential of FDPS based on the reduced bandwidth CQI schemes. We focus on the finite buffer model in the following analysis. In terms of the scheduling policy the PF scheduler in time and frequency is used. Among the FDPS schemes the F-FDM technique is selected for further evaluation, based on the findings of Chapter 5. The reference CQI scheme is AB-CQI, as it provides the maximum FDPS gain potential. Based on settings in Table 6.1 and the finite buffer model the FDPS cell throughput gain with the AB-CQI scheme was found to be 110% and 50%, with the 1x1 and the 1x2 antenna schemes respectively. Similarly, the FDPS coverage gain was found to be 140% and 60% respectively. The reference results assume that the UE speed is set at 3 km/h.

Figure 6.11 illustrates the FDPS potential with the OF-CQI scheme. It is seen that the performance is sensitive to the setting of N_{off}, e.g., a near-linear improvement in gain potential with N_{off} is seen initially. Further, from Figure 6.11 (a) and (b) it is seen that the setting of $N_{off} = 3$ is sufficient to achieve most of the FDPS potential. The trends are similar for both antenna schemes. As seen earlier in the FDLA analysis, when N_{off} is set at a low value there is a loss in perfor-
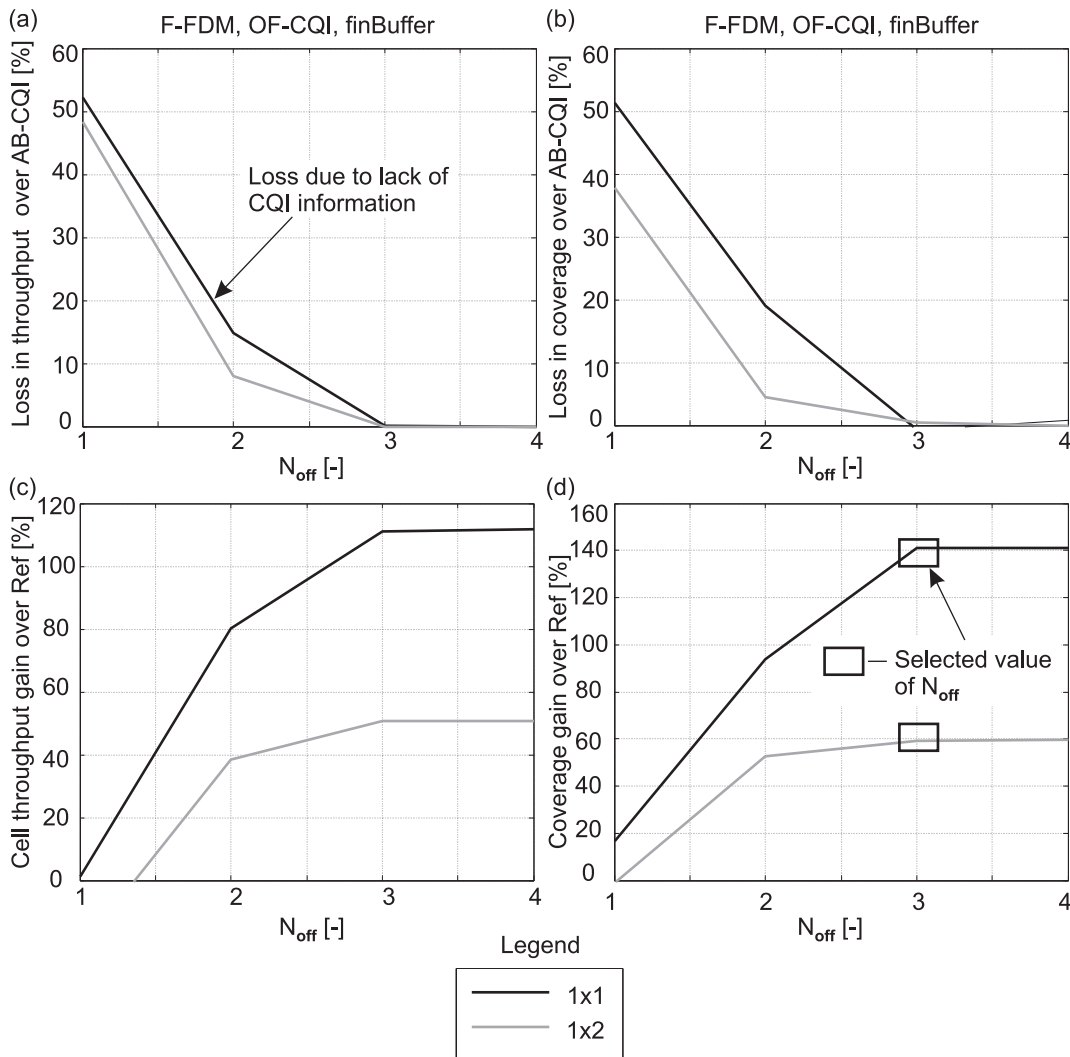
Figure 6.11: F-FDM performance based on the OF-CQI scheme, TD-PF/FD-PF scheduler, finite buffer traffic model, and the Macro case 1 scenario.

mance, due to lack of CQI information at the transmitter side. Figure 6.11 (c) and (d) illustrate the cell throughput and coverage gain over Ref respectively. With the selected value of N_{off} the saving in CQI overhead is around 36% over the reference AB-CQI scheme.

6.12   FDPS Performance Based on the TH-CQI Scheme

The FDPS potential together with the TH-CQI scheme is illustrated in Figure 6.12. Here, the threshold is applied in the SINR domain. Further, cell-level based threshold optimization is preferred to G-factor based optimization, due to the limited potential of the latter technique. The trends are mostly similar to those seen in the FDLA analysis in Figure 6.2. The main difference is that the coverage performance becomes more sensitive to the threshold value. In comparison to FDLA, the coverage potential of FDPS is reduced when the threshold is set at a low value. This is due to the reduction in the multi-user diversity gain caused by the lack of CQI information.
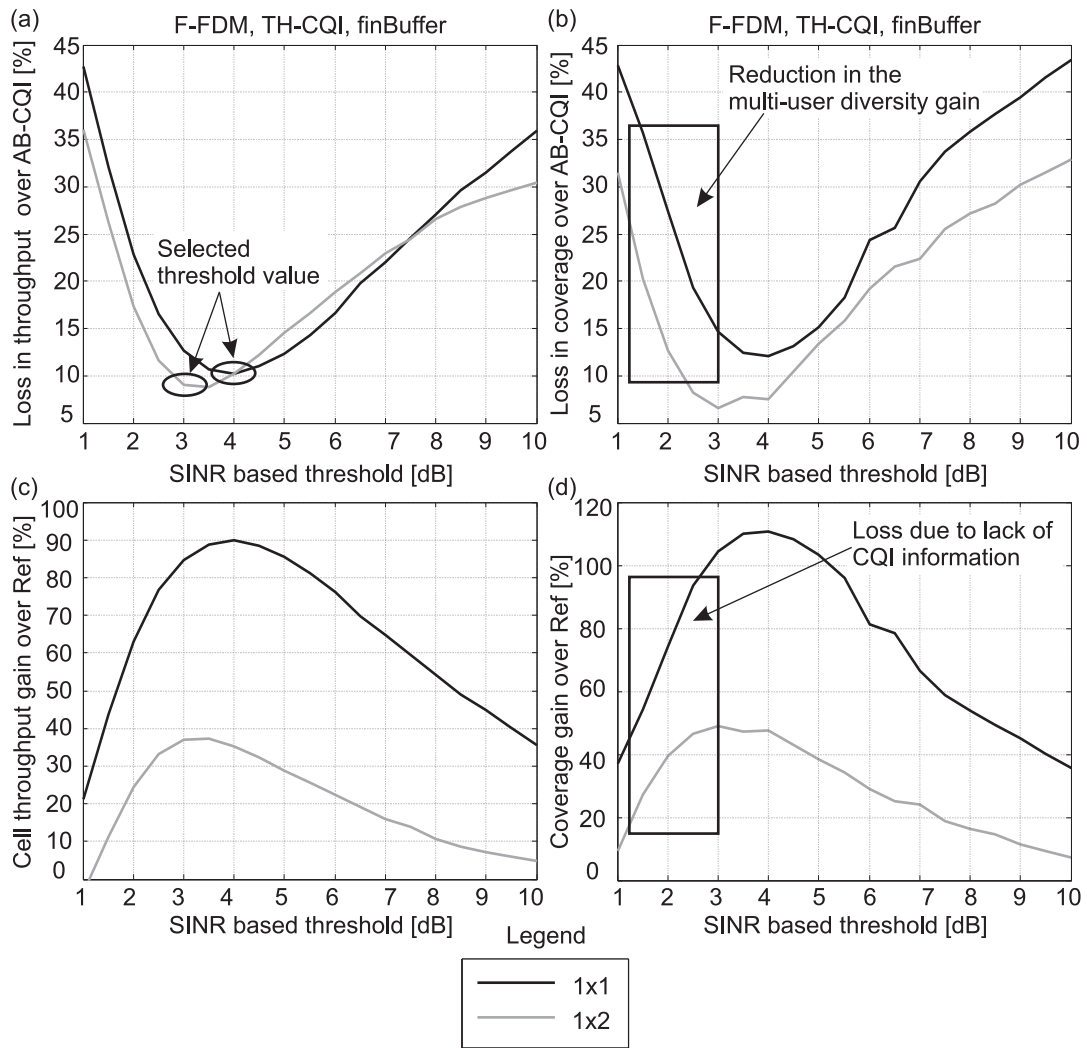
Figure 6.12: FDPS performance based on the TH-CQI scheme, finite buffer model, and non-ideal CQI settings.

Based on the evaluation in Figure 6.12 we have selected the threshold value of 4 dB for the 1x1 scheme and 3 dB for the 1x2 scheme. These settings provide the minimum loss in comparison to the AB-CQI scheme. The loss in FDPS potential is higher with the 1x1 scheme due to the increased channel dynamics. Further, due to the unavailability of detailed knowledge of each RB the optimized TH-CQI scheme cannot match the gain potential available with the OF-CQI scheme, e.g., a loss in cell throughput potential of around 10% - 15% is seen. Among the considered CQI schemes the TH-CQI technique can provide the maximum saving in CQI overhead, around 76%, over the AB-CQI scheme. The threshold optimization for FDPS is, however, dependent on the channel profile, antenna configuration, scheduler type, and UDO.

Figure 6.13 illustrates the performance of the variant TH-CQI scheme where the threshold is applied in the throughput domain. It is denoted as TH-CQI-2, and the results show similar trends as Figure 6.12 (c). Although this technique can improve the FDPS potential over the SINR domain based threshold optimization, the potential is limited, e.g., 1% - 2%. The drawback with the SINR domain optimization is that the mapping of SINR to throughput is non-linear.
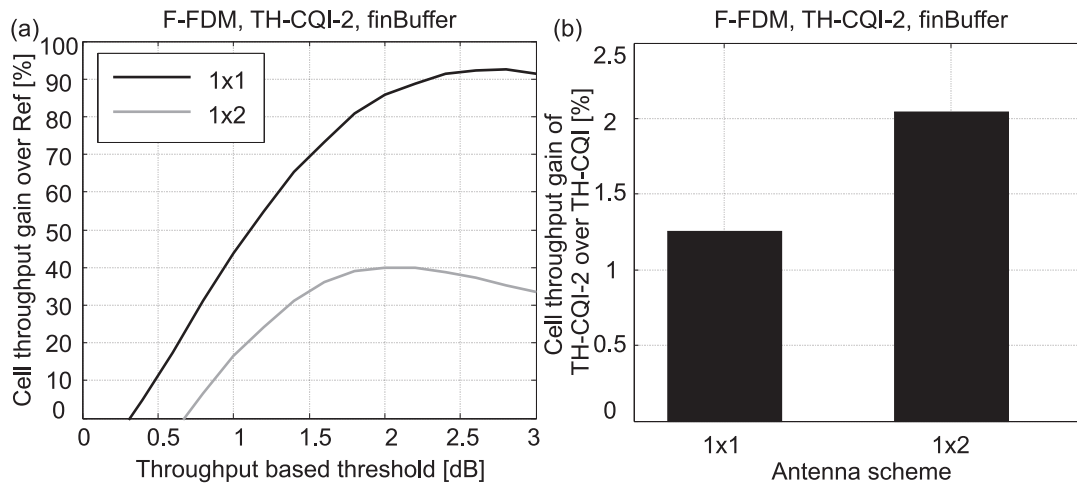
Figure 6.13: FDPS performance based on the variant TH-CQI scheme, where the threshold is applied in the throughput domain.

6.13 Optimization of the TH-CQI Scheme Depending on UDO

As mentioned earlier, the optimization of the TH-CQI scheme is dependent on the UDO. Figure 6.14 illustrates the variation in optimum threshold value as a function of UDO. The trends are expected as the optimized threshold value is a decreasing function of UDO. At a low value of UDO a larger value of threshold is required to improve the utilization of the multi-user diversity gain potential. Further, due to the higher channel dynamics in the 1x1 antenna scheme it requires a larger value of threshold in comparison to the 1x2 case, for the same UDO.
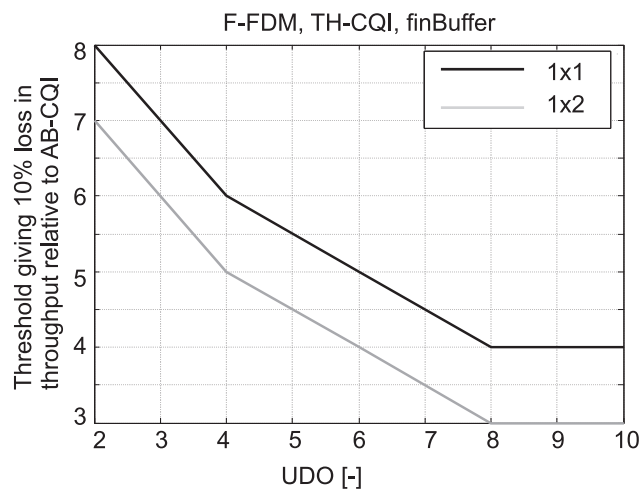

Figure 6.14: Optimization of the SINR based TH-CQI scheme depending on UDO. The results are based on the TU channel profile and Macro case 1 scenario.
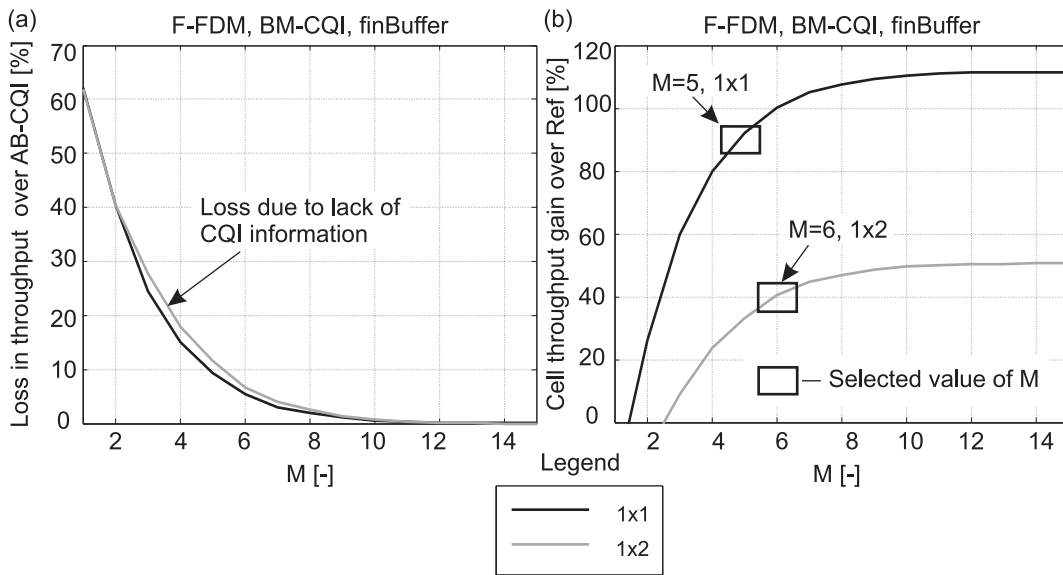
Figure 6.15: FDPS performance based on the BM-CQI scheme. The results are based on the TD-PF/FD-PF scheduler, TU channel profile and Macro case 1 scenario.

6.14   Evaluation of the FDPS Potential With the BM-CQI Scheme

Next, we evaluate the FDPS potential together with the BM-CQI scheme. Figure 6.15 (a) illustrates the loss in cell throughput over the AB-CQI scheme as a function of the parameter M. The trends are similar to the FDLA analysis, shown in Figure 6.4. Initially, there is a significant loss in the FDPS potential due to the reduction in number of RBs with known channel quality, which leads to deterioration in the multi-user diversity gain. Thereafter the performance improves steadily and reaches optimum around $M = 10$. We have selected $M = 5$ for the 1x1 scheme and $M = 6$ for the 1x2 case as they are the smallest values of M which can limit the loss in comparison to AB-CQI to within 10%. Based on the selected values of M the reduction in CQI overhead is around 66% for the 1x1 case and 60% for the 1x2 case.

6.15   FDPS Performance Based on the BM-OF-CQI Scheme

Figure 6.16 illustrates the FDPS performance with the BM-OF-CQI scheme as a function of N_{off}, for the selected values of M. It is seen that the performance is quite sensitive to N_{off} and the setting of $N_{off} = 3$ is sufficient to keep the loss relative to AB-CQI within 10%. At this setting of N_{off} the CQI overhead is reduced by 70% and 66% for the 1x1 case and the 1x2 case respectively. Similarly, in comparison to the BM-CQI scheme the CQI overhead is reduced by 12% and 15%, depending on the antenna scheme. Note that the optimized BM-OF-CQI scheme can provide similar FDPS potential as the TH-CQI scheme. However, it requires an additional 19% and 29% in CQI overhead, depending on the antenna scheme.
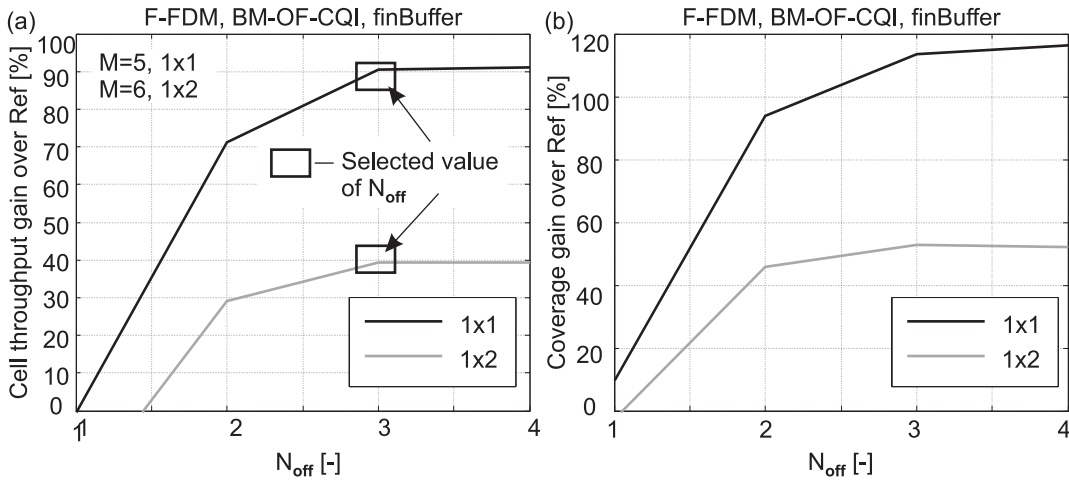
Figure 6.16: FDPS performance based on the BM-OF-CQI scheme, TU channel profile and non-ideal CQI settings.
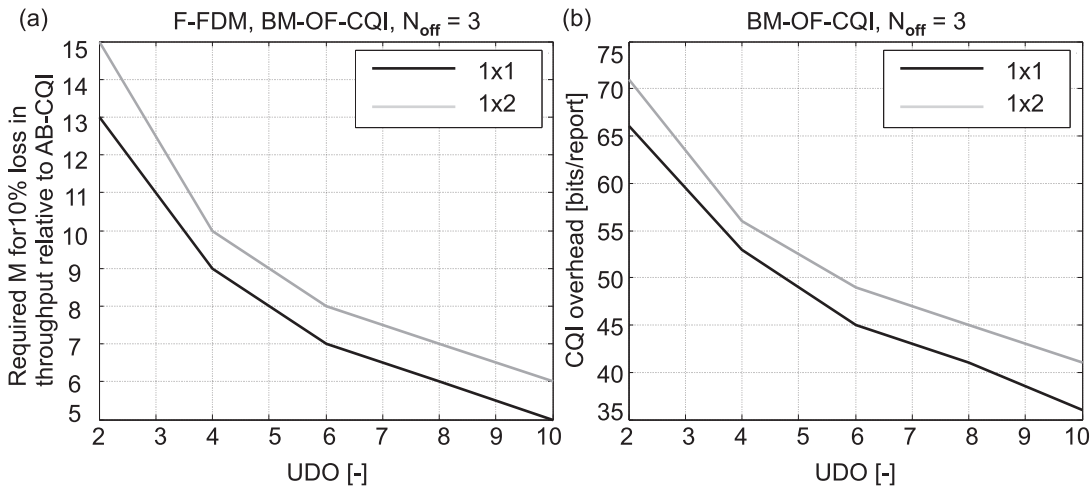

Figure 6.17: Optimization of the BM-OF-CQI scheme depending on UDO. The results are based on the TU channel profile and the Macro case 1 deployment scenario.

6.16   Optimization of the BM-OF-CQI Scheme Depending on UDO

Next, we consider the optimization of the BM-OF-CQI scheme as a function of the UDO. The results shown in Figure 6.17 (a) depict the variation in the lowest value of M for which the cell throughput loss over AB-CQI is within 10%, as a function of the UDO. We have used the setting of $N_{off} = 3$ in these results. It is clear that when the UDO is small a larger value of M is required in order to enable F-FDM to exploit the multi-user diversity gain over the entire system bandwidth. Further, a larger value of M is required under the 1x2 antenna scheme for the same UDO, due to the higher system operating point. Figure 6.17 (b) illustrates the associated CQI overhead with the BM-OF-CQI scheme as a function of the UDO.

6.17   Impact of Reduced CQI Rate on FDPS Performance

Based on the optimized CQI schemes we evaluate the FDPS potential with reduced CQI reporting rate. First, a sub-set of CQI rates is selected for each scheme based on the results in Figure 6.18. The two sets of curves represent the considered antenna schemes. It is clear that the TH-CQI scheme provides the maximum reduction in overhead, while the optimized Best M schemes are superior to the OF-CQI scheme. The selected CQI rates for further analysis are listed in Table 6.5 for the different schemes. The aim is to progressively reduce the CQI rate until it is similar to the Ref scheme, and evaluate the FDPS gain potential as well as mobility support. Further, among the Best M schemes we consider only the BM-OF-CQI scheme for further analysis.

Figure 6.19 (a) and (b) illustrate the FDPS potential with reduced CQI reporting rate when the OF-CQI scheme is employed. Figure 6.19 (c) and (d) illustrate the performance with the TH-CQI scheme and Figure 6.20 illustrates the performance with the BM-OF-CQI scheme. In general the FDPS gain decreases with increase in UE speed, as LA is not able to track fast variations in the channel conditions. Among the considered CQI schemes the TH-CQI scheme is the most robust to UE speed, as it does not depend on detailed knowledge of channel quality. With a similar CQI
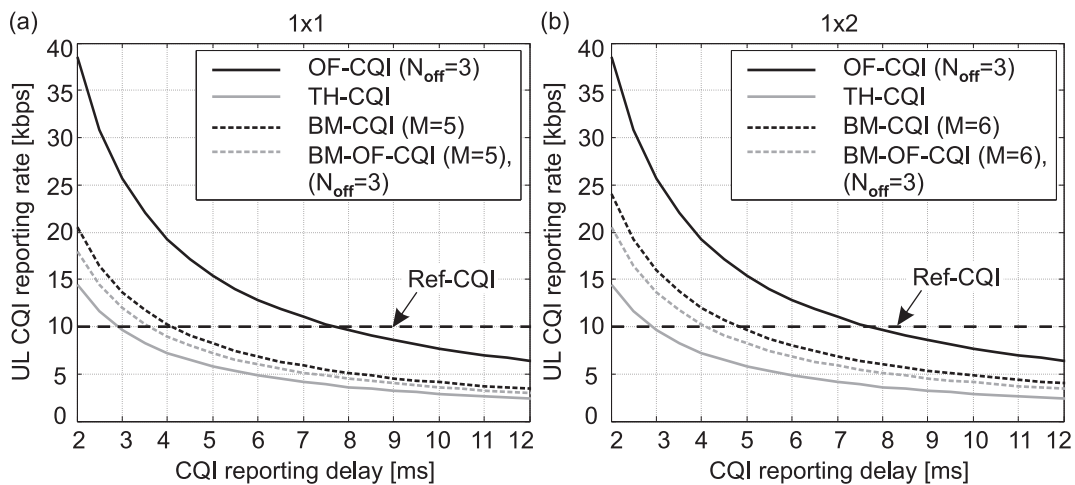

Figure 6.18: CQI rate as a function of the reporting delay, for the optimized CQI schemes.
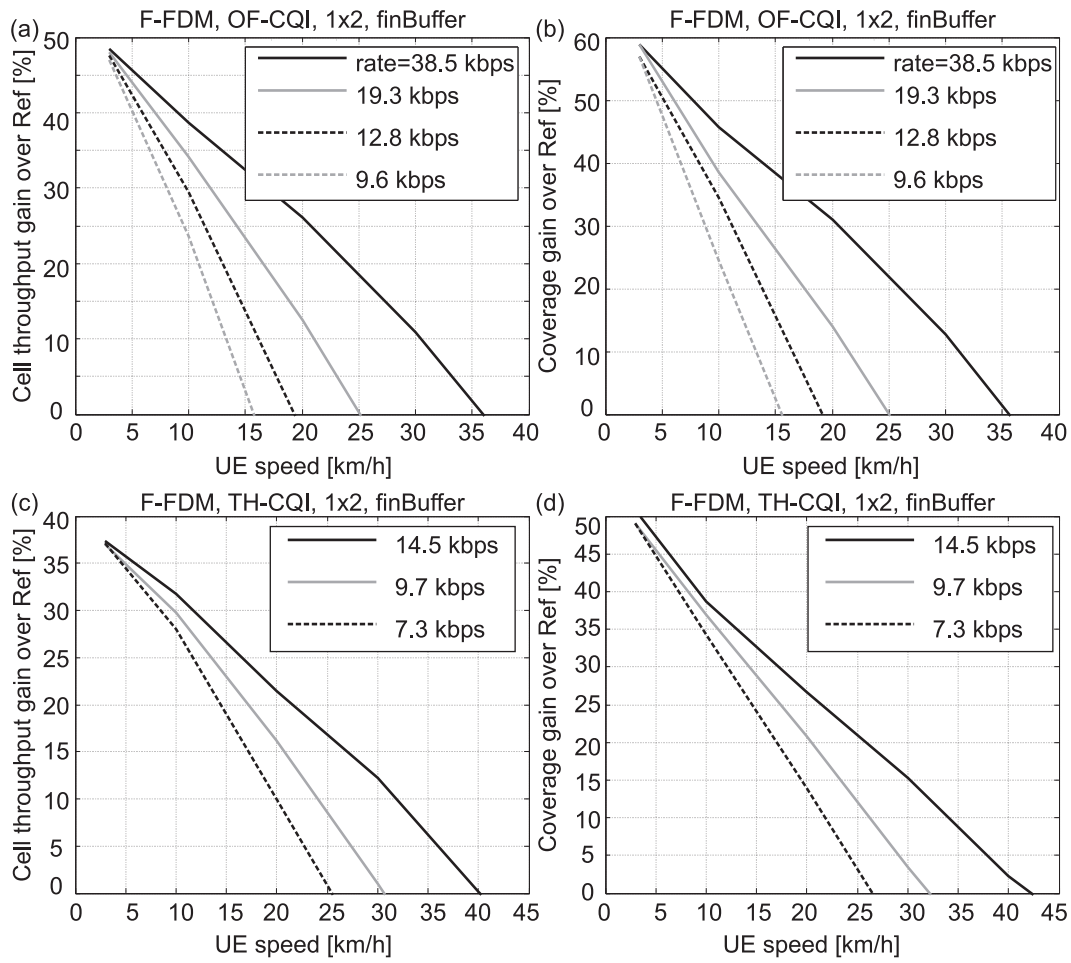
Figure 6.19: FDPS gain potential as a function of the UE speed, for reduced CQI reporting rate. The results are presented for the optimized OF-CQI and the TH-CQI schemes.
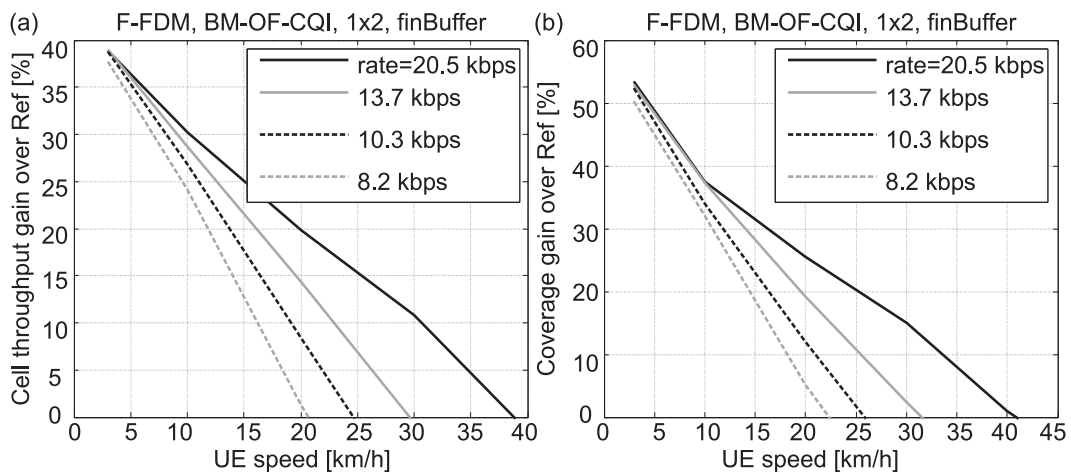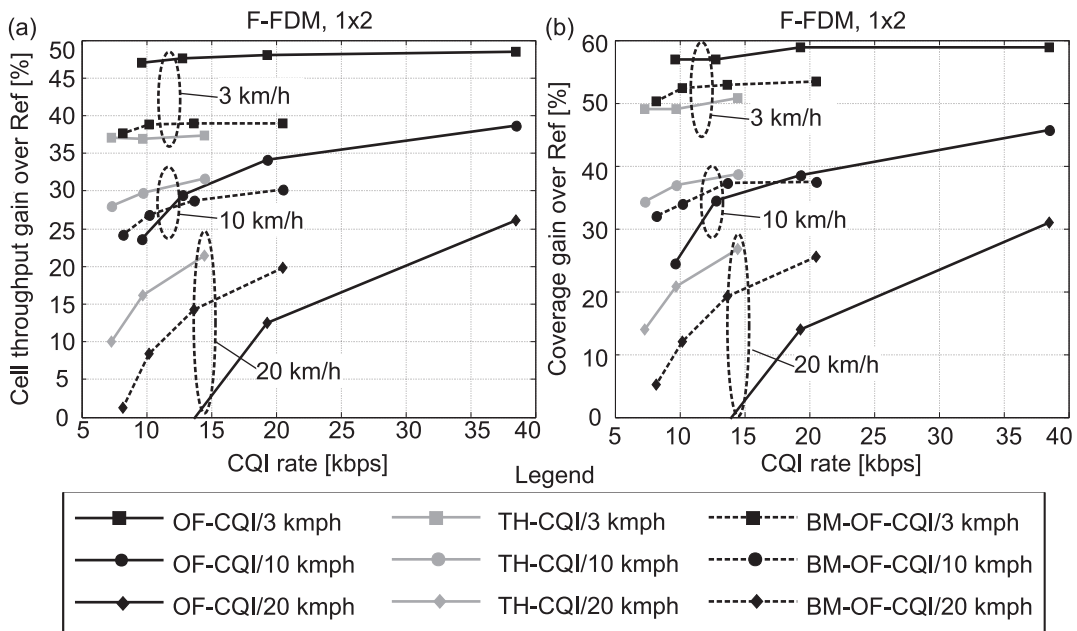

Figure 6.20: FDPS gain potential as a function of the UE speed, for reduced CQI reporting rate. The results are presented for the optimized BM-OF-CQI scheme.

rate as the Ref scheme (10 kbps) we see that the OF-CQI scheme can provide almost the full FDPS gain potential. The TH-CQI scheme can support a maximum cell throughput gain of 36% at the

Table 6.5: CQI parameters for the investigation of delayed CQI reporting, together with FDPS.

CQI scheme	Δ_{cqi} [ms]	W_{cqi} [ms]	CQI rate [kbps]	D_{LA} [sub-frames]
Ref-CQI	0.5	0.5	10	4
AB-CQI	2	2	60	5
OF-CQI	2	2	38.5	5
	4	2	19.3	7
	6	2	12.8	9
	8	2	9.6	11
TH-CQI	2	2	14.5	5
	3	2	9.7	6
	4	2	7.3	7
BM-OF-CQI	2	2	18	5
M=5,N_{off}=3	3	2	12	6
(1x1)	4	2	9	7
	5	2	7.2	8
BM-OF-CQI	2	2	20.5	5
M=6,N_{off}=3	3	2	13.7	6
(1x2)	4	2	10.3	7
	5	2	8.2	8

Figure 6.21: Trade-off between CQI rate and FDPS potential for optimized OF-CQI, TH-CQI and BM-OF-CQI schemes.

CQI rate of 9.7 kbps. This is around 10% lower than the OF-CQI scheme. Similar trends are observed with the BM-OF-CQI scheme. Considering the FDPS gain potential as well as mobility support the TH-CQI scheme provides the best performance. The maximum speed at which FDPS can provide gain over Ref is around 30 km/h, with the 1x2 antenna scheme.

The FDPS gain potential with the reduced CQI reporting rate for the 1x1 antenna scheme is illustrated in Figure C.6. The trends are similar to the 1x2 case, and the TH-CQI scheme provides the best overall FDPS performance. The maximum cell throughput potential with reduced CQI rate is 90%. Further, the maximum speed at which FDPS can provide a gain over Ref is around 35 km/h.

Figure 6.21 illustrates the trade-off between CQI rate and FDPS potential, for the optimized CQI schemes and the 1x2 antenna configuration. Similar to previous results, it is seen that the TH-CQI scheme is the most robust to UE speed. If the CQI rate is kept to around 10 kbps the TH-CQI scheme provides the best FDPS performance beyond the speed of 3 km/h. Similar results for the 1x1 antenna case are illustrated in Figure C.7. The trends are quite similar to the 1x2 case and the TH-CQI scheme provides the best overall performance, considering also the mobility support.

6.18   Impact of Time-Domain Averaging on FDPS Performance

We conclude the CQI analysis by evaluating the potential of averaging in time domain at the UE. As seen previously in Figure 3.18, the advantage of averaging is that the effective number of pilots per RB is increased, which can be used to improve the accuracy of CQI estimation. Figure 6.22 illustrates the FDPS gain potential as a function of the averaging window (W_{cqi}). The results are based on the 1x2 antenna scheme. Further, two different UE speeds have been considered in the
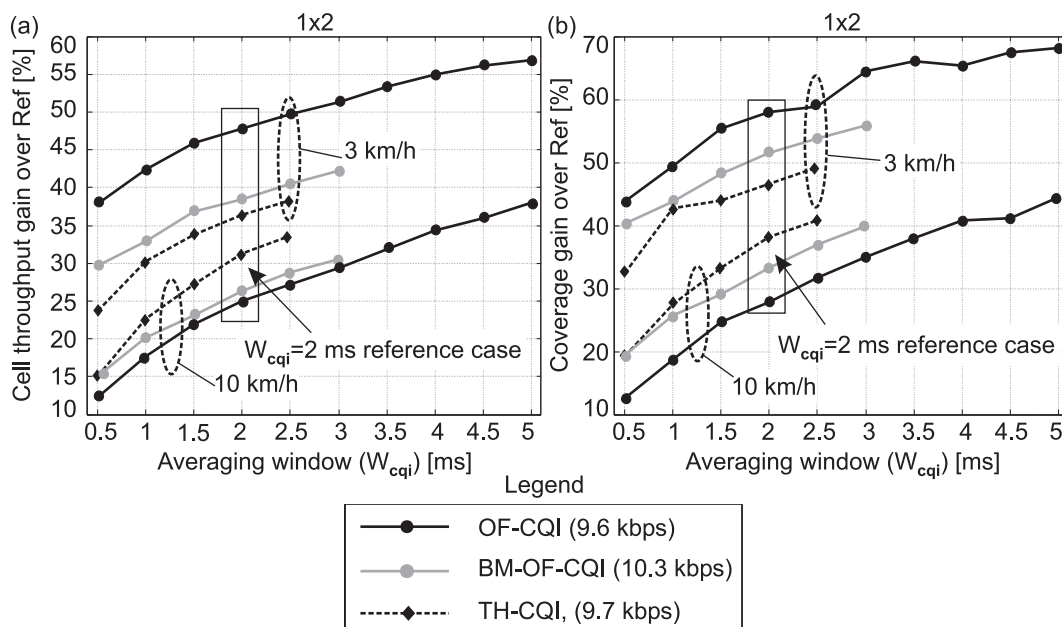

Figure 6.22: FDPS performance as a function of time domain averaging together with reduced CQI reporting rate. The results are based on the 1x2 antenna scheme, TU channel profile, finite buffer model, and the Macro case 1 deployment scenario.

analysis. The std. of CQI error is set at 2.5 dB, based on Figure 3.18.

The performance evaluation shows that the FDPS gain is improved with the increase in the averaging window. Focusing on the performance at $W_{cqi} = 2\,\text{ms}$, which has been used as the reference setting in previous results, we can see that the results in Figure 6.22 match quite well with those shown in Figure 6.19 and Figure 6.20. Note that with an increase in W_{cqi} the channel dynamics are also averaged out, and these are what create the multi-user diversity gain in the first place. This effect is not seen in Figure 6.22 as the considered UE speeds are quite low. The potential of time domain averaging together with the 1x1 antenna scheme has been illustrated in Figure C.8. The trends are quite similar to those for the 1x2 scheme. We conclude that time domain averaging is a useful technique to improve the CQI estimation accuracy, e.g., FDPS cell throughput gain can be improved by around 15% as W_{cqi} is increased from 0.5 ms to 5 ms (1x2 case).

6.19 Conclusions of the FDPS Analysis Based on the Limited CQI BW Schemes

The trade-off between UL signaling overhead and the available FDPS potential (F-FDM) in the DL has been evaluated using three different reduced CQI schemes. Each CQI scheme is optimized individually based on extensive system-level simulations. Further, a highly frequency-selective channel profile, i.e., TU, has been used in the analysis. The AB-CQI scheme is used as reference since it provides the maximum FDPS potential. Based on the finite buffer traffic model it was found that AB-CQI can provide a FDPS cell throughput gain of 110% and 50% with the 1x1 and the 1x2 antenna schemes respectively. However, this scheme requires a large amount of CQI overhead, e.g., the CQI rate needs to be around 60 kbps, which is six times larger than the requirement of the Ref scheme.

We begin by evaluating the FDPS potential based on the offset signaling technique. The analysis has shown that the performance of the OF-CQI scheme is sensitive to the choice of N_{off}. When it is set at a low value, there is a significant deterioration in performance due to a reduction in the multi-user diversity gain potential. The setting of $N_{off} = 3$ was found to be sufficient to achieve most of the FDPS potential, for both antenna schemes.

Next the potential of the TH-CQI scheme is investigated. The analysis has shown that the improvement from applying threshold in the throughput domain is quite limited, compared to the SINR domain. Further, both coverage and cell throughput are sensitive to the choice of threshold value. Considering the optimized TH-CQI scheme it was seen that the FDPS cell throughput gain is around 90% and 40%, depending on the antenna scheme, at low speeds. This performance is achieved with a CQI overhead that is 76% lower than the AB-CQI scheme. The optimization of the TH-CQI scheme depends on the channel profile, antenna scheme, scheduler type, and UDO.

The analysis of the BM-CQI scheme has shown that as FDPS is able to exploit multi-user diversity in both time and frequency, M can be kept at a low value and still achieve within 10% of the maximum potential, e.g., $M = 5$ for the 1x1 scheme and $M = 6$ for the 1x2 scheme. The optimization of the BM-OF-CQI scheme was carried out based on the chosen values of M. It is seen that $N_{off} = 3$ is required to provide sufficient FDPS potential. With the optimized BM-OF-CQI scheme the FDPS gain potential is similar to the TH-CQI scheme. However, it requires an additional 19% and 29% in CQI overhead, depending on the antenna scheme. The optimization of

Table 6.6: Tabulated results of the FDPS gain as a function of the CQI rate, at 3 km/h, based on the finite buffer traffic model.

Parameter	CQI scheme						
	OF-CQI		TH-CQI		BM-OF-CQI		AB-CQI
CQI reporting delay [ms]	6	8	3	4	7	8	2
CQI rate [kbps]	12.8	9.6	9.7	7.3	9 (1x1) 10.3 (1x2)	7.2 (1x1) 8.2 (1x2)	60
FDPS cell throughput gain over Ref [%] (1x1)	109	108	90	90	90	90	110
FDPS coverage gain over Ref [%] (1x1)	132	126	110	105	118	115	140
FDPS cell throughput gain over Ref [%] (1x2)	48	47	37	37	38	37	50
FDPS coverage gain over Ref [%] (1x2)	58	57	49	49	52	50	60

the BM-OF-CQI scheme depends on the channel profile, antenna configuration, and UDO.

In order to reduce the CQI overhead even further, delayed CQI reporting was employed. The main drawback of this technique is that it has an adverse impact on the mobility support. Given that the Ref scheme can be supported with a CQI rate of 10 kbps, the aim is to determine the FDPS gain potential with the optimized CQI schemes at a CQI rate similar to the Ref scheme. It is seen that the maximum gain potential at low UE speeds is provided by the OF-CQI scheme. However, it can support FDPS only up to 15 km/h. The TH-CQI scheme is the most robust to UE speed as it does not depend on detailed channel knowledge. Further, the reporting delay can be kept at a low value as the CQI overhead is inherently lower than the other CQI schemes. At low speeds, the TH-CQI enabled cell throughput gain is within 10% of that provided with the OF-CQI scheme. However, as the speed is increased this scheme provides the best gain potential and can support FDPS up to 30 km/h, based on the 1x2 antenna scheme.

The CQI analysis was concluded with the investigation of the impact of UE based time domain averaging on FDPS performance. It is seen that due to the narrow bandwidth of the RB it is beneficial to employ time-domain averaging, e.g., it can improve gain potential by 15% - 20%. However, as the channel dynamics are also averaged in the process, the size of the averaging window needs to be adjusted according to the UE speed. For reference purposes the FDPS gain potential with the optimized CQI schemes is summarized in Table 6.6. The findings of this study have been published in several conference articles, e.g., [72], [97].

Chapter 7

Practical FDAS Algorithm Design

7.1 Introduction

In this chapter we introduce the advanced multi-cell system simulator that will be used to obtain realistic estimates of the FDAS gain potential over time domain only adaptation and scheduling. Further, algorithm modifications required to take into account practical aspects such as real AMC, and HARQ retransmissions are also covered here.

The chapter is organized as follows: Section 7.2 introduces the new features that have been introduced in the system model. Section 7.3 covers the modeling aspects as well as describes the modifications that are introduced in the FDAS algorithms. Section 7.4 presents the validation of the system simulator. Section 7.5 describes the impact of HARQ strategy on FDLA performance. Section 7.6 presents the evaluation of HARQ strategy on FDPS performance, while Section 7.7 describes the impact of HARQ management scheme on FDPS performance.

7.2 Features Introduced in the System Simulator

The initial evaluation of the FDAS potential was based on a simplified system model that consisted of a single-cell deployment. The location of users was modeled using known G-factor distributions, such as the 3GPP Macro cell out-to-in [64]. Further, several modeling simplifications were introduced in the RRM entities such as LA and HARQ, as described in Chapter 2.

We will now evaluate the FDAS potential with the short-listed schemes using the *system simulator*, where all the relevant RRM entities have been implemented in detail. The average SINR of a user is determined online using the detailed link-budget, as well as co-channel interference from neighboring cells. Further, it is now possible to investigate the impact of restrictions imposed by HARQ retransmissions on the packet scheduler and LA. Similarly, the impact of dynamic other-cell interference (non-AWGN) due to fast fading and variations in traffic, can be evaluated. LA is based on real modulation, and the control channel, coding overhead, and the CRC overhead (24 bits per transport block) have been modeled. Further, the recommended OFDM link-to-system performance mapping function (EESM) will be used in the effective SINR calculations. Similarly, OLLA will be based on the actual HARQ Ack/Nack's received from the UEs.
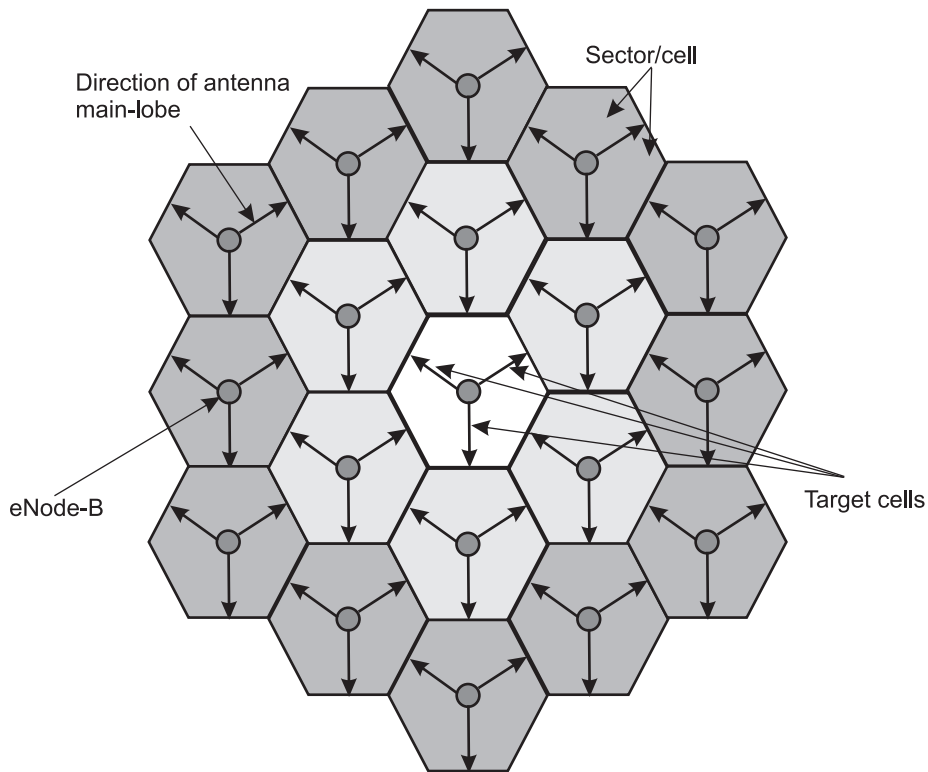
Figure 7.1: The hexagonal regular grid cellular setup implemented in the system simulator according to LTE guidelines, given in [103].

7.3 Description of the System Simulator

The system simulator consists of a detailed multi-cell deployment, based on the latest LTE guidelines [103], [14]. The framework consists of a hexagonal regular grid cellular set up, where the center three target cells are surrounded by two tiers of interfering cells, as shown in Figure 7.1. There are nineteen sites in the simulation area, each consisting of three sectors/cells, giving a total of fifty seven sectors [79]. The orientation of the main lobes of directional sector antenna elements is indicated by solid arrows in Figure 7.1. The PHY layer as well as the primary RRM algorithms such as PS, LA and HARQ are accurately simulated for the center three sectors/cells only. The model is generic in terms of PHY layer parameters, and supports the reference LTE bandwidth scenarios listed in Table 2.2.

A 3-sector network topology with 70 degree eNode-B antennas is assumed for the Macro cell deployment. The propagation modeling consists of the path loss, shadowing and fast fading. The path loss model for the Macro cell case includes a 20 dB outdoor-to-indoor penetration loss [14]. The path loss model was introduced earlier in Table 2.3. Fast fading and temporal dispersion is simulated according to the selected PDP (TU), which is a tapped delay line implementation with uncorrelated Rayleigh fading paths. The location of users is randomly assigned with a uniform distribution within the center three cells. During a packet call the path loss and shadowing component is assumed to be constant for each user, while the fast fading is time-varying. Given this simplification handovers are not explicitly simulated. Shadowing is fully correlated between cells of the same site, while the correlation is 0.5 between sites. The serving cell for a new user is selected according to the lowest total path loss including both distance dependent path loss, shadowing,

effective antenna gains, and the minimum coupling loss.

The RRM related functionalities are explicitly simulated only in the center three target cells, as depicted in Figure 7.1. The remaining cells act as a source of interference. It is assumed that all the cells are transmitting at full load by default. There are six HARQ stop-and-wait processes per user operating in an asynchronous scheme, as described in Section 2.6. The HARQ channel with the longest pending retransmission is selected. The maximum number of HARQ transmission attempts per code-block is equal to 4. Further, ideal HARQ Chase Combining is assumed, and HARQ Ack/Nack signalling delays have been included. Further, error-free detection of the UL control channels is assumed. The system is based on a simple admission control strategy, which keeps the total number of users within the center three cells constant. Ideal channel estimation is assumed throughout. In terms of the DL control channel overhead a fixed number of OFDM symbols are reserved per TTI, while the Pilot channel overhead is not considered. The infinite buffer as well as the finite buffer traffic models described in Section 2.10 have been implemented. The link-to-system level performance mapping is based on the EESM model, which was described earlier in Section 2.8. The β factors for the considered MCS formats have been obtained from extensive link-level simulations, and are listed in Table B.2. The default simulation assumptions are based on the latest LTE recommendations, given in [14], and are summarized in Table 7.1. Note that there are a few changes in the parameter settings in comparison to the initial FDAS evaluation, which reflects the current status in 3GPP.

The interaction between the main entities involved in scheduling, i.e., packet scheduler, LA, HARQ manager and CQI manager was illustrated in Figure 2.4. The overall scheduler is divided into the time-domain (TD) part followed by the frequency-domain (FD) part, as illustrated in Figure 3.12. The minimum resolution for scheduling in the frequency domain is one resource block (RB), and its width is equal to 180 kHz. There are 50 RBs within 10 MHz according to the latest LTE guidelines [14]. However, only 25 CQI reports are reported to the eNode-B. The number of CQI reports has been reduced to lower the overhead, as well as to improve the quality of per RB CQI estimation. The ideal AB-CQI reporting scheme introduced in Section 3.9 is used by default. The modeling of the relevant RRM entities is described hereafter.

7.3.1 CQI Modeling

For the sake of simplicity, we assume that the CQI is equivalent to a simple SINR measurement at the input of decoder. Thus, it includes antenna combining. For the 1x1 receiver case the ideal CQI for RB number n can be expressed in linear scale as:

$$CQI_{ideal}(n) = \frac{\sum_{i=SI}^{EI} P_{pilot,rx}(i)}{\sum_{i=SI}^{EI} I_{tot}(i)} \quad , \tag{7.1}$$

where $I_{tot}(i)$ is the total received interference including receiver noise, on sub-carrier i which is included in RB n, and $P_{pilot,rx}(i)$ is the virtually received pilot power from the serving cell on the i-th sub-carrier. The term "virtually received pilot power" is used here as there is no explicit modeling of pilot symbols. The term $P_{pilot,rx}(i)$ is computed as the product of complete path loss from the serving cell on the i-th sub-carrier and the predefined virtual pilot transmit power. The pilot transmit power is only used for CQI computations. The terms SI and EI in (7.1) denote the start index and end index respectively of the sub-carriers included in RB n.

Table 7.1: System model assumptions based on the 3GPP Macro cell out-to-in deployment, and default simulation parameters [49].

Parameter	Setting
Cellular Layout	Hexagonal grid, 19 cell sites, 3 cells per site
Inter-site distance	500 m
System bandwidth	10 MHz
Sub-carriers per RB	12
Number of RBs (M)	50
Sub-frame/TTI duration	1 ms
Total eNode-B transmit power	46 dBm
Penetration loss	20 dB
Lognormal shadowing standard deviation	8 dB
Correlation between sectors	1.0
Correlation between sites	0.5
Correlation distance of slow fading	50 m
Min. dist. between UE and cell	35 m
Avg. number of users per cell (UDO)	20 (Ref, FDLA), 10 (FDPS)
Max. users multiplexed per sub-frame (N)	1 (Ref, FDLA), 10 (FDPS)
TD scheduling	TD-PF
FD scheduling	F-FDM, FD-PF
Power delay profile	TU, 20 paths
CQI reporting scheme	AB-CQI, periodic reporting
CQI log-normal error std.	1 dB
CQI reporting resolution	1 dB
CQI measurement sub-band (Δf_{cqi})	360 kHz (24 sub-carriers)
Processing delay (D_{cqi})	2 ms
CQI reporting interval (Δ_{cqi})	5 ms
N_{abs}	5 bits
Control channel overhead	21% (3/14 symbols)
Modulation/code rate settings	QPSK (R= 1/3, 1/2, 2/3), 16QAM (R=1/2, 2/3, 4/5), 64QAM (R=1/2, 2/3, 4/5)
HARQ model	Ideal chase combining
Max. No. of HARQ transmission attempts	4
Ack/Nack delay	2 ms
1st transmission BLER target	20%
UE speed	3 km/h
UE receiver	2-Rx MRC
Channel estimation	Ideal
Carrier frequency	2 GHz
eNode-B antenna gain	14 dB
UE antenna gain	0 dBi
UE noise figure	9 dB (-124 dBm/sub-carrier)
Min. distance between UE and cell	≥ 35 m
Frequency re-use	1

In case of the 1x2 MRC scheme the ideal CQI is given by:

$$CQI_{ideal}(n) = \frac{\sum_{i=SI}^{EI} P_{pilot,rx}(i,1)}{\sum_{i=SI}^{EI} I_{tot}(i,1)} + \frac{\sum_{i=SI}^{EI} P_{pilot,rx}(i,2)}{\sum_{i=SI}^{EI} I_{tot}(i,2)} \quad , \qquad (7.2)$$

where $I_{tot}(i,m)$ denotes the total received interference power, and $P_{pilot,rx}(i,m)$ denotes the virtually received pilot power on the i-th sub-carrier at receive antenna number m. In reality, the UEs cannot perfectly estimate the CQI, and the reported CQI is subject to both measurement uncertainties as well as quantization effects, as the CQI needs to be reported with a small finite number of bits. As reported earlier, the basic approach is to add a Gaussian distributed measurement error to the ideal CQI report expressed in decibel, as well as to quantize the CQI to a finite resolution. The formatted CQI report at the receiver for the n-th RB is expressed as:

$$CQI(n) = Quant\left\{ X; \left(10\log_{10}\left(CQI_{ideal}(n) \right) + \epsilon(n) \right) \right\} \quad , \qquad (7.3)$$

where $\epsilon(n)$ is a zero mean Gaussian distributed variable with standard deviation σ_{CQI} ([dB]). The random variables $\epsilon(n)$ and $\epsilon(m)$ are uncorrelated for $n \neq m$. The function $Quant\{x;y\}$ quantizes the value y in steps of x. We assume periodic CQI reporting from each UE, which is also the working assumption in 3GPP [14].

7.3.2 Practical Design of LA Based on Real AMC

The practical design of LA takes into account real AMC, first transmission BLER target, HARQ restrictions, as well as the buffer status. At the transmitter, the effective SINR is calculated on the basis of the CQI reports, MCS format, and the EESM model. The PHY layer performance curves shown in Figure 2.11 are used to determine the BLER for a given effective SINR value and MCS format. We will focus on the detailed analysis of the FDLA-EP algorithm, as it has shown the most potential.

The pseudo-code of the FDLA-EP algorithm taking into account the practical aspects is illustrated in Figure 7.2, based on Matlab notation. Note, that the HARQ retransmission case is not included in Figure 7.2, as it is fairly straightforward to manage. The algorithm loops over the per RB CQI values that have been sorted in descending order of quality. For each combination of RBs the EESM based effective SINR is calculated using (2.22), where γ_i denotes the effective CQI value taking the updated OLLA offset into account. The RB and MCS combination that optimizes throughput under the BLER and buffer occupancy constraints is used in transmission. In case no combination of parameters can satisfy all the constraints the lowest MCS and full bandwidth transmission mode is employed. The design of the Ref scheme is relatively straightforward as there is only one RB available for use.

At the receiver, actual sub-carrier SINR is used to compute the effective EESM SINR. Next, the actual BLER is read from the relevant PHY layer performance curve. The transmission is deemed to be successful if $X < BLER$, where X is a uniformly distributed random variable in the range $[0;1]$. Failed transmissions are afterwards retransmitted using HARQ with ideal Chase Combining. The effect of Chase Combining is captured by linearly adding the EESM values for the different HARQ transmissions.

As the CQI error distribution is assumed to be lognormal, it is likely that LA selects the RBs for transmission which have a positive value of error. In such a scenario the closed loop OLLA

```
sortCQI(1:nPRBs) = sort CQI values in descending order;
sortedIndices(1:nPRBs) = Indices of the sorted CQI values;
maxTP = 0;
PRBallocVector = zeros(1:nPRBs);
powerAllocVector = zeros(1:nPRBs);
numSym = 5;
numCarr = 12;
MCSindex =[ ];
nActPRBs = 0;
for s=1:nPRBs
      tempPowerVector=[ ];
      tempPowerVector(1:s) = P_total/s;
      for t = 1:nNumofMCS
          Calculate γ_eff using (2.22), where β corresponds to the specific MCS
          and γ_i is given by γ_i = (CQI x tempPowerVector) /P_pilot, tx
          Determine the BLER corresponding to γ_eff
          if (BLER <= BLER_target)
              TP_eff,FDLA-EP = (numSym x numCarr x s x MCSToBits) x (1-BLER)
              if ( (TP_eff,FDLA-EP > maxTP) & ( TP_eff,FDLA-EP <= numBitsInBuffer) )
                  maxTP = TP_eff,FDLA-EP ;
                  nActPRBs = s;
                  MCSindex = t;
              end
          end
      end
end
if (maxTP == 0)
      MCSindex=1;
      nActPRBs = nPRBs;
end
for r=1:nPRBs
      if ( r is found in sortedIndices(1:nActPRBs) )
          PRBallocVector(r) = 1;
          powerAllocVector(r) = P_total/nActPRBs;
      end
end
```

Figure 7.2: Pseudo-code of the practical FDLA-EP algorithm employing buffer occupancy information as well as real AMC, based on Matlab notation.

algorithm described in Subsection 2.5.2 is used to reduce the impact of biased CQI errors. The offset factor A_{CQI} is adjusted using the received Ack/Nacks. The same offset is applied to each RB of a user, and only the Ack/Nack of the first transmission is used to adjust the offset factor. The dynamic range of OLLA offset factor is restricted to 4 dB.

7.3.3 HARQ Aware FD Scheduler Design

As described in Section 3.8, packet scheduling is divided into two steps. In Step #1, the TD scheduler selects a sub set of N users from the available users in the cell. These users are frequency multiplexed by the FD scheduler in Step #2. We assume that $N = UDO$, in order to maximize the multi-user diversity gain potential. It is desirable to map users to those RBs where they experience relatively good channel quality. This is a non-trivial optimization problem, which is further complicated by the additional constraint that pending HARQ retransmissions shall be transmitted on the same number of RBs as the original transmission. However, the FD scheduler still has the freedom to select RBs for a retransmission as long as the total number of RBs is the same as for the original HARQ transmission (i.e., adaptive HARQ) [59].

The steps involved in HARQ management at the FD scheduler are illustrated in Figure 7.3. In order to limit the HARQ retransmission delays we choose to give priority to pending HARQ retransmissions in the FD scheduler. Hence, assuming that Q of the N users have pending retransmissions requiring allocation of K RBs, this leaves $Y = M - K$ RBs for transmission of new data from the remaining L users (Step A in Figure 7.3). We begin by allocating up to Y RBs to the L users with new data to transmit (Step B). This gives maximum flexibility in selecting RBs for the users with relatively high channel quality, which tends to maximize the transmitted throughput for new data. The remaining K RBs are subsequently allocated to the Q users with pending retransmissions (Step C). It means that there are less degrees of freedom for selecting good RBs for retransmissions, as compared to new data. This approach is taken because it is less critical to
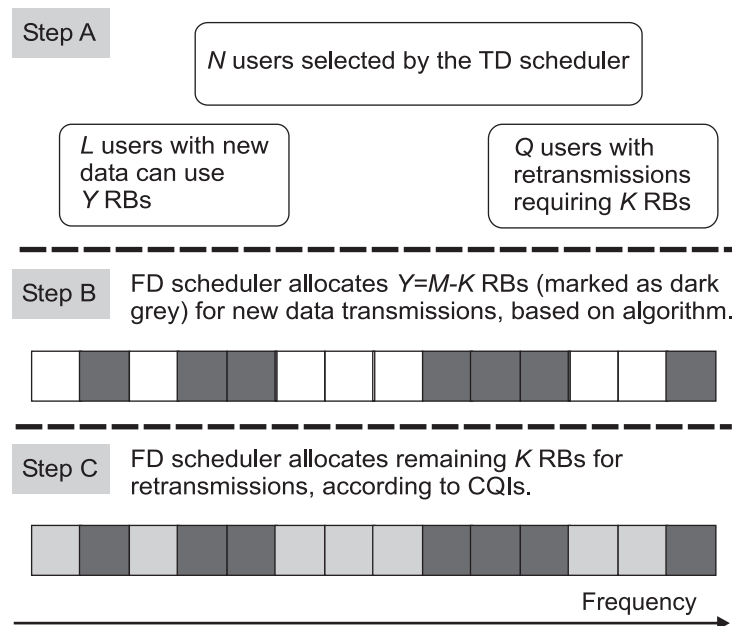

Figure 7.3: HARQ management strategy applied at the FD scheduler, that is required to manage the division of RB resources between first transmissions and retransmissions [59].
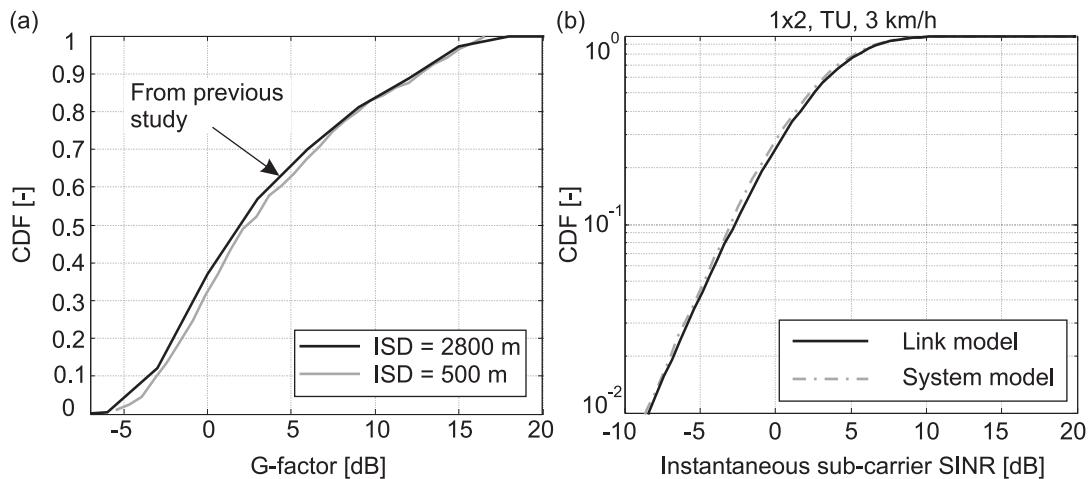
Figure 7.4: (a) Comparison between the G-factor CDF obtained from previous study and the system simulator implemented here. (b) Comparison between the CDFs of instantaneous sub-carrier SINR (TU profile) obtained from link-level model and the system simulator.

have good channel quality for retransmissions, as these will most likely be correctly received due to the HARQ combining gain. The assumption is that the BLER target for the first transmissions is within 10%-20%. We evaluate the impact of selected HARQ management strategy on FDPS performance in Section 7.7.

7.4   Validation of the System Simulator

Figure 7.4 (a) illustrates the CDF curves of the G-factor obtained from the system simulator, as well as from a previous study [64]. The inter-site distance (ISD) in [64] was equal to 2800 m, in comparison to 500 m used here. As a result, it is seen that the CDF curve from the system simulator is shifted slightly to the right, indicating better average SINR conditions. As expected the difference between the curves is mainly seen in the low-medium G-factor range, where the SINR is limited by inter-cell interference.

In Figure 7.4 (b) the CDF curves of instantaneous sub-carrier SINR obtained from the system simulator as well as from the link-level model, described in Appendix A, are shown. These curves are used to investigate the implementation of the channel model and antenna processing. They are obtained for the 1x2 MRC receiver and the TU channel profile. It is seen that the sub-carrier level channel dynamics in the two curves match quite well.

7.5   Impact of HARQ Strategy on FDLA Performance

The impact of adaptive and non-adaptive HARQ transmission on the FDLA performance is illustrated in Figure 7.5. The non-adaptive HARQ scheme restricts the transmitter to allocate the same RBs for retransmission that were used in the original transmission. It is obvious that the performance of coverage limited users is more sensitive to the HARQ strategy, since they normally experience retransmissions due to the severe interference conditions. Further, FDLA performance is sensitive to speed as a result of the CQI and LA processing delays. Thus, we focus on the cover-
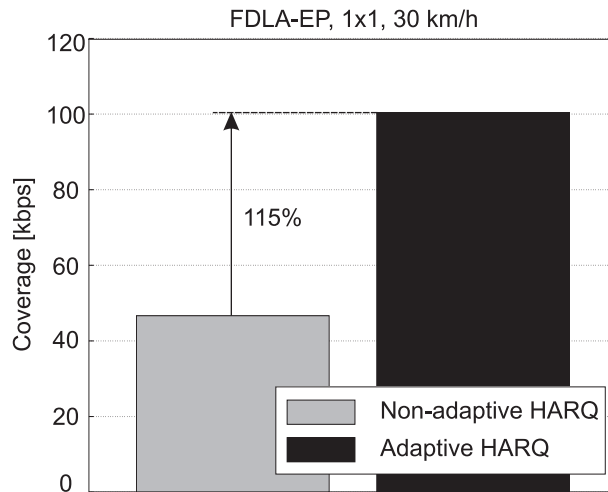
Figure 7.5: Impact of HARQ strategy on coverage performance, based on the 1x1 antenna scheme, infinite buffer traffic model and 30 km/h. The time-domain scheduler is based on the PF principle.

age performance at 30 km/h, and the 1x1 antenna scheme. It is seen in Figure 7.5 that the adaptive HARQ transmission scheme can provide a significant improvement over the non-adaptive scheme in terms of coverage, e.g., over 100%. The FDLA-EP scheme has been used in these results. Thus, it is recommended to employ adaptive HARQ transmission in a practical system.

7.6   Impact of the HARQ Strategy on FDPS Performance

Figure 7.6 illustrates the impact of HARQ strategy (adaptive versus non-adaptive HARQ) on FDPS performance. The results are based on the 1x2 antenna scheme, infinite buffer traffic model, and the speed is set at 30 km/h. It is seen that adaptive HARQ can improve the coverage performance significantly, e.g., around 57%. Similar trends are observed in Figure 7.6 (c), which illustrates the CDF of user throughput. In Figure 7.6 (d) it is seen that due to the reduced degrees of freedom the non-adaptive HARQ scheme occasionally forces a very low FDM order, e.g., around 2-4.

7.7   Influence of the HARQ Management Scheme on FDPS Performance

Finally, the impact of the HARQ management scheme on FDPS performance is evaluated. The proposed HARQ management technique is compared to a scheme that prioritizes multiplexing of retransmissions in frequency, instead of the first transmissions. Figure 7.7 (b) illustrates that although the latter scheme can improve the BLER performance for the first retransmissions, it is not able to improve the coverage significantly, as seen in Figure 7.7 (a). Similar trends were observed in cell throughput. It is recommended to prioritize the multiplexing of first transmissions in frequency, if the objective is to maximize spectral efficiency.
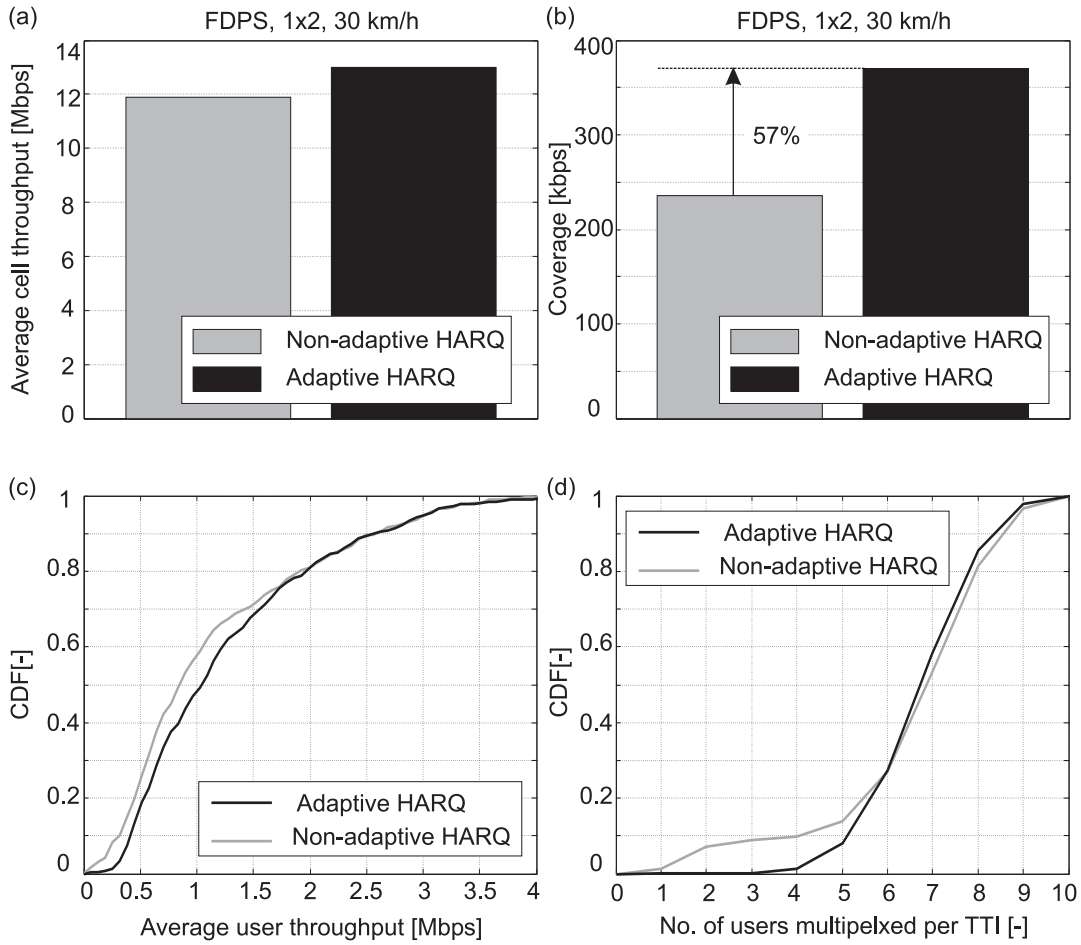
Figure 7.6: Impact of HARQ strategy on FDPS performance, based on the 1x2 antenna scheme, infinite buffer traffic model, and a speed of 30 km/h.
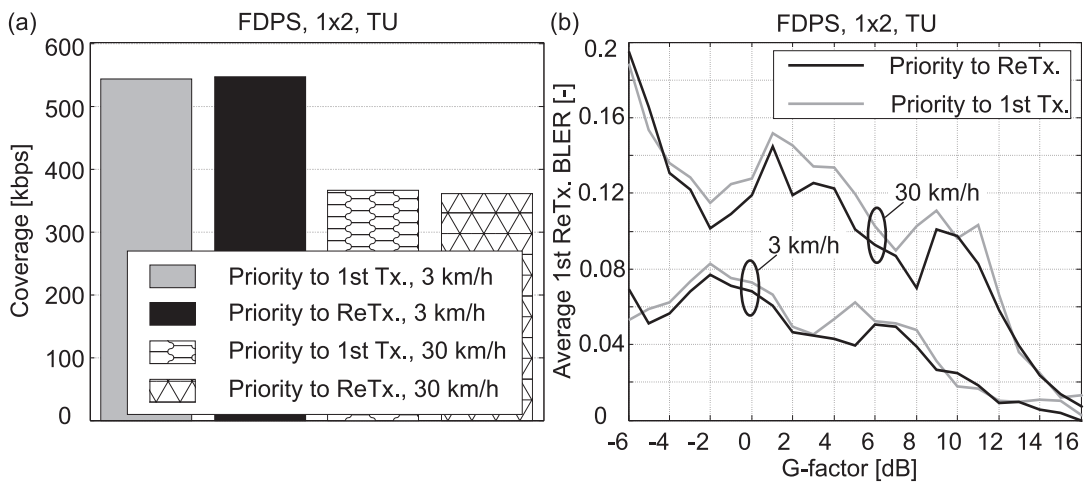

Figure 7.7: FDPS performance as a function of the HARQ management scheme, based on the 1x2 antenna scheme, and the infinite buffer model.

Chapter 8

System Simulator Based Evaluation of the FDAS Potential

8.1 Introduction

In this chapter the system simulator based evaluation of FDAS is presented. The chapter is organized as follows: The algorithms selected for further analysis are short listed in Section 8.2. The detailed performance evaluation of FDLA is described from Section 8.2, and onwards up to Section 8.10. The evaluation of FDPS is presented from Section 8.11, and onwards up to Section 8.16. The conclusions of the FDPS analysis are covered in Section 8.17. Finally, Section 8.18 describes the evaluation of FDPS under fractional load.

8.2 FDAS Schemes Selected for Further Evaluation

Based on the detailed analysis of different LA algorithms in Chapter 4, the FDLA-EP scheme with single-block transmission is selected for further evaluation. Similarly, among the FDPS schemes the F-FDM scheme based on single-block, equal power, and full-bandwidth transmission will be evaluated, on the basis of analysis in Chapter 5. The performance of FDAS schemes is compared against the reference scheme that has been described in Section 3.4.

Among the low bandwidth CQI schemes that can support FDAS the TH-CQI scheme will be used in the detailed analysis, based on the conclusions of Chapter 6. Further, the AB-CQI scheme is employed as the reference CQI scheme for the evaluation of FDAS potential. The complete description of the system simulator has been provided in Chapter 7, and the default simulation parameters have been listed in Table 7.1.
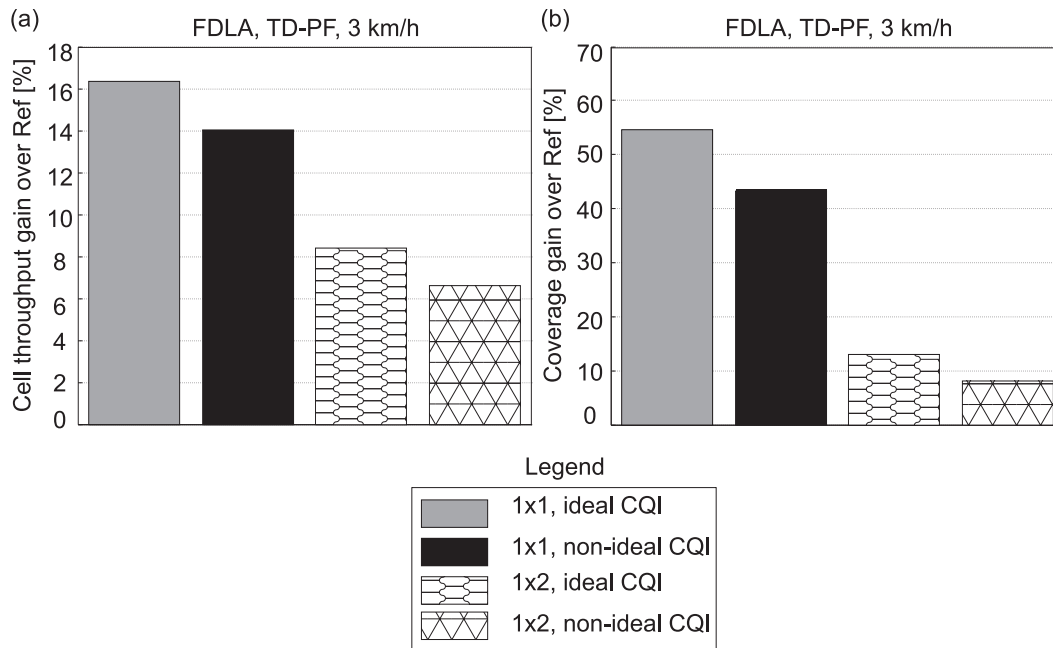
Figure 8.1: (a) FDLA cell throughput gain over Ref as a function of the CQI error and antenna scheme, and (b) FDLA coverage gain over Ref. The results are obtained with the infinite buffer traffic model, and the speed is set at 3 km/h.

8.3 Impact of CQI Error and Receive Antenna Diversity on FDLA Performance

Figure 8.1 (a) and (b) illustrate the FDLA cell throughput and coverage gain over Ref for the 1x1 and 1x2 antenna schemes at 3 km/h, based on PF scheduling in time. Further, the impact of CQI errors on performance is also shown. Similar to the trends in Figure 4.4, it is seen that FDLA gain is reduced in the presence of CQI errors. Furthermore, FDLA is mainly a coverage enhancing mechanism, as seen in Figure 8.1 (b). In the presence of receive antenna diversity the FDLA potential is reduced, due to stabilization of the channel dynamics. These results based on the infinite buffer traffic model and non-ideal CQI settings (AB-CQI) show that the coverage gain of FDLA over Ref is in the order of 10% - 40%, depending on receive diversity.

8.4 Detailed LA Performance Curves

Figure 8.2 illustrates the detailed LA performance curves for the 1x1 and 1x2 antenna schemes. Figure 8.2 (a) and (b) illustrate the cell throughput and coverage respectively, for the FDLA and Ref schemes. In these results the User Diversity Order (UDO) has been fixed at 20. Figure 8.2 (c) illustrates the CDF of the user throughput. While the trends are similar to Figure 4.3 (a), it is observed that the simplified single-cell model gives an optimistic estimate of performance. This can be expected as the previous Shannon theorem based throughput estimation was based on ideal channel coding, continuous rate adaptation, and did not take into account the fact that the decoder performance is dependent on the MCS format (i.e., β factor in (2.22)).

Figure 8.2 (d) illustrates the average number of scheduled RBs as a function of the G-factor.
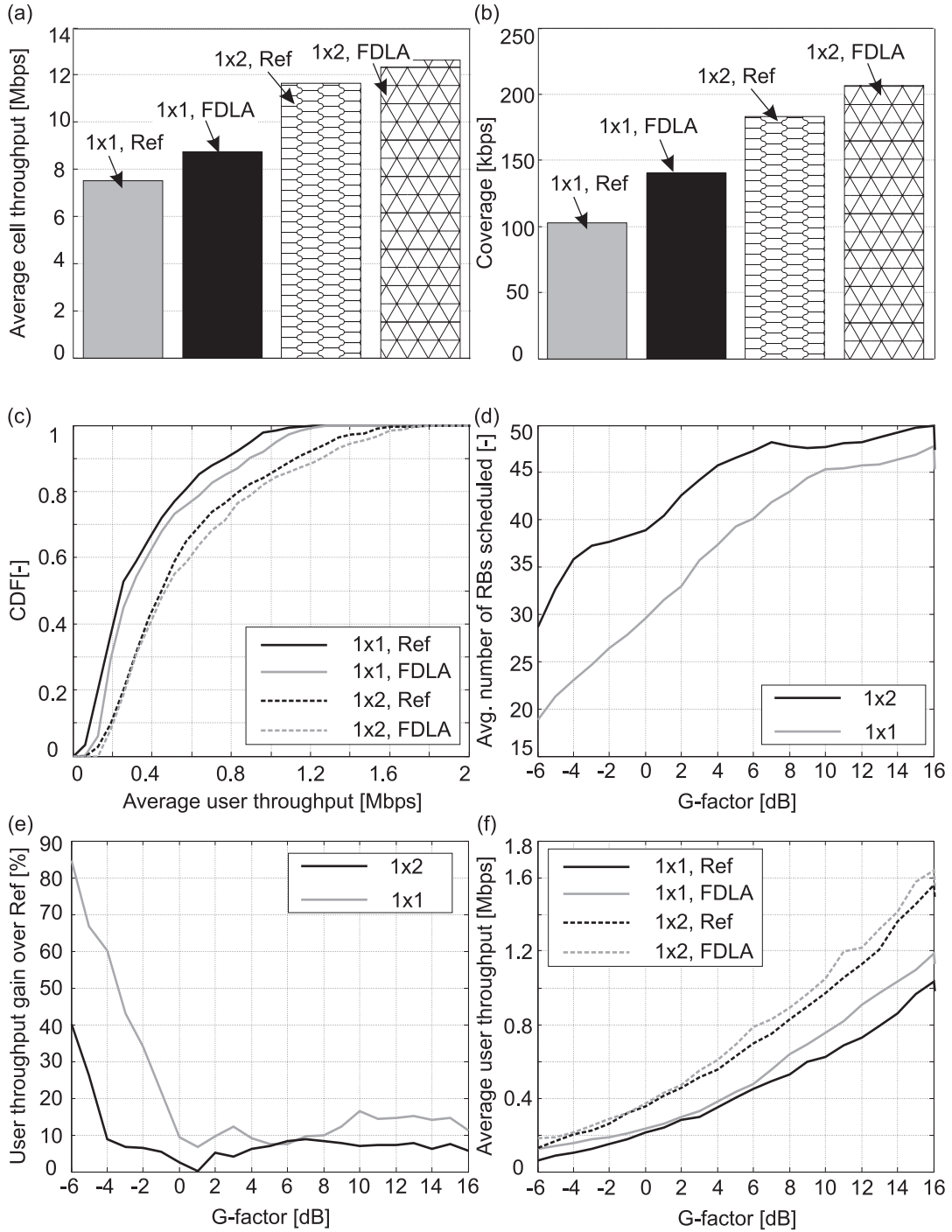
Figure 8.2: Detailed LA performance curves, based on non-ideal CQI settings, the 1x1 and 1x2 antenna schemes, and the infinite buffer traffic model.
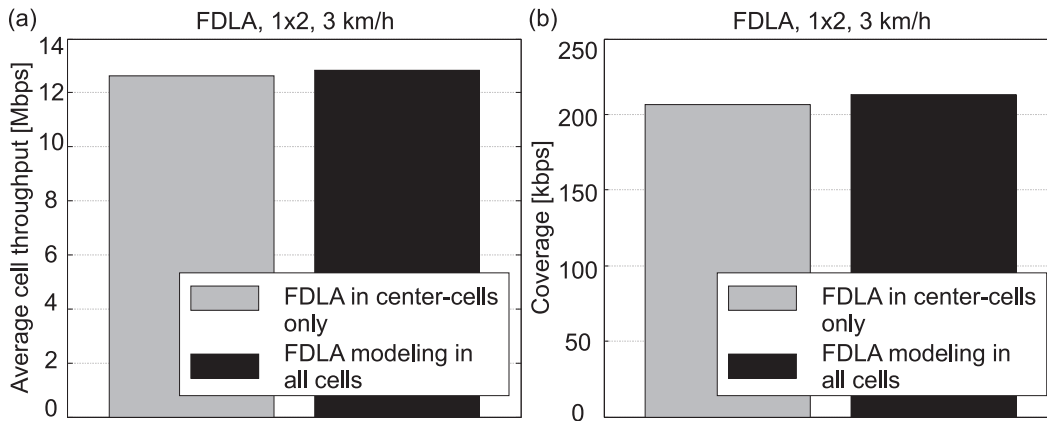
Figure 8.3: Impact of dynamic other-cell interference on FDLA performance, based on the 1x2 antenna case and the infinite buffer model.

In general, the trends are similar to Figure 4.3 (b), and confirm that when the average SINR is low FDLA optimizes the transmit bandwidth under a frequency-selective fading scenario. Figure 8.2 (e) illustrates the FDLA user throughput gain over Ref as a function of the G-factor, and Figure 8.2 (f) illustrates the average user throughput versus the G-factor. In general, the performance trends are similar to Figure 4.3 (d). However, it is observed that due to the EESM model FDLA can also improve performance over Ref at high SINR values.

8.5   Impact of Dynamic Other-Cell Interference on FDLA Performance

The results in Figure 8.2 assume that the interfering cells always transmit at full power, as the detailed modeling of RRM functions is implemented only in the center three cells. Intuitively, we expect the FDLA performance to improve if the other-cell interference is dynamic in nature, e.g., when the RRM functions are implemented in all cells of the network. This is due to the fact that FDLA can avoid transmission on those RBs that are experiencing severe interference, thus improving SINR on the selected RBs. In order to investigate this behavior we model FDLA performance in the interfering cells using the CDF of scheduled PRBs (cell-level), obtained from the analysis in Section 8.4.

The results in Figure 8.3 show that the FDLA performance improves marginally when the other-cell interference is dynamic in nature. Note that the model used here ensures that the RB allocation pattern changes slowly in time at each eNode-B, due to the inability of LA to track fast variations in SINR.

8.6   FDLA Performance as a Function of the Maximum Allowed Power Per RB

In order to limit the dynamic range of SINR variations due to adaptive power allocation as well as to reduce the PAPR of the transmit signal the maximum allowed power per RB, denoted by Power $_{RB,max}$, is parameterized. Figure 8.4 illustrates the FDLA cell throughput and coverage as a function of Power $_{RB,max}$. Here, the interfering cells are transmitting at full power. It is seen
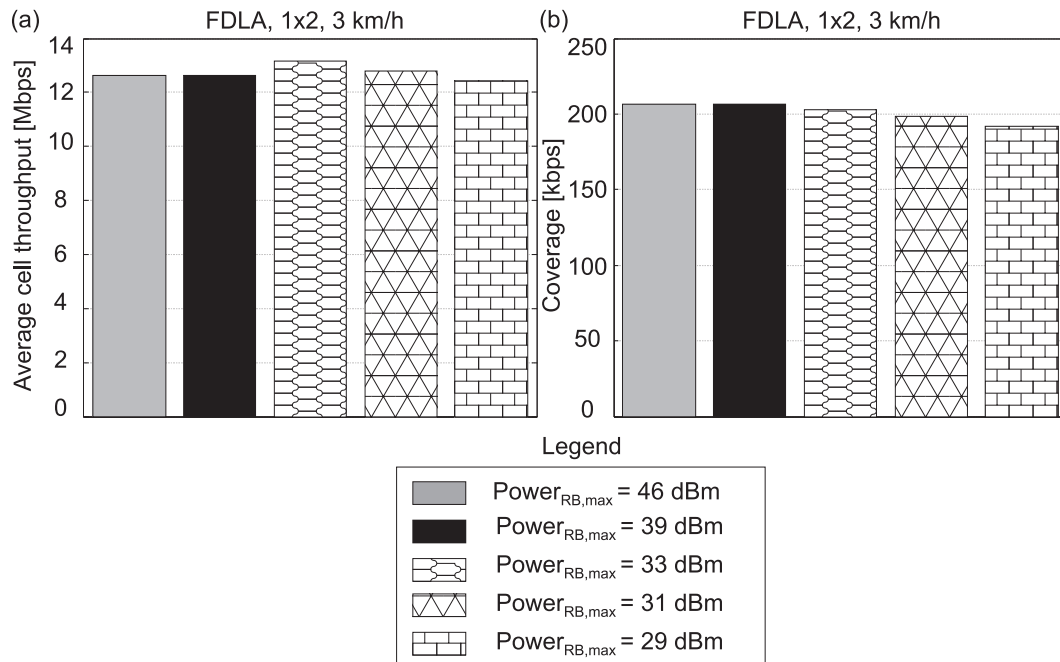
Figure 8.4: Impact of maximum allowed power per RB (Power $_{RB,max}$) on FDLA performance, based on the 1x2 antenna scheme, and the infinite buffer traffic model.

that even though the maximum power per RB is restricted to 2% of full power, there is marginal impact on the FDLA performance. This is due to the fact that the Turbo decoder prefers that all the symbols within the code block have similar SINR conditions, e.g., resulting from limited variations in power. Further, the FDLA algorithm schedules on more than half of the RBs in the average sense, as seen in Figure 8.2 (d), which reduces the impact on FDLA performance.

8.7 Impact of the Traffic Model on FDLA Performance

Figure 8.5 illustrates the impact of traffic model on the FDLA performance. While Figure 8.5 (a) and (b) show the cell throughput and coverage respectively, Figure 8.5 (c) illustrates the CDF of the average user throughput, and Figure 8.5 (d) illustrates the CDF of the scheduled G-factor. It is seen that the absolute value of cell throughput is reduced under the finite buffer traffic model, by around 30%. This traffic model causes the coverage limited users to remain within the simulation set up for a longer duration than the cell-center users, thus reducing the cell throughput. Further, the PF scheduler tries to provide inter-user fairness by scheduling the coverage limited users more often, as seen in Figure 8.5 (d). The coverage performance is not affected by the traffic models considered in this study.

8.8 Significance of OLLA

Figure 8.6 (a) illustrates the relative loss in cell throughput as a function of the std. of lognormal error on the per-RB CQI report. Figure 8.6 (b) illustrates the loss in coverage in comparison to the case with no CQI errors (i.e., $\sigma_{CQI} = 0$). It is seen that OLLA can improve both cell throughput
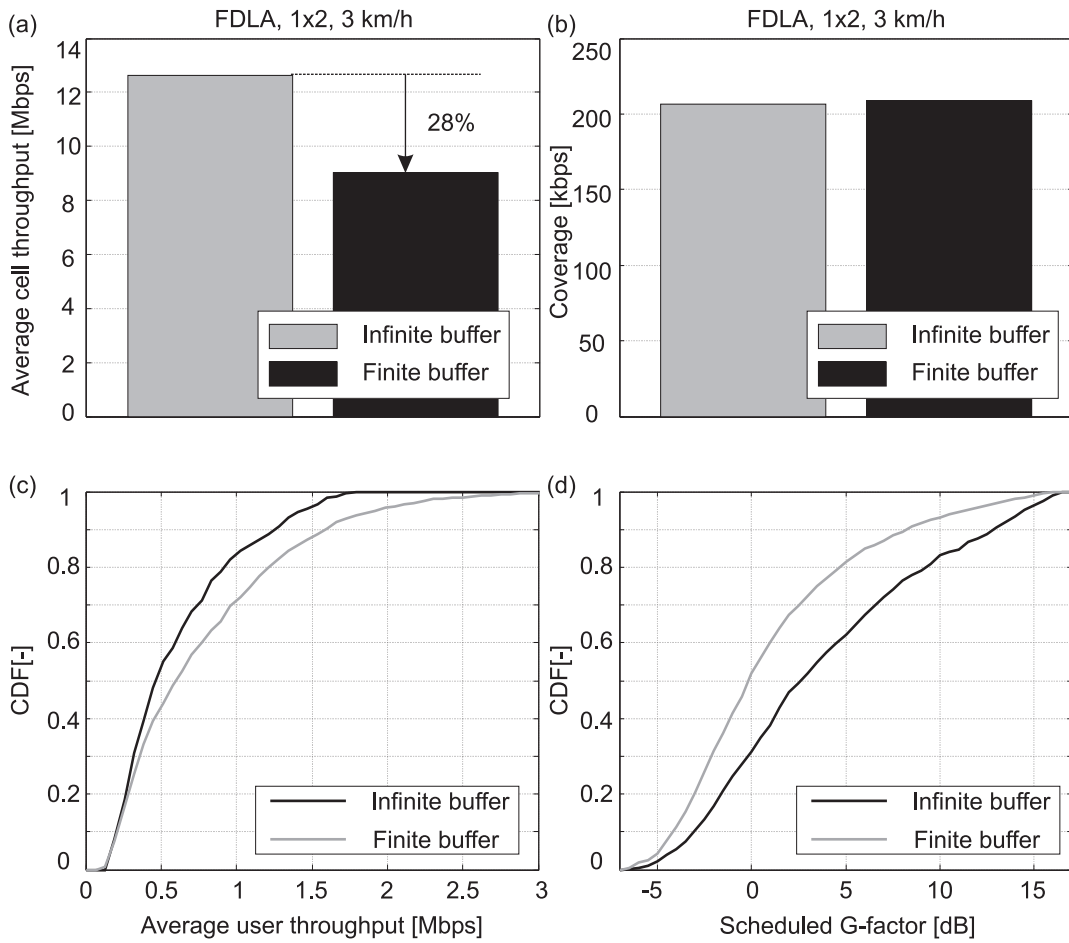
Figure 8.5: Impact of traffic model on FDLA performance, based on the 1x2 MRC antenna scheme.
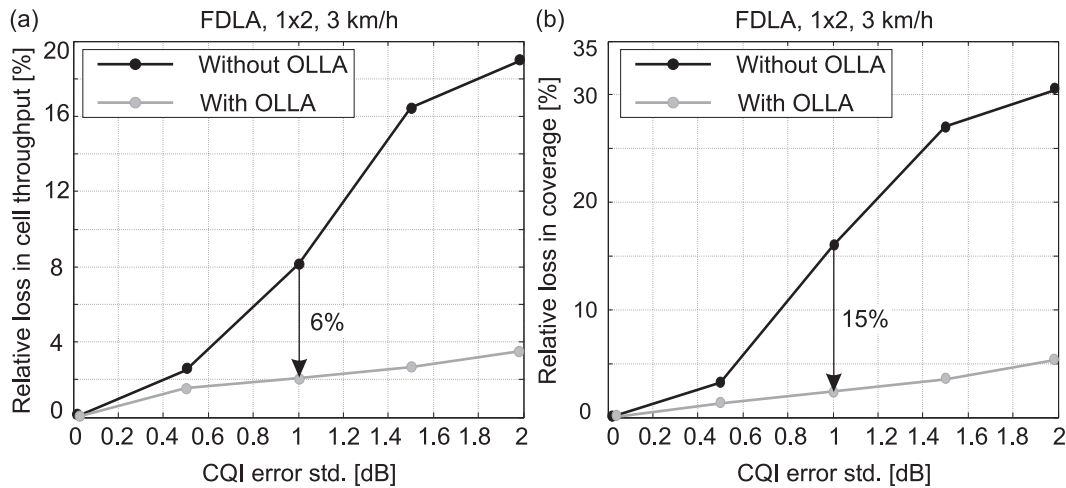

Figure 8.6: Impact of OLLA on FDLA performance when noisy and limited CQI feedback is assumed.

and coverage significantly. The trends are similar to Figure 4.4, and confirm that OLLA should be employed in the practical RRM implementation.

Table 8.1: FDLA gain over Ref for the 1x2 MRC case and the Macro case 1 scenario. Results are based on the AB-CQI reporting scheme at the CQI rate of 25 kbps.

Mobility scenario	Cell throughput gain [%]		Coverage gain [%]	
	Finite buffer	Infinite buffer	Finite buffer	Infinite buffer
Static	18	10	13	13
Low mobility (3 km/h)	8	7	10	10
Medium mobility (30 km/h)	-4	-7	5	5

Table 8.2: FDLA gain over Ref for the 1x1 antenna case and the Macro case 1 scenario. Results are based on the AB-CQI reporting scheme at the CQI rate of 25 kbps.

Mobility scenario	Cell throughput gain [%]		Coverage gain [%]	
	Finite buffer	Infinite buffer	Finite buffer	Infinite buffer
Static	30	29	50	50
Low mobility (3 km/h)	26	14	41	41
Medium mobility (30 km/h)	-3	-5	11	11

## 8.9 Summarized FDLA Results Based on the AB-CQI Scheme

The analysis of FDLA based on the system simulator shows that in general the trends in performance are similar to those obtained with the single-cell model. However, the simplified system model provides an optimistic estimate of the FDLA gain, due to the modeling simplifications. Further, the system settings are also slightly different between the two sets of results. Table 8.1 provides the summarized results of FDLA cell throughput and coverage gain over the reference scheme, for the 1x2 antenna case and the Macro case 1 scenario. The results are provided for both infinite buffer and finite buffer traffic models. Table 8.2 provides similar performance results for the 1x1 antenna scheme. It is seen that FDLA cannot improve the cell throughput over the Ref scheme at 30 km/h, due to the slow CQI feedback.

8.10 FDLA Performance Based on the TH-CQI Scheme

The TH-CQI scheme can reduce the signaling overhead significantly relative to the AB-CQI scheme, as can be seen in Table 8.3. Further, based on the selected parameter settings the CQI rate with the TH-CQI scheme can be made similar to the Ref-CQI scheme. Figure 8.7 illustrates the relative loss in cell throughput and coverage over the AB-CQI scheme as a function of the Threshold value. The trends in terms of cell throughput are similar to Figure 6.2 (a), as there is a unique optimal value of Threshold which maximizes the cell throughput. Further, the optimal

Table 8.3: Parameters for the investigation of low-bandwidth CQI reporting schemes.

CQI scheme	CQI Overhead [bits/report]	Δ_{cqi} [ms]	CQI rate [kbps]
Ref-CQI	$N_{abs} = 5$	1	5
AB-CQI	$M \cdot N_{abs} = 125$	5	25
TH-CQI	$N_{abs} + M = 30$	5	6
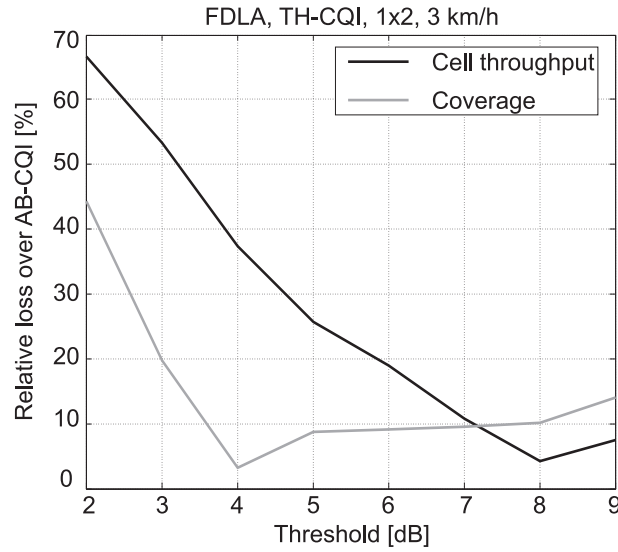
Figure 8.7: Relative loss in FDLA performance as a function of the Threshold value, based on the 1x2 antenna scheme, and the finite buffer traffic model.

Table 8.4: FDLA gain over Ref based on the TH-CQI scheme, and the finite buffer traffic model. Results are provided for the 1x1 and 1x2 antenna schemes.

Mobility scenario	Cell throughput gain [%]		Coverage gain [%]	
	1x1	1x2	1x1	1x2
Static	20	10	40	11
Low mobility (3 km/h)	15	2	40	7
Medium mobility (30 km/h)	-5	-6	10	5

Threshold value is smaller for coverage than cell throughput, as the cell-edge users will generally be scheduled only on a few good RBs. Table 8.4 provides the summarized FDLA performance results for the 1x1 and the 1x2 antenna schemes, based on the finite buffer traffic model and the TH-CQI scheme, at the CQI rate of 6 kbps. This concludes the analysis of FDLA.
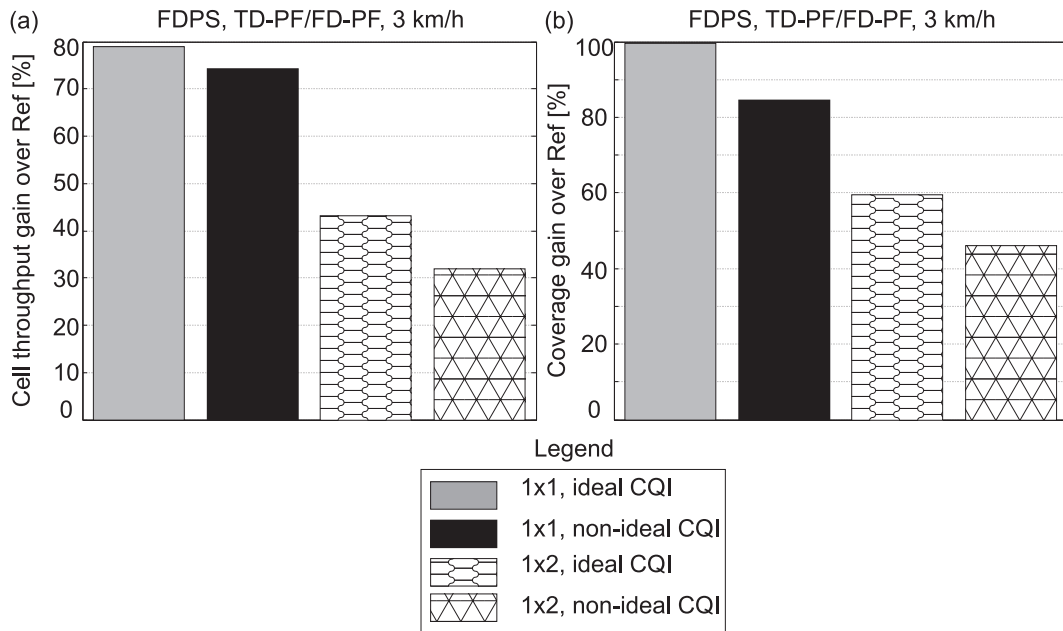
Figure 8.8: Impact of CQI error and antenna scheme on FDPS performance, based on the AB-CQI scheme and infinite buffer traffic model.

8.11 FDPS Performance as a Function of the CQI Error and Receive Antenna Diversity

Next, the investigation of the FDPS potential based on the system simulator is carried out. Figure 8.8 illustrates the impact of receive diversity and CQI error on FDPS performance. The trends are similar to Figure 5.5, and confirm that FDPS can improve performance significantly over the reference scheme. Further, OLLA is able to stabilize the performance in the presence of CQI inaccuracies. The FDPS cell throughput gain over Ref is around 70% - 30%, and the coverage gain is around 80% - 45%, depending on the presence of receive diversity. Comparing the absolute gain with the simplified model it is observed that the previous estimates of the FDPS potential were optimistic, due to the modeling simplifications.

8.12 Impact of Speed on FDPS Performance

FDPS performance as a function of the UE speed is evaluated in Figure 8.9. The trends are similar to Figure 5.6. These results assume non-ideal CQI according to settings in Table 7.1. It is seen that FDPS performance is sensitive to speed as LA is not able to track fast variations in the channel, due to the CQI and LA processing delays. Further, FDPS should be employed in the low-medium mobility scenario, i.e., below 30 km/h.
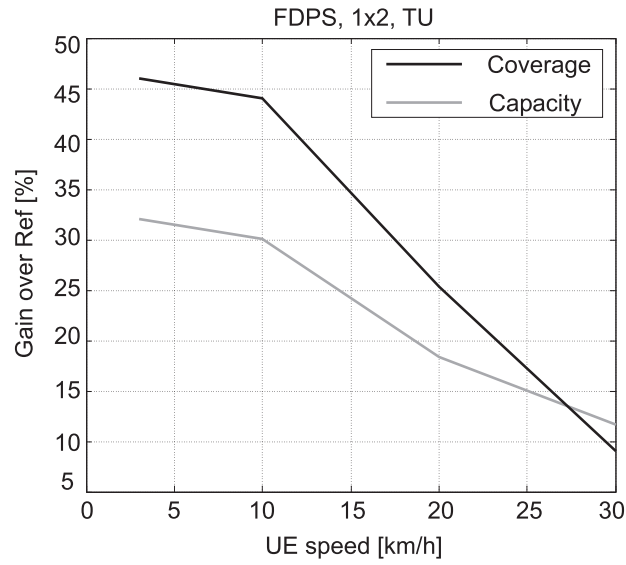
Figure 8.9: FDPS performance as a function of speed, based on the 1x2 MRC scheme and the infinite buffer traffic model.
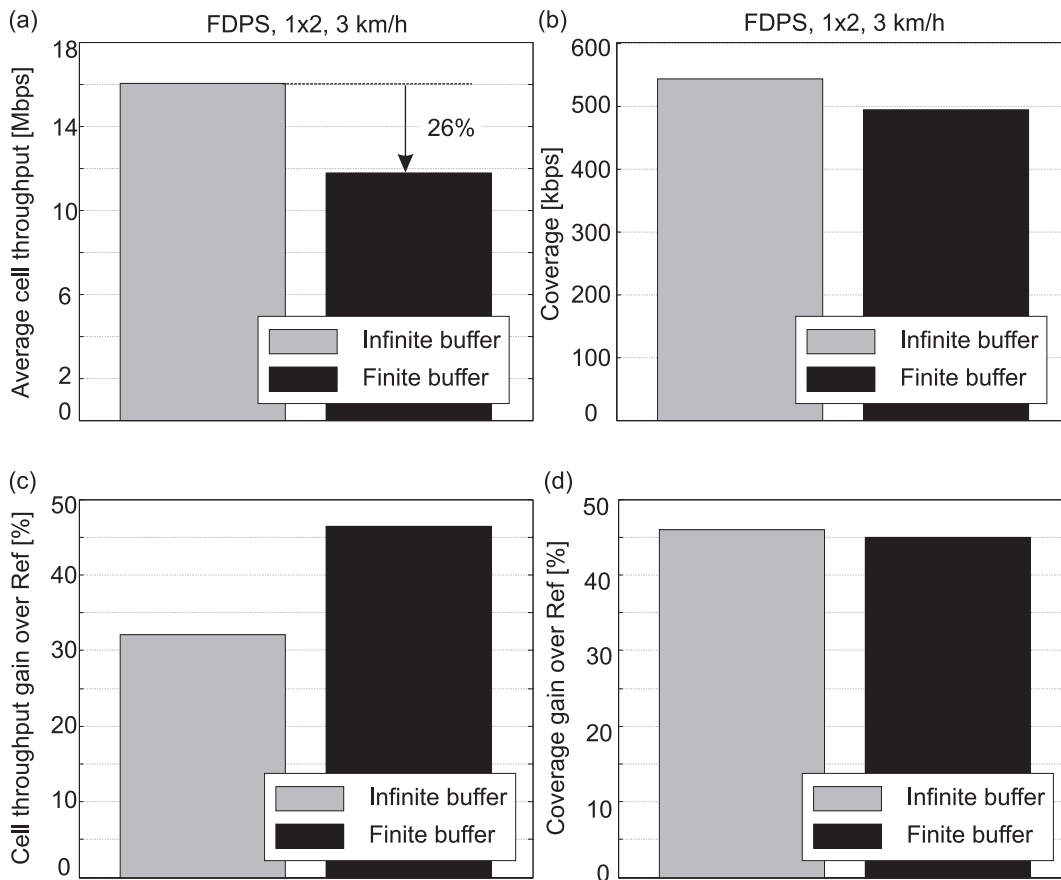

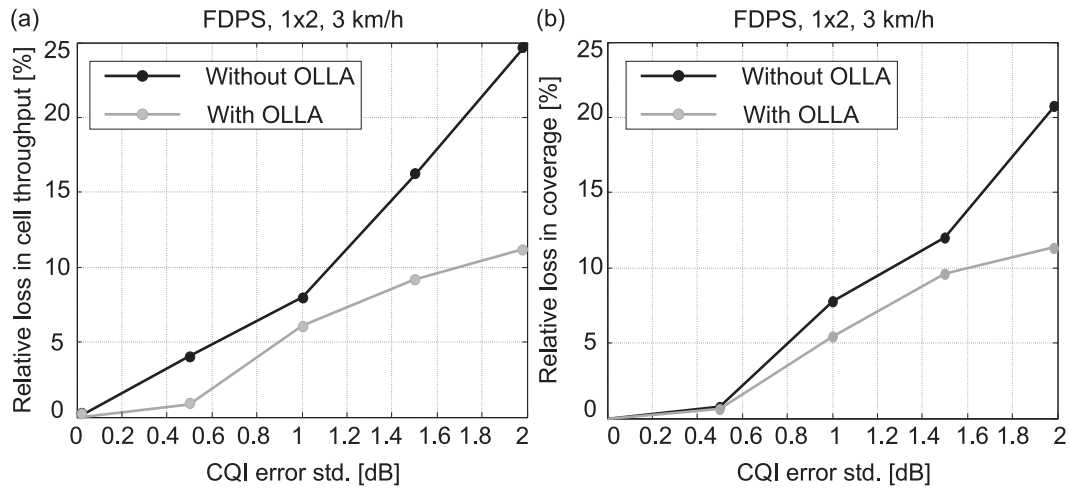**Figure 8.10:** Impact of the traffic model on FDPS performance, based on the AB-CQI scheme.

Figure 8.11: Impact of OLLA on the FDPS cell throughput and coverage. The finite buffer traffic model is employed in these results.

8.13 Impact of Traffic Model on FDPS Performance

Figure 8.10 illustrates the impact of the traffic model on FDPS performance. Similar to the trends in FDLA performance, shown in Figure 8.5, the FDPS cell throughput is also reduced when the data-fair traffic model is employed. However, the PF scheduler is able to maintain the coverage performance. Further, the cell throughput gain over Ref is improved with the finite buffer traffic model, which is similar to the trends in Figure 5.7.

8.14 FDPS Performance Under OLLA

Figure 8.11 illustrates the performance of OLLA when applied together with FDPS. The trends are similar to Figure 5.5, and confirm that OLLA is effective in reducing the impact of biased CQI errors, e.g., OLLA can improve performance by around 10% - 15%. However, there is still a loss of around 5% in both cell throughput and coverage when the per-RB CQI error is around 1 dB. One of the topics for further research is the impact of OLLA convergence on performance. We have assumed a fixed OLLA step size, which is based on previous HSDPA studies.

8.15 FDPS Under Different Degrees of Fairness

Next, FDPS performance under different degrees of fairness is evaluated. Figure 8.12 illustrates performance with four combinations of TD and FD schedulers, which have been described earlier in Section 3.8. It is seen in Figure 8.12 (a) and (b) that different TD and FD scheduler combinations can provide a trade-off between cell throughput and coverage, e.g., the TD-BET/FD-TA scheduler can improve coverage over the TD-PF/FD-PF scheduler by around 15%, without any significant deterioration in cell throughput. The TD-MT/FD-MT scheme is not able to improve the cell throughput even though it prioritizes users with good channel conditions due to the CQI errors and the relatively low FDM order, as seen in Figure 8.12 (f). Further, the TD-PF/FD-ER scheduler tries to allocate equal number of RBs to all users irrespective of their location, as seen
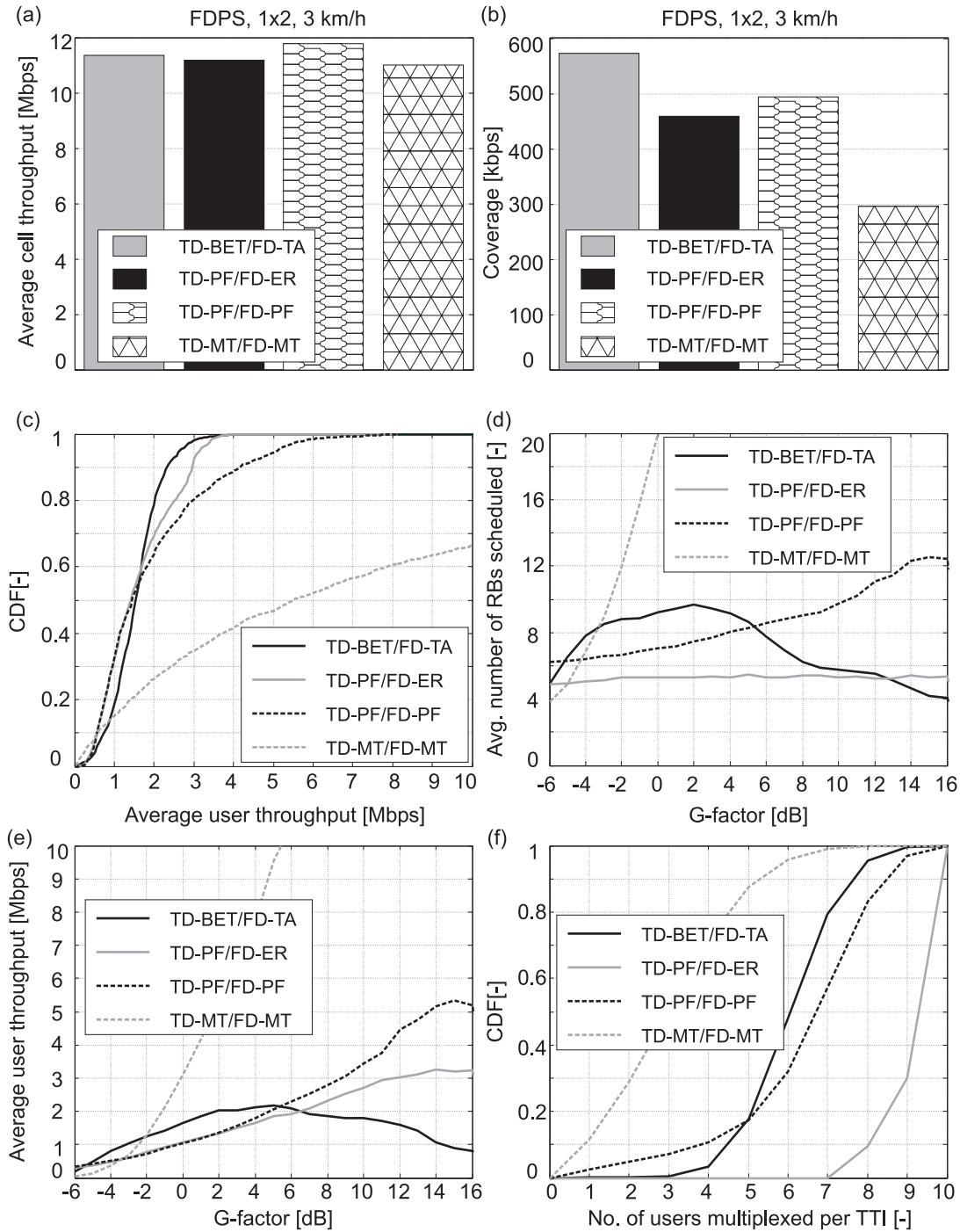
Figure 8.12: Impact of the time-domain and frequency-domain scheduling policy on FDPS performance, based on the finite buffer traffic model.

Table 8.5: FDPS gain over Ref for the 1x2 MRC case, and Macro case 1 deployment scenario. The results are based on the AB-CQI reporting scheme at the CQI rate of 25 kbps, as well as the TD-PF/FD-PF scheduler.

Mobility scenario	Cell throughput gain [%]		Coverage gain [%]	
	Finite buffer	Infinite buffer	Finite buffer	Infinite buffer
Static	56	42	57	57
Low mobility (3 km/h)	46	32	45	45
Medium mobility (30 km/h)	18	12	10	10

Table 8.6: FDPS gain over Ref for the 1x1 case, and Macro case 1 deployment scenario. The results are based on the AB-CQI reporting scheme at the CQI rate of 25 kbps.

Mobility scenario	Cell throughput gain [%]		Coverage gain [%]	
	Finite buffer	Infinite buffer	Finite buffer	Infinite buffer
Static	94	90	86	86
Low mobility (3 km/h)	86	74	83	83
Medium mobility (30 km/h)	23	18	16	16

in Figure 8.12 (d). The TD-BET/FD-TA scheduler tries to provide equal throughput to all users by allocating more RBs to the coverage limited users, as seen in Figure 8.12 (d). More detailed explanation of these results has been provided in [59].

8.16 Summarized FDPS Results Based on the AB-CQI Scheme

The analysis of FDPS based on the system simulator has shown that the performance trends are similar to those obtained with the single-cell model. However, the absolute gain over Ref with the advanced model is lower than that predicted by the simplified model. Table 8.5 provides the summarized results of the FDPS cell throughput and coverage gain over the reference scheme, based on the 1x2 antenna case. Similarly, Table 8.6 provides the FDPS gain numbers for the 1x1 antenna scheme. The results have been provided for both traffic models and for all three mobility scenarios.
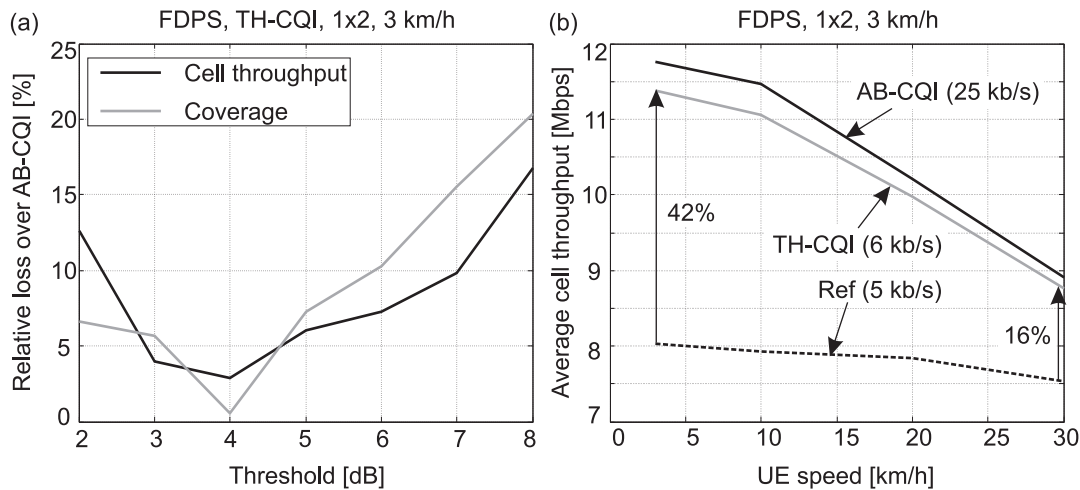
Figure 8.13: (a) Relative loss in FDPS performance as a function of threshold, based on the 1x2 antenna case and the finite buffer model. (b) Variation of FDPS cell throughput as a function of speed, and the CQI scheme. The results are based on the finite buffer traffic model, and for comparison purposes the performance of Ref scheme is also shown.

Table 8.7: FDPS gain over Ref based on the TH-CQI scheme and the finite buffer traffic model.

Mobility scenario	Cell throughput gain [%]		Coverage gain [%]	
	1x1	1x2	1x1	1x2
Static	88	51	75	55
Low mobility (3 km/h)	80	42	70	45
Medium mobility (30 km/h)	20	16	12	10

8.17 FDPS Performance Based on the TH-CQI Scheme

Figure 8.13 (a) illustrates the relative loss in both cell throughput and coverage over the AB-CQI scheme, as a function of the Threshold value. The trends are similar to Figure 6.12 (a) and (b), and a unique optimal Threshold value exists that minimizes the loss. The CQI parameter settings have been taken from Table 8.3.

Figure 8.13 (b) illustrates the variation in FDPS cell throughput as a function of speed. Results are provided for the AB-CQI, TH-CQI and the Ref schemes. In general the trends are similar to Figure 6.21. However, as the AB-CQI scheme is modeled with a larger CQI rate in these simulations it can provide a small gain over the TH-CQI scheme, even at 30 km/h. It is concluded that the TH-CQI scheme is more robust to speed in comparison to the AB-CQI scheme, under the assumption that the CQI rate is fixed at 6 kbps. In summary, the CQI overhead can be reduced significantly with the TH-CQI scheme, e.g., 76%, with around 5% - 10% loss in performance. Table 8.7 provides the summarized FDPS results based on the TH-CQI scheme.

8.18 FDPS Under Fractional Load

Until now we have assumed that there is always sufficient data available at the eNode-B, and that it always transmits on the entire bandwidth. This is referred to as the "full load" scenario. However, in practice the system can experience a situation where there is not enough traffic, e.g., due to lack of users. We denote this as the "fractional load" scenario.

Under fractional load the FDPS scheduler will try to optimize the bandwidth usage by transmitting on the RBs that are experiencing low interference, i.e., it will normally not be required to transmit on the entire system bandwidth. The resulting improvement in SINR (i.e., interference-control) can be utilized to improve the data rate, particularly for the coverage limited users. Thus, FDPS inherently provides a mechanism for interference control, which is particularly effective under fractional load. Further, this is achieved without any centralized management, and without the need for inter eNode-B signaling. Similarly, no modification of the CQI format is required.

The ability of LA to track the fast variations in interference will, however, be limited by the LA and CQI processing delays. As a result, if the scheduler is allowed to change the RB allocation pattern on a TTI basis, the LA error will increase as it will not be able to track the interference variations. In order to reduce the probability of such events we propose to introduce additional constraints on the scheduler. The purpose of this constraint is to restrict transmission on the same RBs for a longer time than the CQI delay, in average sense. Further, the number of RBs that can be used in transmission in each TTI is also regulated in a stochastic sense. Note that the scheduler is still allowed to modify the user-multiplexing order on the selected RBs. Although these constraints will reduce the available degrees of freedom at the scheduler, we expect that FDPS can still provide a gain over round-robin scheduling under fractional load.

A preliminary investigation of the FDPS performance under fractional load based on the above description has been made during this study. A simple two-state Markov chain based model is used to regulate the RB availability at each eNode-B. The modeling details as well as the performance evaluation is presented in Annex I, which is a reprint of the conference article. Taking the round-robin scheduler in time and frequency as reference it was found that FDPS can improve the scheduled SINR significantly, especially at low load, e.g., an improvement of 4 dB was seen at 25% load. This can be attributed to the tendency of FDPS to transmit on the RBs that are experiencing minimum interference. Further, FDPS under fractional load can provide an effective trade-off between cell throughput and coverage, e.g., when the load is 25%, coverage is improved by a factor of two, while the cell throughput is halved compared to the full load case. Other techniques that can regulate the availability of RBs at each eNode-B while satisfying the above mentioned constraints are currently under investigation.

8.19 Acknowledgement

Chapter 9

Overall Conclusions and Recommendations

In this dissertation we have proposed several Frequency-Domain Adaptation and Scheduling (FDAS) algorithms for an OFDMA based system that are suitable for practical implementation. Further, a detailed system-level evaluation of the available FDAS gain potential in Downlink (DL) over time-only adaptation and scheduling (Reference scheme) has been performed. The analysis is based on the UTRA Long Term Evolution (LTE) cellular system framework. The impact of limited and noisy channel-quality feedback has been included in the analysis. Further, several practical system aspects such as control channel and coding overhead, link-to-system performance mapping, Hybrid Automatic Repeat reQuest (HARQ) restrictions, traffic induced variations, and impact of dynamic other-cell interference are included in the evaluation.

The overall evaluation of the FDAS potential has been divided into two parts, depending on the complexity of the system model. In the first part a simplified single-cell based model has been employed, where only the most relevant entities such as the Packet Scheduler (PS), Link Adaptation (LA) and the Channel Quality Information (CQI) control loop have been implemented in detail. The FDAS algorithm design as well as the preliminary performance evaluation has been carried out using the single-cell model. Extensive Monte Carlo simulations based on diverse operating conditions such as different multipath channel profiles, antenna configurations, bandwidth, speed, etc., have been performed in order to make a generalized analysis. The FDAS algorithms with the largest potential were short-listed and further evaluated by using a state-of-the-art multi-cell system simulator in the final part of the study. As a result, realistic estimates of the FDAS gain potential at the system-level over time-domain only adaptation and scheduling have been obtained.

The most important FDAS design parameter is the granularity of adaptation in frequency-domain, where generally an increase in the scheduling resolution leads to an improvement in spectral efficiency. However, the channel-quality feedback needed to support FDAS also increases with an increase in the scheduling resolution. Further, as the signaling overhead reduces the useful data rate in Uplink, it needs to be minimized. The study has shown that most of the FDAS potential can be achieved if the scheduling resolution is in the order of coherence bandwidth. For the typically experienced multipath channel profiles the minimum scheduling bandwidth can be fixed at around 350 kHz, which is similar to the LTE recommendation [14].

9.1 Main Findings of the FDLA Analysis

In order to reduce resource allocation complexity at the transmitter, as well as the overhead of Allocation Table (AT), the single-user per Transmission Time Interval (TTI) scenario is investigated in the thesis. The packet scheduler can still exploit multi-user diversity, but only in the time domain, similar to HSDPA. The parallel sub-channels in OFDMA experience diverse fading conditions over a mobile multipath channel. This frequency-selective fading behavior can be exploited by Frequency-Domain Link Adaptation (FDLA) to improve link throughput, by utilizing bandwidth and/or power adaptation in frequency, as well as Adaptive Modulation and Coding (AMC). The basic idea behind FDLA is that when the SINR is low, it is beneficial to trade bandwidth for SINR (by reallocating power in frequency), as the mapping of SINR to throughput is close to linear (i.e., according to the Shannon Theorem).

It is assumed that the system is operating under a power constraint. Further, the HARQ transmissions must satisfy the target first transmission BLER constraint. These aspects as well as the handling of HARQ retransmissions is included in the proposed FDLA algorithms. In terms of the power allocation strategy apart from the simple equal-power distribution we have also investigated the more advanced Water-filling power distribution in frequency. Further, the inverse Water-filling strategy has also been investigated in the preliminary study.

The system-level analysis in the 3GPP Macro-cell deployment scenario has shown that the adaptation of MCS format within a single HARQ transmission (i.e., multiple code block transmission to a single User Equipment (UE)) does not provide a significant gain over single-block transmission, e.g., less than 5%. FDLA is mainly a *coverage enhancing* mechanism, as frequency-domain adaptation is most suitable when the SINR operating point is low, i.e., beneficial for the cell-edge users that are experiencing severe other-cell interference. In general, the maximum FDLA potential is observed when the average SINR is below 0 dB. Further, considering the performance as well as the signaling overhead requirements, the simpler equal-power distribution in frequency is the most attractive scheme. Water-filling is sensitive to the granularity in power domain, and it leads to increased variability in the symbol quality. This is detrimental to the performance of the selected encoding scheme. The FDLA gain potential is reduced in the presence of transmit and/or receive antenna diversity, as the array gain and/or diversity gain stabilizes the channel dynamics, thus reducing the degrees of freedom. Further, adaptive HARQ transmission can provide a significant gain over non-adaptive HARQ transmission, especially at medium speeds (i.e., 30 km/h).

In terms of the traffic model, two variants of the best-effort traffic have been employed in the analysis. The infinite buffer model is characterized by equal session time for all users, while the finite buffer model allows fixed data for download, irrespective of the user location. As the finite buffer model is a data-fair model the cell-edge users have a significant impact on cell throughput, and it is reduced by around 30% over the infinite buffer case, irrespective of the FDAS scheme.

Depending on the presence of receive antenna diversity, FDLA can provide a coverage gain of 10% - 40% over the reference scheme, at 3 km/h. These results are based on the threshold based CQI scheme (TH-CQI), with periodic CQI reporting at the rate of 6 kbps. Further, the FDLA performance is sensitive to UE speed, and it is not suitable beyond 20 km/h. Performance is also sensitive to the accuracy of CQI reports, and the standard deviation (std.) of CQI error on the resource block (RB) should be kept within 1 dB - 2 dB (assuming lognormal distribution of error). Further, it has been shown that the Outer Loop Link Adaptation (OLLA) mechanism is required to stabilize the FDLA performance under biased errors, i.e., when the CQI reports experience

measurement inaccuracies and processing delays.

9.2   Recommendations for FDPS Algorithm Design

The potential to exploit multi-user diversity in both time and frequency is investigated under Frequency-Domain Packet Scheduling (FDPS). Smart scheduling concepts such as opportunistic scheduling in time and frequency have been utilized to fully exploit the available degrees of freedom in the OFDMA system. A novel scheduling framework has been proposed, where the overall scheduler is divided into a time-domain (TD) part followed by the frequency-domain (FD) part. The main task of the TD scheduler is to control inter-user fairness, while the FD scheduler handles frequency-domain multiplexing aspects. This framework is flexible as it can be tuned according to the complexity and signaling overhead requirements. Further, TD scheduling can be bypassed altogether if the aim is to investigate the potential of optimal user-multiplexing in frequency. Different scheduling policies can be applied at the TD and FD schedulers, depending on whether the goal is to improve cell throughput or coverage.

A novel design for the HARQ aware FD scheduler has been proposed, and the impact of different HARQ management strategies on FDPS performance has been evaluated. The recommended technique is to reserve adequate number of RBs for HARQ retransmissions, while providing the maximum flexibility to the FD multiplexing of first transmissions. Such a strategy will limit the HARQ retransmission delays, and at the same time maximize the transmitted throughput for new data. System level simulations have shown that the selected HARQ strategy can improve the cell throughput, without having a significant impact on coverage.

There is marginal gain in FDPS performance from advanced power distribution in frequency (i.e. Water-filling), over the simpler equal-power distribution and full bandwidth transmission. Further, the latter technique also limits the PAPR of the transmit signal, and it stabilizes the performance of the Turbo decoder (i.e., LTE encoding scheme), which prefers that the symbols have similar quality within a single code block. Thus, it is recommended that the FDPS scheduler should transmit on the entire bandwidth using equal-power distribution in frequency, as long as there is sufficient data to send.

System-level evaluation of FDPS shows that performance is dependent on the user multiplexing flexibility in the frequency domain, e.g., if the FD scheduler is restricted to allocate only adjoining RBs to a user the cell throughput is reduced by 15% - 20%, over the fully flexible solution. Similarly, the performance is sensitive to CQI errors, e.g., the relative loss in cell throughput is around 25% when the std. of CQI error per RB is equal to 2 dB. The impact of noisy channel-quality feedback is reduced by employing the OLLA mechanism, e.g., the cell throughput is improved by around 5% - 10%.

The traffic model has an impact on FDPS performance, e.g., the cell throughput is reduced by around 26% when the finite buffer traffic model is employed. Further, it is observed that the performance is sensitive to UE speed. The FDPS gain over Ref is optimal at low speeds, and it is not suitable to employ channel aware scheduling beyond 30 km/h. At a low speed, e.g., 3 km/h, FDPS can provide a cell throughput gain of 40% - 80% and a coverage gain of 45% - 70%, depending on the presence of receive antenna diversity. These results are based on periodic CQI reporting using the TH-CQI scheme, at the rate of 6 kbps.

The key difference between FDPS and FDLA is that the former does not depend on bandwidth

reduction for the improvement in SINR. It is the order of multi-user diversity in both time and frequency that determine the potential of SINR improvement under FDPS. Thus, it can provide a significant improvement in performance over the reference scheme even at medium-high SINR values, depending on the user diversity order.

9.3 Recommendations for Design of Low-Bandwidth CQI Schemes Enabling FDAS

The potential of FDAS, like any adaptation scheme, is highly dependent on the nature of channel-quality feedback. In order to maximize the gain potential of FDAS in a highly frequency-selective environment the RB width should be quite narrow. However, this implies that only a few pilot symbols will be available for CQI estimation within a single RB, making it difficult to achieve high per-RB CQI measurement accuracy. Simulations have shown that the std. of CQI error can be up to 2.5 dB, when the RB width is equal to 375 kHz

One of the available mechanisms to reduce the CQI error without increasing the RB width is to perform averaging in time at the receiver side, as the effective number of pilots can be increased. However, this will lead to an increase in the link adaptation delay, which will affect the mobility support. Further, excessive averaging can also reduce the perceived channel dynamic range. Ideally, the averaging window at the UE should be adjusted according to its speed. Another approach is to select the window size that can provide a good trade-off between CQI error and mobility support, e.g., the study has shown that the window size should be around 2 ms - 3 ms. The overall goal is to limit the std. of per-RB CQI error to around 1 dB.

Periodic CQI reporting has been assumed in this study, which is also the recommended mode in LTE. Several CQI bandwidth reduction schemes have been investigated, including full CQI reporting (denoted as AB-CQI), smart encoding of CQI information such as combination of absolute and offset signaling (OF-CQI) and signaling of the best M CQIs (BM-CQI, BM-OF-CQI). Additionally, a novel threshold-based CQI scheme (TH-CQI) has been proposed. This scheme is based on signaling of the average channel quality over the best RBs (i.e., threshold is specified in the SINR domain).

Lowering of the CQI rate as a means to reduce overhead has also been considered in the study. The different CQI schemes have been optimized separately for FDLA and FDPS. Based on extensive system-level simulations it was found that the TH-CQI scheme has the most potential, e.g., the CQI overhead can be reduced by around 75% with 5% - 10% loss in performance, compared to near ideal signaling. Further, the TH-CQI scheme is the most robust low-bandwidth CQI scheme against speed and measurement errors.

9.4 Topics for Future Research

One of the key topics for future research is the combination of FDAS and MIMO (e.g., spatial multiplexing, and beam forming techniques). The deployment of antenna arrays is becoming popular as the data rate requirements continues to rise, e.g., LTE supports up to 4x4 antenna configuration. Intuitively, MIMO and FDAS can compliment each other, e.g., a transmit antenna array can be used to induce channel dynamics for static users, which can be exploited by FDAS.

Similarly, in the Micro-cell scenario FDAS alone has limited potential, due to the high average SINR. In this case MIMO can be used to reduce the average SINR per stream, and thereafter it can be combined with FDAS to improve overall performance.

Another important area of research is the design of QoS-aware FDPS scheduler, which can handle a mix of services with different packet delay, data rate, and priority requirements. The performance evaluation of such a scheduler based on a mixture of real-time (e.g., streaming) and non real-time services is necessary to justify practical implementation of FDAS. Similarly, the multiplexing of very low data rate services such as VoIP together with other traffic types needs to be investigated. Further, the results presented in this study need to be modified to include the impact of real channel estimation, pilot channel overhead, and increased MCS granularity.

In this dissertation we have assumed low-medium mobility scenario. In such cases the best user multiplexing strategy in the spectral efficiency sense is to perform channel-aware scheduling in the frequency-domain, i.e., FDPS. However, this is not the case in the high speed scenario. Intuitively, in such cases it makes sense to improve robustness against fast-fading by exploiting the available frequency-diversity. This implies that each transmission is distributed across the entire spectrum, so that burst errors can be avoided. Further, the CQI overhead becomes manageable in the high speed scenario as detailed frequency-selective reports are not required. The design of such multiplexing schemes as well as their performance evaluation is another important research topic.

Appendix A

OFDM Link-Level Model: Description and Performance Analysis

A.1 Introduction

This appendix provides a description of the OFDM link-level model that has been developed during the course of the PhD. Further, basic link-level results are also provided to explain the working of the tool. The aim of this study is to gain better understanding of the OFDM link-level performance. Moreover, the link-level tool was also used to generate the SINR traces that have been used in the single-cell model, as explained in Section 2.12.

The chapter is organized as follows: The description of the link-level processing chain is presented in Section A.2. This is followed by the modeling assumptions in Section A.3. The validation of the OFDM link-level performance is presented in Section A.4, while Section A.5 describes the single user LA curves as well as the cell-level spectral efficiency obtained with the link-level tool.

A.2 Description of the E-UTRA Link-Level Model

Figure A.1 illustrates the block diagram of the OFDM based link-level transceiver chain. The design is based on the E-UTRA PHY layer guidelines given in [14]. Among the important features implemented are channel encoding/decoding based on the 3GPP Rel 6 guidelines [78], HARQ rate matching, MIMO processing and the multipath MIMO channel model [104]. In the DL the transmitter is located at the eNode-B, while the receiver is based in the UE. At the transmitter information bits are generated by the *transport block generator*. The size of the transport block is determined by the LA module and can be based on the instantaneous channel conditions. Specifically, the *transport format and resource combination* (TFRC) information passed by LA is used to calculate the block size. For the sake of simplicity fixed MCS transmission is assumed, i.e., non-adaptive transmission based on the average SINR measured at the input of detector.

The first step of processing at the transmitter is *CRC encoding*. The outcome of CRC decoding at the receiver determines whether the block needs to be retransmitted or not. This is followed by
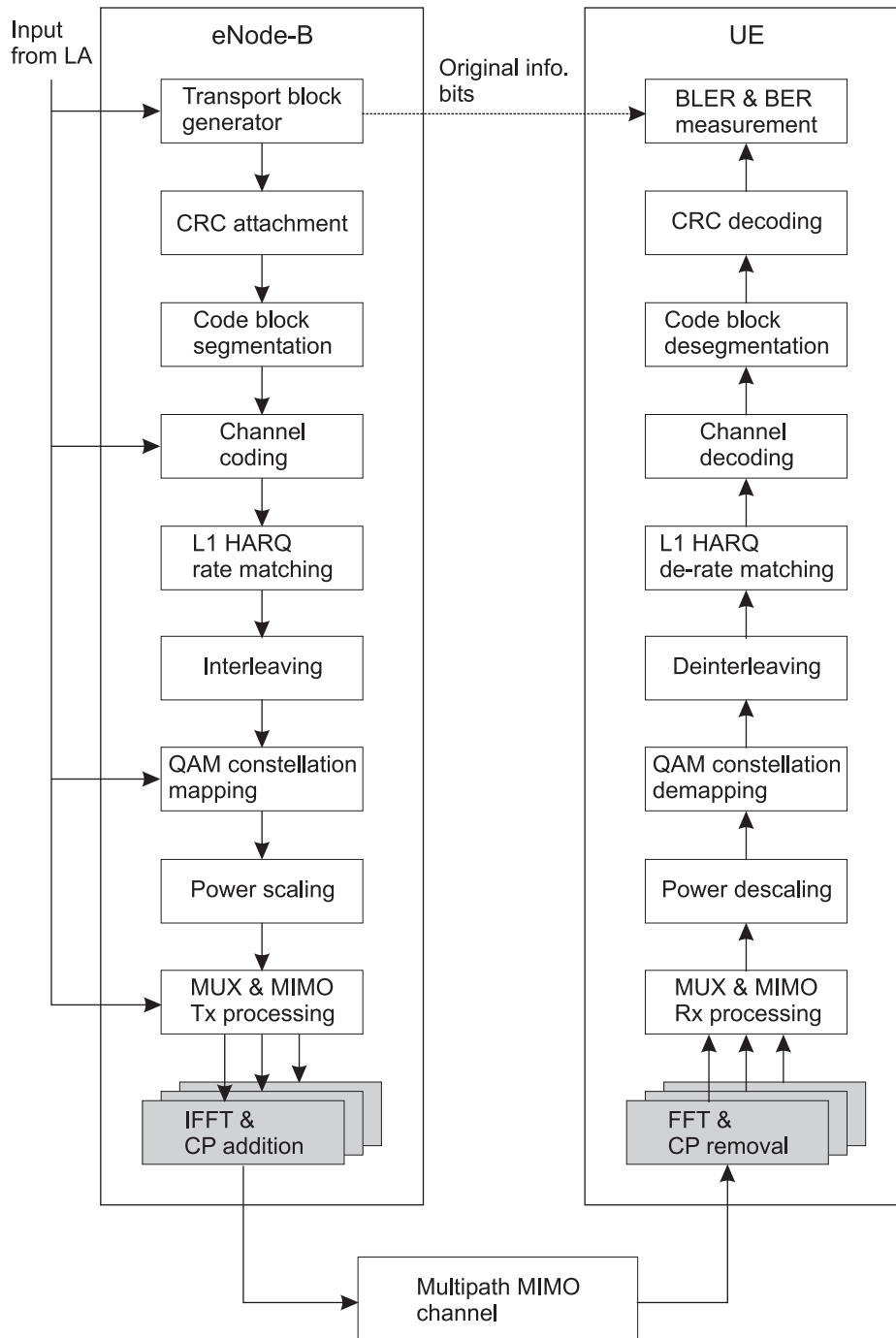
Figure A.1: Block diagram of the OFDM link-level transceiver implemented during the PhD project. The evaluation of the OFDM link-level performance has been published in [62].

code block segmentation. The purpose of this functionality is to ensure that the input to the channel encoder is restricted according to the maximum code block size. If needed the packet is divided into several code blocks before being fed to the channel encoder. The UTRA Release 6 *Turbo encoder* has been employed in this study [78]. Based on the code rate requirement the encoded bits are either punctured or repeated by the *rate matcher*. The code rates can be adjusted from approximately 1/6 to 1/1.

The coded and interleaved bits are modulated according to the selected modulation format. In case of QAM modulation a *QAM re-mapping* is performed according to [78]. The purpose is to relocate the systematic bits at more reliable constellation points in order to improve the decoder performance. The modulated symbols are space-time processed according to the selected MIMO scheme. Each spatial stream is passed through an IFFT module. Further, the cyclic prefix is added before the stream is transmitted over the multipath MIMO channel.

At the receiver side the UE basically performs the inverse operations with respect to the transmitter, as shown in Figure A.1. The receiver perfectly restores the amplitude and phase on each sub-carrier such that only AWGN impairments remain (although scaled by the channel coefficient). If the CRC decoder determines that the data packet is error free, an Ack is signalled back to the eNode-B, otherwise the soft bits are stored in the UE buffer, and a Nack is signalled back. Upon reception of a Nack the eNode-B performs fast PHY layer HARQ retransmission of the data packet [2].

A.3   Modeling Assumptions

A simple LA algorithm is adopted in this analysis where the MCS selection is based on the average SNR (i.e., G-factor). Further, it is assumed that there are no CQI measurement inaccuracies, or reporting delay. The CQI is estimated on a sub-carrier basis. It is assumed that the UL control channel used to transmit the HARQ Ack/Nack messages is received without any errors. Further, the simple TD-RR scheduler is employed in this analysis.

The MIMO channel model used here is based on the implementation in [104], which is a correlation based stochastic MIMO model. In this study it is assumed that the antennas are uncorrelated. Several multipath channel profiles have been implemented, according to the description in Section 2.14. Table A.1 provides the tapped delay line parameters of the considered channel profiles. The PHY layer HARQ scheme is based on Incremental Redundancy (IR) [78]. Note that Chase Combining (CC) is a special case of IR and is thus implicitly supported as well. The maximum number of transmission attempts per data packet is parameterized. In order to maintain a steady flow of data to a single user, several independent SAW based HARQ processes are initiated in parallel (N-channel SAW protocol) [14]. The reference antenna schemes used in this study have been described earlier in Section 2.11.

The default simulation assumptions are listed in Table A.2. Based on these settings and single stream transmission the peak data rates that can be supported are given in Table A.3. The maximum supported rate in the DL with single stream transmission and 64 QAM 4/5 is around 40 Mbps (10 MHz). The overhead due to signalling and pilot channels is not considered here. It implies that multi-stream transmission will be required to meet the peak data rate requirements of LTE (100 Mbps).

Table A.1: Tapped delay line parameters of the Ext. ITU Ped. A, Ext. ITU Veh. A [43] and the COST259 TU [83] channel models, sampled at 30.72 MHz.

Tap	Ext. ITU Ped. A		Ext. ITU Veh. A		COST259 TU		Doppler Spectrum
	Relative Delay (μs)	Avg. Power (dB)	Relative Delay (μs)	Avg. Power (dB)	Relative Delay (μs)	Avg. Power (dB)	
1	0	-5.197	0	-6.153	0	-5.7	CLASSIC‡
2	0.0325	-6.997	0.0325	-7.999	0.217	-7.6	CLASSIC
3	0.0651	-8.897	0.1302	-7.789	0.512	-10.1	CLASSIC
4	0.0977	-7.697	0.3255	-9.602	0.514	-10.2	CLASSIC
5	0.1628	-8.397	0.3580	-6.761	0.517	-10.2	CLASSIC
6	0.1953	-13.197	0.7161	-13.651	0.674	-11.5	CLASSIC
7	0.2929	-21.697	1.0741	-13.142	0.882	-13.4	CLASSIC
8	-	-	1.7252	-18.153	1.230	-16.3	CLASSIC
9	-	-	2.5063	-23.098	1.287	-16.9	CLASSIC
10	-	-	-	-	1.311	-17.1	CLASSIC
11	-	-	-	-	1.349	-17.4	CLASSIC
12	-	-	-	-	1.533	-19.0	CLASSIC
13	-	-	-	-	1.535	-19.0	CLASSIC
14	-	-	-	-	1.622	-19.8	CLASSIC
15	-	-	-	-	1.818	-21.5	CLASSIC
16	-	-	-	-	1.836	-21.6	CLASSIC
17	-	-	-	-	1.884	-22.1	CLASSIC
18	-	-	-	-	1.943	-22.6	CLASSIC
19	-	-	-	-	2.048	-23.5	CLASSIC
20	-	-	-	-	2.143	-24.3	CLASSIC

‡*The "Classic" Doppler spectrum corresponds to the spectrum resulting from uniform distribution in angle of the incident power [19].*

A.4   Validation of the Link-Level Statistics

The CDF of the instantaneous SINR for different antenna cases is shown in Figure A.2. Results are obtained using the TU channel profile. There are two sets of curves depicting the SINR measured on a sub-carrier basis, and the SINR measured on the entire bandwidth (wideband). In a well designed OFDM system with no ISI degradations, the SINR distribution on the sub-carrier will be Rayleigh distributed. The obtained CDF curves for the sub-carrier cases match well with known theoretical distributions for different MIMO schemes, e.g., see in [28], [79].

The CDF curves obtained for the wideband cases in Figure A.2 show that the dynamic range of average SINR is very limited, due to the large bandwidth as well as the frequency-selective channel profile. It implies that the selection of modulation and coding rate is almost constant for

Table A.2: Default simulation parameters used in the link-level analysis of OFDM.

Parameter	Setting
System bandwidth, (BW)	10 MHz
RB bandwidth	10 MHz
FFT size	1024
Sub-frame duration	0.5 ms
Number of useful sub-carriers	600
Number of OFDM symbols per sub-frame	7
CP length (μs)	4.75
Number of users (UDO)	1
Power delay profile	TU
Channel coding	3GPP Rel. 6 compliant Turbo coding with basic rate of 1/3
CRC overhead	24 bits
CQI parameters	Ideal CQI reception
TD scheduling	RR
Selected LA scheme	frequency-blind transmission (Ref)
MCS settings	QPSK: 1/6, 1/3, 1/2, 2/3
	16QAM: 1/2, 2/3, 3/4
	64QAM: 2/3, 4/5
HARQ Type	IR & CC [69]
HARQ SAW channels	6
HARQ Max. number of transmissions	4
UE speed	3 km/h
UE receiver	1x1, 1x2 MRC, 2x2 SFTD
Channel estimation	Ideal
Carrier frequency	2 GHz

a given average SINR or G-factor, and the simple LA model used here can provide a realistic estimate of the system-level performance.

The uncoded BER performance of different modulation schemes has been verified using reference curves in [105]. It is well known that the BER performance of the OFDM signal is dependent on the Doppler frequency, e.g., see [24]. For a fixed sub-carrier spacing the link-level performance deteriorates with increase in UE speed, due to the Inter-Carrier Interference (ICI) degradation. Similarly, for a fixed speed the BER performance deteriorates with a decrease in sub-carrier separation. These aspects are verified in Figure A.3, which shows the uncoded BER performance as a function of the E_b/N_o (SNR per bit) for the following settings of sub-carrier spacing (Δf): 1, 6, 15, 20 [kHz]. Further, the following three UE speeds have been selected for analysis: 3, 30 and 350 [km/h]. The 1x1 antenna scheme, flat fading channel profile, and QPSK modulation scheme are employed in these results.

Figure A.3 (a) illustrates that at 3 km/h ideal OFDM link-level performance in the BER region of interest ($10^{-2} - 10^{-3}$) is achievable if the sub-carrier spacing is at least 6 kHz. When $\Delta f =$

Table A.3: Supported peak data rates based on single stream transmission and settings in Table A.2.

MCS	*Supported single stream data rate [Mbps]*
QPSK 1/6	2.8
QPSK 1/3	5.6
QPSK 1/2	8.4
QPSK 2/3	11.2
16QAM 1/2	16.8
16QAM 2/3	22.4
16QAM 3/4	25.2
64QAM 2/3	33.6
64QAM 4/5	40.3

1 kHz a deterioration in performance is seen when the BER is below 0.001. It implies that in order to achieve ideal OFDM performance at the very low BER values the sub-carrier spacing needs to be much larger than the maximum Doppler frequency, which is around 5 Hz for the 3 km/h case. Figure A.3 (b) and (c) illustrate similar results for the 30 km/h and 350 km/h cases respectively. At 30 km/h the minimum spacing that gives ideal performance is in the order of 15 kHz (also LTE assumption). However, at 350 km/h none of the considered cases can provide very low BER performance and the error floor is observed in all cases.

The turbo decoder implementation has been verified against results in [106]. The decoder performance for some of the considered MCS formats has been shown earlier in Figure 2.11. These curves have been obtained for the AWGN channel and have been verified against similar
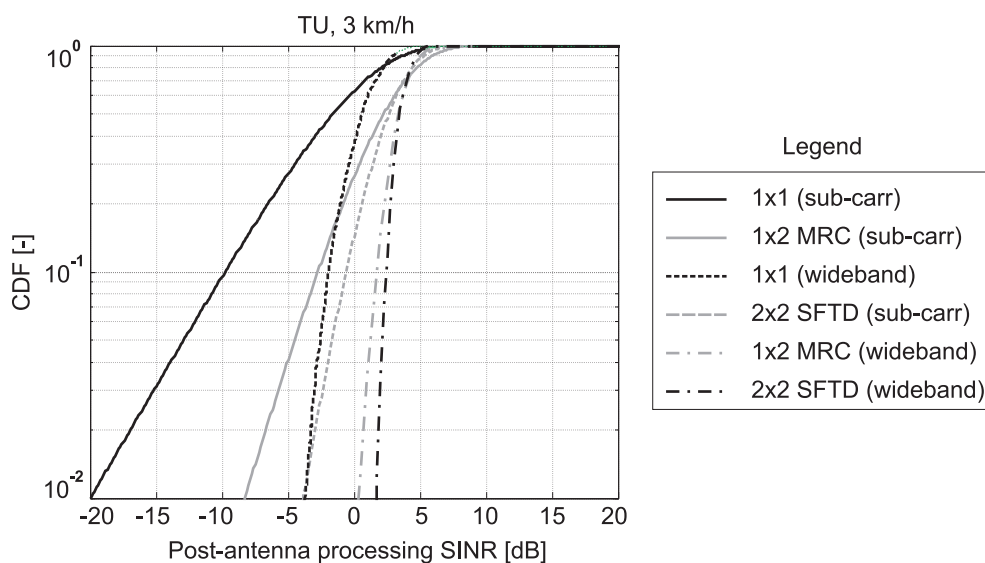
Figure A.2: CDF of the instantaneous SINR measured at the input of detector. Results are based on the TU channel profile at 3 km/h.
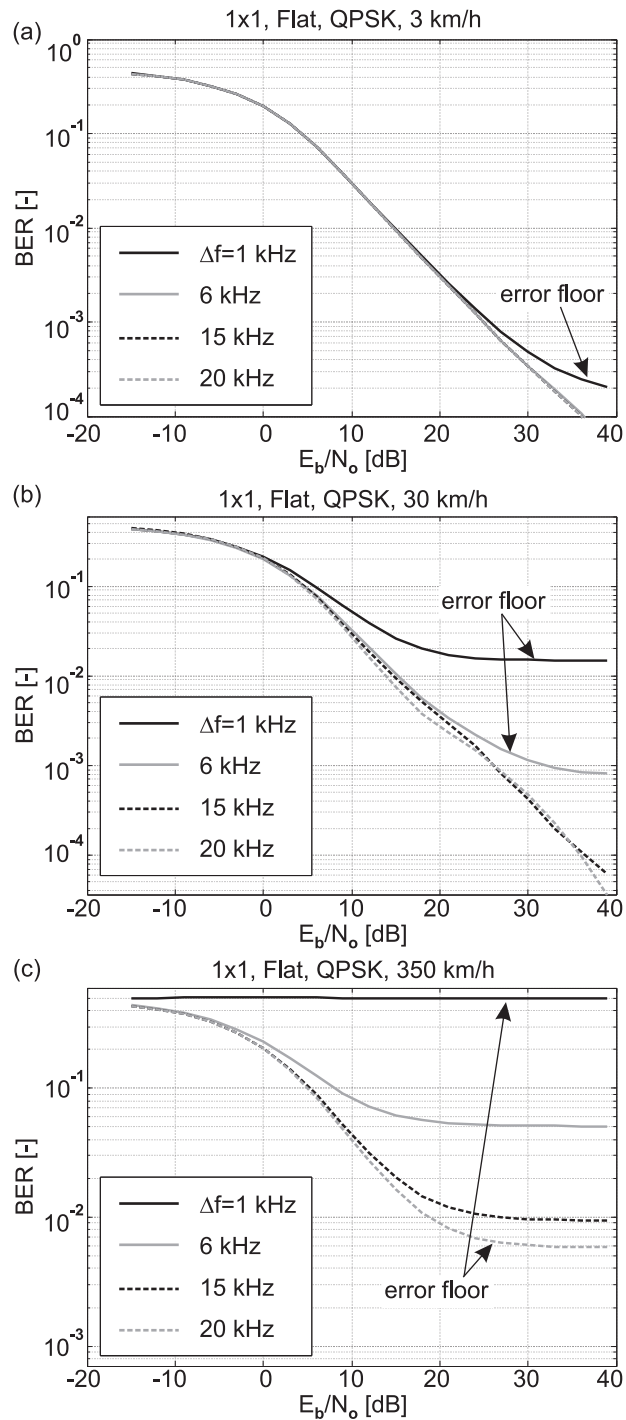
Figure A.3: BER Vs E_b/N_o for the QPSK modulation scheme and the 1x1 antenna configuration. Various combinations of OFDM sub-carrier spacing as well as UE speeds are considered in this analysis, based on the Rayleigh flat-fading channel profile.
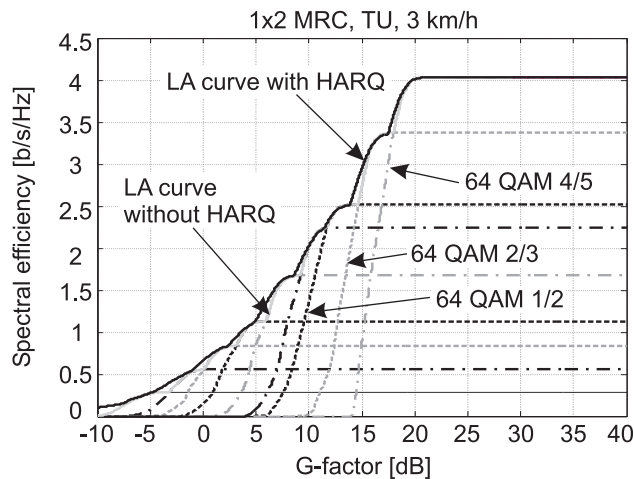
Figure A.4: Link adaptation curve based on wideband transmission in TU channel profile, and the 1x2 antenna scheme.

results in [103].

A.5   Link Adaptation Curves

The link-level performance in terms of BLER Vs SINR curves for the different MCS formats listed in Table A.3 has been used to generate the LA curve, shown in Figure A.4. It is obtained by converting the BLER into an equivalent throughput for each MCS format. Each point on the LA curve gives the maximum supported throughput for a given SINR [2, pp. 129]. In Figure A.4 instead of throughput we have shown spectral efficiency ($\eta_{spectral}$) as the function of long-term average SINR. Further, the influence of HARQ on spectral efficiency can be seen. Here, CC has been used for the code rates below 1/2, while IR is used for the high code rates. The LA curve is dependent on the underlying channel profile as well as on the PHY layer parameters such as the antenna scheme, receiver type, and speed.
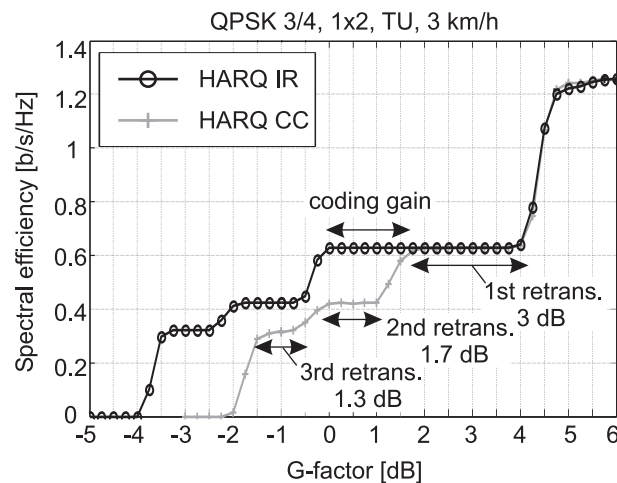
Figure A.5: Illustration of the HARQ retransmission gain based on CC and IR combining.
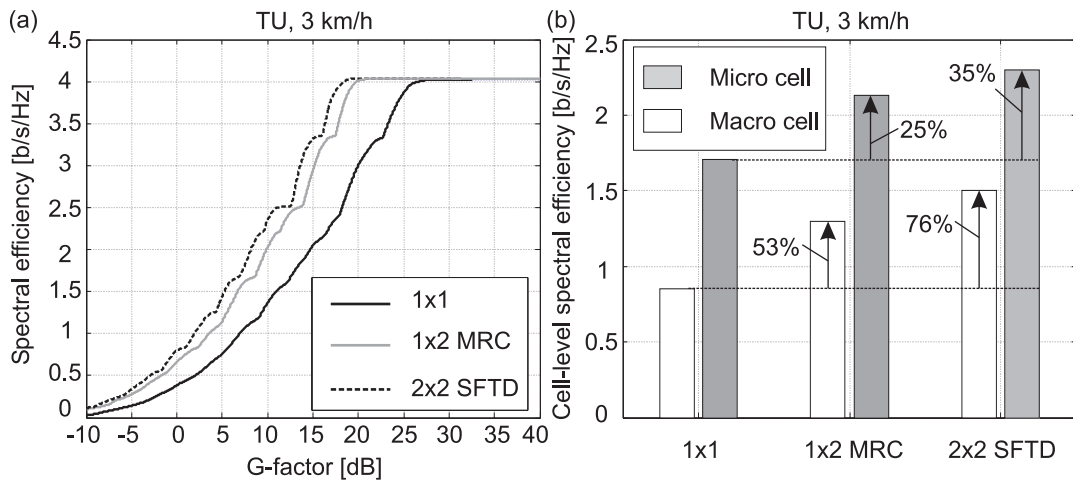
Figure A.6: (a) Comparison of link adaptation curves for different antenna cases. (b) Spectral efficiency as a function of the antenna scheme and cellular deployment scenario.

The difference between CC and IR HARQ schemes is illustrated in Figure A.5, based on the QPSK 3/4 format. In case of CC an identical copy of the signal is sent in each transmission attempt. Thus, the combining gain is equal to 3 dB, 4.7 dB and 6 dB at the first retransmission, second retransmission, and third retransmission respectively. These match well the width of the corresponding steps in the staircase shaped curve for CC in Figure A.5. In case of IR, in addition to the combining gain there is also an extra coding gain with each retransmission, due to the increase in the number of parity bits . The additional parity bits belong to the punctured positions within the original transmission. The effective code rate after one IR retransmission will be 3/8, which is quite close to the mother code rate of 1/3. As a result the coding gain in subsequent IR retransmission attempts is marginal.

Figure A.6 (a) illustrates the LA curves for the considered antenna schemes in the TU channel profile. It is seen that there is a significant improvement in spectral efficiency when an additional receive antenna is added, due to the array gain. However, the improvement due to transmit diversity over the 1x2 case is not significant. Figure A.6 (b) shows the spectral efficiency at cell-level as a function of the antenna scheme and the cellular deployment scenario. The cell-level spectral efficiency is calculated by convolving the LA curve of Figure A.6 (a) with the corresponding G-factor distribution, shown in Figure 2.15. It is seen that based on uncorrelated antennas and the Macro-cell scenario the 2x2 SFTD and the 1x2 MRC antenna schemes can provide a gain of 76% and 53% respectively over the 1x1 case. Similarly, in the Micro-cell scenario the gain in cell-level spectral efficiency over the 1x1 case is around 35% and 25% respectively. Note that these results do not include FDLA as well as of multi-user packet scheduling. The main findings of this study have been published in a conference article [62].

A.6   Acknowledgement

Appendix B

Verification of the EESM Link-To-System Performance Mapping Model

B.1   Introduction

This appendix covers verification of the Exponential Effective SINR Metric (EESM) link-to-system performance mapping model, which is recommended for an OFDM based system such as LTE [14]. The EESM model was introduced earlier in Section 2.8, and it provides a technique to map the link-level performance (in terms of effective SINR) into an equivalent throughput at the MAC layer [75].

The chapter is organized as follows: Section B.2 provides a recapitulation of the EESM model, while Section B.3 describes the modeling assumptions as well as the simulation methodology. The results and discussion are covered in Section B.4.

B.2   Recapitulation of the EESM Model

The EESM model is a counterpart of the Actual Value Interface (AVI) technique used in HSDPA [103]. It is useful in the system-level evaluation as it limits the computational load by reducing link-level processing. The computationally intensive link-level functionalities such as channel decoding, demodulation, etc., are not implemented at the system-level. Instead these are modeled using a link-to-system performance mapping scheme [103]. It is necessary that the model is able to capture the essential link-level characteristics, while it is desirable that it can be applied to different multiple access strategies as well as transceiver types [75].

As introduced earlier in Section 2.8 the EESM model has been recommended for use in an OFDM based system such as LTE [14], [75], where the decoder performance is not only dependent on the average SINR over the code block, but also on the inter-symbol SINR variability. The goal is to define a suitable effective SINR metric (scaler value) which can accurately characterize the decoder performance. In case of the EESM model the effective SINR is given by (2.22), and it

Table B.1: Default simulation parameters for the verification of the EESM model.

Parameter	*Setting*
System bandwidth, (BW)	5, 10 [MHz]
RB bandwidth	10 MHz
Number of users (UDO)	1
Power delay profile	TU, Ped. A, AWGN
Channel coding	3GPP Rel. 6 compliant Turbo coding with basic rate of 1/3
CQI parameters	Ideal
TD scheduling	RR
Selected LA scheme	frequency-blind transmission (Ref)
MCS settings	QPSK: 1/3, 2/3
	16QAM: 4/5
UE speed	3 km/h
UE receiver	1x1, 1x2 MRC
Channel estimation	Ideal
Carrier frequency	2 GHz
Link-to-system mapping	EESM

is similar to the geometric average SINR over the symbols within the code block, conditioned by the beta (β) factor. The beta factor is determined from extensive link-level simulations and it is adjusted for each MCS separately. However, according to theory the beta factor is independent of the system bandwidth and the channel profile. In the following analysis we will verify the suitability of the EESM model to estimate decoder performance under LTE assumptions.

B.3   Modeling Assumptions

The verification of the EESM model is based on the link-level processing chain illustrated earlier in Figure A.1. The simulation methodology has been taken from [76] and [107]. It involves generating several channel realizations for each PDP profile and adjusting the noise power to obtain an estimate of the BLER in the desired operating range, i.e., BLER of 10%-30%. The TU and Ped. A channel profiles have been employed to investigate whether the EESM beta factor needs to be changed under different PDPs. In terms of system bandwidth we have used two cases, 5 MHz and the 10 MHz according to PHY layer parameters given in Table 2.2. Further, the 1x1 and the 1x2 antenna schemes, based on the description in Section 2.11, have been employed in the analysis. The detailed list of simulation assumptions is provided in Table B.1.

B.4   Results and Discussion

Figure B.1 illustrates the BLER Vs EESM effective SINR performance curves for the QPSK 1/3 format, 10 MHz and the 1x2 antenna scheme. The channel realizations are based on the TU and the
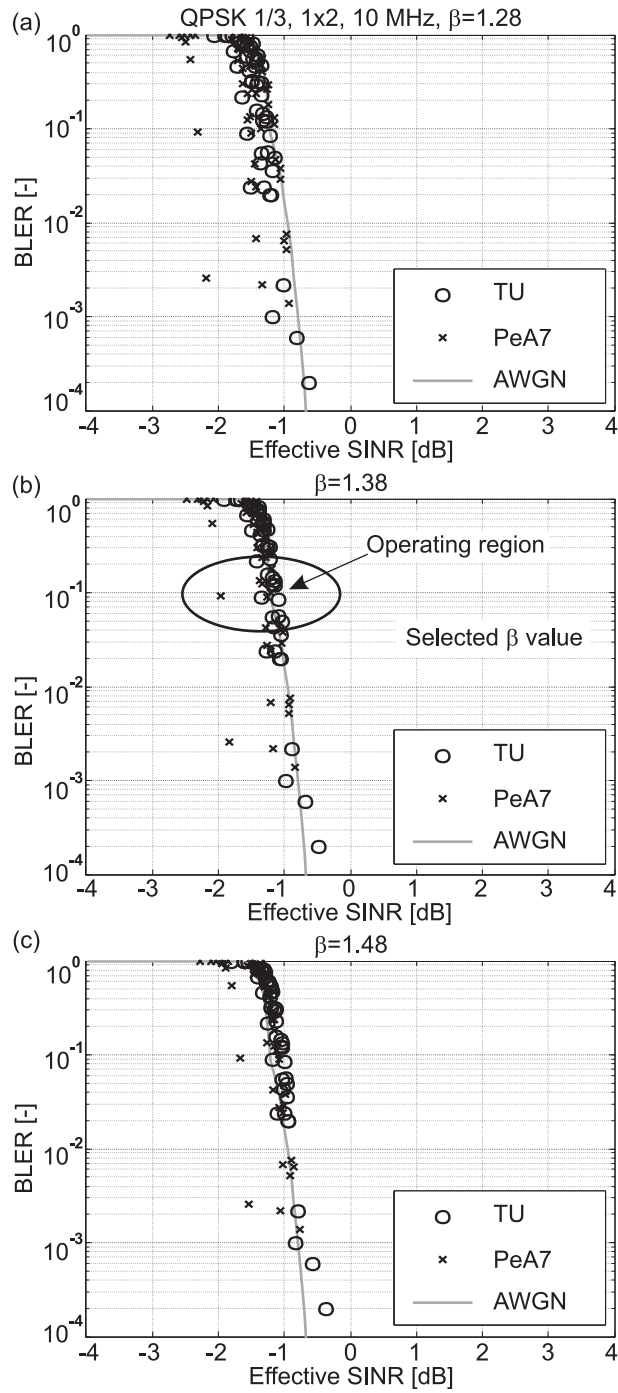
Figure B.1: BLER as a function of the EESM effective SINR for the QPSK 1/3 format, based on the 1x2 antenna scheme and 10 MHz. Three sets of curves are shown for different beta values including the beta value selected for system level simulations.
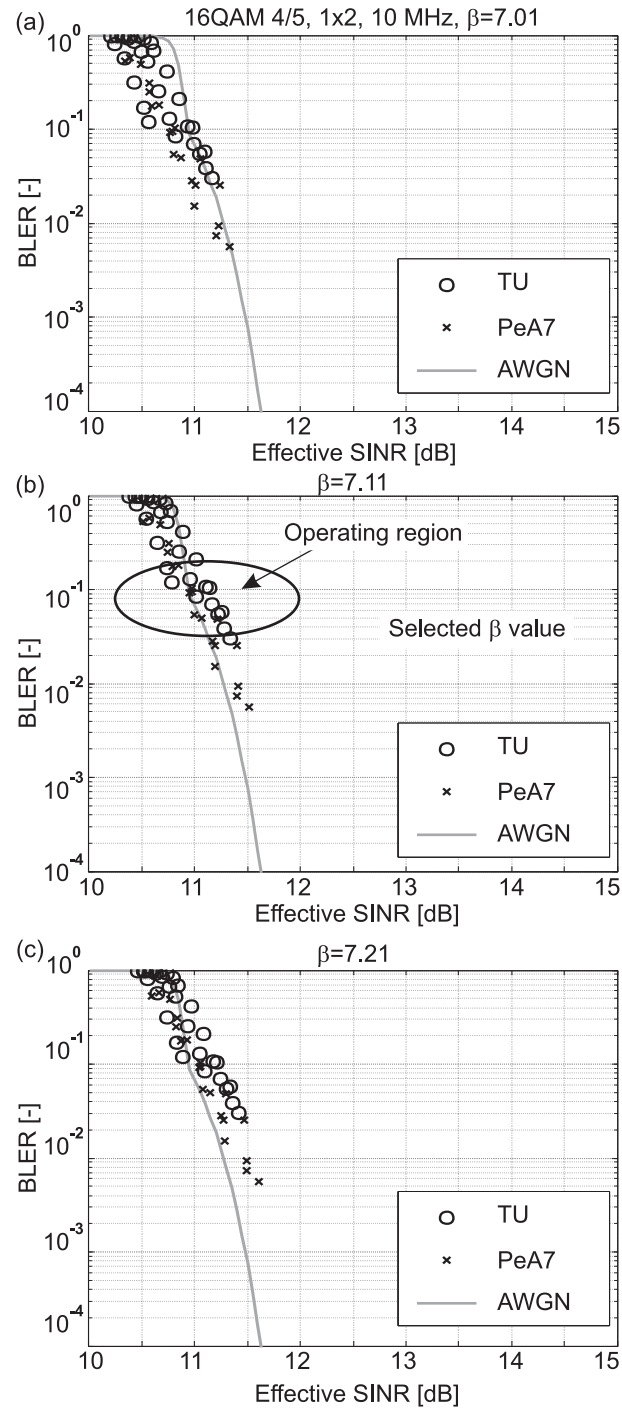
Figure B.2: BLER as a function of the EESM effective SINR for the 16QAM 4/5 format, based on the 1x2 antenna scheme and 10 MHz. Three sets of curves are shown for different beta values.
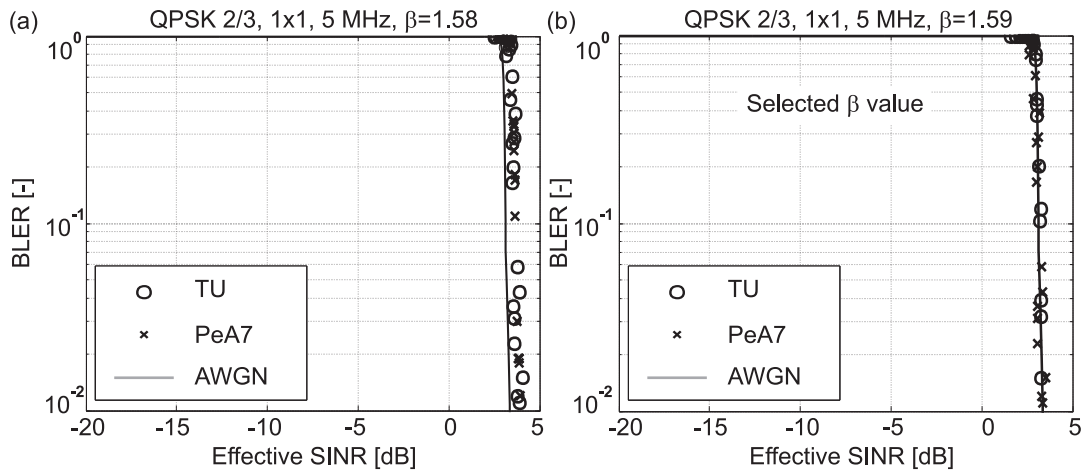
Figure B.3: Comparison between the BLER estimate obtained from detailed link-level simulations and the EESM model. The results are based on the QPSK 2/3 format, 1x1 antenna scheme and 5 MHz.

Ped. A channel profiles. Further, results for three beta values are shown in Figure B.1, including the beta factor used in system level simulations. Similarly, Figure B.2 illustrates the link-level performance based on the 16 QAM 4/5 format. As the BLER target for the first transmission is usually kept in the range of 10-30% [2], [59], we will concentrate on this region. We observe that for the selected β value most of the points obtained from the EESM model lie on the AWGN curve, irrespective of the channel profile. It implies that the EESM model is an effective link-to-system performance mapping scheme for LTE.

Figure B.3 shows the link-level performance using the QPSK 2/3 format, 1x1 scheme and 5 MHz bandwidth. It is seen that the EESM model can provide a reliable estimate of performance at the system-level, without the need for detailed link-level processing. Based on extensive link-level simulations the optimal settings for the β factor are listed in Table B.2, for the MCS formats used in this study.

Table B.2: Optimized setting of β factors for the different MCS formats used in the study.

MCS	β
QPSK 1/3	1.38
QPSK 1/2	1.45
QPSK 2/3	1.59
16QAM 1/2	4.83
16QAM 2/3	6.10
16QAM 4/5	7.11
64QAM 1/2	12.10
64QAM 2/3	21.00
64QAM 4/5	26.64

B.5   Acknowledgement

This study was undertaken in collaboration with fellow PhD student Na Wei.

Appendix C

Low Bandwidth CQI Schemes Enabling FDAS: Supplementary Results

C.1 Introduction

In this appendix we present supplementary results for Chapter 6, which covers the analysis of low bandwidth CQI schemes enabling FDAS. Additional FDLA results are provided for the Ped. A channel profile as well as the 1x1 antenna scheme. The supplementary results for FDPS are mainly for the 1x1 antenna scheme.

C.2 FDLA Performance Based on the OF-CQI Scheme and RR Scheduler

Figure C.1 illustrates the performance of the OF-CQI scheme in the TU channel profile. The results are based on the RR scheduler and the infinite buffer traffic model. The trends are similar to those observed for the PF scheduler in Figure 6.1. We see that $N_{off} = 3$ is sufficient to achieve most of the FDLA potential, irrespective of the antenna scheme.

C.3 Optimization of CQI Parameters Depending on the Channel Profile for FDLA

The dependence of the N_{off} parameter on the channel profile is investigated for the OF-CQI scheme in Figure C.2 (a) & (b), where the Ped. A channel profile has been used. It is seen that $N_{off} = 3$ is sufficient to achieve most of the FDLA gain potential for the OF-CQI scheme, similar to the TU case.

Figure C.2 (c) illustrates the performance of TH-CQI scheme in the Ped. A profile. It is clear that the optimization of threshold is specific to the channel profile. The FDLA performance with the BM-OF-CQI scheme in the Ped. A channel profile is shown in Figure C.2 (d). We can see that due to the nearly flat fading channel profile a large value of M is required to achieve the FDLA
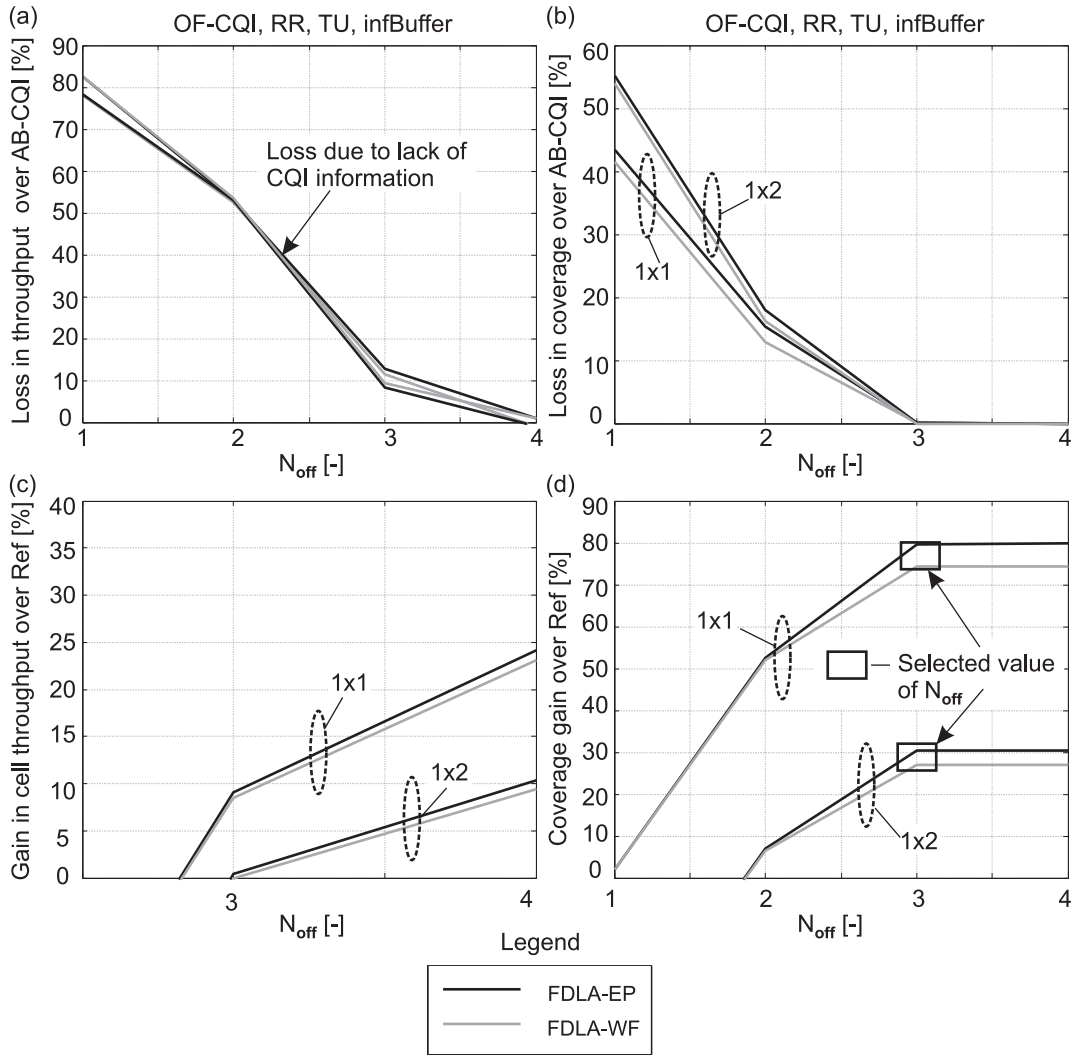
Figure C.1: FDLA performance based on the OF-CQI scheme, TD-RR scheduler and the infinite buffer traffic model. Results are presented for both FDLA schemes as well as for both 1x1 and 1x2 antenna schemes.

capacity similar to Ref. In such cases the Best M schemes are not suitable for implementation as they cannot provide a significant reduction in signaling overhead over the reference AB-CQI scheme.

C.4 Impact of Reduced CQI Reporting Rate on FDLA Performance

Figure C.3 illustrates the FDLA performance with reduced CQI reporting rate. The TH-CQI scheme and the infinite buffer model have been used here. The trends are similar to those observed for the OF-CQI scheme in Figure 6.8. Figure C.4 illustrates the FDLA potential with delayed CQI reporting, and the trends are similar to those observed in Figure 6.9.

Figure C.5 illustrates the FDLA potential as a function of the CQI rate, for selected values of UE speed. The trends are similar to those observed with the 1x2 antenna scheme, shown in Figure 6.10. The TH-CQI scheme is more robust to UE speed as it does not depend on detailed
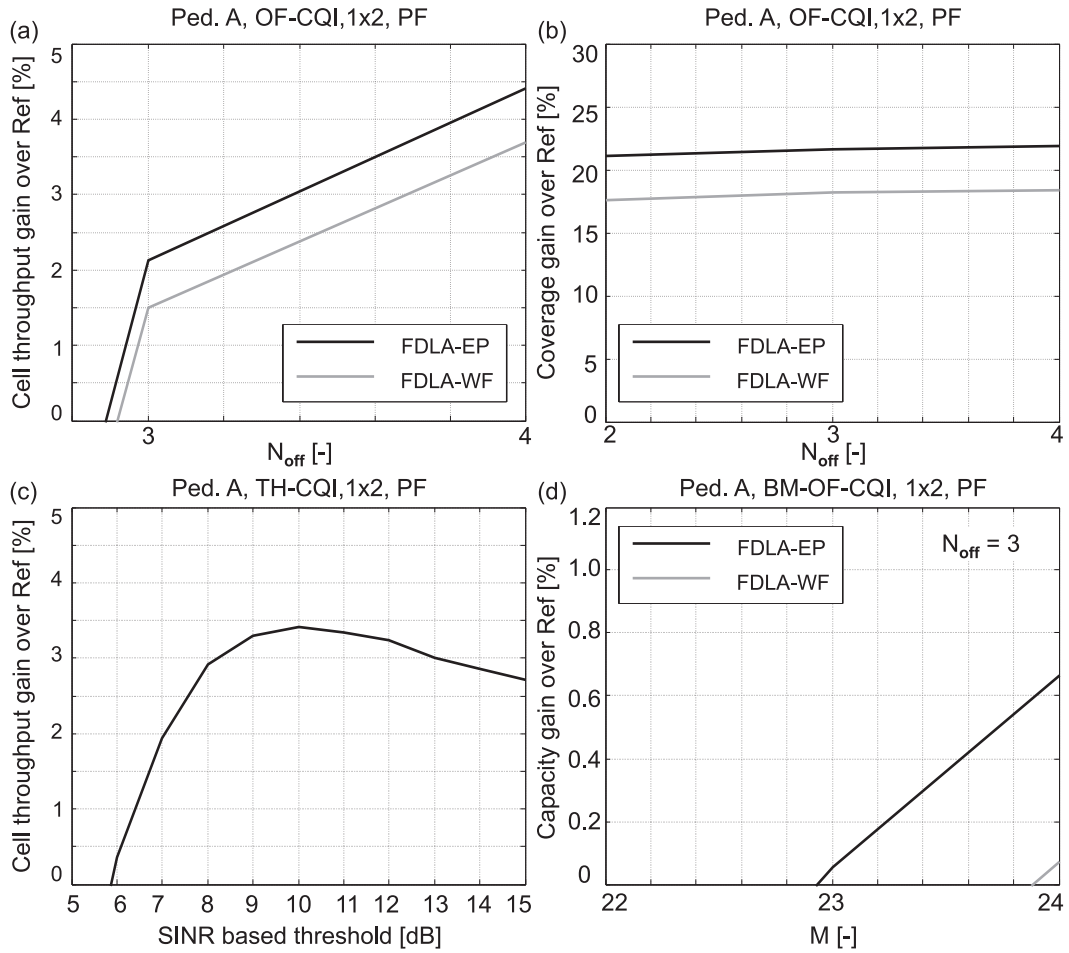
Figure C.2: Optimization of CQI parameters for FDLA based on the Ped. A channel profile and the infinite buffer traffic model.
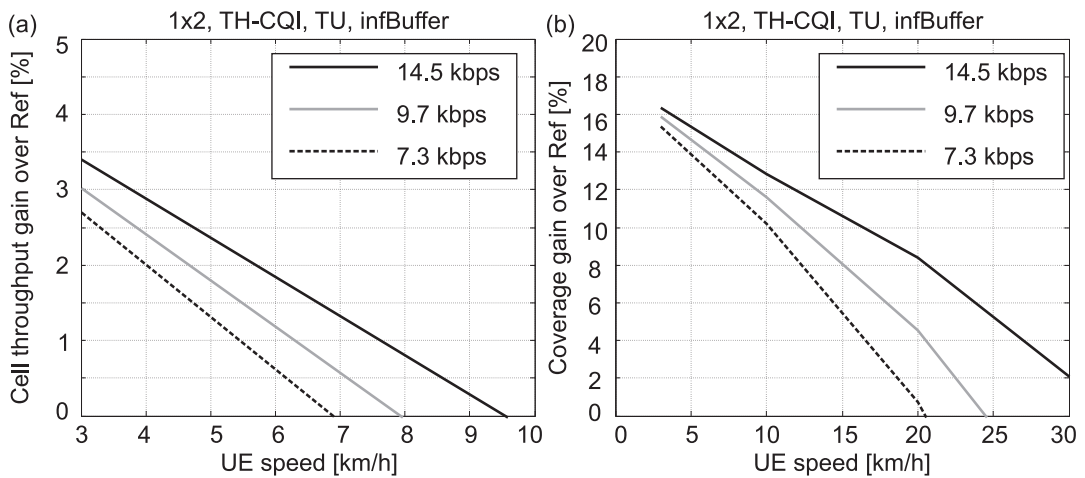
Figure C.3: FDLA-EP performance as a function of the UE speed and CQI reporting delay, for the TH-CQI scheme. Results are based on the infinite buffer traffic model.
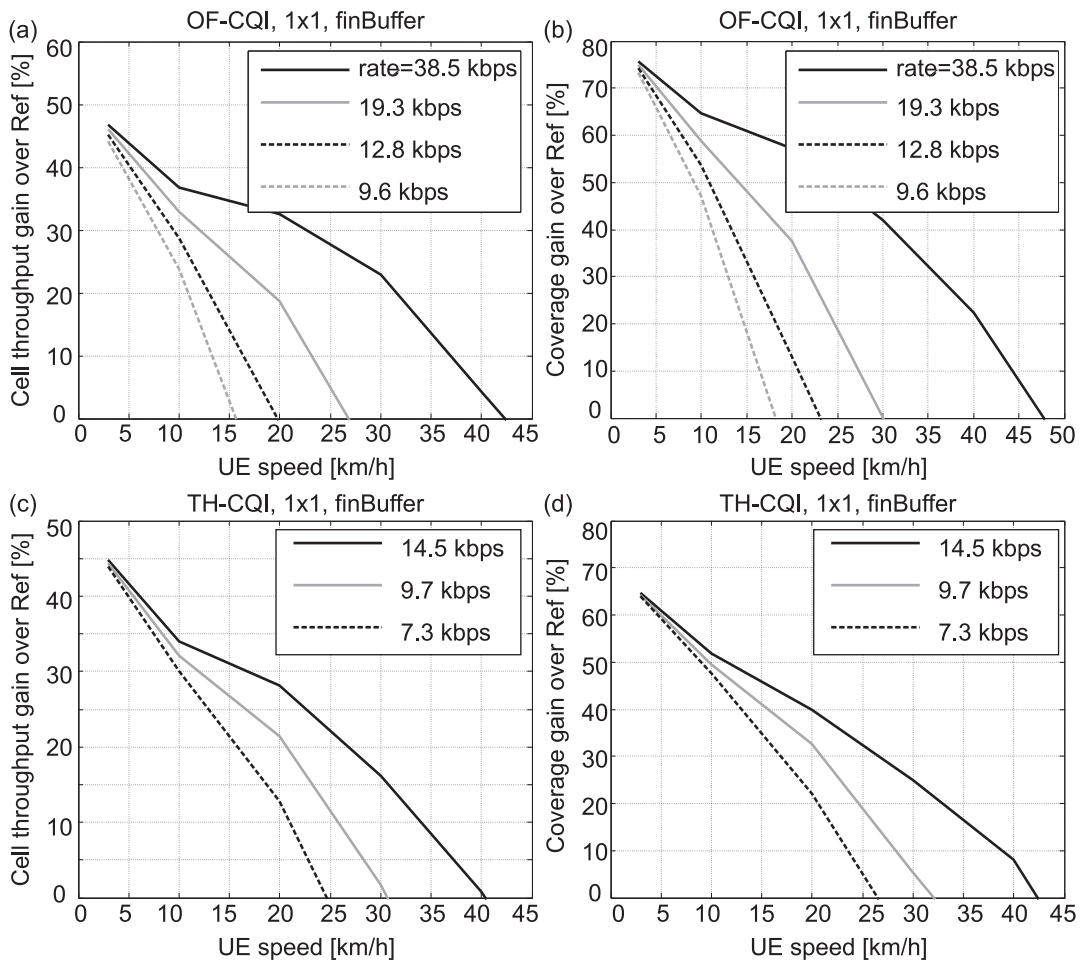
Figure C.4: FDLA-EP performance as a function of the UE speed and CQI reporting rate, for the finite buffer traffic model. Results are provided for the OF-CQI, TH-CQI schemes and are based on the 1x1 antenna scheme.

CQI reports. On the other hand the OF-CQI scheme is very sensitive to speed.

C.5   Impact of Reduced CQI Rate on FDPS Performance

Figure C.6 illustrates FDPS performance with reduced CQI reporting rate. Results are provided for optimized CQI schemes and the 1x1 antenna scheme. The CQI rates for the different schemes have been selected according to the criteria laid down in Section 6.17. The trends are similar to the 1x2 antenna case, as seen in Figure 6.19 and Figure 6.20. It is seen that FDPS can provide an attractive gain over Ref, even when the CQI rate for FDPS is similar to the Ref scheme.

Figure C.7 illustrates the trade-off between CQI rate and FDPS potential, for the optimized CQI schemes and the 1x1 antenna configuration. The trends are similar to those observed in Figure 6.21. The main finding is that among the considered techniques the TH-CQI scheme is the most robust to UE speed. If the CQI rate is kept at around 10 kbps, the TH-CQI scheme provides the best FDPS performance beyond the speed of 10 km/h.
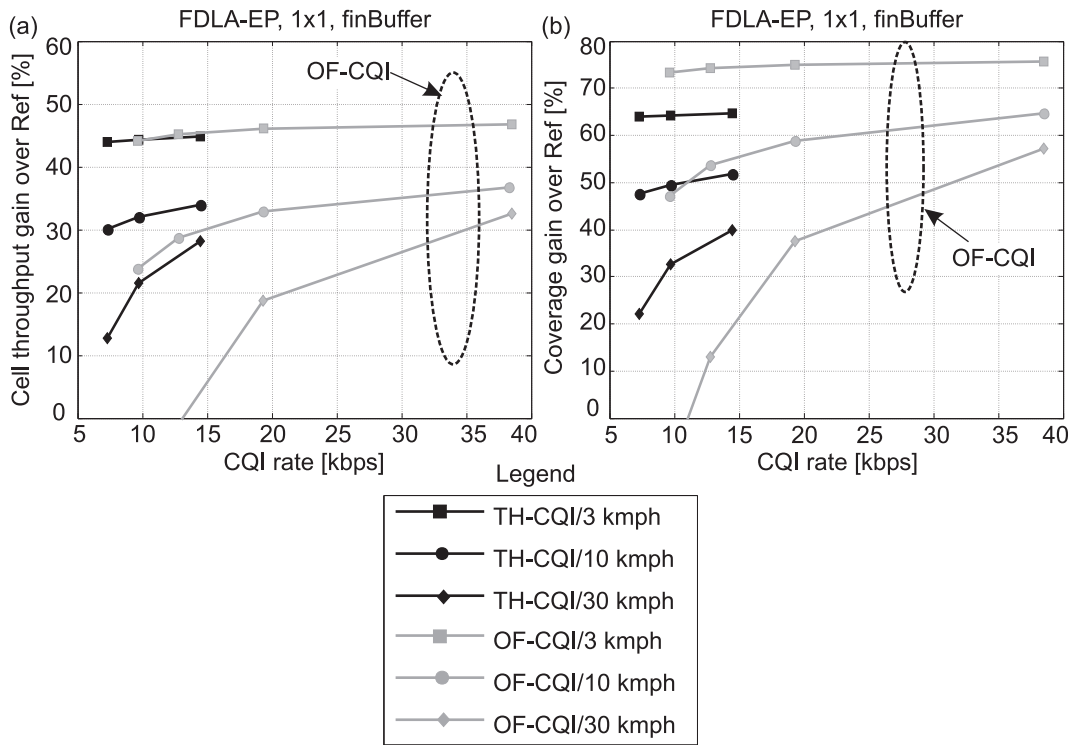
Figure C.5: Trade-off between FDLA potential in the DL and CQI overhead in the UL, based on the finite buffer traffic model and the 1x1 antenna scheme.

C.6 Impact of Time-Domain Averaging on FDPS Performance

Figure C.8 illustrates the FDPS gain potential as a function of the averaging window (W_{cqi}). The results are based on the 1x1 antenna scheme. We observe similar trends as in the 1x2 antenna case, shown in Figure 6.22. As mentioned earlier the advantage of averaging in time is that the effective number of pilots per RB can be increased, thus providing potential to improve the accuracy of CQI estimation. This is also verified in Figure 3.18 where it is seen that the equivalent std. error on RB SINR estimate is reduced with the increase in W_{cqi}.
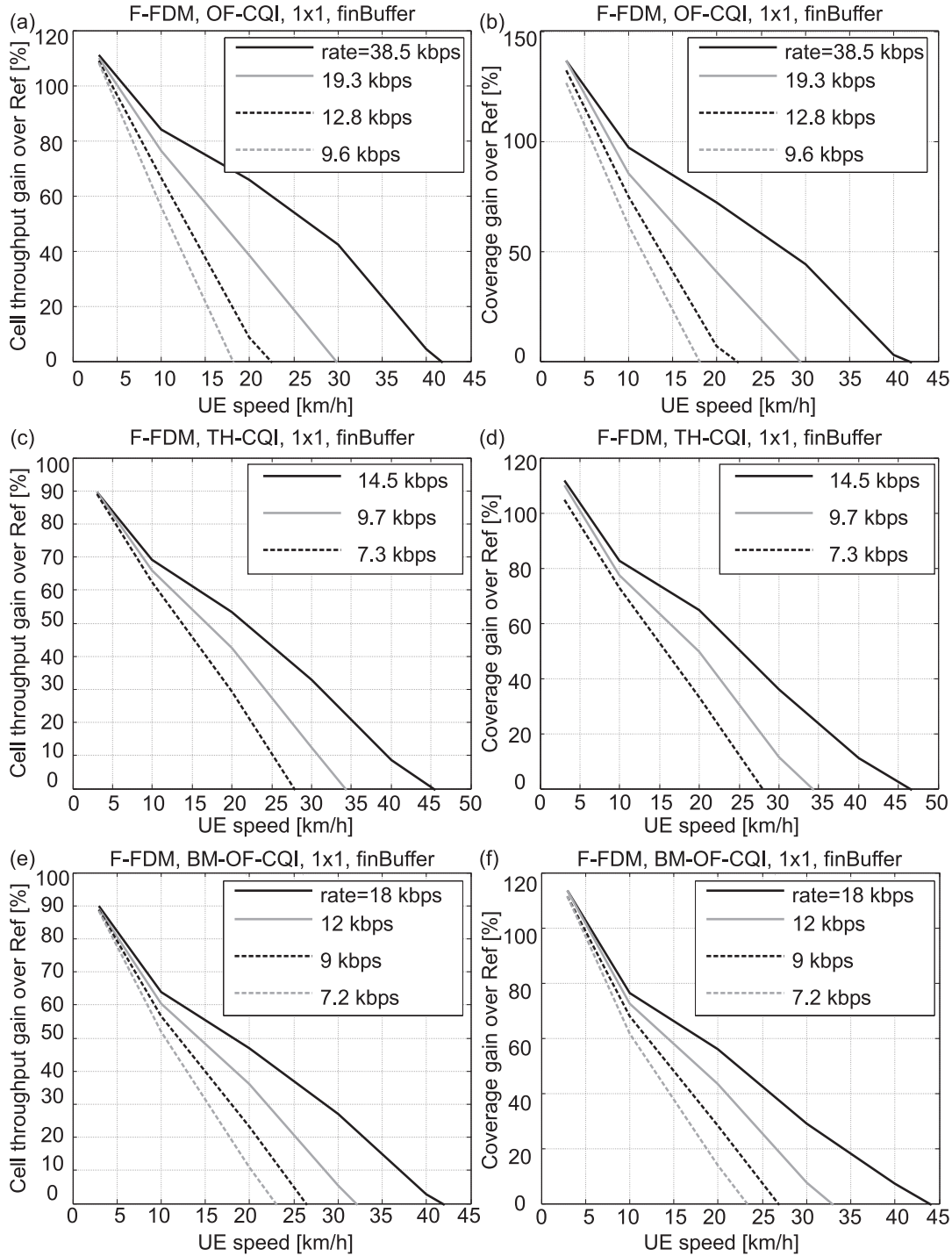
Figure C.6: FDPS performance as a function of the UE speed, for different CQI rates and the 1x1 antenna scheme.
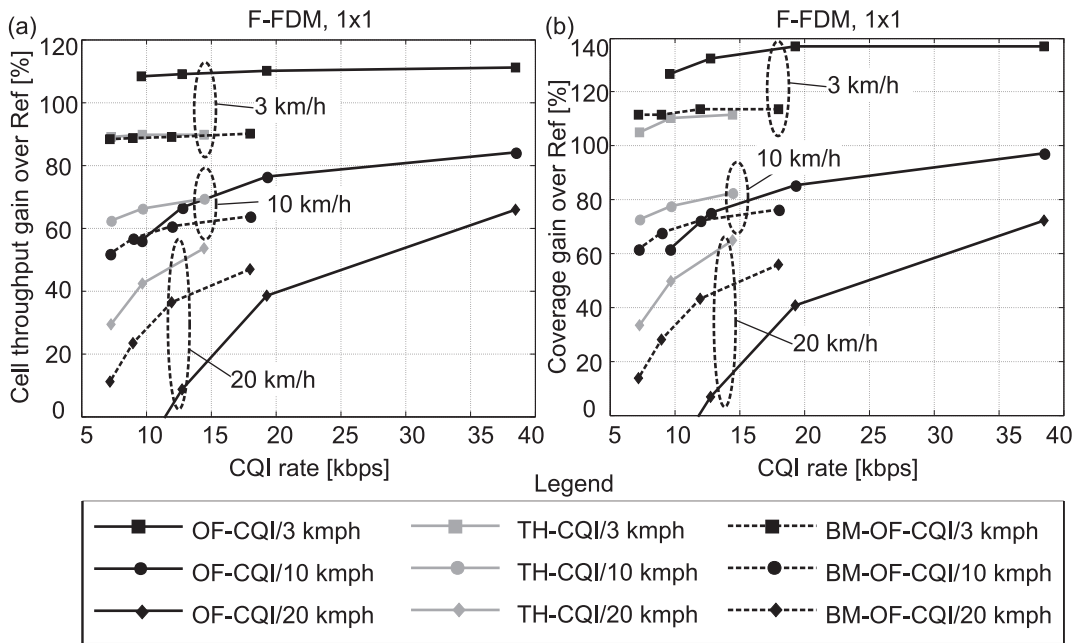
Figure C.7: Trade-off between CQI rate and FDPS potential for optimized OF-CQI, TH-CQI and BM-OF-CQI schemes. Results are based on the 1x1 antenna scheme.
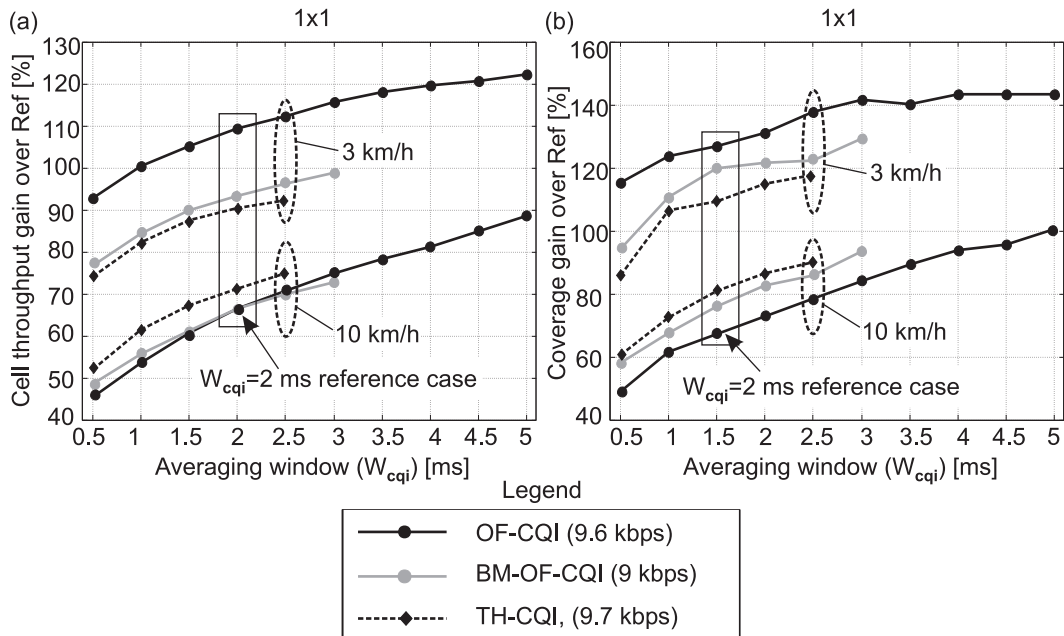

Figure C.8: FDPS performance as a function of time domain averaging together with reduced CQI reporting rate. Results are based on the 1x1 antenna scheme, TU channel profile, finite buffer model, and the Macro case 1 deployment scenario.

Appendix D

Statistical Significance Assessment

D.1 Introduction

The statistical significance assessment of the key performance indicators obtained for a set of reference simulation scenarios is performed here. The chapter is organized as follows: The modeling assumptions are outlined in Section D.2, including the list of selected simulation scenarios. The results and discussion are presented in Section D.3.

D.2 Modeling Assumptions

The statistical significance analysis is based on conducting a large number of simulations (around fifty) with identical parameter setup, but with a different seed of the random number generator. The variation in KPIs is investigated by means of the well known *box and whiskers diagram* [108], [109]. The following KPIs have been considered, which have been defined previously in Section 2.15.

- Average cell throughput

- Average user throughput

- Coverage

D.2.1 Selected Cases for Assessment

The following cases have been selected for evaluation:

1. Verification of the FDLA-EP, FDLA-WF and Ref performance presented in Section 4.9, and based on the infinite buffer traffic model.

2. Verification of the FDLA-EP, FDLA-WF and Ref performance presented in Section 4.9, and based on the finite buffer traffic model.
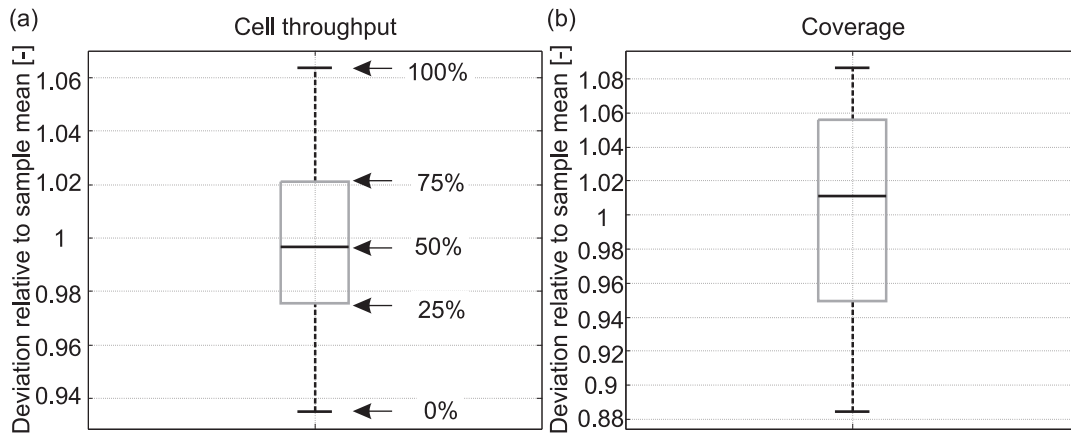
Figure D.1: Box plots of the KPIs obtained for the Ref scheme and the infinite buffer model, in Section 4.9.
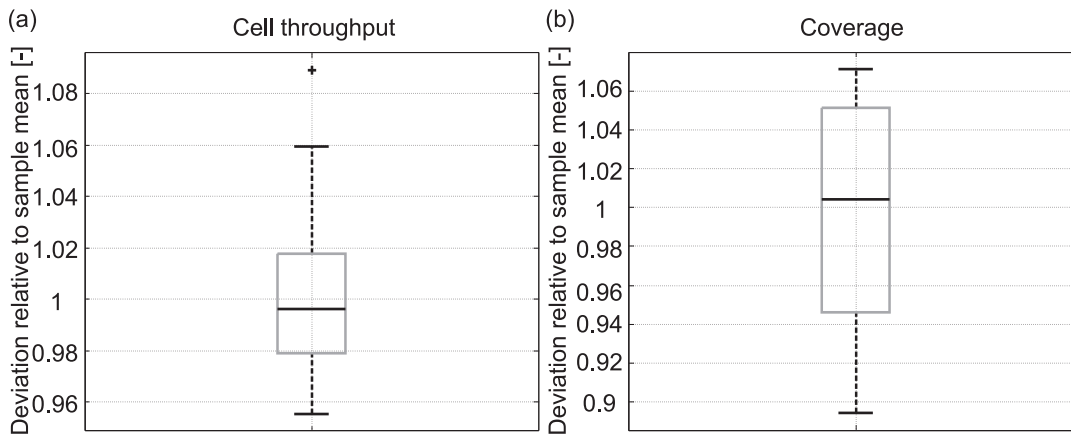

Figure D.2: Box plots of the KPIs obtained for the FDLA-EP scheme with the infinite buffer traffic model, in Section 4.9.

3. Verification of the F-FDM, A-FDM and Ref performance presented in Section 5.9, and based on the finite buffer traffic model.

4. Verification of the Ref and FDPS performance obtained with the system simulator and the infinite buffer model, shown in Section 8.13.

5. Verification of the Ref and FDPS performance obtained with the system simulator and the finite buffer model, shown in Section 8.13.

D.3   Results and Discussion

Figure D.1 illustrates the box and whiskers diagrams for the average cell throughput and coverage obtained for the Ref scheme. The simulation scenario was described earlier in Section 4.9. The KPIs are normalized to the sample mean, i.e., the mean value obtained from all the simulations. In the box and whiskers diagrams the box is drawn from the lower hinge defined as the 25% percentile, to the upper hinge corresponding to the 75% percentile. The median value is shown as a line across the box. The length of the box gives the inter-quartile range, while the whisker
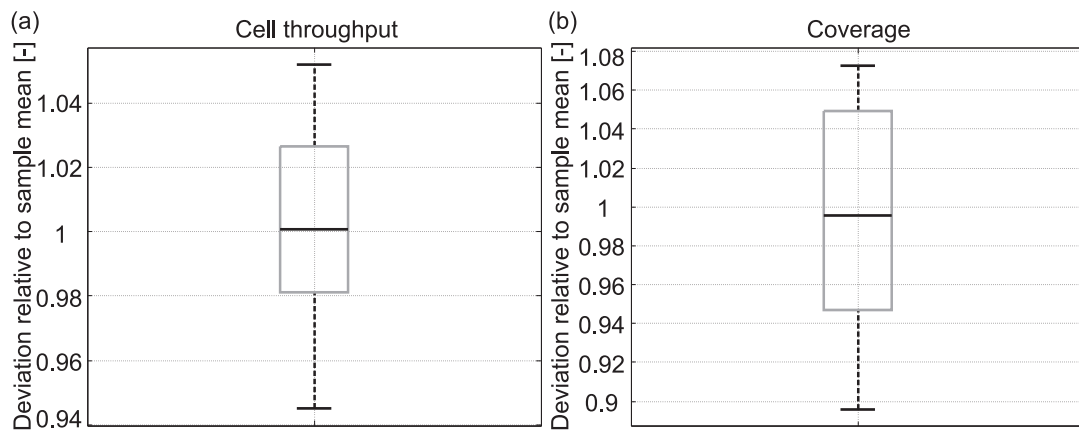
Figure D.3: Box plots of the KPIs obtained for the FDLA-WF scheme and the infinite buffer model, in Section 4.9.
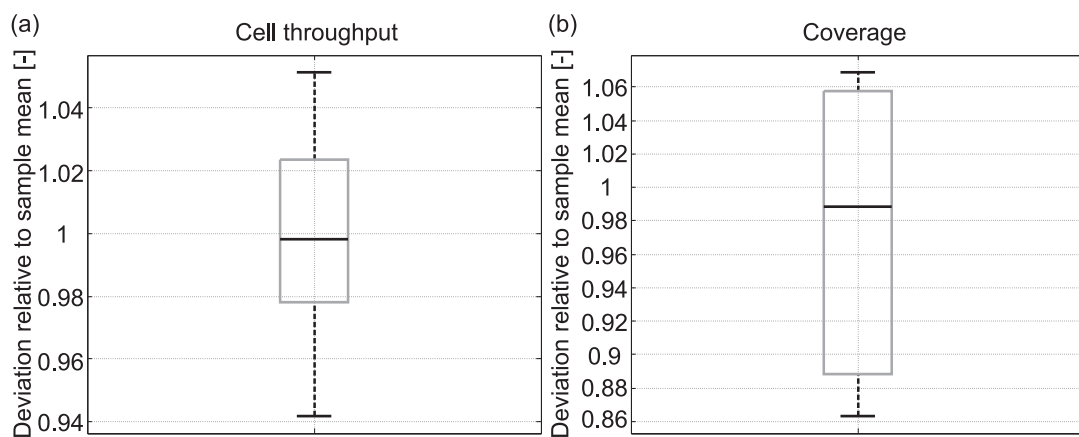

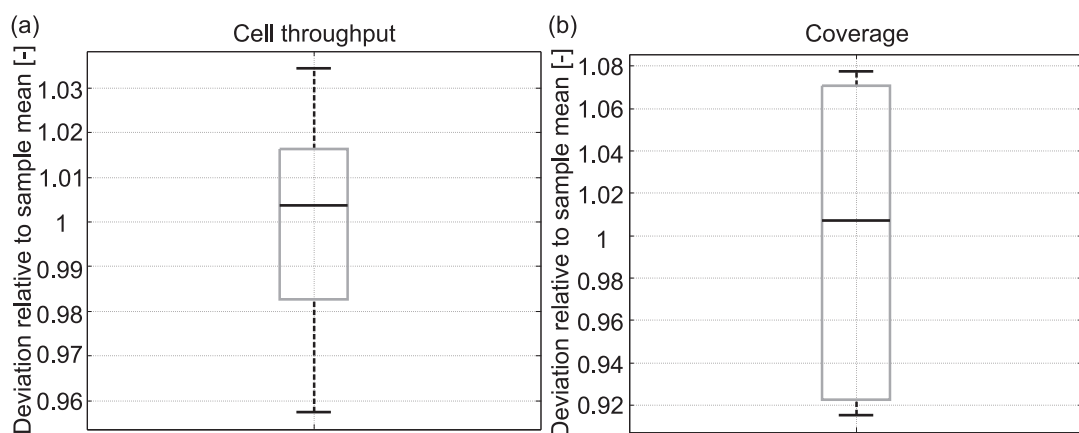**Figure D.4:** Box plots of the KPIs obtained for the Ref scheme and the finite buffer model, in Section 4.9.

Figure D.5: Box plots of the KPIs obtained for the FDLA-EP scheme and the finite buffer traffic model, in Section 4.9.
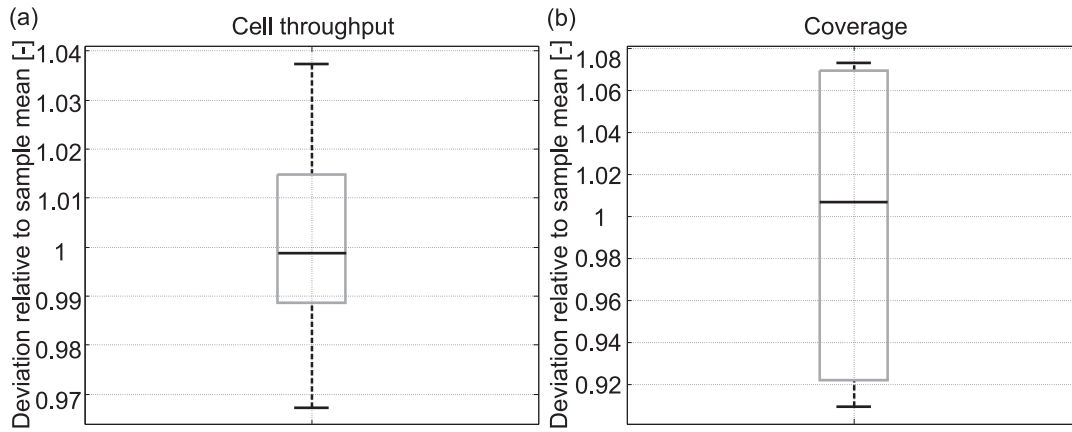
Figure D.6: Box plots of the KPIs obtained for the FDLA-WF scheme and the finite buffer model, in Section 4.9.
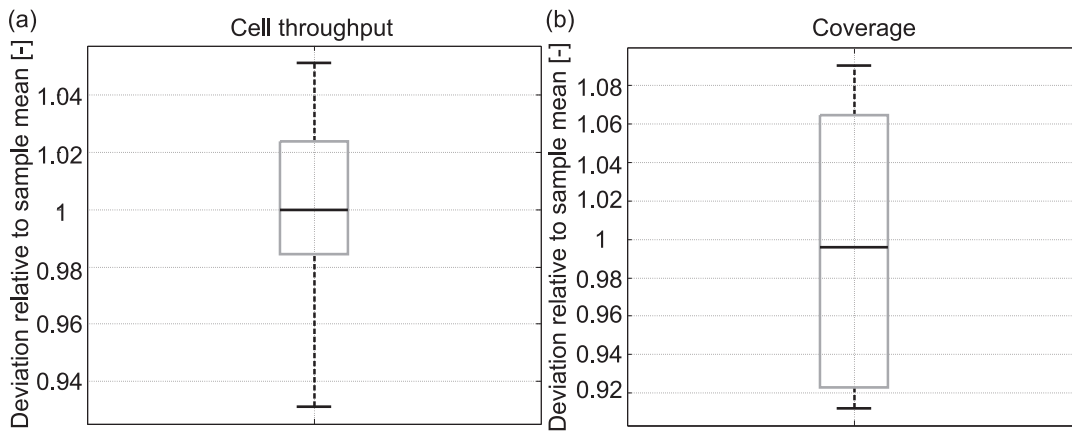

Figure D.7: Box plots of the KPIs obtained for the Ref scheme and the finite buffer model, in Section 5.9.
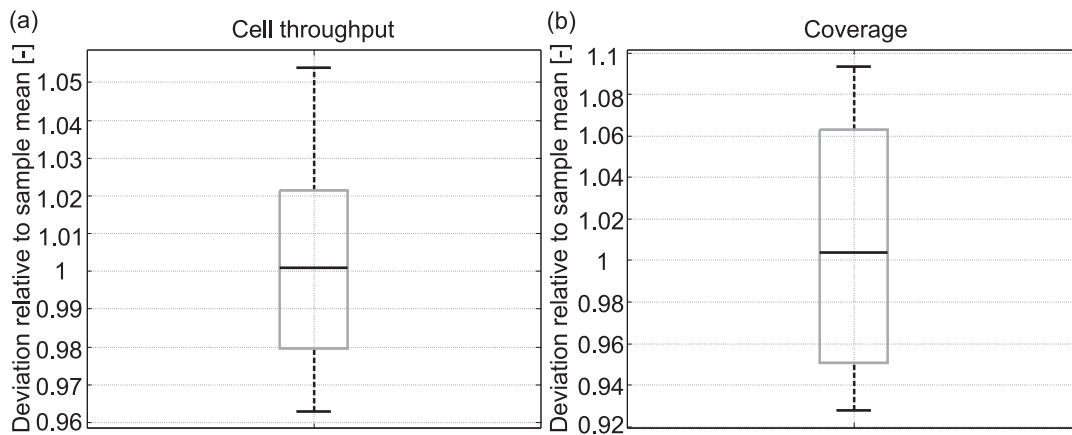

Figure D.8: Box plots of the KPIs obtained for the F-FDM scheme and the finite buffer model, in Section 5.9.
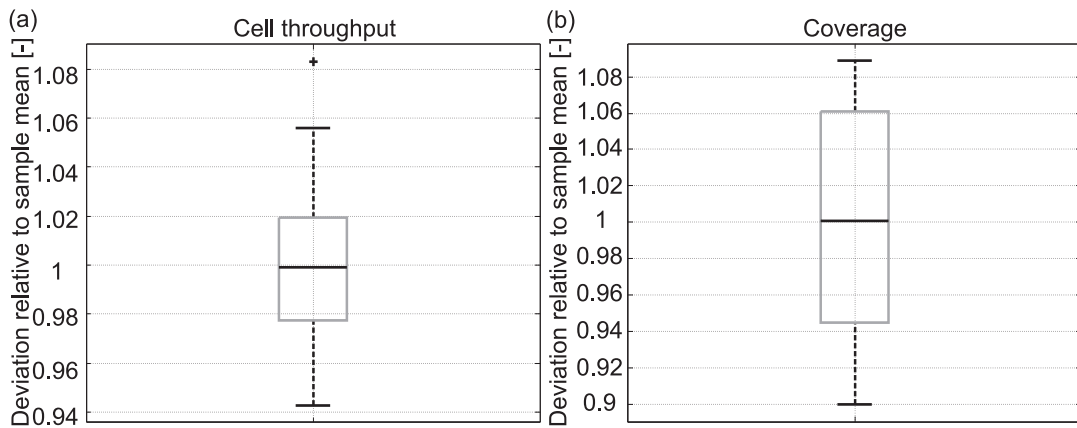
Figure D.9: Box plots obtained for the A-FDM scheme and the finite buffer model, in Section 5.9.
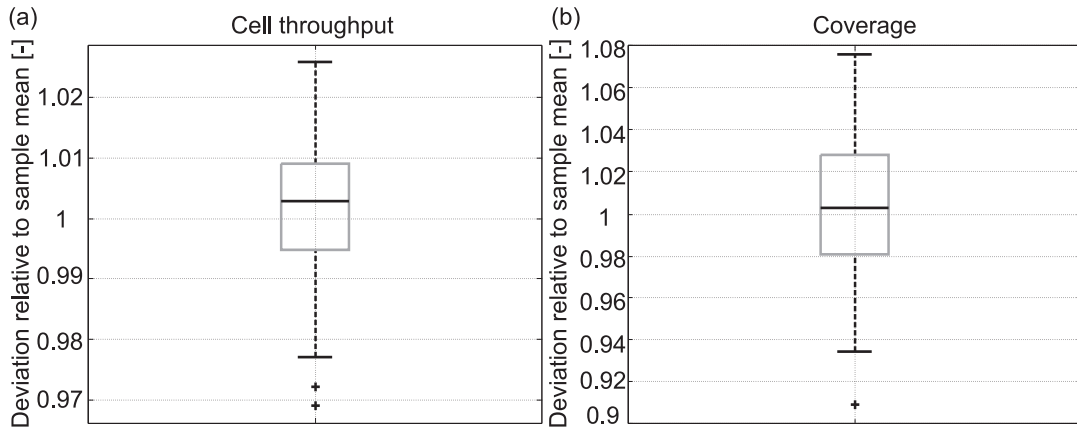

Figure D.10: Box plots obtained for the Ref scheme and the infinite buffer model, obtained with the system simulator.

on each side of the box is extended to the most extreme data values within 1.5 times of the inter-quartile range. Data values lying beyond the ends of the whiskers are marked as outliers [108]. Similar results are presented in Figure D.2 onwards and up to Figure D.9, covering the first three cases listed in Subsection D.2.1.

We see that the deviation in the average cell throughput from its corresponding sample mean is within ±6%, for most cases. Further, in general the distribution of cell throughput is symmetric about the median value. Additionally, the mean and median values are nearly equal in all cases, which implies that the underlying distribution is Gaussian in nature [110].

In terms of coverage performance, the box plots show that the deviation from the sample mean is around ±10%. The distribution of samples is asymmetric about the mean value in several cases, e.g., the samples are concentrated within the 25%-75% region of the CDF. Further, the median and mean values are nearly equal in most cases. The asymmetric nature of the distribution of coverage samples as well as the large deviation in values is due to the lack of uncorrelated link-level statistics. This is a known drawback of the decoupled link and network simulation methodology.

Figure D.10 through to Figure D.13 show the statistical significance assessment of KPIs, obtained from the system simulator based evaluation of FDAS. It is seen that in most cases the deviation in cell throughput and average user throughput from the sample mean is within ±3%,
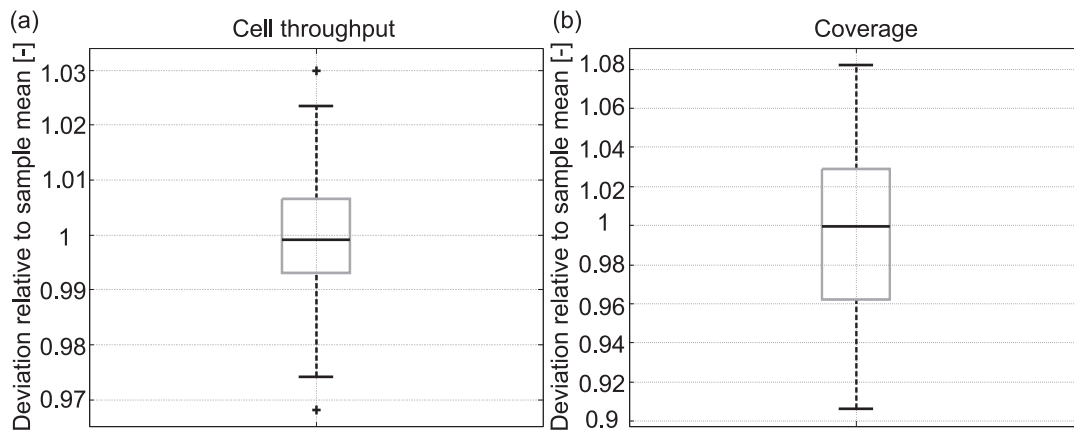
Figure D.11: Box plots obtained for the FDPS scheme and the infinite buffer, obtained with the system simulator.
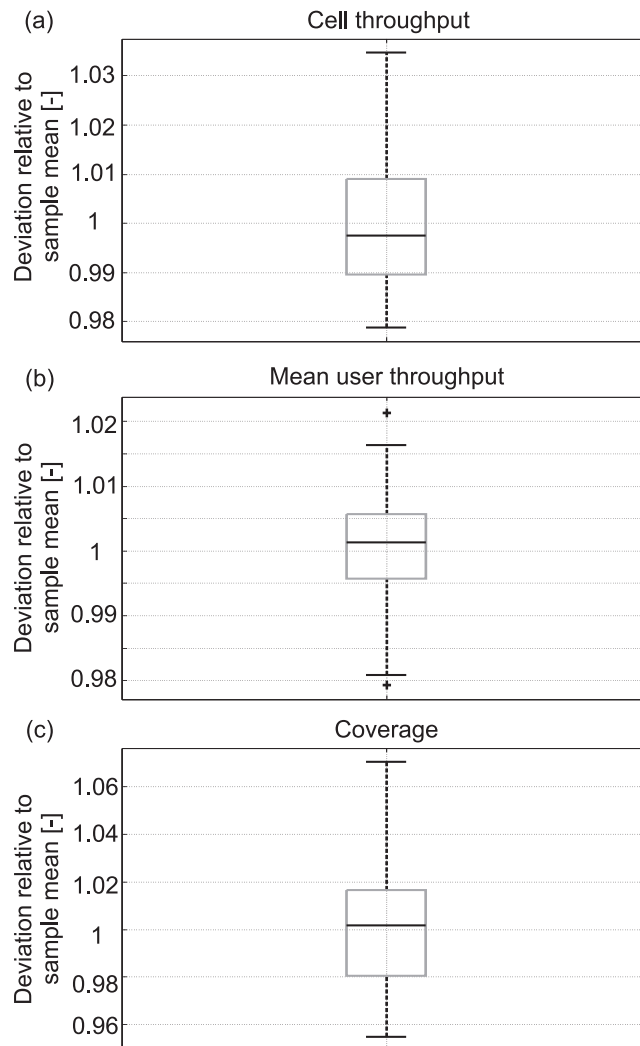
Figure D.12: Box plots obtained for the Ref scheme and the finite buffer, obtained with the system simulator.

Figure D.13: Box plots obtained for the FDPS scheme and the finite buffer, obtained with the system simulator.

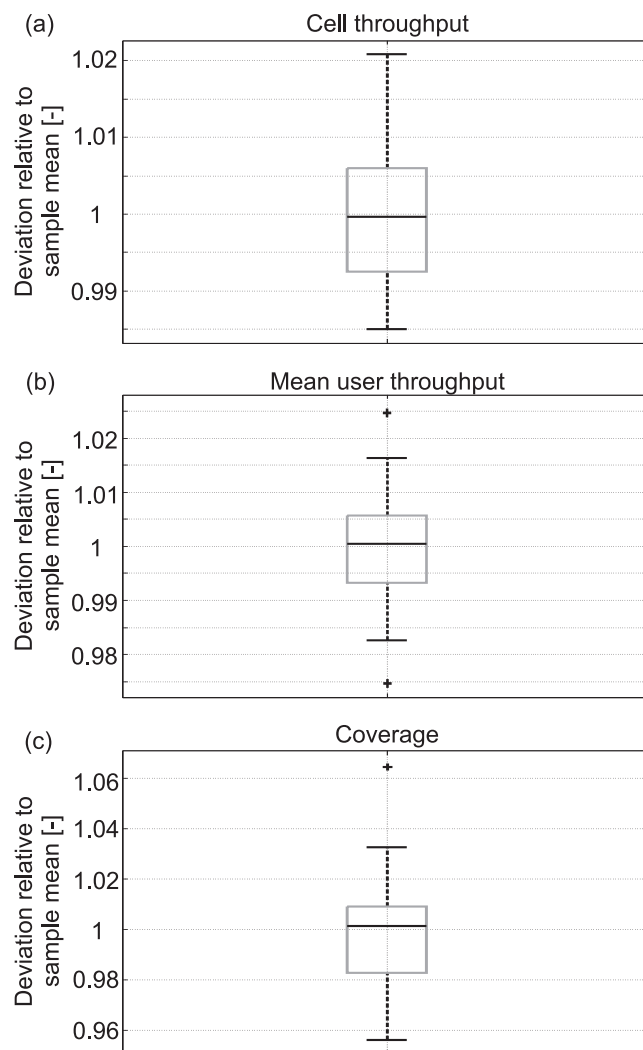which is sufficiently accurate. In terms of coverage, the deviation from the mean value is around $\pm 10\%$ for the infinite buffer cases, while it is around $\pm 6\%$ for the finite buffer cases. Further, the distribution of coverage samples is symmetric about the median value.

Bibliography

[1] H. Holma and A. Toskala, Eds., *WCDMA for UMTS – Radio Access for Third Generation Mobile Communications*, 2nd ed. John Wiley & Sons, 2002.

[2] ——, *HSDPA/HSUPA for UMTS – High Speed Radio Access for Mobile Communications*. John Wiley & Sons Ltd, 2006.

[3] F. Adachi, "Evolution Towards Broadband Wireless Systems," in *Proceedings of the International Symposium on Wireless Personal Multimedia Communications (WPMC)*, vol. 1, Honolulu, Hawaii, October 2002, pp. 19–26.

[4] H. Yang, "A Road to Future Broadband Wireless Access: MIMO-OFDM-Based Air Interface," *IEEE Communiations Magazine*, vol. 43, no. 1, pp. 53–60, January 2005.

[5] B. Classon, K. Baum, V. Nangia, R. Love, Y. Sun, R. Nory, K. Stewart, A. Ghosh, R. Ratasuk, W. Xiao, and J. Tan, "Overview of UMTS Air-Interface Evolution," in *Proceedings of the the IEEE Vehicular Technology Conference (VTC)*, Montreal, Canada, October 2006.

[6] J. Pons, J. Dunlop, and J. Kelliher, "On the application of link adaptation concepts to GSM," in *Proceedings of the IEEE Vehicular Technology Conference (VTC)*, vol. 2, Ottawa, Canada, May 1998, pp. 1219–1223.

[7] Z. Honkasalo, L. Wang, M. Silventoinen, and M. Kajala, "A cell range extension technique for GSM/DCS1800 - using half-rate codec over full-rate channel," in *Proceedings of the International Conference on Universal Personal Communications (ICUPC)*, Florence, Italy, November 1995, pp. 893–898.

[8] W. F. Fuhrmann and V. Brass, "Performance aspects of the GSM radio subsystem," *Proceedings of the IEEE*, vol. 82, no. 9, pp. 1449–1466, September 1994.

[9] M. Rahnema, "Overview of the GSM system and protocol architecture," *IEEE Communications Magazine*, vol. 31, no. 4, pp. 92–100, April 1993.

[10] H. Wang, V. Haikola, and J. Lilleberg, "High Speed Packet Access with Parallel Interference Cancellation and High-order Modulation for Coded FDD CDMA Communications," in *Proceedings of the IEEE Global Telecommunications Conference (GLOBECOM)*, vol. 5, San Antonio, Texas, USA, November 2001, pp. 3140–3144.

[11] 3GPP, "3rd Generation Partnership Project (3GPP) - www.3gpp.org."

[12] H. Holma and A. Toskala, Eds., *WCDMA for UMTS – Radio Access for Third Generation Mobile Communications*, 3rd ed. John Wiley & Sons Inc, 2004.

[13] 3GPP TSG-RAN, RP040461, *Proposed Study Item on Evolved UTRA and UTRAN*, December 2004.

[14] 3GPP Technical Report 25.814, version 7.1.0, *Physical Layer Aspects for Evolved UTRA*, September 2006.

[15] *Mobile WiMAX - Part I: A Technical Overview and Performance Evaluation*, WiMAX Forum, www.wimaxforum.org/home, August 2006.

[16] K. B. Letaief and Y. J. Zhang, "Dynamic Multiuser Resource Allocation and Adaptation for Wireless Systems," *IEEE Wireless Communications*, vol. 13, no. 4, pp. 38–47, August 2006.

[17] E. Dahlman, H. Ekstrom, A. Furuskar, Y. Jading, J. Karlsson, M. Lundevall, and S. Parkvall, "The 3G Long-Term Evolution - Radio Interface Concepts and Performance Evaluation," in *Proceedings of the IEEE Vehicular Technology Conference (VTC)*, vol. 1, Melbourne, Australia, May 2006, pp. 137–141.

[18] 3GPP Technical Report 25.913, version 7.3.0, *Requirements for Evolved UTRA (E-UTRA) and Evolved UTRAN (E-UTRAN)*, March 2006.

[19] T. S. Rappaport, *Wireless Communications — Principles and Practice, second edition*. ISBN 0-13-042232-0: Prentice Hall, 2002.

[20] J. G. Proakis, "Adaptive equalization for TDMA digital mobile radio," *IEEE Transactions on Vehicular Technology*, vol. 40, no. 2, pp. 333–341, May 1991.

[21] B. R. Saltzberg, "Performance of an efficient parallel data transmission system," *IEEE Transactions on Communications Technology*, vol. 15, no. 6, pp. 805–811, December 1967.

[22] B. Hirosaki, "An Orthogonally Multiplexed QAM System Using the Discrete Fourier Transform," *IEEE Transactions on Communications*, vol. 29, no. 7, pp. 982–989, July 1981.

[23] J. A. C. Bingham, "Multicarrier Modulation For Data Transmission: An Idea Whose Time Has Come," *IEEE Communications Magazine*, vol. 28, pp. 5–14, May 1990.

[24] P. O. Vidal, "Analysis of OFDM for UTRAN enhancement," Masters Thesis in Mobile Communications, Aalborg University, Denmark, June 2003.

[25] D. Galda and H. Rohling, "A Low Complexity Transmitter Structure for OFDM-FDMA Uplink Systems," in *Proceedings of the IEEE Vehicular Technology Conference (VTC)*, vol. 4, Bermingham, Alabama, USA, May 2002, pp. 1737–1741.

[26] H. Rohling and Grunheid, "Performance Comparison of Different Multiple Access Schemes for the Downlink of an OFDM Communicaiton System," in *Proceedings of the IEEE Vehicular Technology Conference (VTC)*, vol. 3, Phoenix, Arizona, USA, May 1997, pp. 1365–1369.

[27] G. L. Stuber, J. R. Barry, S. W. Mclaughlin, Y. Li, M. A. Ingram, and T. G. Pratt, "Broadband MIMO-OFDM Wireless Communications," *Proceedings of the IEEE*, vol. 92, no. 2, pp. 271–294, February 2004.

[28] W. C. Jakes, Ed., *Microwave Mobile Communications*. ISBN 0-7803-1069-1: IEEE Press, New Jersey, 1994.

[29] P. Ameigeiras, "Packet Scheduling and Quality of Service in HSDPA," Ph.D. dissertation, Aalborg University – Department of Communication Technology, Aalborg, Denmark, December 2003.

[30] A. J. Goldsmith, "The Capacity of Downlink Fading Channels with Variable Rate and Power," *IEEE Transactions on Vehicular Technology*, vol. 46, no. 3, pp. 569–580, August 1997.

[31] J. F. Hayes, "Adaptive Feedback Communications," *IEEE Transactions on Communication Technology*, pp. 29–34, February 1968.

[32] A. J. Goldsmith and S.-G. Chua, "Variable-Rate Variable-Power MQAM for Fading Channels," *IEEE Transactions on Communications*, vol. 45, no. 10, pp. 1218–1230, October 1997.

[33] J. K. Cavers, "Variable-Rate Transmission for Rayleigh fading Channels," *IEEE Transactions on Communications*, pp. 15–22, February 1972.

[34] W. T. Webb and R. Steele, "Variable-Rate QAM for Mobile Radio," *IEEE Transactions on Communicaitons*, vol. 43, no. 7, pp. 2223–2230, July 1995.

[35] B. Vucetic, "An Adaptive Coding Scheme for Time-Varying Channels," *IEEE Transactions on Communications*, vol. 39, no. 5, pp. 653–663, May 1991.

[36] S. M. Alamouti and S. Kallel, "Adaptive Trellis-Coded Multiple-Phased-Shift Keying for Rayleigh Fading Channels," *IEEE Transactions on Communications*, vol. 42, no. 6, pp. 2305–2314, June 1994.

[37] P. S. Chow, J. M. Cioffi, and J. A. C. Bingham, "A Practical Discrete Multitone Transceiver Loading Algorithm for Data Transmission over Spectrally Shaped Channels," *IEEE Transactions on Communications*, vol. 43, no. 234, pp. 773–775, February 1995.

[38] A. J. Goldsmith and S.-G. Chua, "Capacity of Fading Channels with Channel Side Information," *IEEE Transactions on Information Theory*, vol. 43, no. 6, pp. 1986–1992, November 1997.

[39] IEEE 802.11 Working Group, *The Working Group for WLAN Standards - http://www.ieee802.org/11/*.

[40] J. M. Holtzman, "CDMA Forward Link Water Filling Power Control," in *Proceedings of the the IEEE Vehicular Technology Conference (VTC)*, vol. 3, Tokyo, Japan, May 2000, pp. 1663–1667.

[41] A. Jalali, R. Padovani, and R. Pankaj, "Data Throughput of CDMA-HDR High Efficiency-High Data Rate Personal Communication Wireless System," in *Proceedings of the IEEE Vehicular Technology Conference (VTC)*, vol. 3, Tokyo, Japan, May 2000, pp. 1854–1858.

[42] J. M. Holtzman, "Asymptotic Analysis of Proportional Fair Algorithm," in *IEEE International Symposium on Personal, Indoor and Mobile Radio Communications (PIMRC)*, vol. 2, San Diego, California, USA, September 2001, pp. F33–F37.

[43] T. B. Sørensen, P. E. Mogensen, and F. Frederiksen, "Extension of the ITU Channel Models for Wideband (OFDM) Systems," in *Proceedings of the IEEE Vehicular Technology Conference (VTC)*, vol. 1, Dallas, Texas, USA, September 2005, pp. 392–396.

[44] A. J. Paulraj, D. A. Gore, R. Nabar, and H. Bolcskei, "An Overview of MIMO CommunicationsŮA Key to Gigabit Wireless," *Proceedings of the IEEE*, vol. 92, no. 2, pp. 198–218, February 2004.

[45] W. Na, A. Pokhariyal, T. B. Sørensen, T. E. Kolding, and P. E. Mogensen, "Performance of MIMO with Frequency Domain Packet Scheduling in UTRAN LTE downlink," in *Proceedings of the IEEE Vehicular Technology Conference (VTC)*, Dublin, Ireland, April 2007, pp. 1177–1181.

[46] A. Pokhariyal, T. E. Kolding, F. Frederiksen, P. Olives, T. B. Sørensen, and P. E. Mogensen, "Investigation of Frequency-Domain Link Adaptation for a 5-MHz OFDMA/HSDPA System," in *Proceedings of the IEEE Vehicular Technology Conference (VTC)*, vol. 3, Stockholm, Sweden, May 2005, pp. 1463–1467.

[47] B. Classon, P. Sartori, V. Nangia, X. Zhuang, and K. Baum, "Multi-dimensional Adaptation and Multi-user Scheduling Techniques for Wireless OFDM systems," in *Proceedings of the IEEE International Conference on Communications (ICC)*, vol. 3, Orlando, Florida, USA, May 2003, pp. 2251–2255.

[48] T. E. Kolding, "Link and System Performance Aspects of Proportinal Fair Packet Scheduling in WCDMA/HSDPA," in *Proceedings of 58th IEEE Vehicular Technology Conference (VTC)*, vol. 3, Orlando, Florida, USA, October 2003, pp. 1717–1722.

[49] Orange, China Mobile, KPN, NTT DoCoMo, Sprint, T-Mobile, Vodafone, Telecom Italia, "LTE physical layer framework for performance verification," *3GPP TSG-RAN1#48, R1-070674*, February 2007.

[50] C. Y. Wong, R. S. Cheng, K. B. Letaief, and R. D. Murch, "Multiuser OFDM with Adaptive Subcarrier, Bit, and Power Allocation," *IEEE Journal on Selected Areas in Communicaitons*, vol. 17, no. 10, pp. 1747–1758, October 1999.

[51] B. S. Krongold, K. Ramchandran, and D. L. Jones, "Computationally Efficient Optimal Power Allocation Algorithms for Multicarrier Communication Systems," *IEEE Transactions on Communications*, vol. 48, no. 1, pp. 23–27, October 2000.

[52] R. F. H. Fischer and J. B. Huber, "A new Loading Algorithm for Discrete Multitone Transmission," in *Proceedings of the IEEE Global Telecommunications Conference (GLOBECOM)*, London, UK, November 1996, pp. 724–728.

[53] 3GPP Technical Report 25.813, version 7.0.0, *E-UTRA and E-UTRAN; Radio Interface Protocol Aspects*, June 2006.

[54] G. Song and Y. Li, "Cross-layer optimization for OFDM wireless networks-part I: theoretical framework," *IEEE Transactions on Wireless Communications*, vol. 4, no. 2, pp. 614–624, March 2005.

[55] A. J. Goldsmith and S. B. Wicker, "Design Challenges for Energy-Constrained Ad Hoc Wireless Networks," *IEEE Wireless Communications Magazine*, vol. 9, no. 4, pp. 8–27, August 2002.

[56] G. Song and Y. Li, "Cross-layer optimization for OFDM wireless networks-part II: algorithm development," *IEEE Transactions on Wireless Communications*, vol. 4, no. 2, pp. 625–634, March 2005.

[57] Z. Liu, E. K. P. Chong, and N. B. Shroff, "Oppertunistic Transmission Scheduling with Resource-Sharing Constraints in Wireless Networks," *IEEE Journal of Selected Areas in Communications (JSAC)*, vol. 19, no. 10, pp. 2053–2064, October 2001.

[58] P. Viswanath, D. N. C. Tse, and R. Laroia, "Opportunistic Beamforming Using Dumb Antennas," *IEEE Transactions on Information Theory*, vol. 48, no. 6, pp. 1277–1294, June 2002.

[59] A. Pokhariyal, K. I. Pedersen, G. Monghal, I. Z. Kovacs, C. Rosa, T. E. Kolding, and P. E. Mogensen, "HARQ Aware Frequency Domain Packet Scheduler with Different Degrees of Fairness for the UTRAN Long Term Evolution," in *Proceedings of the IEEE Vehicular Technology Conference (VTC)*, Dublin, Ireland, April 2007, pp. 2761–2765.

[60] M. Nakamura, Y. Awad, and S. Vadgama, "Adaptive Control of Link Adaptation for High Speed Downlink Packet Access (HSDPA) in W-CDMA," in *Proceedings of the Wireless Personal Multimedia Communications Conference (WPMC)*, vol. 2, Honolulu, Hawaii, October 2002, pp. 382–386.

[61] S. Muneta, Y. Matsumoto, N. Mochizuki, and M. Umehira, "A New Frequency-Domain Link Adaptation Scheme for Broadband OFDM Systems," in *Proceedings of the IEEE Vehicular Technology Conference (VTC)*, vol. 1, Amsterdam, Netherlands, September 1999, pp. 253–257.

[62] N. Wei, A. Pokhariyal, C. Rom, B. E. Priyanto, F. Frederiksen, C. Rosa, T. B. Sørensen, T. E. Kolding, and P. E. Mogensen, "Baseline E-UTRA Downlink Spectral Efficiency Evaluation," in *Proceedings of IEEE Vehicular Technology Conference (VTC)*, Montreal, Canada, September 2006, pp. 1–5.

[63] A. J. Goldsmith and S.-G. Chua, "Adaptive Coded Modulation for Fading Channels," *IEEE Transactions on Communications*, vol. 46, no. 5, pp. 595–602, May 1998.

[64] T. E. Kolding, F. Frederiksen, and P. E. Mogensen, "Performance Aspects of WCDMA Systems with High Speed Downlink Packet Access (HSDPA)," in *Proceedings of 56th IEEE Vehicular Technology Conference (VTC)*, vol. 1, Vancouver, British Columbia, Canada, September 2002, pp. 477–481.

[65] P. E. Mogensen, W. Na, I. Z. Kovacs, F. Frederiksen, A. Pokhariyal, K. I. Pedersen, K. Hugl, and M. Kuusela, "LTE Capacity versus Shannon," in *Proceedings of the IEEE Vehicular Technology Conference (VTC)*, Dublin, Ireland, April 2007, pp. 1234–1238.

[66] F. Tang, L. Deneire, M. Engels, and M. Moonen, "Adaptive Link Adaptation," in *Proceedings of the IEEE Global Telecommunications Conference (GLOBECOM)*, vol. 2, San Antonio, Texas, USA, November 2001, pp. 1262–1266.

[67] T. E. Kolding, A. Pokhariyal, N. Wei, and P. E. Mogensen, "Impact of Channel Quality Signaling on Frequency-Domain Link Adaptation Performance," in *Proceedings of the Wireless Personal Multimedia Communications (WPMC) Symposium*, Aalborg, Denmark, September 2005, pp. 932–936.

[68] J. R. F. et al. editor, "Preliminary Design of Multi-user Optimal Transmit and Receive Strategy, D4.1, v1.0," Surface project, European Information Society Technologies, IST-027187, SURFACE, Tech. Rep., December 2006.

[69] F. Frederiksen and T. E. Kolding, "Performance and Modeling of WCDMA/HSDPA Transmission/H-ARQ Schemes," in *Proceedings of the IEEE Vehicular Technology Conference (VTC)*, vol. 1, Vancouver, Cananda, September 2002, pp. 472–476.

[70] ——, "Performance and Modeling of WCDMA/HSDPA Transmission/H-ARQ Schemes," in *Proceedings of 56th IEEE Vehicular Technology Conference (VTC)*, vol. 1, Vancouver, British Columbia, Canada, September 2002, pp. 472–476.

[71] M. Sternad, T. Ottosson, A. Ahlen, and A. Svensson, "Attaining both Coverage and High Spectral Efficiency with Adaptive OFDM Downlinks," in *Proceedings of the IEEE Vehicular Technology Conference (VTC)*, vol. 4, Orlando, Forida, USA, October 2003, pp. 2486–2490.

[72] T. E. Kolding, F. Frederiksen, and A. Pokhariyal, "Low-Bandwidth Channel Quality Indication for OFDMA Frequency Domain Packet Scheduling," in *Proceedings of International Symposium on Wireless Communication Systems (ISWCS)*, Valencia, Spain, September 2006.

[73] F. Kelly, "Charging and rate control for elastic traffic," *European Transactions on Telecommunications*, vol. 8, no. 1, pp. 33–37, January 1997.

[74] P. A. Hosein, "QoS Control for WCDMA High Speed Packet Data," in *Proceedings of the International Workshop on Mobile and Wireless Communication Networks (MWCN)*, Stockholm, Sweden, September 2002, pp. 169–173.

[75] K. Brueninghaus, D. Astley, T. Salzer, S. Visuri, A. Alexiou, S. Karger, and G.-A. Seraji, "Link Performance Models for System Level Simulations of Broadband Radio Access Systems," in *Proceedings of the IEEE Personal Indoor and Mobile Radio Communications Conference (PIMRC)*, vol. 4, Berlin, Germany, September 2005, pp. 2306–2311.

[76] Ericsson, "System-level evaluation of OFDM - further considerations," *3GPP TSG-RAN1, R1-031303*, November 2003.

[77] A. Pokhariyal, "Frequency-Domain Link Adaptation for OFDM/HSDPA," Masters Thesis in Mobile Communications, Aalborg University, Denmark, June 2004.

[78] 3GPP Technical Report 25.858, version 5.0.0, *High Speed Downlink Packet Access: Physical Layer Aspects*, March 2002.

[79] L. T. Berger, "Performance of Multi-Antenna Enhanced HSDPA," Ph.D. dissertation, Aalborg University, Aalborg, Denmark, April 2005.

[80] 3GPP Technical Specification 25.848, version 4.0.0, *Physical layer aspects of UTRA High Speed Downlink Packet Access*, March 2001.

[81] R. G. Gallager, *Information Theory and Reliable Communications*, J. W. . Sons, Ed. John Wiley & Sons, New York, 1968.

[82] I. Z. Kovacs, K. I. Pedersen, J. Wigard, F. Frederiksen, and T. E. Kolding, "HSDPA Performance in Mixed Outdoor-Indoor Micro Cell Scenarios," in *PIMRC*, Helsinki, Finland, September 2006, pp. 1–5.

[83] 3GPP Technical Report 25.943, version 5.1.0, *Deployment Aspects (Release 5)*, June 2002.

[84] Recommendation ITU-R M.1225, *Guidelines for the evaluation of radio transmission technologies for IMT-2000*, February 1997.

[85] 3GPP Technical Report 30.03, version 3.2.0, *Selection procedures for the choice of radio transmission technologies of the UMTS*, April 1998.

[86] Y. Wang, C. Fangjiong, and G. Wei, "Adaptive Subcarrier and Bit Allocation for Multiuser OFDM System Based on Genetic Algorithm," in *Proceedings of the International Conference on Communications, Circuits and Systems*, vol. 1, Hong Kong, China, May 2005, pp. 242–246.

[87] F. F. Digham and M. O. Hasna, "Performance of OFDM with M-QAM Modulation and Optimal Loading over Rayleigh Fading Channels," in *Proceedings of the IEEE Vehicular Technology Conference (VTC)*, vol. 1, Los Angeles, California, USA, September 2004, pp. 479–483.

[88] A. Czylwik, "Adaptive OFDM for Wideband Radio Channels," in *Proceedings of the IEEE Global Telecommunications Conference (GLOBECOM)*, vol. 1, London, UK, November 1996, pp. 713–718.

[89] W. Rhee and J. M. Cioffi, "Increase in Capacity of Multiuser OFDM System Using Dynamic Subchannel Allocation," in *Proceedings of the IEEE Vehicular Technology Conference (VTC)*, vol. 2, Tokyo, Japan, May 2000, pp. 1085–1089.

[90] Y. Kim, N. Haewoon, and B. F. Womack, "An Adaptive Grouped-Subcarrier Allocation Algorithm using Comparative Superiority," in *Proceedings of the IEEE Military Communicaitons Conference (MILCOM)*, vol. 2, Atlantic City, NJ, USA, October 2005, pp. 963–969.

[91] T. C. H. Allen, A. S. Madhukumar, and F. Chin, "Capacity Enhancement of a Multiuser OFDM System Using Dynamic Frequency Allocation," *IEEE Transactions on Broadcasting*, vol. 49, no. 4, pp. 344–353, December 2003.

[92] R. Grunheid, E. Bolinth, and H. Rohling, "A Blockwise Loading Algorithm for the Adaptive Modulation Technique in OFDM Systems," in *Proceedings of the IEEE Vehicular Technology Conference (VTC)*, vol. 2, Atlantic City, New Jersey, USA, October 2001, pp. 948–951.

[93] L. Xiaowen and Z. Jinkang, "An Adaptive Subcarrier Allocation Algorithm for Multiuser OFDM system," in *Proceedings of the IEEE Vehicular Technology Conference (VTC)*, vol. 3, Orlando, Florida, USA, October 2003, pp. 1502–1506.

[94] C. Wengerter, J. Ohlhorst, and A. G. E. v. Elbwart, "Fairness and Throughput Analysis for Generalized Proportional Fair Frequency Scheduling in OFDMA," in *Proceedings of the IEEE Vehicular Technology Conference (VTC)*, vol. 3, Stockholm, Sweden, May 2005, pp. 1903–1907.

[95] A. Forenza and R. H. Jr, "Link adaptation and channel prediction in wireless OFDM systems," in *Proceedings of the Midwest Symposium on Circuits and Systems (MWSCAS)*, Tulsa, Oklahoma, USA, August 2002, pp. 211–214.

[96] S. Catreux, V. Erceg, D. Gesbert, and R. W. H. Jr., "Adaptive modulation and MIMO coding for broadband wireless data networks," *IEEE Communications Magazine*, vol. 40, no. 6, pp. 108–115, June 2002.

[97] K. I. Pedersen, G. Monghal, I. Z. Kovacs, T. E. Kolding, A. Pokhariyal, F. Frederiksen, and P. E. Mogensen, "Frequency Domain Scheduling for OFDMA with Limited and Noisy Channel Feedback," in *Proceedings of IEEE Vehicular Technology Confreence (VTC)*, Baltimore, USA, October 2007.

[98] T. Kashima, M. Rinne, T. Roman, S. Visuri, S. Jarot, J. Kahtava, A. Pokhariyal, T. E. Kolding, and O. Tirkkonen, "Design of channel structures for the Evolved UTRA downlink," in *Proceedings of the Japan Society for Simulation Technology Mobile Communications Working Group Workshop, Evolved UTRA Special Session*, Tokyo, Japan, October 2006, pp. 11–17.

[99] X. Zhang, Y. Wang, and W. Wang, "Capacity Analysis of Adaptive Multiuser Frequency-Time Domain Radio Resource Allocation in OFDMA Systems," in *Proceedings of the IEEE Intl. Symposium on Circuits and Systems (ISCAS)*, vol. 1, Kos, Greece, May 2006, pp. 5676–5679.

[100] A. Das, F. Khan, A. Sampath, and S. Hsuan-Jung, "A Variable Rate Channel Quality Feedback Scheme for 3G Wireless Packet Data Systems," in *Proceedings of the IEEE International Conference on Communications (ICC)*, vol. 2, Seattle, USA, May 2003, pp. 982–986.

[101] B. Ji, C. V. Rensburg, and J.-A. TsaiA, "Analysis of Optimal Use of CQI Channels for OFDMA Systems," in *Proceedings of the IEEE Vehicular Technology Conference (VTC)*, vol. 3, Dallas, Texas, USA, September 2005, pp. 1604–1608.

[102] A. Pokhariyal, T. E. Kolding, and P. E. Mogensen, "Performance of Downlink Frequency Domain Packet Scheduling for the UTRAN Long Term Evolution," in *Proceedings of IEEE Personal Indoor and Mobile Radio Communications Conference (PIMRC)*, Helsinki, Finland, September 2006, pp. 1–5.

[103] 3GPP Technical Report 25.892, version 0.5.2, *Feasibility Study for OFDM for UTRAN enhancement*, December 2003.

[104] L. Schumacher, J. P. Kermoal, F. Frederiksen, K. I. Pedersen, A. Algans, and P. E. Mogensen, "MIMO Channel Characterisation," in *IST Project IST-1999-11729 METRA Deliverable 2*, February 2001.

[105] J. G. Proakis, *Digital Communications, Fourth Edition.* ISBN 0-07-232111-3: Mc Graw Hill, 2001.

[106] J. Vogt and A. Finger, "Improving the max-log-MAP turbo decoder," *Electronic Letters*, vol. 36, pp. 1937–1939, November 2000.

[107] Nortel Networks, "Effective SIR Computation for OFDM System-Level Simulations," *3GPP TSG-RAN1, R1-031370*, November 2003.

[108] R. L. Mason, R. F. Gunst, and J. L. Hess, *Statistical Design and Analysis of Experiments*. John Wiley & Sons, 1989.

[109] C. Rosa, "Enhanced Uplink Packet Access in WCDMA," Ph.D. dissertation, Aalborg University – Department of Communication Technology, Aalborg, Denmark, December 2004.

[110] K. S. Shanmugan and A. M. Breipohl, *Random Signals: Detection, Estimation and Data Analysis*. ISBN 0-471-81555-1: John Wiley & Sons, Inc., 1988.

Paper Reprint

Annex I

Frequency Domain Packet Scheduling Under Fractional Load

A. Pokhariyal, G. Monghal, K. I. Pedersen, P. E. Mogensen, I. Z. Kovacs, C. Rosa and T. E. Kolding, "Frequency Domain Packet Scheduling Under Fractional Load for the UTRAN LTE Downlink", in *Proc. of IEEE Vehicular Technology Conference VTC2007-Spring*, pp. 699-703, Dublin, Ireland, April, 2007.

Frequency Domain Packet Scheduling Under Fractional Load for the UTRAN LTE Downlink

A. Pokhariyal†, G. Monghal†, K. I. Pedersen‡, P. E. Mogensen†,‡, I. Z. Kovacs‡, C. Rosa‡
and T. E. Kolding‡
† Aalborg University, ‡ Nokia Networks — Aalborg, Denmark

Abstract— In this paper we investigate the performance of frequency domain packet scheduling (FDPS) under fractional load (FL), based on the UTRAN Long Term Evolution downlink. Under FL, the packet scheduler does not need to transmit on entire system bandwidth due to lack of traffic in the network, which leads to an improvement in the user experienced SINR. System-level simulations show that the proportional fair scheduler tries to optimize resource allocation by avoiding transmission on frequencies that are experiencing severe interference. As an example, FDPS can provide a gain of 4 dB in SINR over the round-robin scheduler, when the load is equal to 25%. The observed interference control is achieved without any centralized management. Further, FDPS under FL can provide an effective trade-off between cell throughput and coverage. The FDPS performance is dependent on the ability of link adaptation to track variations in interference. This ability is reduced when the frequency usage pattern is changing rapidly over time.

I. INTRODUCTION

The downlink radio access of the 3GPP UTRAN long term evolution (LTE) will be based on the orthogonal frequency division multiple access (OFDMA) scheme. The guidelines for the Physical layer design are described in [1]. As LTE supports frequency-domain adaptation techniques in downlink we will investigate the performance of *frequency domain packet scheduling* (FDPS), which refers to fast channel dependent scheduling in both time and frequency domains. Previous FDPS studies [2], [3], [4] indicate that it has significant potential over time-domain only scheduling, e.g. in [4] it is reported that FDPS can provide a gain of around 40% in cell throughput. The main drawbacks of FDPS are high scheduler complexity and increased signaling overhead in the uplink as well as in the downlink. Previous FDPS studies are based on the full load scenario.

As OFDMA can provide intra-cell orthogonality by means of the cyclic prefix, the main source of interference in downlink is *inter-cell interference* (ICI) [5]. It can severely limit the throughput of users near the cell edge, in a reuse 1 network with continuous coverage. When the network is experiencing a lack of traffic, the packet scheduler optimizes resource allocation by transmitting only on a portion of the system bandwidth. This leads to a reduction in ICI and thereby an improvement in SINR, which can be particularly useful to cell-edge users as their data rate can be improved. The focus of this study is the investigation of FDPS under the *fractional load* (FL) scenario.

We assume that there is no co-ordination between the entities responsible for resource allocation in the neighboring cells. The analysis is based on a detailed LTE system-level model, developed according to the guidelines given in [1]. The important scheduling related functions such as link adaptation (LA) and HARQ have been modeled explicitly. Further, as the FDPS performance is sensitive to the accuracy of *channel quality indication* (CQI) reports, realistic assumptions for achievable CQI accuracy and reporting frequency have been used [4].

The paper is organized as follows: Section II describes the interaction between the different functional entities involved in packet scheduling. It also covers the description of the LA functionality and the FDPS algorithm. Section III provides details on the system-model as well as describes the modeling of FL. Section IV covers the results and analysis, while the conclusions are summarized in Section V.

II. PACKET SCHEDULING FRAMEWORK

Fig. 1 illustrates the interaction between the different entities involved in packet scheduling (PS), which are located at the base station (eNode-B) in order to facilitate fast channel dependent scheduling [6]. Following LTE naming convention the basic time-frequency resource available for data transmission is denoted as the physical resource block (PRB). The PRB consists of a fixed number of adjacent OFDM sub-carriers and represents the
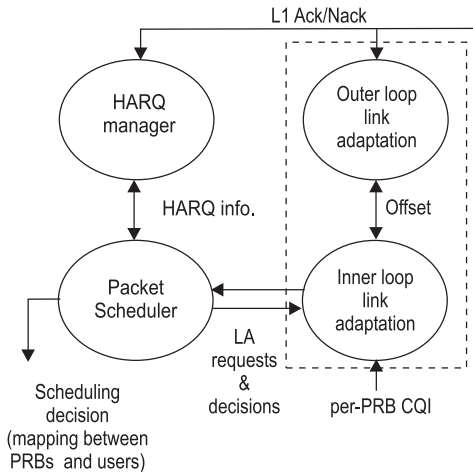
Fig. 1. Interaction between PS, LA, and the HARQ manager entities of the eNode-B that are responsible for dynamic resource allocation.
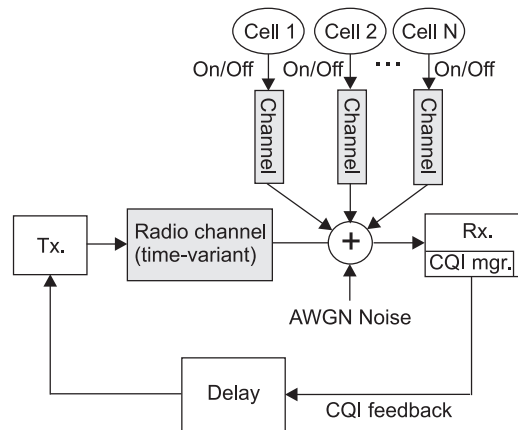

Fig. 2. A single radio link in the reuse 1 LTE downlink, where transmission from neighboring cells leads to ICI. Under FL, the link SINR can vary significantly due to dynamic variations in the ICI.

minimum scheduling resolution in the frequency domain [1]. The PS is the controlling entity in the overall scheduling process. It can consult the LA module to obtain an estimate of the supported data rate for certain users in the cell, for different allocations of PRBs. LA utilizes frequency-selective CQI feedback from the users, as well as Ack/Nacks from past transmissions, to ensure that the estimate of supported data rate corresponds to a certain BLER target for the first transmissions. Further, outer loop link adaptation has been used to stabilize the BLER performance in the presence of LA uncertainties [7]. It provides a user based adaptive offset on a sub-frame interval that is applied to the received CQI reports. This technique can reduce the impact of biased CQI errors on LA performance [8]. Under FL, the scheduler employs a sub-set of PRBs for transmission. Further, restrictions on the allowed power per active PRB can also be enforced in order to control interference variations in the network. The aim of the scheduler is to optimize the cell throughput for the given load condition under the applied scheduling policy, e.g., proportional fair scheduling in time and frequency [8]. The HARQ manager provides buffer status information as well as transmission format of the pending HARQ retransmissions.

A. Link Adaptation

The experienced SINR of a single radio link is formulated with the aid of Fig. 2. The received SINR measured at the sub-carrier frequency f at scheduling interval n is given by:

$$\text{SINR}(f,n) = \sum_{i=1}^{2} \frac{P(f,n) \cdot H_i(f,n)}{N_o(f) + \sum_{k=1}^{N} I_k(f,n)}, \quad (1)$$

where $P(f,n)$ denotes the transmit power from own cell, $H_i(f,n)$ is the channel power gain experienced at the ith receive antenna, $I_k(f,n)$ denotes inter-cell interference power experienced from surrounding cell k, and N_o represents thermal noise. The expression in (1) is based on a 1x2 MRC receiver. Further, there are $N+1$ cells in the network. Note that thermal noise is the only time-invariant parameter in (1). Under FL, the PRB containing sub-carrier f can be either in use or inactive in each of the cells. Moreover, the PRB activity state can vary on a sub-frame basis, which results in larger ICI dynamics in comparison with the full load case. At the eNode-B frequency-domain LA is performed by using the knowledge of prevailing channel conditions obtained through frequency selective CQI reports. Due to processing delays at both ends the CQI report measured at the receiver is not available instantaneously at the transmitter, as shown in Fig. 2. If the ICI conditions change before the packet is finally received, LA will not be able to track those changes, leading to a performance deterioration. As a result under FL, the performance of both LA and FDPS becomes sensitive to the time correlation in the PRB "On" and "Off" activity states. In this regard, as the channel fading is correlated in time it is expected that PRB activity states will also be correlated.

B. Frequency Domain Packet Scheduling

We will focus on localized transmissions in the frequency-domain [1]. The overall scheduler is divided into a time-domain (TD) part followed by the frequency-domain (FD) part. The aim of the scheduler is to maximize the utilization of available multi-user diversity in both time and frequency domains. The details of the scheduler framework

as well as its performance evaluation is provided in the related paper [8]. The motivation behind the partitioning of the scheduler is to reduce the complexity of frequency-domain multiplexing algorithm and to handle the restrictions imposed by HARQ retransmissions in an effective manner. A subset of M users are passed to the FD scheduler by the TD scheduler in each sub-frame. Independent scheduling policies can be applied at each scheduler part. The task of the TD scheduler is to achieve inter-user fairness, while the FD scheduler tries to optimize the spectrum efficiency. The choice of M depends on the scheduler complexity as well as on the allowed DL control overhead. Control signaling is required to notify users of incoming transmissions, and the resulting overhead depends on M. The default scheduler is based on the well known *proportional-fair* (PF) metric, which is applied in both time and frequency. Further, the reference scheduler consists of round-robin scheduling in frequency, while the TD scheduler is based on the PF metric.

III. System Model

The performance evaluation is based on a detailed system-level model of LTE, following the guidelines in [1]. The system bandwidth is fixed at 10 MHz, and the Physical layer settings are based on the LTE working assumptions. The main simulation parameters are listed in Table I, assuming the macro-cell case 1 deployment scenario. We assume that the PRB bandwidth is equal to 375 kHz, resulting in 24 PRBs. Scheduling related functions are explicitly modeled in the three center cells only. The remaining fifty-four cells act as a source of ICI. The link-to-system level mapping is based on the *exponential effective SNR metric* (EESM) model [8]. The location of users is randomly assigned with a uniform distribution within each of the three center cells. It is assumed that the distance dependent path loss and shadow fading is constant during a packet call. A finite buffer best effort traffic model is employed, where each user downloads a 2 Mbit packet. As soon as the download is completed, the session is terminated and a new call is immediately started at a new random location. The serving cell is selected randomly among the strongest cells within a selection margin of 2 dB. The key performance indicators are the average cell throughput, user throughput distribution and coverage at 5% outage.

A. Modeling of Fractional Load

As scheduling is not explicitly simulated in the non-center cells a model is required for FL

TABLE I
DEFAULT SIMULATION PARAMETERS [1].

Parameter	Setting
System bandwidth	10 MHz
Sub-carriers per PRB	25
Cellular Layout	Hexagonal grid, 19 cell sites, 3 cells per site
Inter-site distance	500 m
Total eNode-B transmit power	46 dBm
Penetration loss	20 dB
Shadowing standard deviation	8 dB
Max. users multiplexed per sub-frame	6
Power per active PRB, P_{PRB}	32.2 dBm
C	20 sub-frames
Traffic model	Single 2 Mbit packet
Power delay profile	ITU Typical Urban, 20 paths
Ack/Nack delay	2 ms
CQI log-normal error std.	1 dB
CQI reporting resolution	1 dB
CQI delay	4 ms
Pilot, control channel overhead	28.5% (2/7 symbols)
Modulation/code rate settings	QPSK (R= 1/3, 1/2, 2/3), 16QAM (R=1/2, 2/3, 4/5), 64QAM (R=1/2, 2/3, 4/5)
HARQ model	Ideal chase comb.
No. of HARQ processes	6
1st Tx. BLER target	20%
UE speed	3 km/h
UE receiver	1x2 MRC
Channel estimation	Ideal
Cell selection margin	2 dB

scenario. We have selected the well-known discrete two-state homogenous Markov-chain based stochastic model, as shown in Fig. 3. The states represent whether a PRB is "On" or "Off". The parameters of the Markov model can be tuned to provide a certain average rate of state transitions. This facilitates the modeling of a dynamic FL scenario with known correlation behavior between PRB activity states. Independent Markov chains are used in all the interfering cells in the network, assuming the same state transition probabilities. The activity state of each PRB is updated every 0.5 ms.

Let P_1 denote the probability that a PRB is "On", while $P_0 = 1 - P_1$ denotes the probability that it is "Off". Given the Markov chain in Fig. 3, we can express the state probabilities for PRB "Off" and

Load factor, P_1	Number of active users per cell, L	Avg. num of active PRBs, $\overline{X}$
0.25	5	6
0.50	10	12
0.75	15	18
1.00	20	24

Fig. 4. Statistics for availability of PRBs collected from entire network.

"On" states as,

$$P_0 \;=\; \frac{b}{a+b} \quad, \tag{2}$$

$$P_1 \;=\; \frac{a}{a+b} \quad. \tag{3}$$

Given this simple stochastic model for controlling the On/Off activity for each of the M PRBs in each of the interfering cells, there will be X active PRBs for a given cell in a sub-frame, such that $X \in [0,1,2,\cdots,M]$. The probability of experiencing q consecutive "On" states is geometrically distributed with a mean value given by:

$$C \;=\; \frac{1}{b} \quad. \tag{4}$$

From (3) and (4) and since a and b should be in the range $[0;1]$, parameter C is subject to the following constraint,

$$C \;>\; \max\left\{1, \frac{P_1}{1-P_1}\right\} \quad. \tag{5}$$

The value of C relative to the CQI delay determines how effectively LA can track the SINR variations. We select $C = 20$ sub-frames by default, such that it is much larger than the CQI delay (8 sub-frames). In the center cells, the number of active PRBs is determined by using a Binomial distribution based on the given load factor, P_1. By default constant power allocation in frequency is considered, i.e., fixed power per active PRB denoted by P_{PRB}. We also show performance results for the flexible power allocation scheme, where the total power is divided equally among the active PRBs, for comparison purposes. We investigate FDPS performance under
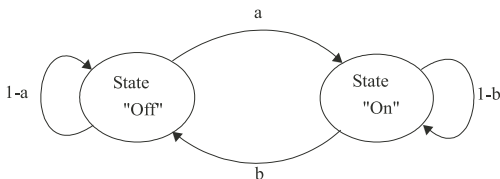

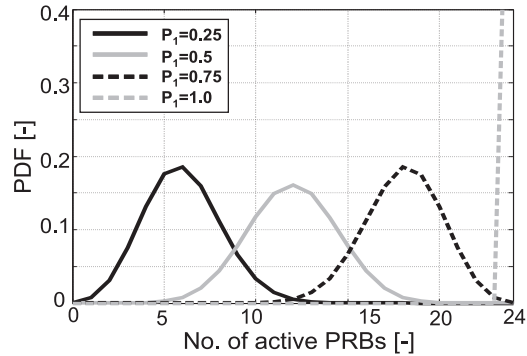Fig. 3. Discrete two-state homogeneous Markov chain used for modeling of FL.

different load conditions enumerated in Table II. The ratio of average number of active PRBs to the number of users L, i.e., $\overline{X}/L$, is kept constant, in order to make a fair comparison.

IV. SIMULATION RESULTS

Fig. 4 shows the probability distribution function (PDF) of the number of active PRBs for different FL scenarios listed in Table II. The statistics are collected from all the cells in the network. The PDF curves follow expected trends with the mean value of active PRBs in each case matching with $\overline{X}$ in Table II.

Fig. 5 illustrates the behavior of key parameters that affect system performance. The results in Fig. 5 (a) confirm that FL results in an improvement in the sub-carrier SINR. Further, a significant gain of FDPS (PF) over reference scheduler is seen especially at low load, e.g., at $P_1 = 0.25$ the SINR improvement with reference scheduler is 6 dB (not shown here), while it is 10 dB with FDPS. The additional gain is attributed to the use of CQI, which lowers the probability of scheduling on the same PRBs in neighboring cells. The interference control seen here is achieved without relying on any centralized management. Fig. 5 (b) illustrates the cumulative density function (CDF) of the total transmit power used at each scheduling node. The curves follow expected trends as the eNode-B tunes the transmit power according to P_1. Fig. 5 (c) depicts the CDF of the experienced SINR measured on a packet basis. We observe a higher gain in SINR than expected at low load, similar to Fig. 5 (a). The CDF curves of Fig. 5 (d) illustrate that LA is able to map the improvement in SINR due to FL into a gain in user throughput, especially at the tail of the throughput distribution, i.e., in terms of coverage. However, the curves converge at the top, which is a result of the limited MCS range, e.g., the highest available MCS, 64QAM 4/5, is selected at around 15 dB, while the SINR can increase up to 40 dB.
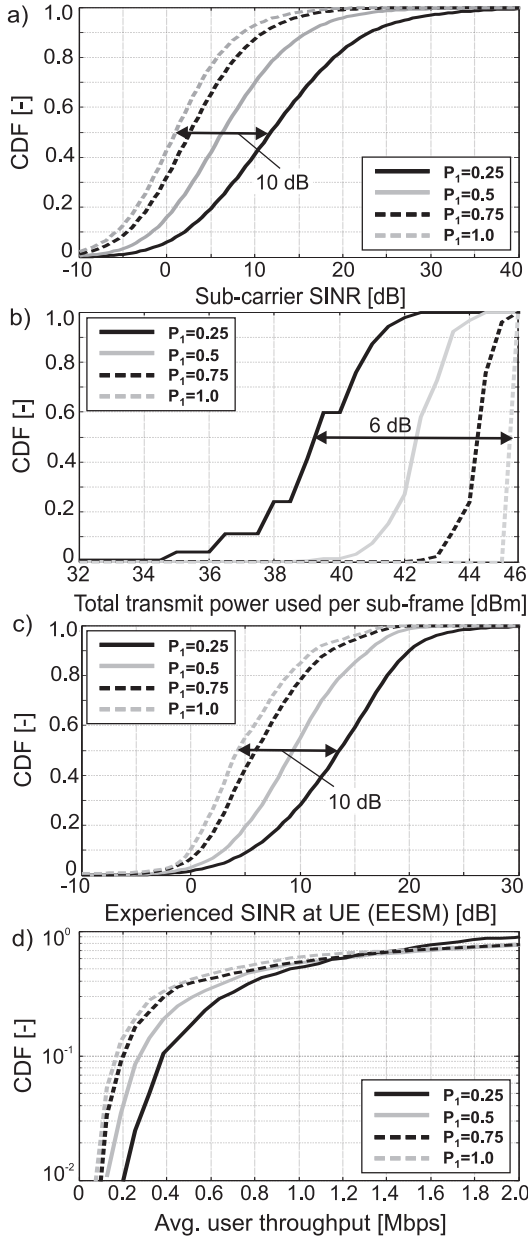
Fig. 5. Behavior of key parameters governing system performance.

Fig. 6. Average cell throughput and coverage performance as a function of P_1. The results for the reference scheduler are shown for two FL cases.

Shannon Theorem based approximation,

$$\text{cell\_tp} \cong W \cdot P_1 \cdot \log 2\left(1 + SINR \cdot \frac{1}{P_1}\right), \qquad (6)$$

where W denotes the bandwidth. P_1 appears twice in (6) to represent the FL induced bandwidth reduction as well as the SINR improvement from the reduction in ICI. By substituting the median value of SINR ($\sim 1\,\text{dB}$) from Fig. 5 (a) and the cell throughput from Fig. 6 (a) for the $P_1 = 1.0$ case into (6) we obtain the Shannon based estimate of the cell throughput for the different cases, also shown in Fig. 6 (a). It can be seen that there is a good match between the estimated and the observed cell throughput values, except for the $P_1 = 0.25$ case. In the latter scenario, due to the limited MCS range LA is not able to map the very high SINR values into corresponding value of throughput. Further, compared to the reference scheduler PF scheduling in frequency can provide an additional gain of 10-15% in throughput and coverage.

Fig. 7 (a) and Fig. 7 (b) illustrate the impact of rate of change of the PRB allocation pattern. Frequent changes in the PRB activity results in a performance loss, due to the inability of LA to track the ICI variations. The impact is significant at low load, e.g., a loss of up to 25% in coverage is seen in Fig. 7 (b).

Fig. 8 illustrates the comparative performance of the constant and the flexible power allocation schemes. The two schemes have quite similar performance as the deployment scenario is mainly interference limited, and the use of higher transmit power does not lead to a similar SINR improvement.

Fig. 6 illustrates the performance of FDPS in terms of average cell throughput and coverage, which is defined as the data rate at 5 % outage. It is observed that FDPS can provide a trade-off between cell throughput and coverage, e.g., when $P_1 = 0.25$, the coverage is improved by a factor of around two, while the average cell throughput is halved, in comparison with the full load case. We compare the results obtained with the following
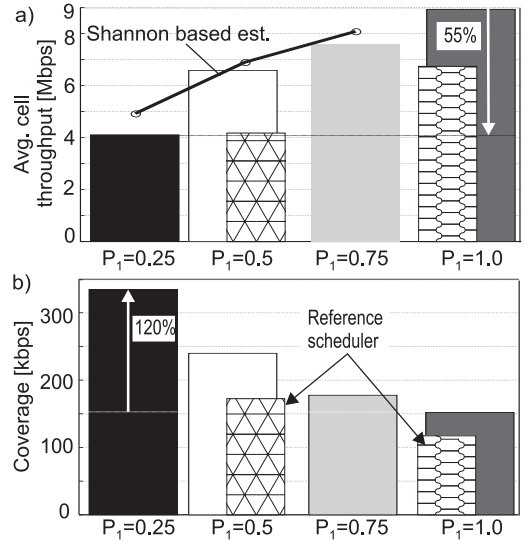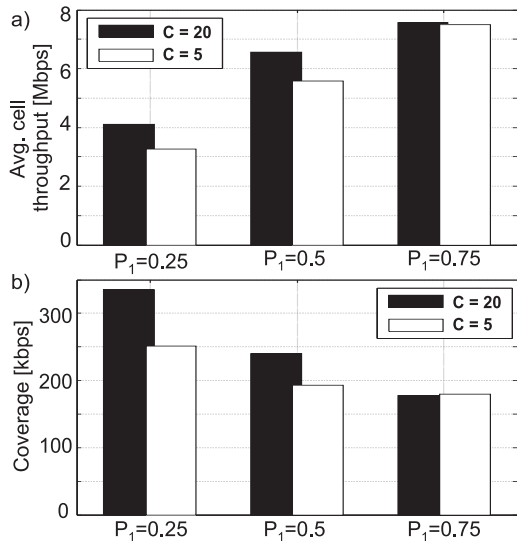
Fig. 7. Impact of the PRB switching rate on FDPS performance.

Fig. 8. Potential of adaptive power allocation with FDPS, $C = 20$.

V. Conclusions

In this paper we have investigated the performance of frequency domain packet scheduling (FDPS) under fractional load (FL) scenario, based on the UTRAN Long Term Evolution downlink. Under FL, the packet scheduler does not need to allocate entire system bandwidth for transmission, due to lack of traffic in the network, which leads to an improvement in the experienced SINR. System-level simulations show that the proportional fair scheduler tries to optimize resource allocation by avoiding transmission on frequencies that are experiencing severe interference. As an example, FDPS can provide a gain of 4 dB in SINR over the frequency-blind scheduler, when the load is equal to 25%. The observed interference control is achieved without relying on any centralized management. Further, FDPS under FL can provide an effective trade-off between cell throughput and coverage, e.g., when the load is 25%, coverage is improved by a factor of two, while cell throughput is halved compared to full load case. The FDPS gain depends on the ability of link adaptation to track the variations in interference. This ability is reduced if the frequency usage pattern is changing at a fast rate.

References

[1] 3GPP Technical Report 25.814, version 7.1.0, *Physical Layer Aspects for Evolved UTRA*, September 2006.

[2] B. Classon, P. Sartori, V. Nangia, X. Zhuang, and K. Baum, "Multi-dimensional Adaptation and Multi-user Scheduling Techniques for Wireless OFDM systems," in *IEEE ICC International Conference on Communications*, vol. 3, Orlando, Florida, USA, May 2003, pp. 2251–2255.
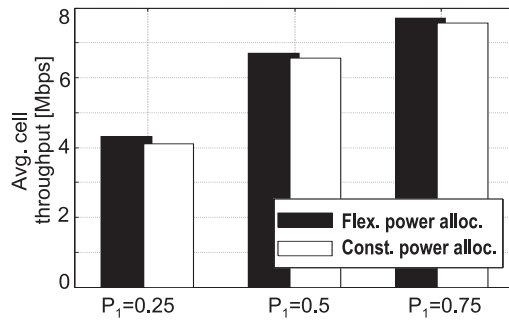
[3] S. Nagata, Y. Ofuji, K. Higuchi, and M. Sawahashi, "Optimum Resource Block Bandwidth for Frequency Domain Channel-Dependent Scheduling in Evolved UTRA Downlink OFDM Radio Access," in *Proceedings of IEEE Vehicular Technology Conference (VTC)*, Melbourne, Australia, May 2006.

[4] A. Pokhariyal, T. E. Kolding, and P. E. Mogensen, "Performance of Downlink Frequency Domain Packet Scheduling for the UTRAN Long Term Evolution," in *Proceedings of IEEE Personal Indoor and Mobile Radio Communications Conference (PIMRC)*, Helsinki, Finland, September 2006.

[5] Texas Instruments, "Performance of Inter-Cell Interference Mitigation with Semi-Static Frequency Planning for EUTRA Downlink," *3GPP TSG-RAN1, R1-060368*, February 2006.

[6] H. Holma and A. Toskala, Eds., *HSDPA/HSUPA for UMTS – High Speed Radio Access for Mobile Communications*. John Wiley & Sons Ltd, 2006.

[7] M. Nakamura, Y. Awad, and S. Vadgama, "Adaptive Control of Link Adaptation for High Speed Downlink Packet Access (HSDPA) in W-CDMA," in *Proceedings of Wireless Personal Multimedia Communications Conference (WPMC)*, vol. 2, Honolulu, Hawaii, October 2002, pp. 382–386.

[8] A. Pokhariyal, K. I. Pedersen, G. Monghal, I. Z. Kovacs, C. Rosa, T. E. Kolding, and P. E. Mogensen, "HARQ Aware Frequency Domain Packet Scheduler with Different Degrees of Fairness for the UTRAN Long Term Evolution," in *Proceedings of the IEEE Vehicular Technology Conference (VTC)*, Dublin, Ireland, April 2007.